FACULTY OF SCIENCE
DEPARTMENT OF CHEMISTRY
MOLECULAR DESIGN & SYNTHESIS
Celestijnenlaan 200F box 2404
B-3001 HEVERLEE, BELGIUM
B-3001 Heverlee, Belgium
dzenita.kasapovic@.kuleuven.be
https://chem.kuleuven.be/en/research/mds/lic

Dženita Avdibegović

RECOVERY OF RARE EARTHS FROM BAUXITE RESIDUE LEACHATES BY FUNCTIONALISED SORBENTS

July 2018

KU LEUVEN

ARENBERG DOCTORAL SCHOOL
FACULTY OF SCIENCE

RECOVERY OF RARE EARTHS FROM BAUXITE RESIDUE LEACHATES BY FUNCTIONALISED SORBENTS

DŽENITA AVDIBEGOVIĆ

Supervisor(s):
Prof. Dr. Koen BINNEMANS
Dr. Mercedes REGADÌO

Dissertation presented in partial fulfilment
of the requirements for the degree of
Doctor of Science (PhD): Chemistry

July 2018

RECOVERY OF RARE EARTHS FROM BAUXITE RESIDUE LEACHATES BY FUNCTIONALISED SORBENTS

Dženita Avdibegović

Supervisor:

Prof. Dr. Koen BINNEMANS

Co-supervisor:

Dr. Mercedes REGADÌO

Examination Committee:

Dr. Joris ROOSEN

Dr. Risto KOIVULA (external member)

Prof. Dr. Tatjana PARAC-VOGT

Prof. Dr. Ir. Tom VAN GERVEN

Prof. Dr. Wim DE BORGGRAEVE (chairperson)

Prof. Dr. Ir. Yiannis PONTIKES

July 2018

Uitgegeven in eigen beheer, Dženita Avdibegović, Celestijnenlaan 200F, B-3001 Heverlee.

If you can dream it, you can do it…

Acknowledgement (Dankword)

It has been a long but a fruitful journey and the time has come to write a totally different part of the thesis…

First of all, thank you *Prof. Koen Binnemans* for putting your trust in me, for letting me experience wonders of scientific research and for giving me the opportunity to learn so much during the past three years. It has been a real honor for being a part of such great, progressive, creative, hard-working, open-minded (you name it…) group with you as a head of the team.

Mercedes (my *Mer*) thank you for being not only a co-supervisor of my dreams, but also my friend and one of the nicest persons I have met. Thank you for all your infinite patience for all my beginner's mistakes and for being so devoted to everything you do. I have learned so much from you…

I would like to thank to all of my jury members for reading the thesis, their valuable comments, ideas and nice discussion during my preliminary defense. *Wim*, thank you for making sure that everything runs smoothly during my preliminary defense and for being always so student-friendly. *Tom*, thank you for all the valuable suggestions starting from my nine month presentation until now. *Yiannis*, it has been a pleasure for being a part of the same REDMUD (or BR) team. Thank you for all motivation that you were giving to the ESRs and for the nice atmosphere during our meetings. *Risto*, thank you for all your support, for being a great host during my stay in your group at University of Helsinki, and for a great collaboration. *Tanja*, thank you for a great motivation after every talk with you and for being a true role model of a great woman in science and a great person. *Joris*, thank you for all your effort in improving my manuscripts and especially the thesis. I always find the inspiration for my research by reading your work and thank you for being one of the persons from who I learned a lot.

Rita, *Rabab*, *Lucian*, *Dirk*, *Paul*, *Bart*, *Domink*, thank you all for your help whenever needed.

I would like to thank to the members of the supervisory board of the REDMUD project for a great collaboration and fruitful meetings: Ken Evans, Katy Tsesmelis, Gyorgy Banvolgyi, Marios Katsiotis, Vicky Vassiliadou, Carsten Dittrich, Milena and Srecko Stopic, Alan Tkaczyk, Dimitris Panias, Thymis Balomenos, Anna Bjorklund, Bernd Friedrich. I would like to offer special thanks to Risto Hariula, who, although no longer with us, continues to inspire by his example.

A big thanks to my dear friends and colleagues from the REDMUD project for their support and good collaboration during these three memorable years: *Buhle (mr. X)*, *Bengi*, *David*, *Tobias*, *Johanes*, *James*, *Andrei.*

Special thanks to my REDMUD ladies for the great atmosphere, for our talks, jokes and our ladies trip (I hope we can do it again somewhere soon): *Stergi* (always positive and smiley), *Chiara B.* (*mia Chiarona*) and *Chiara C.* (*Chiaretta*), *Gozde* (my *canim*), *Pritii* (sunshine). I can't wait to meet with all of you again.

Rodolfo, *Rodolfito*, the *boss*, *α*, but above all my friend, thanks for all the great time we had from the very beginning of this journey, for all the laughter (what a laugh), fun, trips, all the moments with the big group of friends and I guess I can dare to say sports ☺ Thank you for being always willing to help in everything, for the scientific discussions with a great coffee from the fourth floor. I am glad to have such open-minded and energetic friend and a colleague like you.

Wenzhong, I can never forget all the effort you put in making sure that I feel comfortable and that everything goes well during my stay in Helsinki. I enjoyed our trips, talks and discussions, and I cherish deeply all the moments. Thank you for being always so nice, friendly, patient when I got confused, for all the time you devoted in helping me in million different situations, for trying to teach me some Chinese words (although there is still much room for improvement :) for all efforts you put to make sure that the work is done in the best possible way, for always being willing to be there for a friend… You are a genuine person and I am truly happy to have a friend and a colleague like you.

Junhua, thank you for the hospitality and kindness during my stay in Helsinki. I am very grateful to you for showing me, together with *Wenzhong*, a part of amazing Chinese culture and cuisine and for making the period of my secondment enjoyable.

Surachet (O_2), one of the most amazing persons I have ever met! I appreciate all nice talks about Asian culture and life in general, shopping times, trips with *Wenzhong*, and simply the moments while walking towards our, at that time new home in *Vuolukiventie*. It was a pleasure to have met you and wherever in this whole world I may be know that you can always count on me, my friend.

A big thanks to all people I met at University of Helsinki for their generosity and good collaboration.

Thanks to *Michiel*, *Tu*, *Lukas*, *Nerea*, *Zheng*, *Stijn R*, *Stijn VR*, *Heleen*, *Arne*, *Jonas*, *Jeroen*, *Sven*, *Isadora*, *Liubov*, *Basit*, *Giacomo*, *Raju*, *Babu*, *Piet*, *Lieven*, *Chenna*, *Laura*, *Alexandra*, *Alexander*, *Alexandr*, *Jens*, *David*, *Tom VDH*, *Bram*, *Niel*, *Sandra*, *Eleonora*, for being great colleagues and friends.

Clio and *Bieke*, thanks for all work-related help and in general when needed, ever since I arrived in the group.

Sofia, thanks for being always in a good mood for a talk, for sharing advices and your experience and for being so inspiring!

Daphne, thank you for all the kindness, patience, and very nice and inspiring talks. Thanks for being willing to extend your hand to help me with the work in the lab or anything else that I needed (not to mention your help when I would receive a mail in Dutch ☺ I miss you in the LIC group!

Brecht, thank you for showing me the diversity of Belgian culture and for being my *kleine broertje*.

Emir and *Merve*, one of the most inspiring and enthusiastic couples I have seen. Thank you for all the nice moments we shared, for being my friends and my dear neighbors! I am very happy to have learned even more from you about Turkish culture.

Recai, thanks for the motivation (in your own style :) friendship and help, especially in the recent critical moments with the thesis-related work! I appreciate it very much!!!

Simona, my *Simi* (*Simonka*), I am happy to have met you (and *Matej*), really kind, friendly and creative person, a true pearl. I appreciate all the times we had and I sense there is much more yet to come.

Martina, bella Martiiii…. you know that I love you so much!!! Thank you for your optimism, for motivation, for all the talks and everything we shared. The effort you put in teaching me some Italian is admirable and I am very grateful for that. I am glad to have met a dreamer similar to me. You are my colorful butterfly and whatever the future might bring, know that I will gladly be there for you.

Special thanks to *Caravan team*, *Oscar*, *Gaston*, *Carla*, *Fabio*, *Francesco*, *Carmen*, for organising social events and for the great time.

Thank you *Asma* and *Ghania* for the good time we shared while you were still living in Leuven.

Thanks to my office-mates *Sharron*, *Kumar*, *Thupten*, for wonderful working environment, and for great talks about life in general. I appreciate that I learned something about your cultures and that through that I broaden my view and managed to understand another kinds of realities. *Pieter*, thanks to you as well for the nice atmosphere while you were still in our office, for being patient during our "*morning sessions of compliments*" and for being always willing to listen to my troubles with experiments (and the entropy :)

Federica, my *Fede*, my dear friend, a companion from my first day in Belgium… I was incredibly lucky to have met you and to have shared with you all these days, all the hardness at the beginning, and all the relieve that came afterwards (freedom moments :) You are the reason that I cherish this lifetime experience even more. Thank you for listening to all my detailed (and exhausting) descriptions of emotions and philosophical thoughts about life and society and for sharing also yours with me. It is a true blessing to have a friend like you, so gentile, honest and reliable!

Thanks from the bottom of my heart to my Bosnian friends that are always there for me, although we can't meet each other that often: *Selma* (*kuma* and *mala*), *Admira* (forever *Konchy*), *Alema* (*Ale*, leader), *Almir* and *Almira* (the sweetest researchers), *Emir* (traveler), *Senada* (organiser), *Azra* (*misi*), *Sabina* (optimist), *Elma* (*Konchy 2*). Special thanks to you *Sanita*, my dear, lifetime friend, for all your support in all these years. I will always remember and appreciate all the moments of joy we had with simple things.

I could never thank enough to my family, especially to my beloved parents *Senija* and *Fikret Kasapovic*, for all their unconditional love, support, encouragement that I can succeed, for putting their trust in me, for being the powerful wind that moves when I felt like I can't go further, and for much more beyond what words can express. I want to thank to my brother *Elvir Kasapovic* and to my sister-in-law *Hena Kasapovic* for their love and support. Special thanks to my two beautiful babies, my niece and nephew *Ajlin* and *Afan*, for making my days joyful even when I just think of you. Thanks to my mother and father-in-law, *Ramiza* and *Hamza Avdibegovic* for their love, support and encouragement. My *Semir*, my lovely husband, the list of things to thank you for is too long for this thesis, but know that I am happy from the bottom of my heart to have spent all these years with you. Thank you for being there for me…

Lastly, the research leading to results obtained in this PhD has received funding from the European Community's Horizon 2020 Programme under Grant Agreement number 636876 (REDMUD – H2020-MSCA-ITN-2014). Project website: etn.redmud.org.

Preface

This PhD thesis entitled ”Recovery of rare earths from bauxite residue leachates by functionalised sorbents” comprises the introduction, objectives, six experimental chapters and conclusions of the work.

Chapter 1 presents general information about rare-earth elements. An overview of bauxite residue reserves, alumina production and bauxite residue deposits is given. Fundamentals of sorption processes, sorption isotherms, kinetics and column chromatography operations are discussed. Specific routes for the synthesis of sorbents used during this PhD research and their characteristics are described. A literature review is given about the sorbents that have been developed for the rare earths recovery in liquid-solid extraction system.

Chapter 2 describes the specific objectives of this PhD thesis.

Chapter 3 discusses the synthesis of supported ionic liquid phases. The most promising supported ionic liquid phase was then investigated for the recovery of rare-earth elements, with special attention to recovery of scandium. The basics of the sorption mechanism of scandium are discussed.

Chapter 4 discusses the application of the supported ionic liquid in column chromatography for the recovery of rare-earth elements. A detailed study of the separation of rare earths from the base elements in bauxite residue leachates is presented. The optimised column chromatography method is then applied for the recovery and separation of rare earths from leachates obtained under non-optimised leaching of bauxite residue.

Chapter 5 focuses on the separation of rare earths and base elements from the leachate obtained by high pressure leaching of the bauxite residue slag, which is generated after smelting reduction of bauxite residue for iron removal.

Chapter 6 discusses the combined processes of selective precipitation of iron and a subsequent column chromatography for the separation of rare earths from a simulated bauxite residue leachate.

Chapter 7 discusses the separation of scandium from bauxite residue leachates using zirconium phosphate. The studies cover the performance of zirconium phosphate batchwise and by column chromatography.

Chapter 8 discusses the synthesis of novel sorbents for mutual separation of rare earths. Detailed characterisation of the synthesised materials is provided.

Chapter 9 concludes the experimental work and gives an outlook for further work.

Lastly, a list of publications and attended conferences are presented.

.

Abstract

Bauxite residue, better known as red mud, is a waste product of the alumina industry, but with many unexploited values. The estimated inventory of bauxite residue in operating and closed alumina refineries reaches the value of several billion of tonnes. Stockpiling of huge amounts of residue can create environmental problems. Bauxite residue comprises iron, aluminium, titanium, sodium and even more interestingly, valuable rare-earth elements (REEs). Although a lot of research has been done on bauxite residue valorisation, to date there are no large-scale applications of bauxite residue yet. The REEs, and scandium in particular, are generally more enriched in residues originating from karst bauxites. Interestingly, bauxites found in the southern region of Europe belong to the group of karst bauxites. Europe currently has no operating REE mine, although these elements are getting an increasing role as materials for the transition to cleaner energy and the production of high-tech devices.

In this PhD thesis sorbents were synthesised and investigated for the recovery of REEs from bauxite residue leachates. The leachates can be prepared by direct leaching of bauxite residue with mineral acids, or as a processing step after recovery of other valuable metals. The leachates typically comprise low concentrations of REEs, whereas base elements like iron or aluminium are concentrated. Liquid-solid extraction is a suitable method for recovery of elements from dilute streams. This process requires sorbents selective for elements of interest. Supported ionic liquid phases (SILPs) and crystalline zirconium-phosphate (α-ZrP) were synthesised, characterised and examined for the REEs recovery and separation from other element present in bauxite residue leachates. Moreover, hybrid materials prepared by grafting of short *n*-alkyl chains (ethyl, *n*-propyl and *n*-butyl) to titanium(IV) phosphate functionalised mesoporous MCM-41 silica were tested for mutual separation of REEs.

Two routes for SILPs preparation were investigated: physical impregnation of ionic liquids on a solid support or chemical immobilisation by covalent bonding of the ionic liquid anion to the solid support. The SILP betainium sulfonyl(trifluoromethanesulfonylimide) poly(styrene-*co*-divinylbenzene), [Hbet-STFSI-PS-DVB], prepared by covalent bonding of ionic liquid to the resin resulted in a sorbent suitable for scandium recovery. The SILP was tested batchwise to

reveal its basic performance for scandium recovery from synthetic acidic solutions, such as selectivity, kinetics, influence of pH and sorption capacity. [Hbet-STFSI-PS-DVB] was packed in a column and detailed studies on REEs separation from base elements were performed under column operating conditions. [Hbet-STFSI-PS-DVB] performance for separation of REEs and the base elements in bauxite residue was evaluated with real acidic bauxite residue leachates. The leachates were obtained by direct leaching of bauxite residue by acids and by high-pressure leaching of a slag generated after smelting reduction of bauxite residue for iron recovery. In both cases, a proof-of-principle for the REEs recovery and separation from base elements by the [Hbet-STFSI-PS-DVB] was confirmed. The performance of [Hbet-STFSI-PS-DVB] was further evaluated in a simplified study with a simulated H_2SO_4 leachate. From this leachate, iron was selectively precipitated and the remaining solution was subsequently tested for the REEs recovery by the [Hbet-STFSI-PS-DVB]. After precipitating iron, scandium uptake from the sulfate media was boosted. Moreover, the purity of scandium obtained after column chromatography was superior to the purity obtained after $ScPO_4$ precipitation.

Furthermore, the selectivity for scandium over iron of several metal(IV) phosphates was investigated from acidic solutions. It was found that α-ZrP exhibits a strong affinity towards scandium, superior to other tested metal(IV) phosphates. Therefore scandium uptake by α-ZrP was investigated in depth. After evaluating batchwise its performance for scandium recovery, α-ZrP was packed in a column. Scandium separation by the α-ZrP column was examined with a leachate obtained by direct leaching of bauxite residue with HCl. A prominent selectivity for scandium over the vast majority of other elements present in bauxite residue was observed.

Due to the small differences between the different REE, they are often recovered from leachates by liquid-liquid or liquid-solid extraction as a group of elements. Still, for certain applications their separation into individual elements is required. The grafted MCM-41 materials were examined for separation of mixtures of REEs. The separation between scandium and lanthanum was found to be remarkable, whereas neodymium and dysprosium separation was comparable to the separation obtained in liquid-liquid extractions with typical extractants such as tributyl phosphate (TBP).

Samenvatting

Bauxietresidu is een afvalproduct van de alumina-industrie met een hoge potentiële, maar onbenutte waarde. Tot op heden werden meer dan enkele miljarden tonnen aan bauxietresidu opgeslagen in stortplaatsen van operationele en gesloten aluminaraffinaderijen. De opslag van deze enorme hoeveelheden residu kan milieuproblemen veroorzaken. Anderzijds bevat bauxietresidu ijzer, aluminium, titanium, natrium en significante concentraties aan zeldzame aarden. Hoewel de valorisatie van bauxietresidu reeds lange tijd intensief wordt onderzocht, zijn er tot op heden nog geen grootschalige toepassingen gecommercialiseerd. In Europa, bijvoorbeeld Griekenland en Hongarije, is voornamelijk karstbauxiet aanwezig in de bodem. Dit type bauxiet bevat typisch hoge concentraties aan zeldzame aarden, met scandium in het bijzonder. Europa heeft momenteel echter geen operationele mijn voor de winning van zeldzame aarden, hoewel deze metalen een steeds grotere rol spelen als bouwsteen voor hoogtechnologische materialen die essentieel zijn voor de overgang naar een schonere maatschappij.

Dit proefschrift handelt over de synthese en toepassing van sorptiematerialen voor de winning van zeldzame aarden uit loogoplossingen van bauxietresidu. Loging van bauxietresidu wordt uitgevoerd door direct contact met minerale zuren, of na een bewerkingstap voor de winning van de andere waardevolle metalen. Loogoplossingen bevatten typisch slechts lage concentraties aan zeldzame aarden en hoge concentraties aan de basiselementen zoals ijzer en aluminium. Vloeistof-vast-extractie is een geschikte methode voor de winning van elementen uit verdunde oplossingen en vereist het gebruik van adsorptiemiddelen die selectief zijn voor de beoogde elementen. Drie vaste materialen werden onderzocht, namelijk 1) ionische vloeistof op een vaste drager, ook wel supported ionic liquid phases of SILP genaamd, en 2) kristallijn zirkoniumfosfaat (α-ZrP) en 3) hybride materialen van mesoporeus MCM-41-silica gefunctionaliseerd met titanium(IV) fosfaat en korte lineaire alkylketens, meer bepaald met een ethyl-, propyl- en n-butylgroep. Alle materialen werden gesynthetiseerd, gekarakteriseerd en toegepast op de winning en scheiding van zeldzame aarden uit loogoplossingen van bauxietresidu.

Voor de bereiding van de SILPs werden twee routes onderzocht: (1) fysische impregnatie van de ionische vloeistoffen op een vaste drager en (2) chemische immobilisatie door covalente binding van het anion van de ionische vloeistof op een vaste drager. De SILP betaïnium sulfonyl(trifluoromethaansulfonylimide) poly(styreen-co-divinylbenzeen) [Hbet-STFSI-PS-DVB], bereid door chemische immobilisatie, was geschikt voor de adsorptie van scandium. De performantie van deze SILP werd onderzocht in batchtesten aan de hand van enkele parameters waaronder selectiviteit, kinetiek, invloed van de pH en sorptiecapaciteit. Vervolgens werd [Hbet-STFSI-PS-DVB] gepakt in een kolom voor gedetailleerde kolomexperimenten voor de scheiding van de zeldzame aarden van de basiselementen uit werkelijke loogplossingen van bauxietresidu. De loogoplossingen van twee processen werden gebruikt, namelijk het direct logen van bauxietresidu met sterke zuren en het logen van een slak gegenereerd na het reductief smelten van bauxietresidu voor de winning van ijzer. Verder werd [Hbet-STFSI-PS-DVB] ook toegepast in de winning van zeldzame aarden uit een loogoplossing bekomen door directe behandeling met zwavelzuur, maar waarbij het ijzer eerst selectief werd neergeslagen. Hierdoor werd de opname van scandium door [Hbet-STFSI-PS-DVB] versterkt. De zuiverheid van scandium was beter in vergelijking met neerslagvorming van scandium als scandiumfosfaat.

Vervolgens werd de selectiviteit van verschillende vaste metaal(IV)fosfaten getest voor opname van scandium en ijzer uit zure oplossingen. Hieruit bleek dat α-ZrP een superieure affiniteit vertoonde voor scandium vergeleken met de andere onderzochte metaal(IV)fosfaten. Daarom werd de winning van scandium met α-ZrP grondiger onderzocht in zowel batchexperimenten als kolomexperimenten, vanuit een loogoplossing bekomen door het direct logen van bauxietresidu met HC1. Scandium vertoonde een duidelijk hogere selectiviteit voor het materiaal vergeleken met de andere elementen aanwezig in de startoplossing.

Omdat de chemische eigenschappen van zeldzame aarden slechts minimaal verschillen, worden ze vaak als een groep elementen gewonnen via vloeistof-vloeistofextractie en vloeistof-vastextratie. Toch is het voor bepaalde toepassingen nodig dat de zeldzame aarden worden gescheiden in de individuele elementen. Daarom werden als laatste deel in dit proefschrift het hybridemateriaal MCM-41 onderzocht voor de scheiding van zeldzame aarden. De scheiding tussen scandium en de lanthaniden was opmerkelijk hoog, terwijl de scheiding van neodymium

en dysprosium vergelijkbaar was met de scheiding met klassieke vloeistof-vloeistofextractie met extractanten zoals tributylfosfaat (TBP).

Abbreviations

[A336] [CA-100]	trialkylmethylammonium *sec*-nonylphenoxy acetate
$[C_8mim][PF_6]$	1-octyl-3-methylimidazolium hexafluorophosphate
$[Hbet][Tf_2N]$	betainium bis(trifluoromethylsulfonyl)imide
BR	bauxite residue
BV	bed volume
c_{eq}	equilibrium concentration
c_{ini}	initial concentration
CMC	critical micelle formation
CRMs	critical raw materials
D2EHPA	di-(2-ethylhexyl)phosphoric acid
DGA	diglycolamide
DOODA	3,6-dioxaoctanedioic acid
DTPA	diethylenetriamine pentaacetic acid
EDASiDGA	silica gel particles modified with diglycol amic acid groups
EDTA	ethylenediaminetetraacetic acid
EGTA	ethyleneglycol tetraacetic acid
EU	European Union
FDGA	furan-2,4-diamido-propyltriethoxysilane
Fmoc-SBA-15	lysine-functionalized mesoporous material
FT-IR	Fourier-transform infrared spectroscopy
HREE	heavy rare earth elements
IL	ionic liquid
ILs	ionic liquids
IUPAC	International Union of Pure and Applied Chemistry
k_1	pseudo-first-order rate constant
k_2	pseudo-second-order rate constant
K_d	distribution coefficient
K_F	Freundlich constant
k_{int}	intra-particle rate constant
K_L	Langmuir constant
LREEs	light rare earth elements
m	mass
MREEs	medium rare earth elements
MRI	magnetic resonance imaging
n	sorption intensity
q	amount of metal ions sorbed onto a sorbent
REE	rare-earth element

REEs	rare-earth elements
REO	rare-earth oxides
SF	separation factor
SILP	supported ionic liquid phase
SILPs	supported ionic liquid phases
SOFCs	solid oxide fuel cells
TBP	tri-*n*-butyl phosphate
TENORM	Technologically Enhanced Naturally-Occuring Radioactive Material
TMOS	tetramethyl orthosilicate
TMS-EDTA	N-[(3-trimethoxysilyl)propyl]-ethylenediaminetriacetic acid
V	volume
α-TiP	α-$Ti(HPO_4)\cdot H_2O$
α-ZrP	α-$Zr(HPO_4)\cdot H_2O$
γ-ZrP	γ-$Zr(PO_4)(H_2PO_4)\cdot 2H_2O$

Table of contents

Chapter 1

Introduction

1.1 RARE-EARTH ELEMENTS

1.1.1 Rare-earth elements properties and occurrence

The rare-earth elements (REEs) include the 15 lanthanide elements (Ln, atomic numbers 57-71) and the elements scandium and yttrium (atomic numbers 21 and 39, respectively).[1] REEs are generally categorised into two groups based on their double-salt solubility (IUPAC classification): the light rare-earth elements (LREEs, elements from lanthanum to europium; and the heavy rare-earth elements (HREEs, elements from gadolinium to lutetium).[2] Yttrium is usually grouped with the HREEs due to their similarity in physical and chemical properties, as well as their co-occurrence in nature. The REEs can be also categorised into three groups based on their extractability with acidic extractants: the REEs from lanthanum to neodymium are called LREEs; from samarium to gadolinium, the medium rare earth elements (MREEs) and from terbium to lutetium including yttrium, the HREEs. There is no agreement among the definition of LREE and HREE. For instance, they are defined differently in Europe and in China. In this PhD thesis the IUPAC classification is followed. Scandium is included in neither the LREEs group nor the HREEs group due to its different physical properties determined by its smaller atomic and ionic radius than those of the other REEs. Nevertheless, in aqueous systems scandium behaves more similar to yttrium and other REEs, than to aluminium or titanium. When crossing the series from lanthanum to lutetium, there is a decrease in both the atomic and the ionic radii, more markedly at the start of the series.[3] This is known as the *lanthanide contraction* and is caused by the shielding of 4f orbitals by the filled 5s and 5p orbitals. The lanthanide contraction is not a unique phenomenon as similar phenomena take place with the actinides and the d-block transition series. However, the lanthanides adopt primarily the (+3) oxidation state in their compounds, and therefore demonstrate the steady and subtle changes in their properties in a way that is not observed in other blocks of elements.[3,4]

The term *rare earth* might suggest that these elements have a low abundancy, but this is not the case. However, it is quite unusual to find rare earths in concentrations high enough to support economic exploitation.[3] The REEs are found naturally in a wide range of minerals, including silicates, carbonates, oxides and phosphates. Lighter lanthanides are more abundant than the heavier ones, and more interestingly the elements with even atomic number are more abundant

than those with odd atomic number (this is the so-called Oddo–Harkins rule). The main REEs sources are bastnasite $LnFCO_3$, monazite (Ln, Th)PO_4 (richer in LREE), xenotime (Y, Ln)PO_4 (richer in later HREE), and ion-adsorption clays (aluminosilicate minerals which are richer in MREEs).[3] Thortveitite $(Sc,Y)_2Si_2O_7$, euxenite $(Ln,Y,Ca,U,Th)(Nb,Ta,Ti)_2O_6$, and gadolinite $(Ln,Ce,Y)_2FeBe_2Si_2O_{10}$, are rare minerals rich in scandium.[5,6] Bauxite and laterite nickel deposits can be considered as REE resources as well.[4,7]

The mining district Bayan Obo in China is the largest REE deposit in the world. Chinese REEs deposits are responsible for more than 90% of the global production. Other productive countries are Australia, Canada, South Africa, Brazil, India, Malaysia, and Sri Lanka.[4] Mountain Pass in the USA was the second largest REE deposit, but the company operating the mine (Molycorp) went bankrupt in 2015. Europe currently has no primary REE mining activity, but it does have several valuable REEs deposits *e.g.* Kvanefjeld and Kringlerne in Greenland, Fen in Norway, Sokli in Finland, and Norra Kärr in Sweden.[8]

1.1.2 Rare earth applications and importance for Europe

One of the first REEs applications go back to 1885, when Austrian scientist Auer von Welsbach reported a patent for a lanthanum-zirconium incandescent mantle. Since then, the REEs have been used in numerous applications: batteries, polishing powders, glass additives, catalysts for the petroleum industry and for air pollution control, contrast agents for magnetic resonance imaging (MRI), magnets *etc.* Currently, permanent magnets are the most important application of rare earths.[1] There are two main types of rare-earth magnets: samarium–cobalt magnets and neodymium–iron–boron magnets, the latter dominating the market. Rare-earth magnets are of high importance for automotive, military, aerospace industry and wind turbines. High-purity REE production is a critical component in commercial defense and other high-value applications. Scandium is presently used in few applications because of its limited availability and its high price. Some applications are aluminum alloys for aerospace and guns due to their light weight and high strength, then products such as phosphors, fluorescent and energy-saving lamps and solid oxide fuel cells (SOFCs). SOFCs are at present the most important application of scandium.[1] In the SOFCs, scandium is applied in scandia-stabilised zirconia, which has a

higher conductivity than yttria-stabilised zirconia, and allows lower operating temperatures. Yttrium is widely used in consumer products, garnets, lasers, phosphors, alloys, medical devices, and superconductors.

The global annual production of REEs is typically expressed in tonnes of REOs. The majority is produced in China, while Europe lacks primary production mines and the major concern is how to secure reliable and unhindered access to certain raw materials.[1] To address this challenge, the European Commission created a list of so-called Critical Raw Materials (CRMs) in 2011, which has already been updated twice, in 2014 and 2017. CRMs are raw materials of a high importance to the economy of the European Union (EU) and of which the supply is associated with a high risk. Based on their high economic importance and lack of primary production, the REEs are assessed as CRMs for the EU (Figure 1.1).[9] There are different solutions that can help to alleviate the shortage of raw materials like REEs. One of the solutions involves the replacement of one REE element by another one in a given application or replacement of REEs by non-REEs. However, this can lead to products with inferior performance. For example, rare-earth magnets can be replaced by ferrite or alnico magnets, but these magnets have much lower energy densities. Another possible solution is recycling and closing the materials loop. With this aim, several European research projects set-up to deal with recycling of end-of-life products or industrial waste materials and set the basis for the development of a European REEs industry (REDMUD, EURARE, DEMETER, EREAN).[10–13] Using industrial metallurgical waste as secondary source for REE exploitation would not only be profitable but would also minimize the environmental impact of the primary metallurgical industry. The work presented here is focused on the bauxite residue as a potential resource for REEs and is part of the MSCA-ETN REDMUD project. The project was initialised with the aim of developing a zero-waste valorisation of bauxite residue. Instead of considering BR as a toxic waste, in the REDMUD project it is considered as a valuable resource of metals and matrix for building materials and a lot of research efforts have been given for the development of innovative processes.[14–18]

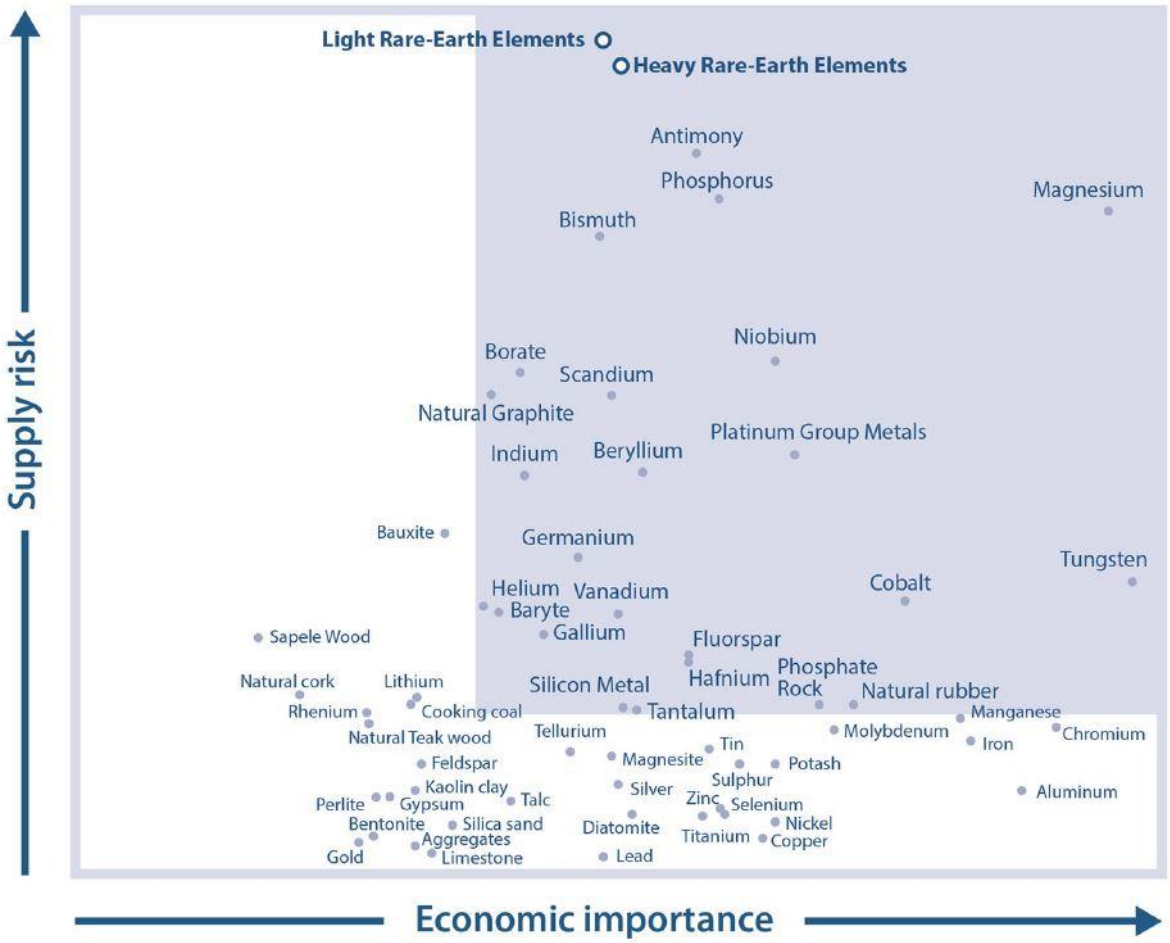

Figure 1.1. Critical Raw Materials (CRMs) according to the 2017 report of the European Commission.[1,9]

1.2 BAUXITE RESIDUE (RED MUD)

1.2.1 Bauxite residue (red mud) generation and properties

Aluminium (Al) is the most abundant metal in the Earth's crust and is used in a variety of applications, such as transportation, building industry, and packaging for food and beverages. Its global production has increased over the years reaching the value of about 63 million tonnes in 2017.[19] Aluminium does not occur naturally as a pure metal, and instead is a constituent of many rocks, minerals and ores. Therefore aluminium has to be extracted and converted to a metal

through a combination of chemical and electrolytic processes. Bauxite is the most important ore of aluminium.[20,21] Bauxites are a typical exogenous type of mineral source () and are consisted of a mixture of aluminium minerals such as gibbsite ($Al(OH)_3$), boehmite (γ-AlO(OH)) and diaspore (α-AlO(OH)), but also minerals like hematite (Fe_2O_3), goethite (FeO(OH)), quartz (SiO_2), rutile/anatase (TiO_2) and kaolinite ($Al_2Si_2O_5(OH)_4$). Different criteria are used to classify bauxites. According to the bauxite mineralogy, they can be classified into: gibbsitic bauxites (consisted mainly of gibbsite), mixed bauxites (consisting of both gibbsite and boehmite) and monohydrate bauxites (consisting mainly of boehmite or diaspore). Based on their geological formation, bauxites can be divided into: lateritic (formed in situ from weathering of aluminous parent rocks in tropical and temperature regions), sedimentary (formed during the mechanical washout of lateritic bauxites), and karst bauxites (transformed bauxite materials washed and accumulated in eroded limestone cavities where further transformation can occur).[7,22] Furthermore, bauxites can be classified according to their known deposits into: Surinamean type (a pseudonym for gibbsitic bauxite), European type (composed mainly of boehmite) and Jamaican type (very fine grained high-iron gibbsitic bauxite containing minor quantities of boehmite). The majority of the refineries in Europe are located in the southern part (Figure 1.2) and they are using karst bauxite (*e.g.* alumina refinery in Greece).

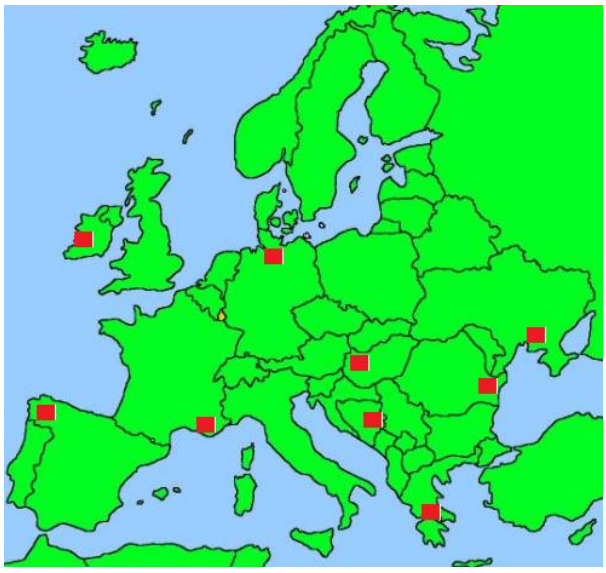

Figure 1.2. Location of bauxite refineries in Europe.

The standard precursor to aluminium metal from its ores is aluminium oxide (Al_2O_3, alumina). The international aluminium industry is based for more than 95% on the use of high-quality bauxites for alumina production by the Bayer process. The Bayer process for low silica and high-grade bauxite involves two steps: 1) the pressure leaching of bauxite with NaOH solution to obtain a sodium aluminate solution ($NaAl(OH)_4$), and 2) precipitation of $Al(OH)_3$ from this solution by seeding with fine crystals of $Al(OH)_3$ (Figure 1.3).[23] The obtained $Al(OH)_3$ is further calcined to form alumina which is used as a feed to produce pure aluminium by the Hall-Héroult electrolytic process. To date, the Bayer process is considered as the simplest and the most economical process for alumina production. There are a few examples of alternative processes including lime sinter process applied to nephelines ($(Na,K)AlSiO_4$), lime-soda sinter process applied to siliceous bauxites which are not suitable for the Bayer process, and the process developed by Orbite Aluminae Inc. which is suitable for variety of aluminous ores.[24–26] In the lime sinter process a mixture of nepheline and lime is sintered and $(Na, K)_2O{\cdot}Al_2O_3$ is formed, which is then leached with an alkali solution. The solution is desilicified and alumina recovery is carried out by carbonation. The lime-soda sinter process is similar to the sinter process. The alumina bearing material is sintered with lime and soda ash. In this process silica and lime combine to Ca_2SiO_4 and alumina and sodium oxide combine to $NaAlO_2$. $NaAlO_2$ is leached from the sinter with hot Na_2CO_3 or NaOH solution. The aluminate solution is then desilicified, and the hydrated alumina is separated by carbonation and seeding. In the Orbite process aluminous ore is leached at high temperature using HCl. All the metals, except of titanium, dissolve as chlorides. The insoluble silica and titanium are removed by filtering. The leachate is processed by HCl gas to precipitate the $AlCl_3{\cdot}6H_2O$, which is then calcined and transformed into alumina.

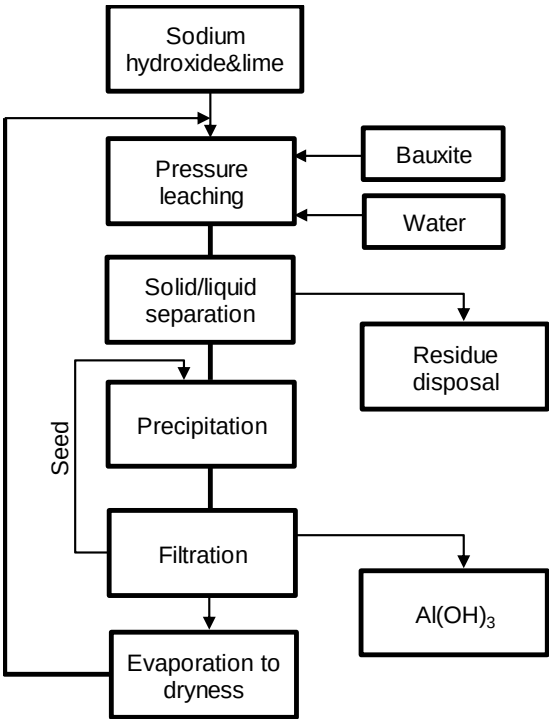

Figure 1.3. Bayer process flow chart.

The residual material arising from the alumina production by the Bayer process is called bauxite residue (BR) or red mud. The residue is generally very alkaline slurry (pH ≈ 12). After drying, the slurry becomes a reddish-brown fine material (particle size typically less than 100 μm) (Figure 1.4).[23] In the past, BR was disposed of in estuaries or sea lagoons nearby refineries. Some storage areas have been sealed to minimise leakage to the underlying ground and ground water. Many refineries use lagoon storage (refineries in Germany, USA, Canada). More recently, the dry disposal ("dry" stacking) has been the preferred method (*e.g.* alumina refineries in Greece and France). The water content is reduced before disposal for instance using a filter press. Nevertheless, BR storage remains a challenge for the alumina industry. When the BR is stored as the alkaline slurry, it creates safety and environmental hazards due to potential exposure to humans and wildlife, and contamination of surface and ground waters. There are several examples of industrial incidents with BR that caused damage to the environment and tragic effects to humans. The BR of the Alunorte alumina refinery in Barcarena (Brazil) overflowed the drainage channels around a deposit, and seep into the Murucupi river. In China two villages in Henan Province were covered in mud after a BR pond dam of the Xiangjiang

Wanji Aluminium refinery collapsed releasing 2 million cubic meters of waste. In Ajka (Hungary) a damn reservoir of the Ajkai Timföldgyár alumina refinery collapsed and around 8 hundred thousand cubic meters of highly alkaline BR was released to the neighboring localities.[27] Many scientific studies have been conducted to assess the key risks and impacts associated with the release of BR. The key risks after the spill were associated with the highly alkaline nature of the slurry and the fine particle size, which could be released into the atmosphere by wind once dry.[27] However, research findings revealed that BR dust, based on its size distribution and composition, can be considered less hazardous to human health than urban particulate matter.[27,28] Still, the high resuspension potential and alkalinity might pose problems such as the irritation of the upper respiratory tract and eyes. Additionally, BR disposal sites occupy vast areas of land which could be used for other purposes, for instance in agriculture. Despite the long-standing recognition of BR as an issue, it has never been satisfactorily resolved. The estimated total inventory of BR in operating and closed sites is around $3 \cdot 10^9$ tonnes.[29] The worldwide annual production of BR is difficult to assess as it fluctuates markedly from year to year, but is estimated at about 140 million tonnes, of which only minor quantities are being productively used.[27,29]

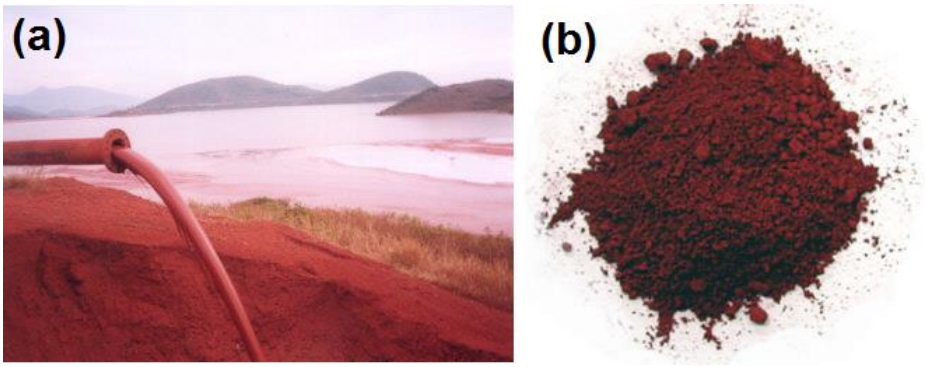

Figure 1.4. Disposal of bauxite residue slurry (a) and appearance of bauxite residue after drying (b).[30]

The key parameters that need to be considered in order to find an application for BR and solve the storage issue, are the chemical composition and the physical characteristics of the material.

The variation in composition is extremely wide (Table 1.1), and it can be even wider for some bauxites. Besides the major components presented in Table 1.1, BR contains significant quantities of other metals, including REEs, uranium, thorium, vanadium, zirconium and gallium.[31] Since the majority of the uranium and thorium from the bauxite ore report to the residue during the Bayer process, BR is considered as a Technologically Enhanced Naturally-Occuring Radioactive Material (TENORM). Numerous research efforts have attempted to utilise BR as a raw material source for iron, alumina or titania production by hydro- and pyrometallurgical methods, or by combining both methods. Iron recovery has been explored by direct magnetic separation from BR to reduce the energy consumption, but iron recovery by this process is low.[31] Therefore, iron recovery from BR has been thoroughly investigated by pyrometallurgical processes, where BR is either reduced in the solid state followed by magnetic separation to recover iron, or reduced by smelting in a blast, electric or low shaft furnace to produce pig iron.[23,31–33] Alumina can be recovered from BR by hydrometallurgy using organic or inorganic acids (H_2SO_4, HNO_3, HCl, citric, oxalic acid), by bio-leaching or by alkali roasting (sintering).[31] Titanium can be recovered from BR slag generated during the pyrometallurgical recovery of iron. Besides, the slag can be digested for recovery of aluminium, and other valuable compounds like REEs.

Table 1.1. Major components of BR and their typical range. Adapted from the reference.[29]

Component	**Typical range (%)**
Sodalite ($3Na_2O{\cdot}3Al_2O_3{\cdot}6SiO_2{\cdot}2NaCl$)	4–40
Al-goethite ($(Fe,Al)_2O_3{\cdot}nH_2O$)	1–55
Haematite (Fe_2O_3)	10–30
Magnetite (Fe_3O_4)	0–8
Silica (SiO_2) crystalline and amorphous	3–20
Calcium aluminate ($3CaO{\cdot}Al_2O_3{\cdot}6H_2O$)	2–20
Boehmite (AlOOH)	0–20
Titanium dioxide (TiO_2) anatase and rutile	2–15
Muscovite ($K_2O{\cdot}3Al_2O_3{\cdot}6SiO_2{\cdot}2H_2O$)	0–15
Calcite ($CaCO_3$)	2–20
Kaolinite ($Al_2O_3{\cdot}2SiO_2{\cdot}2H_2O$)	0–5
Gibbsite ($Al(OH)_3$)	0–5
Perovskite ($CaTiO_3$)	0–12
Cancrinite ($Na_6[Al_6Si_6O_{24}]{\cdot}2CaCO_3$)	0–50

1.2.2 Bauxite residue as a potential source of rare-earth elements

Mineral forms of REE in bauxite deposits are often the same as found in the REE ores (monazite, bastnäsite and xenotime).[34] Abedini *et al.* observed the existence of a pronounced rare-earth tetrad-effect in titanium-rich bauxites, which can be used as a geochemical indicator to evaluate the depositional conditions of bauxites.[7] Generally, REEs are more enriched in karst bauxites than in lateritic (typical values are presented in Table 1.1).[35] As already discussed in the section 1.2.1, the bauxite reserves found in Europe mainly belong to the group of karst bauxites, although there are some exceptions (for instance the alumina refinery in Greece uses about 80% of Greek karst bauxite and 20% of lateritic bauxite from Ghana or Brazil).[36] Based on case studies of lanthanum, scandium, cerium and yttrium distribution in the Bayer process, it can be concluded that the REEs are almost entirely transferred from the bauxite ore to the BR.[36] This results in a concentration of the REE in the BR with a factor of approximately 2 (Table 1.2). The use of BR as a REEs secondary resource might offer a solution for the European REEs supply risk, and in particular for scandium.[37] According to the current price of scandium and its general abundance in BR, scandium represents more than 95% of the economic value of REEs in BR.[38] The annual production capacity of the alumina refinery in Greece exceeds 800,000 tonnes of alumina. At least the same amount of BR is generated in the process, which can therefore act as a potential scandium resource. Shaoquan and Suqing reported in 1996 that minerals in which the scandium content is larger than 0.002% (20 g tonne^{-1}) can generally be considered as important scandium resources.[39] Worldwide BR reserves contain substantial concentrations of scandium. Jamaican, Australian, Chinese, Greek and Hungarian BR each have a scandium content of 55 g tonne^{-1}, 54 g tonne^{-1}, 158 g tonne^{-1}, 127 g tonne^{-1} and 54 g tonne^{-1} respectively.[37,40–43] However, the cost effectiveness of exploiting scandium resources is affected by the fluctuating market demand.[1]

In order to recover scandium and other REEs from BR, direct acid leaching of BR was attempted in several studies.[44,45] However, with this method, large amounts of base elements are dissolved (iron, aluminium, titanium) as well, which creates issues in further recovery process steps such as solvent extraction or ion exchange.[45] Moreover, large volumes of effluents are generated and the volume of solid residue to be stored is not significantly reduced.[25]

Table 1.2. Typical concentrations of REEs and thorium in lateritic bauxite in Ghana and karst bauxite in Greece, and in BR of Greek origin. Adapted from the references.[36,37]

Elements	Lateritic bauxite in Ghana	Karst bauxite in Greece	BR in Greece
	Concentration (g tonne^{-1})		
La	19.1±1.3	57±7	130±1
Ce	34±1	206±8	480±26
Pr	ND[a]	15±1	29±2
Nd	13±1	53±6	107
Sm	2.0±0.2	9.8±1.0	19.4±0.2
Eu	0.8±0.2	2.4±0.9	4.6±1.1
Gd	ND[a]	10.6±0.6	22.0±0.3
Tb	<0.5	2.3±0.5	3.3
Dy	ND[a]	9.8±0.3	20.1±0.1
Ho	ND[a]	2.1±0.1	4.1±0.1
Er	ND[a]	7.2±0.8	13.3±0.3
Tm	ND[a]	<2	<2
Yb	2.5±0.3	7.0±0.4	13.8±0.3
Lu	0.4±0.0	55±9	2.2
Y	ND[a]	51±2	108±2
Nb	ND[a]	55±9	100±1
ΣLn[b]		382.3	854.4
Sc		59.0±3.7	127.9±14.7
ΣREE[c]		492.3	1090.3
Th	22.7±2.3	51±2	105±2

[a] ND – not detected; [b] Sum of lanthanides; [c] Sum of lanthanides, yttrium and scandium.

Recently, an ionic liquid betainium bis(trifluoromethylsulfonyl)imide, [Hbet][Tf_2N], was applied in direct leaching of BR.[46] About 45% of scandium and more than 70% of REEa and were recovered, with less than 5% of iron and 30% of aluminium recovery. In another study, [Hbet][Tf_2N] was applied in recovery of scandium from sulfation-roasted BR leachates.[47] The

scandium concentration in the leachate was increased three times by applying multi-stage leaching, compared to single-stage leaching. Scandium was subsequently purified from the obtained sulfate leachate by solvent extraction with [Hbet][Tf_2N]. One of the major concerns when using ionic liquids is their high price compared to the mineral acids.

Large-scale reuse of BR as a REEs resource could be considered profitable if all its valuable components (iron, aluminium, titanium) would be recovered by economical processes in an integrated processing flow sheet, with minimum or zero waste. To date, zero-waste valorisation of BR is not occurring yet. Recovery of iron by smelting followed by slag leaching could be a good option for recovering iron, aluminium, titanium, and REEs.[33] However, this process requires large amounts of flux due to the high alumina content of the bauxite residue. This issue can be resolved by alkali roasting for alumina removal prior to smelting. The alkali roasting–smelting–leaching process allows recovery of aluminum, iron, titanium, and REEs generated residue could be used in building materials and cementitious binders. One of the most promising processes for BR valorisation was developed by Orbite Aluminae Inc.[48] After base element recovery (aluminium, iron, alkali metals), the REEs were extracted with di-(2-ethylhexyl) phosphoric acid (D2EHPA) and tri-*n*-butyl phosphate (TBP). In this process, the base metals and REEs were recovered in a yield of around 90%. The majority of the acid used is recycled back into the process, making it a near-zero-waste process. Generally, solvent extraction and ion exchange are the most preferred processes for obtaining REEs of high purity after leaching of BR, with or without pyrometallurgical treatment. Wang *et al.* obtained the best extraction of Sc(III) from synthetic H_2SO_4 leachates of Australian BR when using D2EHPA and TBP, over other extractants.[41] In 2002, Ochsenkühn-Petropoulou and co-workers published a pilot-plant study on the recovery of scandium from Greek BR. The process consisted leaching with nitric acid, followed by ion-exchange chromatography with Dowex 50W-X8 to separate the REE from the base metals, and and ending with a solvent extraction step to separate scandium from other REEs using D2EHPA in *n*-hexane.[49] Roosen *et al.* recovered and purified scandium highly selectively from a Greek BR leachate with an innovative biopolymer as sorbent material.[50] Besides biopolymers sorbents, also titanium phosphate has been applied as a sorbent material to recover scandium from a simulated BR leachate.[16] The selectivity for scandium over iron was improved by reducing iron from its trivalent to the divalent state by sodium sulfite.

Although a lot of research has been done in this field, until recently BR has not been used industrially as a resource for REEs or other valuable metals. In 2016 a Russian company RUSAL made a successful pilot unit for scandium concentrate recovery from BR by carbonisation technology.[51] Scandium concentrate is processed into scandium oxide (Sc_2O_3). If the unit achieves a full-scale production, the company plans to utilise Sc_2O_3 in the production of aluminium-scandium alloys.

1.3 SORPTION STUDIES AND SORBENTS FOR THE RECOVERY AND SEPARATION OF RARE-EARTH ELEMENTS

Liquid-solid extraction is the process of transferring a substance from a liquid to an appropriate solid phase. It has been receiving growing attention in various industries for several decades. The use of liquid-solid extraction allows either all compounds to be removed from a solution or particular compounds to be selectively separated. Usually it is a preferred technology over liquid-liquid extraction for recovery of compounds from dilute solutions. *Sorption* is a general term that is used to describe the retention of a substance (*sorbate*) on or in a solid (*sorbent*).[52] Adsorption and ion exchange are specific cases of sorption. *Adsorption* may be described as an enrichment of compounds, for instance from fluids on a surface of the solid state material.[53] The solid surface may be regarded as a site with certain electric and sterical properties characteristic for the solid (*adsorbent*) matrix structure, which induce energetically heterogeneous energy levels based on the degree of interaction with the fluid phase (*adsorptive*). Adsorption may be reversible or irreversible process. *Ion exchange* phenomena exhibit numerous similarities with adsorption processes, but there are also some differences. Ion exchange process refers to a removal of dissolved ions by exchange materials via electrostatic interactions.[54] Ion-exchange is a reversible and stoichiometric process. A strict differentiation between adsorption and ion exchange is sometimes impossible, for instance with exchange and adsorption resins (polymeric adsorbents with large internal surface areas).[53] Besides, a *chelation exchange* can be considered as a different type of sorption mechanism, where generally a coordination bond is formed during

the exchange process between the metal ion and the functional group on the surface of the sorbent.[55]

The following sections provide the basic fundamentals of the sorption process that were used during this PhD study for the recovery of REE, including sorption isotherms, reaction kinetics, materials and operating modes.

1.3.1 Sorption studies

1.3.1.1 Batch sorption experiments

Batch sorption experiments are used to investigate the performance of sorbents for metal uptake. Typically, batch sorption experiments are performed by agitating a fixed amount of sorbent in a defined volume of solution, containing the studied metal ions. After reaching the equilibrium conditions, the sorbent is removed from the solution, for example, by filtration or centrifugation, after which the sorbent can be reused or disposed of. The metal ion concentration is determined from the equilibrated solution.

The amount q of the metal ions adsorbed onto the sorbent (mmol g^{-1} of dry adsorbent) is calculated by *Eq. 1.1*.

$$q = \frac{(c_{ini} - c_{eq}) \cdot V}{m} \qquad (Eq.\ 1.1)$$

The initial metal ion concentration in the solution (mmol L^{-1}) is c_{ini}, the equilibrium concentration of metal ions in the solution (mmol L^{-1}) is c_{eq}, V is the volume of the solution (L) and m is the mass of a dry sorbent (g).

The amount of metal ions desorbed with a suitable agent can be calculated with *Eq. 1.2*.

$$Desorption\ (\%) = \frac{c_1}{c}.100 \qquad (Eq.\ 1.2)$$

c_1 is the concentration of metal ions (mmol L^{-1}) in the solution after desorption at equilibrium. c (mmol L^{-1}) is calculated as follows:

$$c = \frac{(c_{ini} - c_{eq}).V}{V_{ac}} \qquad (Eq.\ 1.3)$$

where V_{ac} (L) is the volume of acid used for desorption.

The metal uptake can also be expressed by the *distribution coefficient* (K_d) (*Eq. 1.4*).

$$K_d = \frac{q}{c_{eq}} \qquad (Eq.\ 1.4)$$

K_d (L g^{-1}) is the ratio of the sorbed amount of metal ions by the sorbent (q) divided by metal ions concentration in solution at equilibrium (c_{eq}).

The separation between two metal ions A and B is quantified by the separation factor ($SF_{A/B}$). It is defined as the ratio of the distribution coefficient of two metals (*Eq. 1.5*).

$$SF_{A/B} = \frac{K_{dA}}{K_{dB}} \ (K_{dA} \geq K_{dB}) \qquad (Eq.\ 1.5)$$

The most common and simplest models to describe the sorption of metal ions are empirical Langmuir and Freundlich models.[56,57] The sorption mechanisms are investigated by varying the initial concentration of metal ions and the equilibrium data are then fitted to linearized Langmuir and Freundlich equations (*Eq. 1.6* and *Eq. 1.7*, respectively).

The linearised Langmuir equation is described as follows:

$$\frac{c_{eq}}{q} = \frac{1}{K_L \cdot q_m} + \frac{c_{eq}}{q_m} \qquad (Eq.\ 1.6)$$

c_{eq} is the concentration of metal ions at equilibrium (mmol L^{-1}), q is the amount of metal ions adsorbed by dry sorbent (mmol g^{-1}), K_L is the Langmuir constant (L $mmol^{-1}$), q_m is the maximum adsorption capacity (mmol g^{-1}). The Lanqmuir model is based on the assumption that the sorption occurs at a monolayer on the surface of a sorbent which has a finite amount of sorption sites.

The linearised Freundlich equation is described by following equation:

$$\log\ q = \log K_F + \frac{1}{n} \log\ c_{eq} \qquad (Eq.\ 1.7)$$

K_F is the Freundlich isotherm constant and n is the adsorption intensity. A plot of log q versus log c_{eq} represents the Freundlich adsorption isotherm at room temperature. The Freundlich model is used to describe a multilayer sorption. This empirical model further suggests that the binding sites on the surface of sorbent are not equivalent.

In order to examine the rate-controlling step for sorption, the widely used pseudo-first-order, pseudo-second-order and intra-particle diffusion kinetic models can be applied (*Eq. 1.8*, *Eq. 1.9* and *Eq. 1.10*, respectively).[56,58]

The linearised pseudo-first-order kinetic model is described as follows:

$$\log\ (q_m - q_t) = \log q - \frac{k_1}{2.303} \cdot t \qquad (Eq.\ 1.8)$$

q_m and q_t are the amounts of metal ions per amount of sorbent (mmol g^{-1}) at equilibrium and at time t, respectively, k_1 is the pseudo-first-order rate constant (min^{-1}).

The linearised pseudo-second-order kinetic model is described as follows:

$$\frac{t}{q_t} = \frac{1}{k_2 \cdot q_t^2} + \frac{t}{q_m} \qquad (Eq.\ 1.9)$$

k_2 is the pseudo-second-order rate constant (g $mmol^{-1}$ min^{-1}). The pseudo-second-order kinetic model suggests that the reaction rate is controlled by a chemisorption process.

Finally, the intra-particle diffusion model is described by following equation:

$$q_t = k_{int} \cdot t^{\frac{1}{2}} + C \qquad (Eq.\ 1.10)$$

k_{int} (mmol g^{-1} $h^{1/2}$) is the intra-particle rate constant and C is a constant (mmol g^{-1}) which is proportional to the extent of the boundary layer thickness. According to this model intra-particle diffusion is the only rate controlling step.

1.3.1.2 Column chromatography

Chromatography is a physical method of separation in which the components to be separated are distributed between two phases, one of which is stationary (stationary phase) while the other (the mobile phase) moves in a definite direction. If the separation is carried out on a column, the term *column chromatography* is used. When applied to a metal recovery, it involves a stationary phase (*sorbent*) through which the mixture of metal ions flows, and a mobile phase (*eluent*), which is a solution that carries the mixture of metal ions that need to be separated.[53] Column chromatography separation involves several steps (Figure 1.5):

1. Sorbent conditioning – The pH and ionic strength of the column are equilibrated to starting conditions to allow binding of the desired metal ions;
2. Loading stage – The sample is applied on the column and metal ions with affinity for the sorbent bind to it. In the case of ion exchange, metal ions displace the original counter-ions. The sample can be loaded until the metal concentration in the solution leaving the column exceeds a certain threshold level;
3. Wash stage – Unbound metal ions are washed out with the solution that was used in the conditioning step;
4. Elution stage – Bound metal ions are sequentially eluted by isocratic elution (when the eluent composition is kept constant) or gradient elution (when the eluent composition is varied during the separation);
5. Regeneration stage – A suitable column regeneration solution is applied to restore the initial conditions of the column before the next separation.

The recovery of metal ions during the loading stage can be calculated from *Eq. 1.11*.

$$Recovery\ (\%) = \frac{m - m_1}{m} \cdot 100 \qquad (Eq.\ 1.11)$$

m and m_1 are the metal amounts (mg) in the feed before column loading and in the subsequently collected fraction, respectively.

Separation by column chromatography is based on the principle of selectivity, where metal ions with a higher affinity for the sorbent bind more strongly than ions with a lower affinity for the

sorbent material. Higher affinity can be based on the differences in physical and chemical properties of the constituents of a mixture, such the charge and ionic radius of the metal ions.

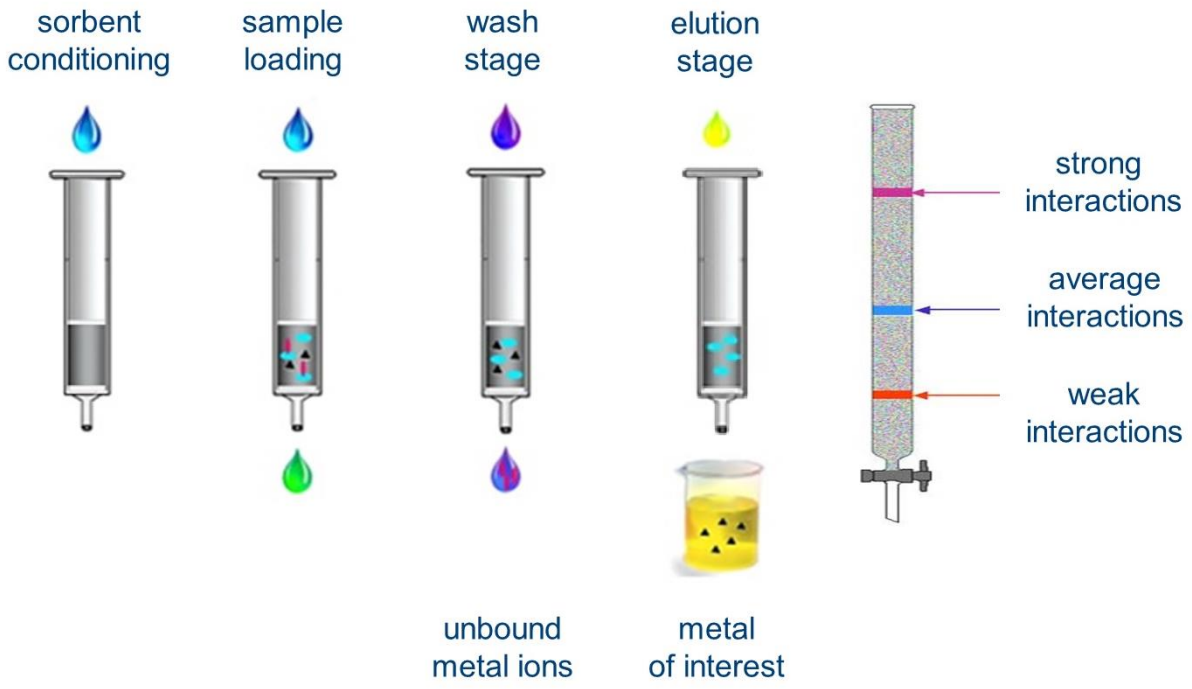

Figure 1.5. Separation of metal ions by the principle of column chromatography.

Due to the difference in the affinity for the sorbent material, metal ions travel through the column at different rates during the elution stage. The metal ions that exhibit the highest affinity for the sorbent will migrate slowly through the column and elute latest. Besides, the separation of metal ions can be affected by several other parameters such as particle size distribution of the sorbent, column length, inner diameter and the packing method and the flow rate at which the separation is being carried out.

By collecting the metal ions in distinct fractions, a full separation of the metal mixture can be achieved. A chromatogram is then constructed from the distinct fractions by plotting the metal concentration as a function of the elution volume, elution time or the bed volume (*BV*, regarded as the total volume of the sorbent together with the void volume in the column).

1.3.2 Sorbents

1.3.2.1 Supported ionic liquid phases (SILPs)

The simplest and widest definition of ionic liquids (ILs) is that ILs are compounds consisting exclusively of ions.[59,60] They can consist of organic or inorganic salts, with a low melting temperature. The most commonly used IL cations are based on imidazolium (*e.g.* 1,3-dialkylimidazolium), pyridinium (*e.g.* *N*-alkylpyridinium), ammonium (*e.g.* tetraalkylammonium) or phosphonium (*e.g.* tetraalkylphosphonium).[59] The most commonly used IL anions are nitrate ($[NO_3]^-$), acetate ($[CH_3COO]^-$), tetrafluoroborate ($[BF_4]^-$), bis(trifluoromethylsulfonyl)imide (bistriflimide, $[Tf_2N]^-$), trifluoromethanesulfonate ($[TfO]^-$), hexafluorophosphate ($[PF_6]^-$) and the halogenides (Cl^-, Br^- and I^-).[61] Besides, specific functional groups can be incorporated into the structure of the cation or anion to design functionalised ILs.[62–65] Changes in the nature of the different substituents in the cationic fragment as well as modifications in the structure of the counteranion provide an essentially infinite series of ILs with modulated properties, and for this reason they are also known as designer solvents. The most important properties of ILs include their negligible vapor pressure, good electrochemical stability and conductivity, broad electrochemical window, low flammability and broad liquidus range.[66–75] However, due to the high degree of intermolecular interactions, the viscosity of ILs is generally higher than that of common organic solvents.[66] Viscosity is an important parameter when scaling-up an ionic liquid process, since a high viscosity slows down mass transfer and complicates pumping of the solvent.

A new class of materials, named *supported ionic liquid phases* (SILPs), was introduced to avoid the disadvantage of the high viscosity of ILs. SILPs include combination of ILs and porous solid supports. Similar variations in the structure as in the case of ILs can be used to tune the characteristic of the SILPs, which may lead to advanced materials with adjustable chemical and physical properties. Immobilization of ILs on porous materials can be achieved simply by physical immobilisation (physisorption) or by chemical binding to the support (chemisorption) (Figure 1.6).[2,76–78] The SILPs prepared by physical immobilisation are composed of IL spread on the surface of a solid material in the form of a thin layer or in the cavities of a solid material. The forces between the ILs and the support are weak Van der Waals forces. Thicknesses of the IL

layer between 50 and 500 mm can be obtained.[79] Ideally, all advantages of the ILs retain in SILPs thus circumventing the issue of the high viscosity. The SILP concept may result in a very efficient use of the IL, because of the relatively short diffusion distances for the reactants compared to those in conventional IL two-phase systems.[80]

Several methodologies can be followed for physical immobilisation of ILs onto a solid support (Figure 1.6):[81]

a) Impregnation – A solid support is placed in contact with a solution of IL in an appropriate solvent (*e.g.* acetone, ethanol), the mixture is shaken for a period of time and then the solvent can be removed either by evaporation (*dry method*) or by filtration (*wet method*). Alternatively, a modifier (*e.g.* dibutylpolypropylene glycol) which promotes water penetration into the support can be added to the IL solution (*modifier addition method*). The solvent is then evaporated as in the dry method. Moreover, the IL can be impregnated onto a solid support by pumping its solution through a column packed with the support (*column method*). During the impregnation the IL gradually fills the pore space from the smallest pores up to macropores.[82]

b) Sol-gel method – The basic idea that is developed in the sol-gel method is to confine the IL within an oxide matrix (*e.g.* silica) through a one-step process.[83] A gel is defined as a solid interconnected network spreading throughout a liquid phase. In classical sol-gel processing, the liquid phase is removed, the targeted material being the porous solid obtained after drying. However, since the ILs have low vapor pressure it permits to use the gel with the IL confined in the structure. The resulting materials are often called ionogels. In the systems with silica-based ionogels, gelation is understood to occur through the initial formation of colloidal particles containing bulk Si–O–Si bonds, followed by particle aggregation and hence the formation of an extended silica matrix.[84] As it grows, this solid network becomes three-dimensionally interpenetrated by the IL phase. One possible approach to ionogels is the synthesis of compounds by the conventional hydrolysis–condensation reaction of a silica compound such as tetramethyl orthosilicate (TMOS) in a water–methanol solution and subsequent swelling of the silica material in the selected IL. Another approach is a non-aqueous sol–gel route, which uses TMOS as precursor for silica particles and a catalytic agent *e.g.* formic acid as, to prepare

compounds with different IL content.[85,86] The final structure and properties of the ionogel are highly affected by variations in the experimental conditions.

c) Encapsulation – This method is used as an additional step to one of the previously mentioned methods, when the prepared SILP is additionally coated with a polymer layer (*e.g.* polysulphone) in order to stabilise the IL layer on the support.[87]

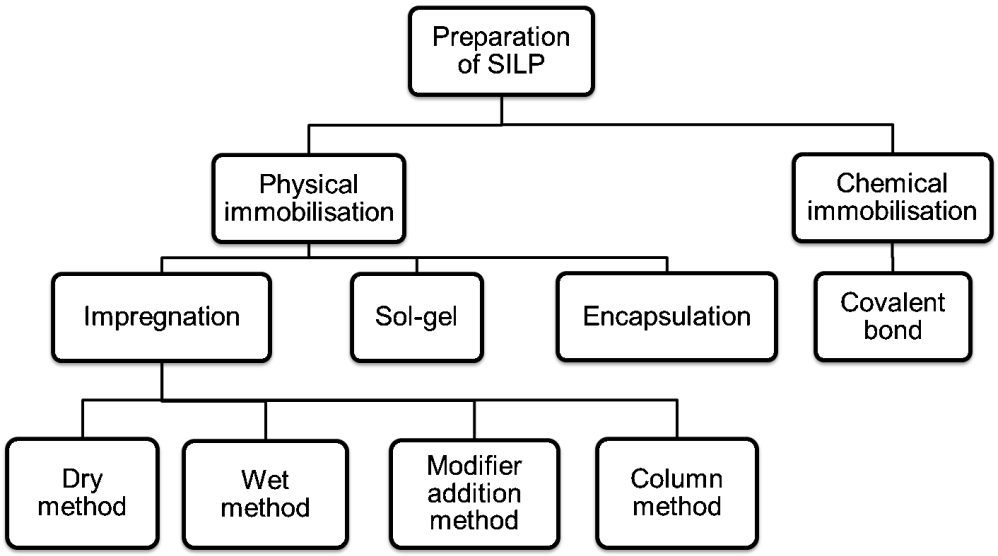

Figure 1.6. Frequent preparation methods of supported ionic liquid phases (SILPs).

An example of the appearance and surface morphology of a SILP prepared by the dry impregnation of an IL on a resin, as examined by optical microscopy, is represented in Figure 1.7. The surface coating of the resin can be observed.

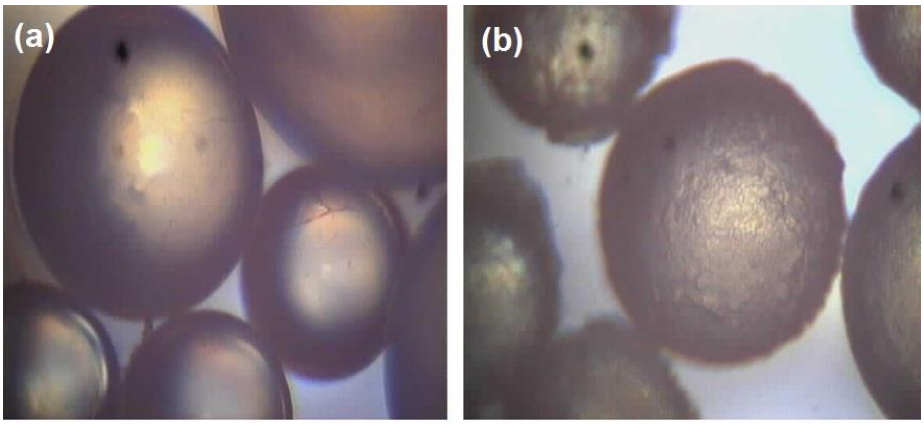

Figure 1.7. An example of a surface morphology of a resin (a) and a SILP prepared by the dry impregnation method (b).[78]

It is known that ILs may tend to dissolve in water quite well, which could lead to significant losses to the reaction media and, finally, to the environment.[68] Dissolution of the IL component of the SILP may further cause the loss in performance of the material. Salting-out is a potential technique that can solve the dissolution issue of ILs, both in liquid-liquid and liquid-solid extractions, but this technique is still limited to fundamental studies.[68,88] The most appropriate way to prevent losses of IL is by preparing SILPs with covalently linked ILs via cation or anion (chemical immobilisation).[89] In this type of SILPs, ILs are present as a monolayer on a surface of a solid support, although multilayers can also be obtained.[90] A downside of the SILPs prepared by the chemical method is that most of the properties of bulk ILs are lost.

The most frequently used solid supports for immobilisation of ILs are polymer resins and silica-based materials. The polymer resins used for immobilisation are usually polystyrene-based resins. Polymer resins exhibit a good thermal and chemical stability, a high mechanical robustness and an easy availability at a relatively low price. Also silica based materials have the advantage of a porous structure, a large surface area, a good mechanical strength and a high thermal stability. Various functional groups can easily be immobilised on silica-based materials by functionalisation of silanol groups. However, silica-based materials are only stable at moderate acidic conditions and degrade under basic conditions. Silica-based materials, especially mesoporous silica with a low density and a small particle size are more difficult to separate from

the aqueous phase than resins, and this might pose difficulties for continuous industrial separation process. Other supports employed for immobilisation may include zeolites, alumina, carbon nanotubes, magnetic nanoparticles, cellulose and membranes.[91–101]

1.3.2.2 Metal(IV) phosphates

Metal(IV) phosphates are intensively investigated as ion exchangers. They are generally prepared in both amorphous and crystalline form. Amorphous metal(IV) acid phosphates were intensively investigated in the years 1955-1965, especially for their potential use as inorganic ion exchangers in processes occurring at high temperatures or in the presence of ionizing radiation.[102,103] In 1964, Clearfield and Stynes discovered the first crystalline member of this class, namely the layered zirconium hydrogenphosphate monohydrate (α-$Zr(HPO_4)_2 \cdot H_2O$ or α-ZrP). α-ZrP is a layered compound in which zirconium atoms lie slightly above and below the plane and are connected by phosphate groups (Figure 1.8a).[102,104–106] Three oxygen atoms of each phosphate group are bonded to three different zirconium atoms. The last oxygen atom of the phosphate is protonated and points either into the interlayer of the material or is on the surface. The resulting structure contains octahedral ZrO_6 cross-linked by tetrahedral PO_4 groups, forming a layer. The interlayer region houses a single water molecule per unit formula, which is stabilised by hydrogen bonding with the interlayer phosphate groups. The interlayer distance is 7.56 Å, and the thickness of the layer, calculated as the shortest distance between the center of the oxygen atoms of the P-OH groups present on the opposite sides of one layer, is 6.3 Å. The distance between adjacent P-OH groups on one side of the layer is 5.3 Å and the "free area" around each phosphate group is 24.0 $Å^2$. The structure of other α-layered M(IV) phosphates is essentially the same, but the nature of the central metal atom causes significant differences in the interlayer distance, in the distance between phosphate groups, and in the "free area" available to guest species.

Further development in layered metal(IV) phosphates was made after a discovery of another layered structure of zirconium phosphate, γ-$Zr(PO_4)(H_2PO_4) \cdot 2H_2O$ or γ-ZrP (Figure 1.8b).

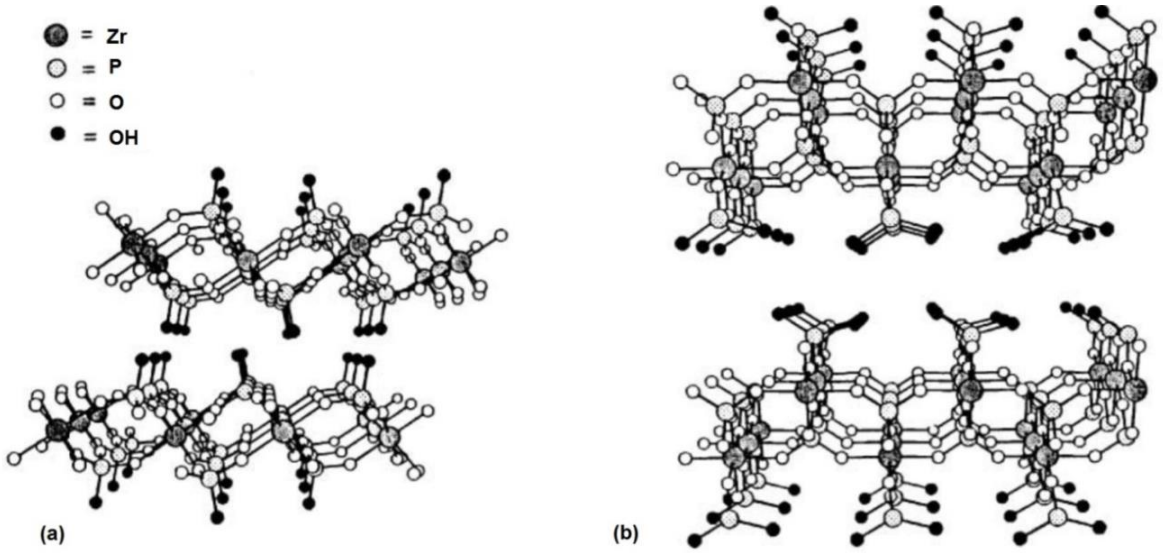

Figure 1.8. Crystal structure representations of: (a) α-zirconium phosphate, $Zr(HPO_4)_2 \cdot H_2O$ (α-ZrP), and (b) of γ-zirconium phosphate, $Zr(PO_4)(H_2PO_4) \cdot 2H_2O$ (γ-ZrP).[107]

γ-ZrP is constituted of two ideal planes containing the zirconium atoms bonded by tetrahedral PO_4 and H_2PO_4 groups. The PO_4 group shares all four oxygen atoms with four zirconium atoms while the H_2PO_4 shares two oxygen atoms with two different zirconium atoms and points the remaining two OH groups towards the interlayer region. The adjacent layers are linked through hydrogen bonds involving the two water molecules and the $P(OH)_2$ groups. The γ-ZrP has more-rigid layers than the α-compounds and shows a stronger acidic character. The ion exchange in the α-phases takes place by diffusion of the cations from the external parts of the layered crystals towards the bulk with an advancing phase boundary. Thus, the process takes place with a discontinuous phase transition and occurs at constant composition of the solution. At acidic pH values, only a limited number of cations (*e.g.* Li^+, Na^+) are able to exchange the protons of α-ZrP at a high rate. Large monovalent or divalent cations such as Cs^+ or Ba^{2+} or highly hydrated trivalent cations such as Cr^{3+}, replace the protons of α-ZrP at room temperature at very slow rates, due to the high activation energy required for the expansion of the interlayer region. On the other hand, the γ-ZrP shows lower steric hindrance towards diffusion of large cations.

Intercalation in α-ZrP proceeds by three main mechanisms: ion exchange, acid-base reaction, and/or electron transfer.[104] The most common of these are the ion exchange and acid–base

mechanisms. For the ion-exchange process, cations displace the acidic protons of the hydroxy phosphate groups in the interlayer region of α-ZrP, forming a new phase. On the other hand, the intercalation via an acid−base reaction takes place when a Brønsted base is protonated by the acidic protons of the hydroxy phosphate groups, forming an ionic pair between deprotonated phosphate and the protonated base. The largest entrance to the interlayer region of α-ZrP is 2.61 Å. Therefore ions above this size cannot enter the interlayer by direct ion exchange. Further investigation showed that although these ions were not able to enter the interlayer at low pH, they were able to displace exclusively the surface protons of α-ZrP by ion exchange. More recently, it was demonstrated that the ion-exchange chemistry of α-ZrP could be used to deposit metal ions exclusively on the surface of the nanoparticles.[104] The metal ion layer can then be functionalised with phosphonic acids, resulting in surface functionalised α-ZrP. As a new area of focus, the surface functionalisation of the α-ZrP particles can offer new possibilities to materials chemistry for the preparation of tailor made compounds, with a structure and reactivity that can be tuned for specific purposes.[108–112]

Many layered metal(IV) phosphates and phosphonates may be considered as solid acids with ion-exchange properties. The properties of several frequently used members of metal(IV) phosphates are included in Table 1.3.

Table 1.3. Characteristics of layered metal(IV) phosphates. Adapted from the reference.[102]

	Unit cell parameters				Interlayer distance [Å]	Free area [Å^2]	Ion-exchange capacity [mmol H^+ g^{-1}]
	a [Å]	*b* [Å]	*c* [Å]	β [°]			
α-$Zr(HPO_4)\cdot H_2O$	9.060	5.297	15.414	101.71	7.56	24.0	6.64
α-$Ti(HPO_4)\cdot H_2O$	8.630	5.006	16.189	110.2	7.56	21.6	7.76
α-$Hf(HPO_4)\cdot H_2O$	9.014	5.257	15.477	101.64	7.60	23.7	5.15
γ-$Zr(PO_4)(H_2PO_4)\cdot 2H_2O$	5.386	6.363	24.806	98.70	12.2	17.8	6.27
γ-$Ti(PO_4)(H_2PO_4)\cdot 2H_2O$	5.181	6.347	11.881	102.59	11.60	16.5	7.25

1.3.2.3 Mesoporous silica materials

Silicate mesoporous materials have received widespread interest in potential applications as supports for catalysis, and novel functional materials for separation of compounds. In 1992, researchers at American Mobil Corporation discovered the family of mesoporous silicate molecular sieves with exceptionally large uniform pore structures and a high surface area (> 700 m^2 g^{-1}). The system with a hexagonal array of pores, known as *Mobile Crystalline Material 41* (MCM-41), is the most important member of the family. MCM-41 possesses surface areas larger than 1000 m^2 g^{-1}, and well-defined pore sizes of about 2.0 to 10.0 nm, therefore surpassing the pore-size constraint (< 2.0 nm) of microporous zeolites (Figure 1.9). Besides hexagonal MCM-41 silica, other members of this family have been identified, like lamellar (MCM-50) and cubic (MCM-48) phases (Figure 1.10). MCM-41 is generally extensively investigated because the other members in this family are either thermally unstable or difficult to obtain. MCM-41 shows relatively poor hydrothermal stability so elements like aluminium were introduced in the structure of these mesoporous materials to increase the hydrothermal stability.[113]

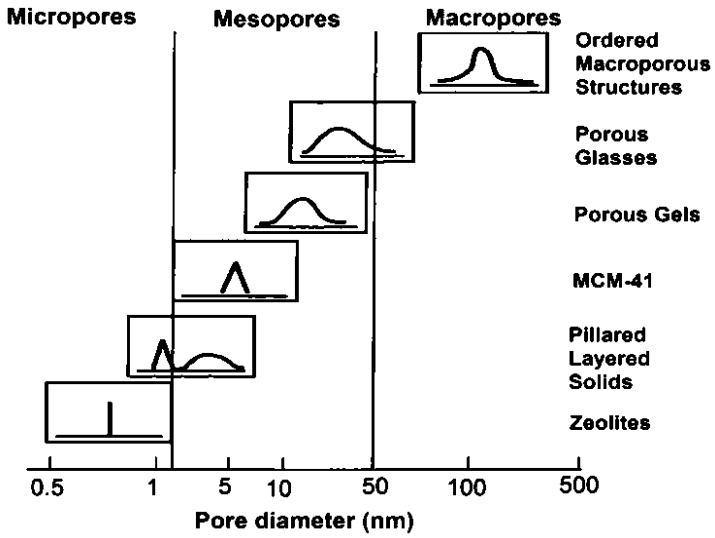

Figure 1.9. Schematic illustration of the pore size distribution of some porous materials. Adapted from the reference.[114]

Generally, mesoporous silica synthesis involves the addition of a silicate source, *e.g.* tetraethyl orthosilicate, TEOS, to an aqueous surfactant solution (Figure 1.11).[115,116] Hydrolysis and condensation leads to a silica framework which builds around the surfactant micelles. The surfactant is removed by solvent extraction or by calcination in air. The latter is preferred as it results in a more regular pore size.[117,118] Other surfactant removal processes include supercritical fluid extraction and ozone treatment.[119,120]

The structure, composition, and pore size of these materials can be tailored during synthesis, by variation of the reactant stoichiometry, the nature of the surfactant molecule, the reaction conditions, or by post-synthesis functionalization techniques.[114] They can be synthesised using anionic, cationic or neutral surfactants. Instead of using small organic molecules as templating compounds, as in the case of zeolites, long chain surfactant molecules are employed *e.g.* hexadecyltrimethylammonium bromide (CTAB). At low concentrations, the surfactants exist as monomolecules.[114] With increasing concentration, surfactant molecules combine together to form micelles. The *critical micelle concentration* (CMC) is defined as the concentration of surfactants above which micelles form. In the micelle core, which essentially consists of liquid hydrocarbon, there is greater freedom for movement and so the entropy associated with the hydrocarbon tails increases. As the concentration process continues, hexagonal close packed arrays appear, producing the hexagonal phases. The next step in the process is the coalescence of the adjacent, mutually parallel cylinders to produce the lamellar phase

Figure 1.10. Schematic representation of the MCM materials: MCM-50 (layered), MCM-41 (hexagonal) and MCM-48 (Cubic).[114]

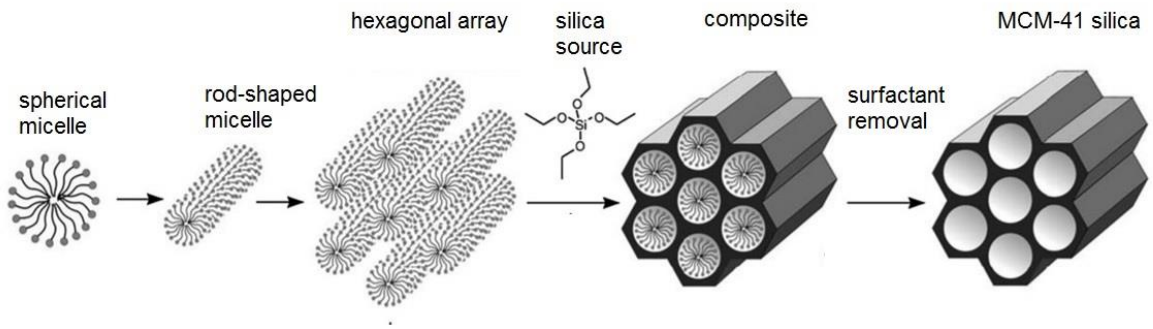

Figure 1.11. Schematic illustration of MCM-41 preparation. Adapted from the reference.[116]

The formation of a particular phase in a surfactant aqueous solution at a given concentration depends not only on the concentrations but also on the nature of the surfactant itself, such as the length of the hydrophobic carbon chain and counter ion in the case of ionic surfactants. Moreover, it depends on the experimental parameters, such as pH, temperature, ionic strength and solvent. Generally, the CMC decreases with the increase of the surfactant chain length due to the increase in the magnitude of the negative free energy of micellisation. Increasing the ionic strength in the solution and increasing the valence of the counter ions also lead to a reduction in the CMC. On the other hand, the CMC increases with increasing counter ion radius, pH, and temperature.

Besides MCM mesoporous silica, other types of mesoporous silica materials are being researched in the same field of applications as the MCM group, namely Santa Barbara Amorphous n^{o} 15 (SBA-15) and highly ordered cubic Korea Advanced Institute of Science and Technology–6 (KIT-6).[114,115,121] SBA-15 exhibits a larger pore size (from 4.6 to 30 nm) and better thermal, mechanical and chemical resistance properties than MCM silica. KIT-6 silica is an attractive material with a three dimensional pore structure and large pore size, with growing research attention.[122]

Mesoporous silica materials contain residual silanol groups, that can be further functionalised in order to modify their surface properties by grafting of different organic groups.[118,123,124] In the grafting method, the surface silanol groups serve as anchoring groups where both free (≡Si–OH) and geminal silanols (=Si(OH)$_2$) are responsible for functionalization, while hydrogen-bonded

silanol groups are less accessible. Another way to modify mesoporous silica is by a direct modification through a sol-gel process based on the co-condensation of silica precursors and one or more organoalkoxysilane precursors with Si–C bonds.[125] Siloxane precursors act as the main framework of the mesoporous materials while the organoalkoxysilane precursors contribute to the building of the framework and serve as functional groups on the surface. Modified mesoporous materials are of great interest because of their potential applications in various areas such as catalysis, adsorption, chromatography, nanotechnology, metal ion extraction, and imprinting for molecular recognition.

1.3.3 Developments in recovery and separation of rare-earth elements by sorbents

The SILPs were first introduced in catalysis, since ILs are also applied as catalysts or as a medium for immobilisation and recovery of catalytic species. As the research in the field of REE recovery by ILs expanded, the use of SILPs in liquid-solid extraction of metal ions was considered. Sun *et al.* studied the separation of REEs by the task-specific IL trialkylmethylammonium *sec*-nonylphenoxy acetate, [A336] [CA-100], impregnated on XAD-7 resin.[126] By varying the pH of the solution, the separation factors of scandium to yttrium, europium and cerium reached the values of 16.49, 62.73, and 87.12, respectively. However, a good separation between scandium and other REEs was only achieved when the pH was higher than 5, whereas there was no selectivity from strongly acidic solution. In another study, Sun *et al.* tested Cyanex 923 dissolved in the IL 1-octyl-3-methylimidazolium hexafluorophosphate, $[C_8mim][PF_6]$, and impregnated on Amberlite XAD-7 resin, for REEs separation.[127] The resulting SILP could effectively separate yttrium from scandium, holmium, erbium and ytterbium by adding ethylenediaminetetraacetic acid (EDTA) as a complexing agent.

Most SILPs that are used for REEs separation and prepared by chemical immobilisation comprise imidazolium-based ILs. Zhu and Chen prepared a SILP by anchoring *N*-methylimidazole to the Merrifield resin to form *N*-methylimidazolium functionalised SILP in chloride [Cl^-] form.[128] The SILP was further modified with $NaNO_3$ to prepare the SILP in nitrate [NO_3^-] form. The SILP was then tested for sorption of cerium from nitric acid media. It was

found that nitric acid in the concentration range from 2 to 6 mol L^{-1} did not significantly affect the uptake of cerium. The authors concluded that the imidazolium-based SILP showed selectivity for cerium over lanthanum, gadolinium and ytterbium. In another study focusing on scandium separation, Zhu *et al.* tested a similar immidazolium-based SILP but in hexafluorophosphate [PF_6^-] form and impregnated with Cyanex 923.[129] The SILP was found to be effective for scandium recovery by a neutral extraction mechanism at a pH of 4.3. Scandium was selectively separated from thulium, ytterbium and lutetium, with separation factors of 4.50, 5.36, 4.46, respectively. The SILP was additionally investigated for scandium uptake when Cyanex 923 was dissolved in [C_8mim][PF_6]. In this case, scandium uptake followed a cation exchange mechanism. Turanov *et al.* prepared a novel bifunctional IL, trioctylmethylammonium 1-phenyl-3-methyl-4-benzoylpyrazol-5-onate.[130] The IL was used as a silica sol-gel material for recovery and separation of REEs from HNO_3 solutions. Scandium sorption from aqueous solutions was much better than sorption of the other REEs, and their separation was achieved by a simple pH adjustment of the aqueous phase.

Ma *et al.* synthesised a novel lysine-functionalised mesoporous material (Fmoc-SBA-15) using a two-step post-grafting method to obtain an adsorbent that can selectively adsorb scandium from aqueous solution.[131] The material possessed high selectivity for scandium from a mixed REE solution at pH = 5. The recent advances in the field of mesoporous silicas designed for liquid–solid extraction of REEs and actinides are summarised in a review by Florek, Kleitz and co-workers.[132] Negrea *et al.* used cellulose with thiourea as an efficient and environmentally friendly material to recover europium and neodymium from aqueous solutions.[133] An overview of the work on the removal of REEs from aqueous solution by different low cost adsorbents is summarised in the review by Anastopoulos and co-workers.[134]

Other hybrid materials and ion-exchange resins were investigated for the separation between the REEs and other metal ions. Among different sorbents that are selective for REEs, the diglycolamide (DGA)-based materials have attracted increasing attention as one of the most effective sorbents (Figure 1.12). Ogata and co-workers synthesised silica gel particles modified with diglycolamic acid groups (EDASiDGA), which exhibited higher sorption for the HREE than for the LREE.[135] Moreover, the sorbent was packed in a column and evaluated for the uptake of REEs at pH 1.0 from a simulated solution containing low concentrations of REEs and

high concentrations of base metal ions (mainly aluminium, calcium and iron).[136] The sorbent showed a remarkable selectivity for the REEs, and especially for the HREEs. The REEs were desorbed by 1 mol L^{-1} H_2SO_4. The molar ratios of the REEs to base metals in the solution after desorption were three to four orders of magnitude higher than the initial molar ratios. To clarify the sorption mechanism, several derivatives of EDASiDGA were investigated for the sorption of REE ions.[137] It was concluded that adsorbents with diglycolamic acid ligands adsorb REE ions via the three oxygen atoms of the ether, amide, and carboxylic acid group of the diglycolamic acid ligands, and that this tridentate chelation confers high selectivity for REE ions. Van Nguyen, Nakamura and co-workers used the same resin with diglycolamic acid for separation of scandium from a model solution containing scandium, cerium, lanthanum, and aluminum.[138] The highest selectivity for scandium over the other REEs and aluminium was obtained at pH = 1. The selectivity for scandium was confirmed batchwise and using column chromatography. The authors explained the selectivity for scandium based on the pore size of the resin and the ionic radius of scandium. The average radius of the resin pores was measured by the Brunauer–Emmett–Teller (BET) method and found to be 0.89 Å. Scandium is known to be the smallest ion among the REEs ions and it can easily penetrate the resin (Table 1.4).[139] However, the selectivity for scandium over aluminium cannot be explained by the pore size, but probably by the lower hydration enthalpy of scandium over aluminium (Table 1.4).[140]

Table 1.4. Ionic radii (coordination number 6) and hydration enthalpies of Al(III) and several REEs.

Metal ion	Ionic radius (Å)	Hydration enthalpy $-\Delta H_{hyd}$ (kJ mol^{-1})
Al(III)	0.535	4665
Sc(III)	0.745	3897
La(III)	1.032	3296
Ce(III)	1.010	3337

Roosen *et al.* synthesised chitosan–silica particles functionalised with the chelating ligands diethylenetriamine pentaacetic acid (DTPA) and ethyleneglycol tetraacetic acid (EGTA) and tested these for scandium recovery from bauxite residue leachates.[50] It was observed that only EGTA-functionalised chitosan–silica appeared to be highly selective for scandium over iron. A remarkable separation between scandium and other base elements in bauxite residue leachate was achieved by column chromatography with a HNO_3 eluting solution at pH 0.50. In another study by Roosen *et al.*, DTPA-chitosan–silica showed a higher selectivity than EDTA-chitosan-silica towards adsorption of dysprosium in comparison with neodymium.[141] Subsequently, neodymium and dysprosium were well separated by DTPA-chitosan-silica column chromatography. Florek, Kleitz and co-workers synthesised a series of diglycolamide (DGA)-based sorbents by grafting the ligands on the high-surface area KIT-6 silica and tested these for REEs uptake.[142] The 3,6-dioxaoctanedioic acid (DOODA) grafted on mesoporous silica (KIT-6) showed preference for the uptake of smaller lanthanides (HREE), over aluminium and iron. The sorbent with furan-2,4-diamido-propyltriethoxysilane (FDGA) exhibited high distribution coefficient values for extracting scandium from a mixture of REEs. The selectivity was achieved with solutions at pH = 4. The authors concluded that more selective sorption of REEs could be achieved when tuning the *bite angle* of chelating ligands by changing the ligand structure. Moreover, Giret *et al.* demonstrated the potential of using the unmodified mesoporous KIT-6 silica for the selective separation of scandium from other REEs. In this case, a 100 times higher concentration of scandium was achieved.[143] Still, the unmodified KIT-6 silica sorbent did not exhibit selectivity for scandium over iron and aluminium.

Recently, a low-cost sorbent was synthesised by anchoring *N*-[(3-trimethoxysilyl)propyl]-ethylenediaminetriacetic acid (TMS-EDTA) to oxidised activated carbon (AC) for the recovery of REEs from aqueous solutions.[144] The sorbent showed selectivity towards the REEs over nickel and cobalt, and especially a high selectivity towards the HREE. Inorganic ion exchangers like zirconium and titanium phosphates were also applied in REEs separation from the base metals. Zirconium phosphate was proven to be efficient in separating neodymium and dysprosium from cobalt, as well as for the mutual separation between the two REEs.[145,146] Zhang and co-workers purified scandium from a simulated bauxite residue leachate using titanium phosphate, as previously discussed in section 1.2.2 (Page 12).[16]

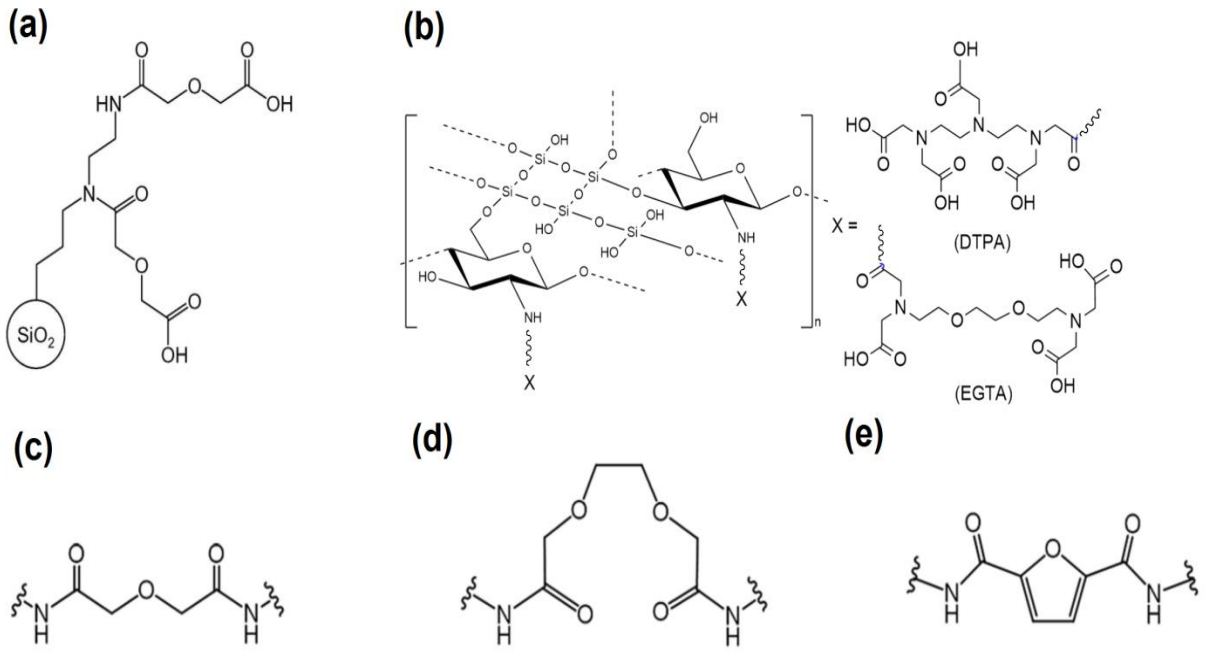

Figure 1.12. Sorbents selective for REEs: (a) immobilized diglycolamic acid ligand on silica gel (EDASiDGA), (b) chitosan–silica particles functionalized with ethyleneglycol tetraacetic acid (EGTA) and diethylenetriamine pentaacetic acid (DTPA), (c) diglycolamide (DGA), (d) 3,6-dioxaoctanedioic acid (DOODA) and (e) furan-2,4-diamido-propyltriethoxysilane (FDGA) ligands grafted on KIT-6 silica.[50,135,142]

The first large-scale separation of REEs by column chromatography was performed by Spedding *et al.* in 1947.[147] The REEs were loaded on Amberlite IR-100, a sulfonic acid cation-exchange resin, and ammonium citrate/citric acid solution was used as eluent to selectively elute the REEs based on the difference in the stability constants of the REE-citrate complexes. Nowadays, more commercial products for REEs separation are available. For instance, the company "Axion – Rare and Noble metals" developed the ion-exchange resin AXION-P6-32 for REEs uptake from highly concentrated NH_4NO_3 solutions (180 g L^{-1}).[148] The total dynamic exchange capacity (the capacity in a column) by REEs equals 3.0 mmol g^{-1}. Another resin AXION HL can be used for recovery of HREEs from highly acid nitric and phosphoric acid solutions without preliminary neutralisation, resulting in a concentration factor of 10.

1.4 REFERENCES

1 K. Binnemans, P. T. Jones, T. Müller, L. Yurramendi, *J. Sustain. Metall.*, 2018, **4**, 126–146.

2 J. Zhang, B. Zhao, B. Schreiner, *Separation Hydrometallurgy of Rare Earth Elements*, Springer, Cham, Switzerland, 2016.

3 S. Cotton, *Lanthanide and Actinide Chemistry*, Wiley, Chichester, United Kingdom, 2006.

4 Y. Kanazawa, M. Kamitani, *J. Alloys Compd.*, 2006, **408-412**, 1339–1343.

5 W. Wang, Y. Pranolo, C. Y. Cheng, *Hydrometallurgy*, 2011, **108**, 100–108.

6 L. Gao, Y. Chen, *J. Rare Earths*, 2010, **28**, 622–626.

7 A. Abedini, A. A. Calagari, M. R. Azizi, *J. Geochem. Explor.*, 2018, **186**, 129–142.

8 K. M. Goodenough, J. Schilling, E. Jonsson, P. Kalvig, N. Charles, J. Tuduri, E. A. Deady, M. Sadeghi, H. Schiellerup, A. Müller, G. Bertrand, N. Arvanitidis, D. G. Eliopoulos, R. A. Shaw, K. Thrane, N. Keulen, *Ore Geol. Rev.*, 2016, **72**, 838–856.

9 European Commission, Directorate-General for Internal Market, Industry, Entrepreneurship and SMEs (2017) Study on the review of the list of Critical Raw Materials: executive summary.

10 REDMUD, available at: http://etn.redmud.org/. Accessed on 30.04.2018.

11 DEMETER, available at: http://www.demeter-eu-project.eu/. Accessed on 30.04.2018.

12 EURARE, available at: http://www.eurare.eu/. Accessed on 30.04.2018.

13 EREAN, available at: http://erean.eu/. Accessed on 30.04.2018.

14 T. Hertel, B. Blanpain, Y. Pontikes, *J. Sustain. Metall.*, 2016, **2**, 394–404.

15 R. M. Rivera, B. Ulenaers, G. Ounoughene, K. Binnemans, T. Van Gerven, *Miner. Eng.*, 2018, **119**, 82–92.

16 W. Zhang, R. Koivula, E. Wiikinkoski, J. Xu, S. Hietala, J. Lehto, R. Harjula, *ACS Sustain. Chem. Eng.*, 2017, **5**, 3103–3114.

17 D. Avdibegović, M. Regadío, K. Binnemans, *RSC Adv.*, 2018, **8**, 11886–11893.

18 G. Alkan, B. Yagmurlu, S. Cakmakoglu, T. Hertel, Ş. Kaya, L. Gronen, S. Stopic, B. Friedrich, *Sci. Rep.*, 2018, **8**, 5676.

19 World of Aluminium., http://www.world-aluminium.org/statistics/#histogram, Accessed 18.04.2018.

20 V. Sibanda, S. Ndlovu, G. Dombo, A. Shemi, M. Rampou, *J. Sustain. Metall.*, 2016, **2**, 167–184.

21 X. Hao, K. Leung, R. Wang, W. Sun, Y. Li, *Geosci. Front.*, 2010, **1**, 81–89.

22 B. A. Bogatyrev, V. V. Zhukov and Y. G. Tsekhovsky, *Lithol. Miner. Resour.*, 2009, **44**, 135–151.

23 Z. Liu, H. Li, *Hydrometallurgy*, 2015, **155**, 29–43.

24 V. M. Sizyakov, V. Y. Bazhin, E. V. Sizyakova, *Metallurgist*, 2016, **59**, 1135–1141.

25 C. R. Borra, B. Blanpain, Y. Pontikes, K. Binnemans, T. Van Gerven, *J. Sustain. Metall.*, 2016, **2**, 365–386.

26 Y. Tian, X. Pan, H. Yu, Y. Han, G. Tu and S. Bi, in *Light Metals 2016*, ed. E. Williams, Springer International Publishing, Cham, 2016, pp. 5–9.

27 W. M. Mayes, I. T. Burke, H. I. Gomes, Á. D. Anton, M. Molnár, V. Feigl, É. Ujaczki, *J. Sustain. Metall.*, 2016, **2**, 332–343.

28 A. Gelencsér, N. Kováts, B. Turóczi, Á. Rostási, A. Hoffer, K. Imre, I. Nyirő-Kósa, D. Csákberényi-Malasics, Á. Tóth, A. Czitrovszky, A. Nagy, S. Nagy, A. Ács, A. Kovács, Á. Ferincz, Z. Hartyáni, M. Pósfai, *Environmental science & technology*, 2011, **45**, 1608–1615.

29 K. Evans, *J. Sustain. Metall.*, 2016, **2**, 316–331.

30 REDMUD, http://redmud.org/red-mud/disposal/, Accessed 18.04.2018.

31 Y. Liu, R. Naidu, *Waste manag.*, 2014, **34**, 2662–2673.

32 F. Kaußen and B. Friedrich, *Chem. Ing. Tech.*, 2015, **87**, 1535–1542.

33 C. R. Borra, B. Blanpain, Y. Pontikes, K. Binnemans, T. Van Gerven, *J. Sustain. Metall.*, 2016, **2**, 28–37.

34 F. Habashi, *Can. Metall. Q.*, 2013, **52**, 224–233.

35 I. Valeton, *Developments in Soil Science 1.*, In *Bauxites*, Elsevier, Amsterdam, The Netherlands, 1972.

36 J. Vind, A. Malfliet, B. Blanpain, P. Tsakiridis, A. Tkaczyk, V. Vassiliadou, D. Panias, *Minerals*, 2018, **8**, 77.

37 M. Ochsenkühn-Petropulu, T. Lyberopulu, G. Parissakis, *Anal. Chim. Acta*, 1994, **296**, 305–313.

38 K. Binnemans, P. T. Jones, B. Blanpain, T. Van Gerven, Y. Pontikes, *J. Clean. Prod.*, 2015, **99**, 17–38.

39 X. Shaoquan, L. Suqing, *Hydrometallurgy*, 1996, **42**, 337–343.

40 R. P. Narayanan, N. K. Kazantzis, M. H. Emmert, *ACS Sustain. Chem. Eng.*, 2017, **6**, 1478–1488.

41 W. Wang, Y. Pranolo, C. Y. Cheng, *Sep. Purif. Technol.*, 2013, **108**, 96–102.

42 Y. Qu and B. Lian, *Bioresource Technol.*, 2013, **136**, 16–23.

43 É. Ujaczki, Y. Zimmermann, V. Feigl, M. Lenz, In: Y. Pontikes (ed) Proc. Bauxite Residue Valoris. Best Pract. Conf. 5–7 October 2015, Leuven (Belgium), 339–346.

44 K. Sugita, Y. Kobayashi, Y. Taguchi, S. Takeda, Y. Ota, M. Ojiri, K. Oda, H. Sano, 2015, US Patent US20150086449.32.

45 C. R. Borra, Y. Pontikes, K. Binnemans, T. Van Gerven, *Miner. Eng.*, 2015, **76**, 20–27.

46 P. Davris, E. Balomenos, D. Panias, I. Paspaliaris, *In: Martin O. (eds.), Light Metals 2018, TMS 2018, The Minerals, Metals and Materials Series*, 2018, Springer, Cham, Switzerland.

47 B. Onghena, C. R. Borra, T. Van Gerven, K. Binnemans, *Sep. Purif. Technol.*, 2017, **176**, 208–219.

48 R. Boudreault, J. Fournier, D. Primeau, M.M. Labrecque-Gilbert, 2015, US Patent US20150275330.

49 M. T. Ochsenkühn-Petropoulou, K. S. Hatzilyberis, L. N. Mendrinos, C. E. Salmas, *Ind. Eng. Chem. Res.*, 2002, **41**, 5794–5801.

50 J. Roosen, S. van Roosendael, C. R. Borra, T. Van Gerven, S. Mullens, K. Binnemans, *Green Chem.*, 2016, **18**, 2005–2013.

51 Aluminium INSIDER, https://aluminiuminsider.com/rusal-mulling-industrial-scale-production-scandium-oxide-red-mud/. Accessed on 30.04.2018.

52 D. L. Sparks, *Sorption*, in: *Encyclopedia of Soils in the Environment*, Elsevier, Oxford, United Kingdom, 2005, 532–537.

53 J. Kammerer, R. Carle, D. R. Kammerer, *J. Agric. Food Chem.* 2011, **59**, 22–42.

54 Inamuddin, M. Luqman, *Ion Exchange Technology I Theory and Materials*, Springer, Dordrecht, Netherlands, 2012.

55 P. Jones, P. N. Nesterenko, *J. Chromatogr. A*, 1997, **789**, 413–435.

56 A. Balouch, M. Kolachi, F. N. Talpur, H. Khan, M. I. Bhanger, *Am. J. Analyt. Chem.*, 2013, **04**, 221–228.

57 A. R. Vaino, K. D. Janda, *J. Comb. Chem.*, 2000, **2**, 579–596.

58 Y Y.S. Ho, G. McKay, *Process Biochem.*, 1999, **34**, 451–465.

59 N. V. Plechkova, K. R. Seddon, *Chem. Soc. Rev.*, 2008, **37**, 123–150.

60 G.-C. Tian, J. Li, Y.-X. Hua, *Trans. Nonferrous Met. Soc. China*, 2010, **20**, 513–520.

61 N. Hatano, T. Takekiyo, H. Abe, Y. Yoshimura, *Int. J. Spectrosc.*, 2011, **2011**, 1–5.

62 P. Nockemann, B. Thijs, S. Pittois, J. Thoen, C. Glorieux, K. van Hecke, L. Van Meervelt, B. Kirchner, K. Binnemans, *J. Phys. Chem. B*, 2006, **110**, 20978–20992.

63 V. M. Egorov, D. I. Djigailo, D. S. Momotenko, D. V. Chernyshov, I. I. Torocheshnikova, S. V. Smirnova, I. V. Pletnev, *Talanta*, 2010, **80**, 1177–1182.

64 W. Wang, Y. Liu, A. Xu, H. Yang, H. Cui, J. Chen, *Chin. J. Chem. Eng.*, 2012, **20**, 40–46.

65 D. Depuydt, W. Dehaen, K. Binnemans, *Ind. Eng. Chem. Res.*, 2015, **54**, 8988–8996.

66 R. Germani, M. V. Mancini, N. Spreti, P. Di Profio, G. Savelli, *Green Sustain. Chem.*, 2011, **01**, 155–164.

67 D. Depuydt, W. Dehaen, K. Binnemans, *ChemPlusChem*, 2017, **82**, 458–466.

68 B. Onghena, K. Binnemans, *Ind. Eng. Chem. Res.*, 2015, **54**, 1887–1898.

69 Z. Li, X. Li, S. Raiguel, K. Binnemans, *Sep. Purif. Technol.*, 2018, **201**, 318–326.

70 S. Riaño, K. Binnemans, *Green Chem.*, 2015, **17**, 2931–2942.

71 M. Matsumiya, Y. Kikuchi, T. Yamada, S. Kawakami, *Sep. Purif. Technol.*, 2014, **130**, 91–101.

72 T. Vander Hoogerstraete, K. Binnemans, *Green Chem.*, 2014, **16**, 1594–1606.

73 G.-T. Wei, Z. Yang, C.-J. Chen, *Anal. Chim. Acta*, 2003, **488**, 183–192.

74 D. Villemin, M. Didi, *Orient. J. Chem*, 2013, **29**, 1267–1284.

75 A. Rout and K. Binnemans, *Dalton Trans.*, 2015, **44**, 1379–1387.

76 J.-Q. Wang, X.-D. Yue, F. Cai, L.-N. He, *Catal. Com.*, 2007, **8**, 167–172.

77 E. Guibal, A. F. Piñol, M. Ruiz, T. Vincent, C. Jouannin, A. M. Sastre, *Sep. Sci. Technol.*, 2010, **45**, 1935–1949.

78 N. Kabay, J. L. Cortina, A. Trochimczuk, M. Streat, *React. Funct. Polym.*, 2010, **70**, 484–496.

79 F. Giacalone, M. Gruttadauria, *ChemCatChem*, 2016, **8**, 664–684.

80 J. Lemus, J. Palomar, M. A. Gilarranz, J. J. Rodriguez, *Adsorption*, 2011, **17**, 561–571.

81 A. Negrea, L. Lupa, M. Ciopec, P. Negrea, I. Hulka, *IJCEA*, 2014, **5**, 424–428.

82 R. S. Juang, *Proc. Natl. Sci. Counc. ROC(A)*, 1999, **23**, 353–364.

83 M.-A. Néouze, J. Le Bideau, P. Gaveau, S. Bellayer, A. Vioux, Ionogels, *Chem. Mater.*, 2006, **18**, 3931–3936.

84 C. J. Brinker, *J. Non-Cryst. Solids*, 1988, **100**, 31–50.

85 L. Viau, M.-A. Néouze, C. Biolley, S. Volland, D. Brevet, P. Gaveau, P. Dieudonné, A. Galarneau, A. Vioux, *Chem. Mater.*, 2012, **24**, 3128–3134.

86 A. Martinelli, L. Nordstierna, *Phys. Chem. Chem. Phys.*, 2012, **14**, 13216–13223.

87 D. Muraviev, L. Ghantous, M. Valiente, *React. Funct, Polym.*, 1998, **38**, 259–268.

88 D. Dupont, K. Binnemans, *Green Chem.*, 2015, **17**, 2150–2163.

89 V. Compañ, S. Molla, E. García Verdugo, S. V. Luis, M. I. Burguete, *J. Non Cryst. Solids*, 2012, **358**, 1228–1237.

90 X. Zhang, W. Geng, C. Yue, W. Wu, L. Xiao, *J. Environ. Chem. Eng.*, 2016, **4**, 2565–2572.

91 C. P. Mehnert, E. J. Mozeleski, R. A. Cook, *Chem. Commun.*, 2002, 3010–3011.

92 S. Eyley, W. Thielemans, *Chem. Commun.*, 2011, **47**, 4177–4179.

93 M. H. Valkenberg, C. Castro, W. F. Hölderich, *Top. Catal.*, 2001, **14**, 139–144.

94 J.-M. Andanson, A. Baiker, *J. Phys. Chem. C*, 2013, **117**, 12210–12217.

95 L. Vidal, M.-L. Riekkola, A. Canals, *Anal. Chim. Acta*, 2012, **715**, 19–41.

96 W. Miao, T. H. Chan, *Acc. Chem. Res.*, 2006, **39**, 897–908.

97 A. Eftekhari, T. Saito, *Eur. Polym. J.*, 2017, **90**, 245–272.

98 A. Vioux, L. Viau, S. Volland, J. Le Bideau, *C. R. Chim.*, 2010, **13**, 242–255.

99 B. Gadenne, P. Hesemann, J. J. E. Moreau, C*hem. Commun.*, 2004, 1768–1769.

100 G. Lv, Z. Li, W.-T. Jiang, P.-H. Chang, L. Liao, *Mater. Chem. Phys.*, 2015, **162**, 417–424.

101 L. Wu, C. Yang, L. Mei, F. Qin, L. Liao, G. Lv, *Appl Clay Sci.*, 2014, **99**, 266–274.

102 G. Alberti, M. Casciola, U. Costantino, R. Vivani, *Adv. Mater.*, 1996, **8**, 291–303.

103 A. Clearfield, *Inorganic ion exchange materials*, CRC Press, Boca Raton, Florida, 1982.

104 B. M. Mosby, M. Goloby, A. Díaz, V. Bakhmutov, A. Clearfield, *Langmuir*, 2014, **30**, 2513–2521.

105 B. M. Mosby, A. Díaz, A. Clearfield, *Dalton Trans.*, 2014, **43**, 10328–10339.

106 C. Trobajo, S. A. Khainakov, A. Espina, J. R. García, *Chem. Mater.*, 2000, **12**, 1787–1790.

107 A. Clearfield, Z. Wang, *J. Chem. Soc., Dalton Trans.*, 2002, 2937–2947.

108 R. Vivani, G. Alberti, F. Costantino, M. Nocchetti, *Microporous Mesoporous Mater.*, 2008, **107**, 58–70.

109 Y. Zhou, I. Noshadi, H. Ding, J. Liu, R. Parnas, A. Clearfield, M. Xiao, Y. Meng, L. Sun, *Catalysts*, 2018, **8**, 17.

110 A. Díaz, V. Saxena, J. González, A. David, B. Casañas, C. Carpenter, J. D. Batteas, J. L. Colón, A. Clearfield, M. D. Hussain, *Chem. Commun.*, 2012, **48**, 1754–1756.

111 V. Luca, J. J. Tejada, D. Vega, G. Arrachart, C. Rey, *Inorg. Chem.*, 2016, **55**, 7928–7943.

112 M. Pica, *Catalysts*, 2017, **7**, 190 (18).

113 C. Jiang, A. Su, X. Li, T. Zhou, D. He, *Powder Technol.*, 2012, **221**, 371–374.

114 Z. Al Othman, *Materials*, 2012, **5**, 2874–2902.

115 L. T. Gibson, *Chem. Soc. Rev.*, 2014, **43**, 5163–5172.

116 F. Hoffmann, M. Cornelius, J. Morell, M. Fröba, *Angew. Chem. Int. Ed.*, 2006, **45**, 3216–3251.

117 C. P. Guthrie, E. J. Reardon, *J. Phys. Chem. A*, 2008, **112**, 3386–3390.

118 A. Corma, *Chem. Rev.*, 1997, **97**, 2373–2420.

119 S. Kawi, *Chem. Commun.*, 1998, **13**, 1407–1408.

120 T. J. M. Keene, R. Denoyel, P. L. Llewellyn, *Chem. Commun.*, 1998, **20**, 2203–2204.

121 H. Tüysüz, C. W. Lehmann, H. Bongard, B. Tesche, R. Schmidt, F. Schüth, *J. Am. Chem. Soc.*, 2008, **130**, 11510–11517.

122 C.-W. Lee, K. C. Roh, K.-B. Kim, *Nanoscale*, 2013, **5**, 9604–9608.

123 A. Matsumoto, K. Tsutsumi, K. Schumacher, K. K. Unger, *Langmuir*, 2002, **18**, 4014–4019.

124 A. Wani, E. Muthuswamy, G. H. L. Savithra, G. Mao, S. Brock, D. Oupický, *Pharm. Res.*, 2012, **29**, 2407–2418.

125 N. I. Vazquez, Z. Gonzalez, B. Ferrari, Y. Castro, *Bol. Soc. Esp. Ceram. Vidr.*, 2017, **56**, 139–145.

126 X. Sun, Y. Ji, J. Chen, J. Ma, *J. Rare Earths*, 2009, **27**, 932–936.

127 X. Sun, B. Peng, Y. Ji, J. Chen, D. Li, *Sep. Purif. Technol.*, 2008, **63**, 61–68.

128 L. Zhu, J. Chen, *J. Rare Earths*, 2011, **29**, 969–973.

129 L. Zhu, Y. Liu, J. Chen, W. Liu, *J. Appl. Polym. Sci.*, 2011, **120**, 3284–3290.

130 A. N. Turanov, V. K. Karandashev, N. S. Sukhinina, V. M. Masalov, G. A. Emelchenko, *J. Environ. Chem. Eng.*, 2016, **4**, 3788–3796.

131 J. Ma, Z. Wang, Y. Shi, Q. Li, *RSC Adv.*, 2014, **4**, 41597–41604.

132 J. Florek, S. Giret, E. Juère, D. Larivière, F. Kleitz, *Dalton Trans.*, 2016, **45**, 14832–14854.

133 A. Negrea, A. Gabor, C. M. Davidescu, M. Ciopec, P. Negrea, N. Duteanu, A. Barbulescu, *Sci. Rep.*, 2018, **8**, 316.

134 I. Anastopoulos, A. Bhatnagar, E. C. Lima, *J. Mol. Liq.*, 2016, **221**, 954–962.

135 T. Ogata, H. Narita, M. Tanaka, *Hydrometallurgy*, 2015, **152**, 178–182.

136 T. Ogata, H. Narita, M. Tanaka, *Hydrometallurgy*, 2015, **155**, 105–109.
137 T. Ogata, H. Narita, M. Tanaka, *Hydrometallurgy*, 2016, **163**, 156–160.
138 N. Van Nguyen, A. Iizuka, E. Shibata, T. Nakamura, *Hydrometallurgy*, 2016, **165**, 51–56.
139 R. D. Shannon, *Acta Cryst. A*, 1976, **32**, 751–767.
140 D.W. Smith, *J. Chem. Educ.*, 1977, **54**, 540–542.
141 J. Roosen, J. Spooren, K. Binnemans, *J. Mater. Chem. A*, 2014, **2**, 19415–19426.
142 J. Florek, A. Mushtaq, D. Larivière, G. Cantin, F.-G. Fontaine, F. Kleitz, *RSC Adv.*, 2015, **5**, 103782–103789.
143 S. Giret, Y. Hu, N. Masoumifard, J.-F. Boulanger, J. Estelle, F. Kleitz, D. Larivière, S *ACS Appl. Mater. Interfaces*, 2018, **10**, 448–457.
144 C. M. Babu, K. Binnemans, J. Roosen, *Ind. Eng. Chem. Res.*, 2018, **57**, 1487–1497.
145 J. Xu, E. Wiikinkoski, R. Koivula, W. Zhang, B. Ebin, R. Harjula, *J. Sustain. Metall.*, 2017, **3**, 646–658.
146 J. Xu, R. Koivula, W. Zhang, E. Wiikinkoski, S. Hietala, R. Harjula, *Hydrometallurgy*, 2018, **175**, 170–178.
147 F. H. Spedding, E. I. Fulmer, T. A. Butler, E. M. Gladrow, M. Gobush, P. E. Porter, J. E. Powell, J. M. Wright, *J. Am. Chem. Soc.*, 1947, **69**, 2812–2818.
148 JSC "Axion – Rare-earth and Noble Metals", http://axion-rnm.com/page/71162, Accessed 15.04.2018.

Chapter 2

Objectives

"No amount of experimentation can even prove me right; a single experiment can prove me wrong." A. Einstein

For many years, both academia and industry have been trying to find a viable way to valorise bauxite residue, which has been piling up for many decades, resulting in an estimated total inventory of several billions of tonnes. However, to date very few industrial applications of bauxite residue are known. In Chapter 1, the potential routes of bauxite residue valorisation were discussed, with the emphasis on bauxite residue as a valuable source of rare-earth elements (REEs). The main objective of this PhD thesis is the development of new sorbents suitable for the recovery of REEs from acidic solutions.

At first, the development of supported ionic liquid phases (SILPs) will be explored. The challenge here is to select the right combination of ionic liquid and support and integrate them into a SILP material that can meet the criteria of selective recovery of REEs from bauxite residue leachates. The developed SILPs need to be stable under the operating conditions. The SILPs need to be characterised in detail and investigated batchwise for the recovery of REEs. After proving their basic performance batchwise, the SILPs can be packed in a column and are further investigated for REEs separation from bauxite residue leachates produced by various leaching procedures. The study will allow determining whether the SILPs can be used to recover REEs directly from non-treated bauxite residue leachates or whether is it necessary to consider the use of SILPs in an integrated flow sheet, where base metals are recovered in advance.

Secondly, well-established ion-exchangers, metal(IV) phosphates, will be considered for separating scandium from iron. Scandium represents the majority of trace metal value in bauxite residue. The iron concentration in bauxite residue leachates is in general rather high (several 1000 mg L^{-1}) and its separation from scandium imposes difficulties. The ion-exchangers will be screened batchwise for scandium and iron separation. The most promising ion-exchanger can then be thoroughly investigated for scandium recovery from bauxite residue leachates.

Lastly, novel sorbents will be developed by surface modification of MCM-41 silica and tested for the separation of mixtures of REEs. The mixtures of REEs can be concentrated from the leachates by SILPs or metal(IV) phosphates. The REEs can then be split into subgroups or individual elements by these functionalised MCM-41 silica materials.

Chapter 3

Recovery of Sc(III) from diluted aqueous solutions by a supported ionic liquid phase (SILP)

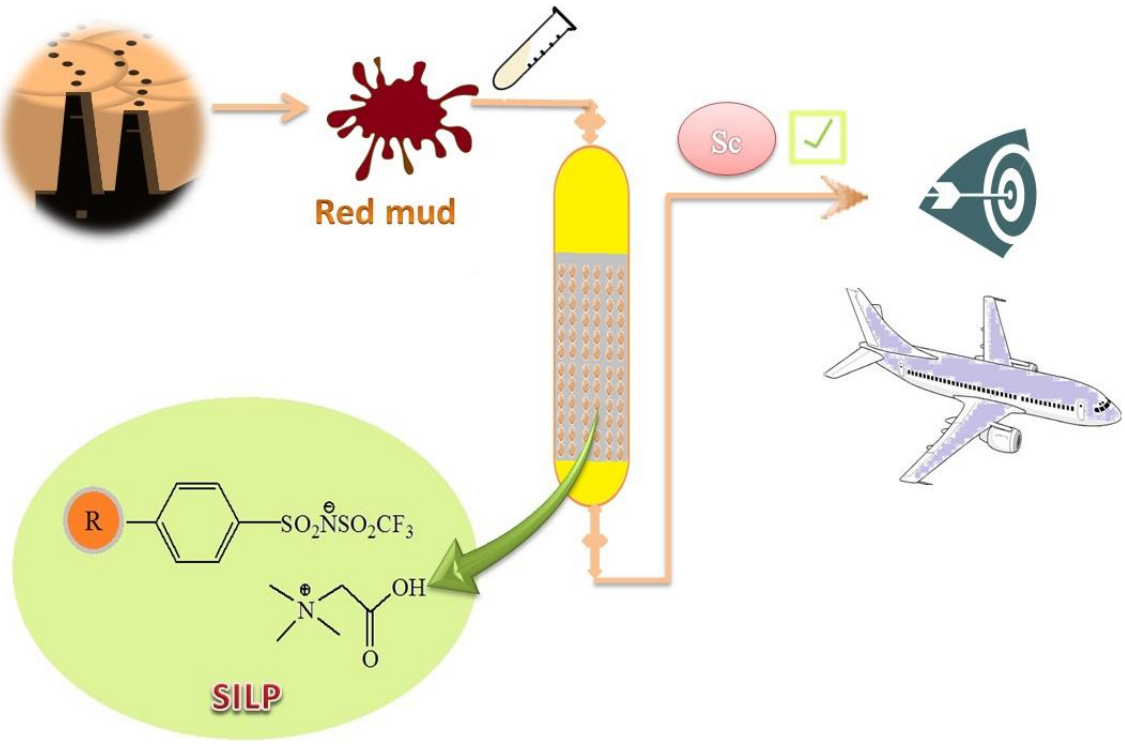

Recovery of scandium from diluted aqueous solutions by a supported ionic liquid phase.

This chapter is based on the published paper:

Avdibegović D., Regadío M., Binnemans K. (2017). Recovery of scandium(III) from diluted aqueous solutions by a supported ionic liquid phase (SILP). *RSC Advances*, **7**, 49664-49674.

The text may contain slight adjustments compared to the original publication.

Author contributions:

K.B, M.R. and D.A. conceived the research. D.A. conducted all experiments and wrote the manuscript. All the authors commented on the manuscript.

Authors wish to thank Dirk Henot (KU Leuven) for performing CHN measurement and Bart Van Huffel (KU Leuven) for performing BET measurement.

ABSTRACT

The sorption of scandium from diluted, acidic solutions by a supported ionic liquid phase (SILP) was investigated, as part of a process for the recovery of scandium from bauxite residue (red mud). Both dry impregnation and covalent linking were studied for the SILP preparation. The SILP betainium sulfonyl(trifluoromethanesulfonylimide) poly(styrene-*co*-divinylbenzene) [Hbet-STFSI-PS-DVB] was prepared by covalent linking of the ionic liquid to the resin and this resulted in a sorbent suitable for scandium recovery. The effects of pH, contact time, sorption capacity, desorption, reusability of sorbent and the influence of Fe(III), Al(III) and Ca(II) on the Sc(III) sorption were studied from HCl solutions. The sorption of Sc(III) from HNO_3 and H_2SO_4 feed solution under optimal conditions were studied as well. The sorption kinetics followed a pseudo-second order kinetic model. Equilibrium studies at room temperature showed that the experimental data could be fitted well to the Langmuir isotherm model. The stripping of Sc(III) from the loaded SILP was achieved with 1 mol L^{-1} H_2SO_4. The SILP was stable and could be reused for seven sorption/desorption cycles without significant losses in its sorption efficiency for Sc(III).

3.1 INTRODUCTION

Scandium belongs to the group of rare-earth elements (REEs) and finds applications in aluminum alloys, halide lamps and fuel cells.[1] However, it is an expensive metal with small global production volumes. Although scandium is relatively abundant in the Earth's crust (22 mg kg^{-1}), there are few scandium minerals and it rarely occurs in rich ore deposits. It is mainly recovered as by-product from the production of other metals (REEs, U, Ti, W, Al, Ni, Ta and Nb).[2–4] Bauxite residue (red mud), the waste industrial product of the Bayer process for alumina production from bauxite ore, can contain up to 130 mg kg^{-1} of scandium and it is potentially a valuable scandium resource.[5,6] Scandium can be partially recovered from bauxite residue by acid leaching, although in this way many metal impurities go into the leach solution as well and in concentrations much higher than that of scandium.[1,7,8]

Liquid-liquid extraction is used for the recovery of Sc(III),[9] but it requires much higher initial concentrations of Sc(III) than the ones that can be found in the pregnant leach solutions.[1] Nevertheless, for recovery of low concentrations of Sc(III) its enrichment with a selective sorbent in high capacity ion exchange columns could be an efficient technique.

Much of the research work on Sc(III) recovery by sorption and extraction has been performed with resins,[10–13] modified carbon nanotubes,[14] activated carbon,[15] SBA-15,[16] silica sol-gel material[17] or extractants impregnated onto a solid support.[18–21] Ionic liquids (ILs) show a great potential for application in hydrometallurgy, both solvent extraction[22–24] and leaching.[25,26] ILs are solvents that consist entirely of ions, and they have been investigated as non-volatile alternatives for organic solvents. However, ILs have a high viscosity which may involve drawbacks in process design. To overcome these issues different methods are used to immobilize ILs onto the surface of a solid support forming supported ionic liquid phases (SILPs).[27,28] Ideally, ILs in SILPs obtain a large specific surface area and mechanical properties of the support and maintain the extractive properties of ILs. This further makes SILPs suitable not only for applications in catalysis,[29–32] but also for metal ions sorption and preconcentration.[28,33–35] SILPs are classified in two groups. The first group consists of the classic SILP materials where the IL is impregnated on a porous support material and the forces between the IL and the support are weak, physical Van der Waals forces (physisorption of the IL). The second group comprises

covalently linked IL phases, where the IL cation (or anion) is chemically bonded to the solid support.[36] The first class of SILPs is relatively easy to prepare and these SILPs exhibit a straightforward mechanism of interactions of ILs with metal ions.[37] The main disadvantage of SILPs prepared by physisorption is the loss of the impregnated IL due to the solubility of the IL in the aqueous phase.[35,38,39] Consequently, this leads to a steady loss of sorption capacity and the SILPs become ineffective after several cycles of application. Moreover, leakage is not acceptable because ILs are expensive compounds and their components can contaminate the aqueous effluents.[37] In the second class of SILPs there is no discrete IL phase in the structure of the solid support. Instead, the IL can be considered as a covalently anchored ligand. Covalent linking ensures that the IL will not be leached from the support.[32,40]

The objective of this work was to develop a stable SILP for the sorption of Sc(III) from the leach solution of industrial process residues or tailings, such as bauxite residue. The SILP was tested for the recovery of low concentrations of Sc(III) from acidic feed solution.

3.2 EXPERIMENTAL

3.2.1 Chemicals

$AlCl_3 \cdot 6H_2O$ (99%), nitric acid (65%), ammonia (25%), standard solutions of scandium, yttrium, neodymium, dysprosium, lanthanum, gallium, aluminum, iron and calcium (1000 ± 10 µg mL^{-1}) were purchased from Chem-Lab NV (Zedelgem, Belgium). $Sc(NO_3)_3 \cdot 5H_2O$ (99.9%), $YCl_3 \cdot 6H_2O$ (99.9%), $NdCl_3 \cdot 6H_2O$ (99.9%) were purchased from Strem Chemicals (Newburyport, USA). $DyCl_3 \cdot 6H_2O$ (99.9%) was purchased from abcr (Karlsruhe, Germany). $CaCl_2 \cdot 2H_2O$ [(100 ± 2)%] was purchased from Merck (Overijse, Belgium). $FeCl_3$ anhydrous (98%), hexadecyltrimethylammonium bromide (CTAB) (99%), betaine hydrochloride [Hbet][Cl] (99%), triethylamine (99%), and sulfuric acid (96%) were purchased from Acros Organics (Geel, Belgium). Lithium bis(trifluoromethylsulfonyl)imide (99%) was purchased from IoLiTec (Helibronn, Germany). NaOH (97%), hydrochloric acid (37%) were purchased from VWR (Leuven, Belgium). Polystyrene-divinylbenzene (PS-DVB) sulfonyl chloride resin (0.91 mmol g^{-1}, 200-400 mesh) was purchased from RappPolymere (Tübingen, Germany). Trifluoromethanesulfonamide (98%) was purchased from J&K Scientific GmbH (Pforzheim,

Germany). Dichloromethane (DCM) (*p.a.*) and acetone (*p.a.*) were purchased from Fisher Chemical (Loughborough, UK). Silicone solution in isopropanol was purchased from SERVA Electrophoresis GmbH (Heidelberg, Germany). Tetraethyl orthosilicate (TEOS) (98%) and Amberlite XAD-16 resin (20-60 mesh) were purchased from Sigma Aldrich (Diegem, Belgium). Sc_2O_3 (99.99%) was cordially provided by Solvay (La Rochelle, France). Hydrated $ScCl_3$ was prepared by dissolving Sc_2O_3 in concentrated hydrochloric acid, followed by heating and evaporation of the acid near dryness. A Sc(III) stock solution (≈ 10 g L^{-1}) was prepared by dissolving $ScCl_3$ in ultrapure water. Working solutions of Sc(III) were prepared by diluting 10 times in ultrapure water. In order to prepare a $Sc_2(SO_4)_3$ solution, $Sc(OH)_3$ was precipitated from 5 mL of $ScCl_3$ stock solution by the addition of ammonia (25%). The precipitate was washed several times to remove the remaining chloride anions, which was confirmed by the AgCl precipitation test. The precipitate of $Sc(OH)_3$ was then dissolved in sulfuric acid and the solution was diluted with ultrapure water. The resulting solution contained ≈ 5 g L^{-1} of Sc(III). The concentrations of the stock solutions were measured by TXRF or ICP-OES (see next section). Amberlite XAD-16 resin was washed prior to use according to the literature procedure and dried for 2 h in a vacuum oven at 50 °C.[41] MCM-41 silica was prepared as previously described in the literature.[42] Briefly, CTAB (2.0 g) was added to the ammonia solution, which was then homogenized. TEOS (10 mL) was added and a white slurry was formed. Finally, the product was filtered, dried and calcined in the air at 550 °C for 5 h. The IL betainium bis(trifluoromethylsulfonyl)imide [Hbet][Tf_2N] was synthesised in a reaction between an aqueous solution of betaine hydrochloride and an aqueous solution of lithium bis(trifluoromethylsulfonyl)imide.[43]

3.2.2 Equipment

FT-IR spectra were recorded on a Bruker Vertex 70 spectrometer (Bruker Optics) via the attenuated total reflectance (ATR) technique with a Bruker Platinum ATR accessory. Analyses were performed with the OPUS software package. The carbon, hydrogen, and nitrogen content of the resin and SILP were determined using a CHN elemental analyser (Thermo Scientific FLASH 2000). Scanning electron microscopy (SEM) images of platinum coated samples were

recorded with Philips XL30. The specific surface area was determined by a surface area analyzer (Quantchrome NOVA 2200e). Prior to the surface area measurements, the samples were degassed under vacuum and 50 °C for 19 h. N_2 sorption was measured at -196.15 °C and the Brunauer-Emmett-Teller (BET) equation was used to calculate the specific surface area. Batch sorption and desorption experiments were performed using a VWR International water bath shaker (Type 462-0355). The synthesis of SILP was performed using Thermo Fisher Scientific MaxQ 2000 open-air platform shaker. For the desorption experiments on the recovery of Sc(III) from the loaded SILP after sorption tests, the samples were centrifuged (Heraeus Labofuge 200). A total reflection X-ray fluorescence (TXRF) spectrometer (Bruker Picofox S2) was used to determine the concentration of Sc(III) of single-element solutions. Lanthanum internal standard was used for quantification and gallium internal standard for quality control. To avoid significant matrix effects an inductively coupled plasma - optical emission spectrometer (ICP-OES) (Perkin Elmer OPTIMA 8300) was used to determine the concentration of elements from multielement and scandium sulfate solutions. The calibration solutions and all samples were prepared by dilution with 2 wt% HNO_3. In order to obtain a better accuracy and precision of the ICP-OES measurement lanthanum internal standard was used. Thermogravimetric analysis (TGA) was performed on a TA Instruments T500 thermogravimeter under nitrogen flow (heating rate: 5 °C min^{-1}, from 20 up to 600 °C). The pH was measured with a Mettler-Toledo pH meter SevenCompact pH/Ion S220 after calibration with standard buffer solutions of pH 1, 4, 7 and 10.

3.2.3 Synthesis of SILPs

3.2.3.1 Dry impregnation method

[Hbet][Tf_2N] (1.0 g) was dissolved in acetone (11 mL) and Amberlite XAD-16 resin or MCM-41 silica (1.0 g) was added. The mixture was shaken for 24 h at room temperature at 300 rpm. Finally, the acetone was removed by a rotary evaporator. The products [Hbet][Tf_2N]-Amberlite XAD-16 and [Hbet][Tf_2N]-MCM-41 silica were characterized by FT-IR.

3.2.3.2 Covalent linking

Trifluoromethanesulfonamide (0.179 g or 1.24 mmol) was dissolved in DCM (18 mL). Polystyrene sulfonyl chloride resin (1 g, 1 eq.) and triethylamine (0.512 mL, 4 eq.) were added to the solution. The mixture was shaken for 48 h at room temperature and speed of 300 rpm. The resulting product (**1)** was filtered and washed with DCM. A sample of [Hbet][Cl] (0.419 g, 3 eq.) was dissolved in water (6 mL) and acetone (6 mL) was added to enhance the swelling of the resin and to make the reactive sites accessible. Then, the resulting solution of [Hbet][Cl] (**2)** was added to the intermediate product (**1)** and shaken for 24 h at room temperature at 300 rpm. The final product (**3)** was filtered, washed with acetone and finally with ultrapure water. The obtained wet product was used in the batch sorption experiments. The SILP and the sulfonyl chloride resin were dried at 50 °C for 24 h in a vacuum oven prior to FT-IR, SEM, CHN analysis and TGA for determining the decomposition temperature.

3.2.3.3 Sorption and desorption tests

For batch sorption experiments 0.050 g of wet SILP prepared by the covalent linking was added to 10 mL of an aqueous solution of Sc(III) in a 20 mL glass vial. Unless otherwise specified, the concentration of Sc(III) was 1.1 mmol L^{-1}, the shaking speed 300 rpm and the equilibration time 90 min. The experiments were carried out at room temperature in chloride media. The pH was adjusted between 0.5 and 3.5 using diluted HCl (or other corresponding acid: H_2SO_4 in sulfate and HNO_3 in nitrate media) or NaOH solution. After equilibration the solutions were filtered through a cellulose syringe filter with a pore size of 0.45 µm. The pH of the filtrate was measured and the metal ion concentration was determined by TXRF or ICP-OES. The amount of the metal ions sorbed onto the SILP was calculated from *Eq. 1.1* (Page 16, 1.3.1.1), based on the dry mass of the SILP. The average moisture content, estimated by the TGA, was 32%. Desorption and recovery of metal ions from the loaded SILP was performed with 2 mL of the tested acids (HCl, HNO_3 and H_2SO_4). Prior to the addition of acid, the solution was centrifuged for 2 min at 3000 rpm and the supernatant was taken by a pipette. The SILP was washed two times with 10 mL of ultrapure water to remove eventually residual metal ions and centrifuged again. The same procedure was applied for the reusability studies under the optimised conditions, where after each desorption and washing step 10 mL of Sc(III) feed solution was added. The desorbed amount (%) was calculated from *Eq. 1.2* (Page 16, 1.3.1.1).

3.2.3.4 Stability tests of SILPs prepared by the dry impregnation method

TGA was used to estimate the amount of IL prior to and after performing the Sc(III) sorption tests with SILPs prepared by a dry impregnation method. An amount of 0.10 g of impregnated SILPs was added to 5 mL of aqueous solutions containing 2.2 mmol L^{-1} of Sc(III). The experiments were carried out at room temperature, a shaking speed of 300 rpm and an equilibration time of 90 min. The initial pH (pH_{ini}) was adjusted to 3.5. After equilibrating, the mixtures were centrifuged for 2 min at 3000 rpm. The supernatant was taken by a pipette for TXRF analysis of the Sc(III) concentration. The remaining SILPs were dried in a vacuum oven for 24 h at 50 °C prior to the TGA measurements. The content of the IL in SILPs was estimated from the observed percentage of mass loss in the temperature range of the IL decomposition.

3.3 RESULTS AND DISCUSSION

3.3.1 SILPs characterisation

The dry impregnation method was employed for the preparation of SILPs containing the ionic iquid [Hbet][Tf_2N], which is known to be a good extractant for Sc(III) (Figure 3.13).[7] Two solid supports were tested for impregnation of [Hbet][Tf_2N]: Amberlite XAD-16 and MCM-41 silica. The prepared SILPs were characterized by FT-IR (Figure 3.14, Figure 3.15*)*. The characteristic absorption frequencies arising from the cation and anion of the IL were found in SILPs. Amberlite XAD-16 resin exhibits a high surface area (≈ 800 m^2 g^{-1}) and large pore volumes (200 Å).[40] The support with a polystyrene–divinylbenzene (PS-DVB) matrix is unlikely to affect the metal ion sorption processes. Therefore only the IL will play an active role in the sorption process. MCM-41 silica was selected as a support because it is one of the most important members of the family of mesoporous molecular sieves.[44] Mesoporous silicas are often used as solid supports due to their large surface area (≈ 1000 m^2 g^{-1}), fast sorption kinetics and controllable pore size (between 2 and 50 nm) and pore arrangement.[45]

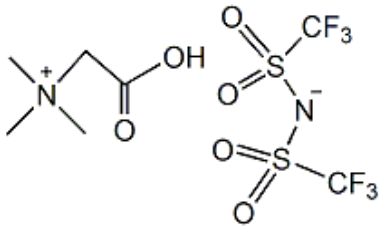

Figure 3.13. Chemical structure of the IL [Hbet][Tf_2N].

It was not possible to precisely determine the IL content in the Amberlite XAD-16 SILP by TGA, because of the overlapping of thermal decomposition of the IL and Amberlite XAD-16 between 300 and 500 °C (Figure 3.16a). However, the change in the height drop of the TGA curve of the tested SILP in the temperature range from 300 to 400 °C indicated that the content of the IL after one sorption test had decreased from 50 wt% to approximately 20 wt%. From the TGA data (Figure 3.16b) the estimated amount of the IL in the SILPs after impregnation of the MCM-41 silica was ≈50 wt%. There was a clear distinction between the decomposition temperature of the IL and the MCM-41 silica support.

The content of the IL in the silica-based SILP after one batch sorption test had decreased from 50 wt% to approximately 13 wt%. In addition to the losses of IL from both supports, the reproducibility of the Sc(III) sorption results was poor due to the solubility of the IL in the acidic aqueous feed solution. According to previous studies, the solubility of [Hbet][Tf_2N] in water (1:1 ratio) is approximately 14 wt%, if no high concentrations of salting-out agents are present.[7] When testing the stability and sorption properties of SILPs with impregnated [Hbet][Tf_2N] high liquid-to-solid ratios were applied (50:1). Therefore a higher solubility of the IL was anticipated than in the case of liquid-liquid extraction. Even with supports exhibiting a high surface area, the IL loading of 50 wt% could not be maintained over time and severe IL losses occurred. The solubility of [Hbet][Tf_2N] can potentially be decreased by addition of salting-out agents to the aqueous phase (for instance Na_2SO_4) to further optimize the sorption procedure.[26] However, this would require high inorganic salts consumption. Additionally, the ions of the inorganic salt may interfere in the downstream processes to recuperate a high yield of pure scandium.

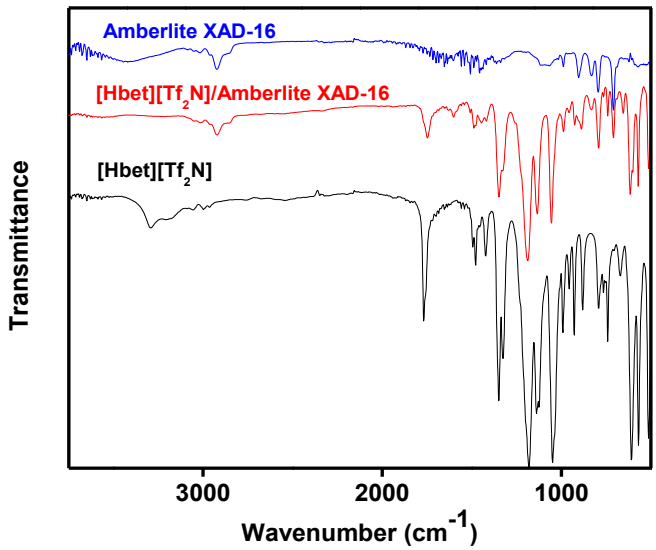

Figure 3.14. FT-IR spectra of [Hbet][Tf_2N] and SILP prepared by dry impregnation method with [Hbet][Tf_2N] and the Amberlite XAD-16 support.

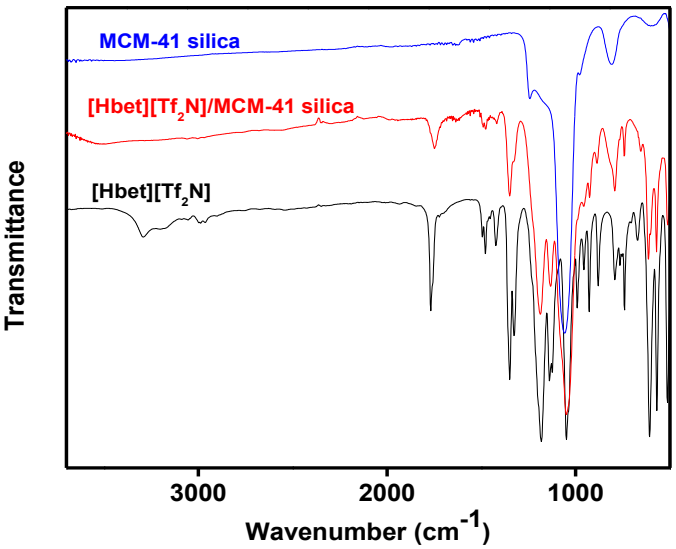

Figure 3.15. FT-IR of [Hbet][Tf_2N] and SILP prepared by dry impregnation method with [Hbet][Tf_2N] and MCM-41 silica support.

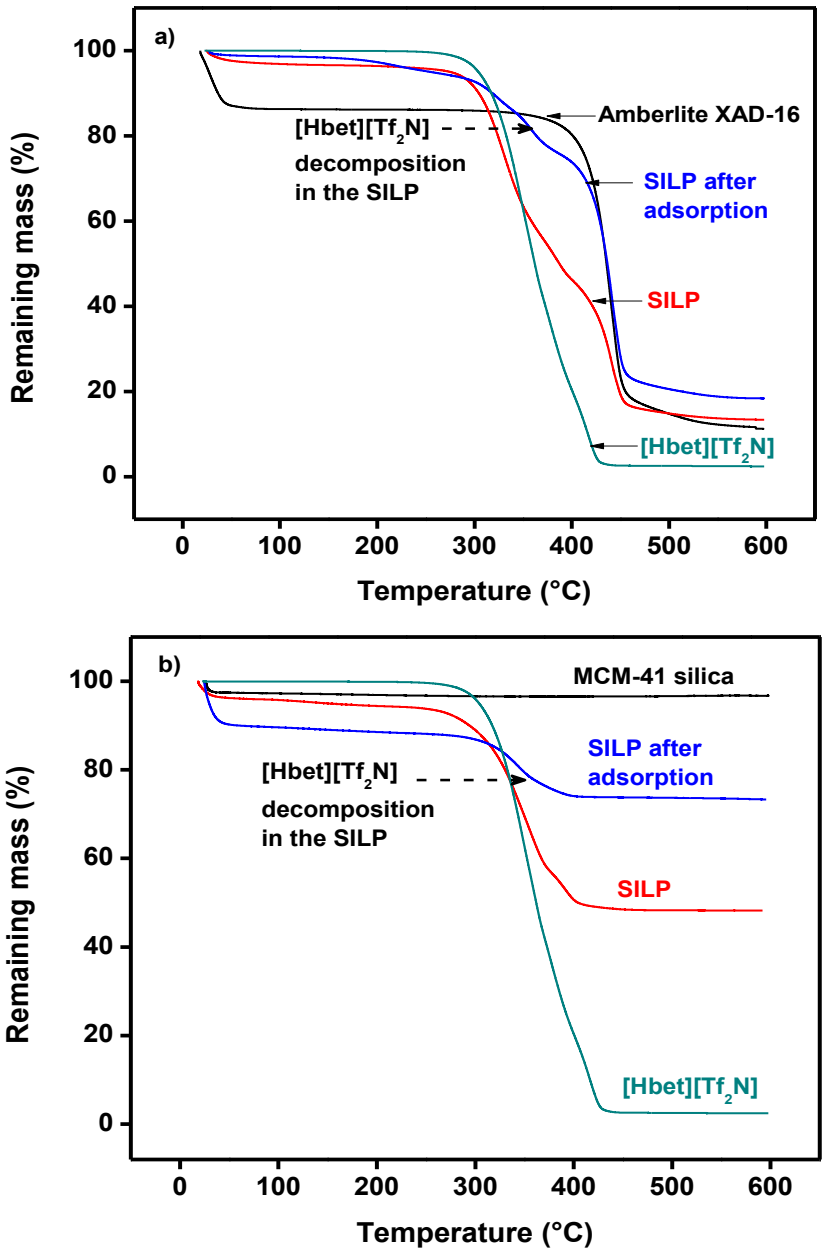

Figure 3.16. TGA of the SILPs [Hbet][Tf_2N]–Amberlite XAD-16 (a) and [Hbet][Tf_2N]–MCM-41 silica (b) prior and after the sorption test. Nitrogen atmosphere, heating rate: 5 °C·min^{-1}, from 20 to 600 °C.

Because of the losses of IL from the SILPs prepared by impregnation, covalent linking of the IL onto the support was performed. Carboxylic acid extractants and ILs with carboxyl functional group are useful for extraction and separation of metal ions.[9–11,46–48]

In this study a SILP mimicking the structure of [Hbet][Tf_2N] was synthesized (Figure 3.17). El Kadib et al. previously reported the synthesis of a SILP prepared by covalent linking with periodic mesoporous organosilica and trisilylated guanidinium-sulfonimide IL.[49] The IL was covalently anchored to the silica surface *via* both the organo-cationic and the organo-anionic moieties.[49] Instead of preparing the silylated sulfonamide precursor for surface grafting to SBA-15 and MCM-41 silica, the SILP was synthesised starting from a PS–DVB-based resin as a support with sulfonyl-chloride reactive sites. Silica-based materials suffer from a lack of stability in strongly acidic or alkaline conditions, low breakthrough for polar analytes,[40] collapse of the mesoporous structure in water due to silicate hydrolysis[45] and the need to use more expensive starting compounds such as 2-(4-chlorosulfonylphenyl)ethyl-trimethoxysilane instead of a sulfonyl chloride resin.

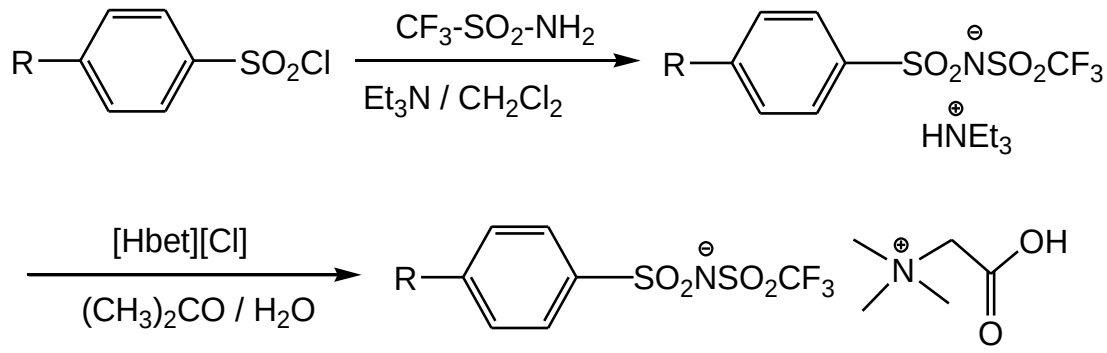

Figure 3.17. Synthesis of the SILP Hbet-STFSI-PS-DVB.

Polymer-based supports have better tolerance towards samples and eluents with extreme pH values and moreover PS-DVB resins show high mechanical rigidity and stability,[50] making them convenient for preparing sorbents that are used in highly acidic media. A sulfonimide was thus synthesized by reaction of PS-DVB sulfonyl chloride resin and trifluoromethanesulfonamide in the presence of excess of triethylamine (top Figure 3.17). By the addition of excess amount of betaine hydrochloride the triethylammonium cation was then exchanged for betainium (bottom

Figure 3.17). In the final synthesis step, acetone was used to enhance the swelling of the support. If the support is not well swollen, the accessibility of the reactive sites is poorer and the reaction rates are slower. Therefore, the reaction solvent must be carefully chosen since cross-linked polystyrene resins will not swell in solvents that are too polar like water.[42,43,51] If the resin is sufficiently porous, the reactive sites are accessible even without extensive swelling. Still, it is necessary that the resin swells to accommodate larger organic ions during the synthesis of the SILP.[52] FT-IR was used to characterize the SILP (Figure 3.18). The most characteristic peaks in the IR spectra of the SILP were the C=O asymmetric stretching in the carboxylic group of the cation at 1750 cm^{-1} and S=O asymmetric stretching which shifted from 1375 cm^{-1} in the SILP, indicating that the reaction between sulfonyl chloride group and trifluoromethanesulfonamide has taken place.[53,54]

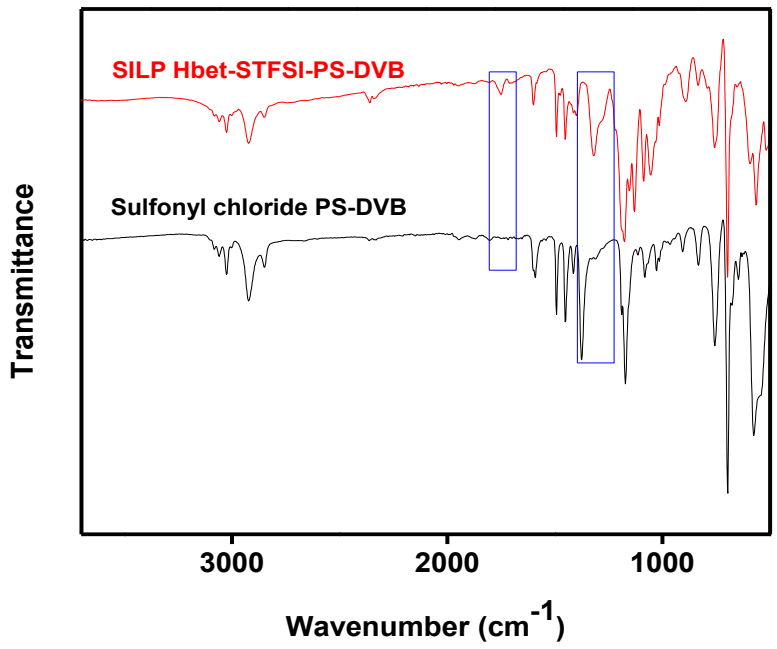

Figure 3.18. FT-IR spectra of the SILP Hbet-STFSI-PS-DVB and sulfonyl chloride resin. The most characteristic peaks are emphasized by blue rectangles.

Moreover, the CHN analysis results for sulfonyl chloride resin were: 81.12% C, 7.12% H and 0.00% N. The synthesis of the SILP by covalent linking was confirmed by the presence of

nitrogen in the SILP: 71.64% C, 6.30% H and 1.81% N. From the N content the degree of functionalization of the sulfonyl chloride resin was estimated to be around 71%. The BET specific surface area of the resin was 49 $m^2 g^{-1}$, while when accommodating the ion pairs in the SILP the specific surface area decreased to 15 $m^2 g^{-1}$. The SILP had the same spherical shape as the resin that was used as support (Figure 3.19).

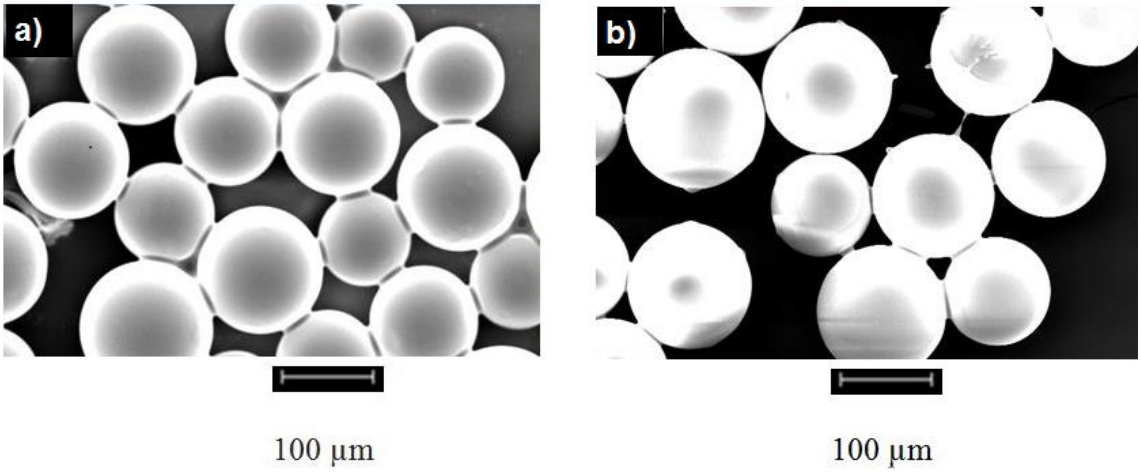

Figure 3.19. SEM images of sulfonyl chloride resin (a) and SILP Hbet-STFSI-PS-DVB (b). Acceleration voltage 10.0 kV, working distance 10.0 mm, 500× magnification.

Sulfonyl chloride resin with particle size between 200 and 400 mesh was selected as a starting material for the synthesis. Sorbents with too small particle size can cause issues with the solid-liquid separation in batch sorption experiments. Furthermore, if applied in chromatography column separations, issues with leakage or clogging might occur. On the other hand, if the particle size is large, it can negatively affect the sorption kinetics and the sorption capacity, since the uptake by smaller particles is more favoured due to greater accessibility of the functional groups.[55]

To examine whether the thermal stability of the SILP differed significantly from the starting resin, a TGA of both materials was performed. In the sulfonyl chloride resin, the thermal decomposition of polystyrene matrix was between 320 and 440 °C (Figure 3.20). The thermal decomposition of the SILP started at a lower temperature, but above 200 °C. With the covalent attachment of ion pairs onto the resin, the thermal stability range of the polymer support was

slightly decreased (> 95% of the polystyrene was decomposed at 410 °C). Normally the working temperatures for metal sorption from aqueous solution are below 100 °C. The slight decrease in the thermal stability range of the polymer support after covalent linking of ion pairs does not diminish the usability of the SILP in metal ion separation.

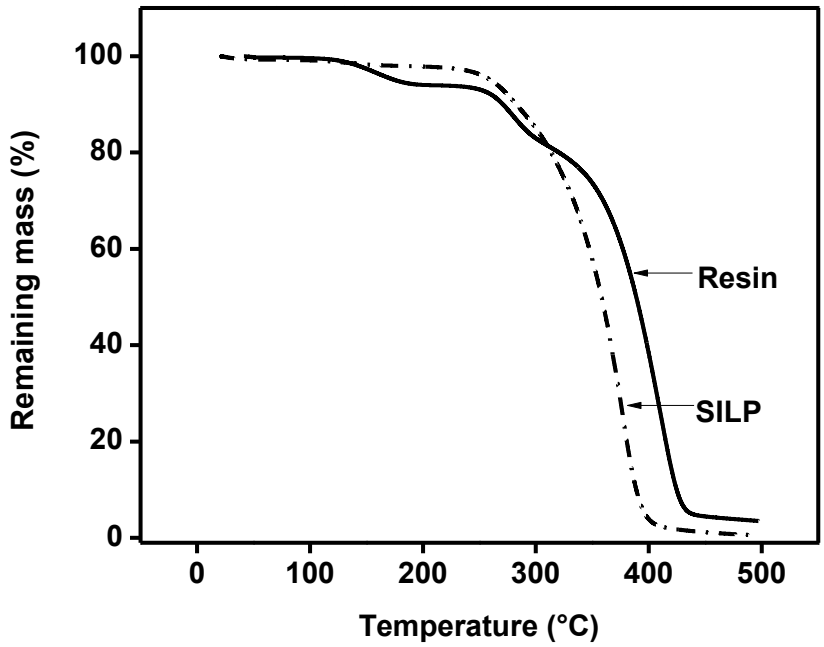

Figure 3.20. TGA of sulfonyl chloride resin and the SILP [Hbet-STFSI-PS-DVB]. Nitrogen atmosphere, heating rate: 5 °C min^{-1}, from 20 to 500 °C.

3.3.2 Effect of pH

To recover Sc(III) from acidic leachates, a convenient sorbent must be able to sorb Sc(III) at low pH. To prevent the precipitation of $Sc(OH)_3$, the pH was kept below 4 (although the actual pH at which $Sc(OH)_3$ starts to precipitate depends on the scandium concentration).[7,56] The same consideration has to be taken into account for the common accompanying elements in the bauxite residue leachates which are present in significantly higher concentrations than Sc(III). Losses of Sc(III) by coprecipitatation of other metal hydroxides might occur. For instance, in bauxite residue leach solutions the concentration of Sc(III) is only a few mg L^{-1} compared to the thousands of mg L^{-1} of major elements (Fe, Al, Ca, Si, Ti).[1] Therefore, the effect of the pH_{ini} on

Sc(III) sorption was investigated for the range 0.5 < pH < 3.0 and the equilibrium pH was monitored as well (Figure 3.21). With the increase in pH_{ini}, the sorption of Sc(III) also increased, accompanied by a decrease in equilibrium pH. Even at pH < 1.5, the amount of sorbed Sc(III) is in the same range as observed for sorbents that have been previously used for Sc(III) recovery from bauxite residue leach solutions.[57] Furthermore, over the entire investigated acidic pH range the SILP showed superior sorption capacity for Sc(III) over previously reported sorbents selective for scandium.[16,58] Therefore the SILP could be considered as a suitable sorbent for recovery of Sc(III) from acidic media.

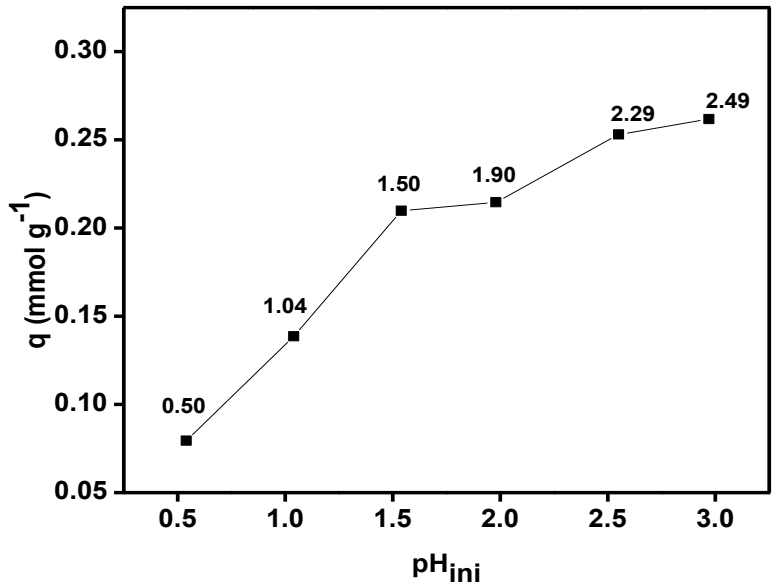

Figure 3.21. Effect of the initial (pH_{ini}) and equilibrium pH (pH_{eq} values are labeled in the graph) on Sc(III) sorption with [Hbet-STFSI-PS-DVB]: aqueous phase = 10 mL, 0.05 g of SILP, Sc(III) concentration 1.1 mmol L^{-1}, 90 min, 300 rpm, room temperature.

Furthermore, the sorption mechanism under acidic conditions and the stability of the SILP under basic conditions were investigated by FT-IR. The stability of the SILP in basic solution was studied to compare its behavior with the IL [Hbet][Tf_2N]. [Hbet][Tf_2N] alkali-metal salts are water soluble and in alkaline solutions the IL becomes completely water miscible.[51] A sample of 0.05 g of wet SILP was added to 1 mL of 5.1 mmol L^{-1} Sc(III) (pH_{ini} = 2.8, pH_{eq} = 2.5) and NaOH solution (pH_{ini} = 12.9). The samples were shaken for 3 h at 1000 rpm and afterwards

centrifuged. The remaining SILP was washed with ultrapure water and dried for 24 h in a vacuum oven at 50 °C. The absorption band at 1750 cm^{-1} that corresponds to the COOH group had shifted to 1649 cm^{-1} after Sc(III) sorption and to 1664 cm^{-1} after Na(I) sorption (Figure 3.22). The later absorption bands correspond to the conjugated base COO^-, which confirmed that the presence of the betainium cation in the SILP Hbet-STFSI-PS-DVB is essential for sorption of Sc(III). Moreover, a similar SILP with the Et_3N^+ cation instead of the betainium cation (top Figure 3.17) was not able to sorb Sc(III) from aqueous solution, due to the lack of carboxylic functional group. These findings are similar to what was observed for liquid-liquid extraction of Sc(III) when using the ionic liquids [Hbet][Tf_2N][7] and tri-*n*-butyl(carboxymethyl)-phosphonium chloride, [$P_{444}C_1COOH$][Cl].[46]

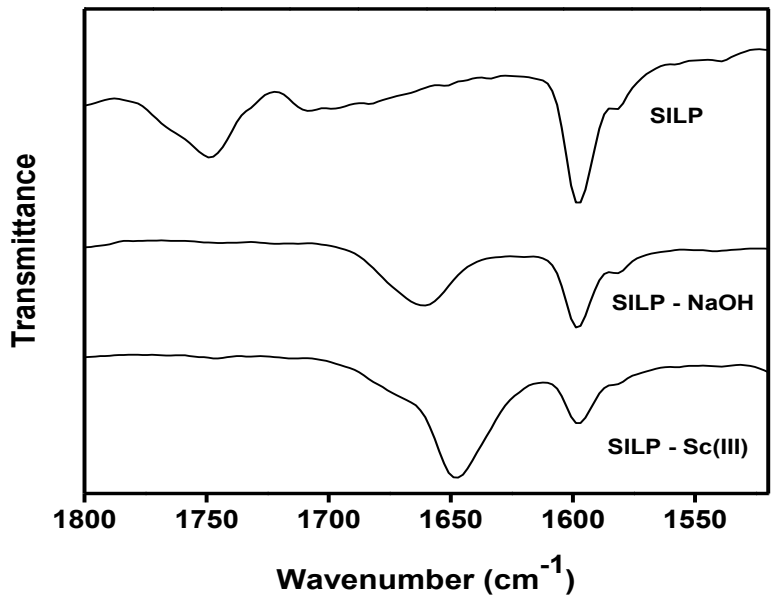

Figure 3.22. FT-IR spectra of the carboxylic acid/carboxylate peak of the SILP Hbet-STFSI-PS-DVB before sorption tests and sorption under acidic and alkaline conditions: aqueous phase = 1 mL, 0.05 g of SILP, 270 min, 1000 rpm, room temperature. pH of NaOH solution = 12.9. Sc(III) concentration = 5.1 mmol L^{-1}, pH_{ini} = 2.8, pH_{eq} = 2.5.

Unlike the IL [Hbet][Tf_2N], when mixed with a NaOH solution (pH = 12.9) the SILP [Hbet-STFSI-PS-DVB] did not lose its ion pairs to the aqueous phase. This was evident from the presence of the COO^- absorption band. In principle, the miscibility of ILs depends on its ionic

species. In the SILP, the IL was covalently attached *via* the anion to the polymer which strongly contributed to the stability of the SILP even in alkaline solutions.

3.3.3 Sc(III) sorption isotherms from different media

The sorption of Sc(III) at room temperature was studied from chloride, nitrate and sulfate media since the corresponding acids can be used for leaching of metals from bauxite residue. Scandium(III) chloride, nitrate and sulfate salts were used to prepare the tested feed solution. From chloride and nitrate media, Sc(III) sorption with the SILP [Hbet-STFSI-PS-DVB] increased with the increase in initial and equilibrium Sc(III) concentration. In principle, rare-earth chloride and nitrate negatively charged complexes are not stable at low chloride and nitrate concentration.[59] On the other hand, the sorption in sulfate media was low (Figure 3.23). This can be explained by the formation of scandium(III) sulfate complexes. Schrodle *et al*. showed that Sc(III) in sulfate media forms both inner- and outer-sphere 1:1 $[ScSO_4]^+_{(aq)}$ complexes.[60] Higher-order inner-sphere complexes predominate in more concentrated solutions of scandium sulfate, and most likely *fac*-$[Sc(SO_4)_3(OH_2)_3]^{3-}$ is the major species present. The electrostatic interactions of small Sc(III) ions (0.745 Å for coordination number of 6)[2] with the sulfate ligands are strong which makes sorption of Sc(III) by the SILP *via* H^+ exchange in the cation difficult.

The Langmuir and Freundlich sorption models were applied to describe the sorption process of Sc(III) from chloride and nitrate media.[61] Although these models do not provide information about the type of reaction involved, the effect of ionic strength, the pH or the composition of the media, they are widely used as empirical models to describe very the sorption process in a simple way. Thus, they can provide an estimate for the maximum sorption capacity and the type of sorption.[62] The linearised Langmuir equation is given by *Eq. 1.6* (Page 17, 1.3.1.1) and the linearised Freundlich equation is represented by *Eq. 1.7* (Page 18, 1.3.1.1). Sorption of Sc(III) in chloride and nitrate media followed the Langmuir sorption isotherm model with correlation coefficient of 0.98 and 0.99, respectively (Table 3.5). Freundlich sorption isotherms gave correlation coefficients of 0.87 in chloride and 0.91 in nitrate media.

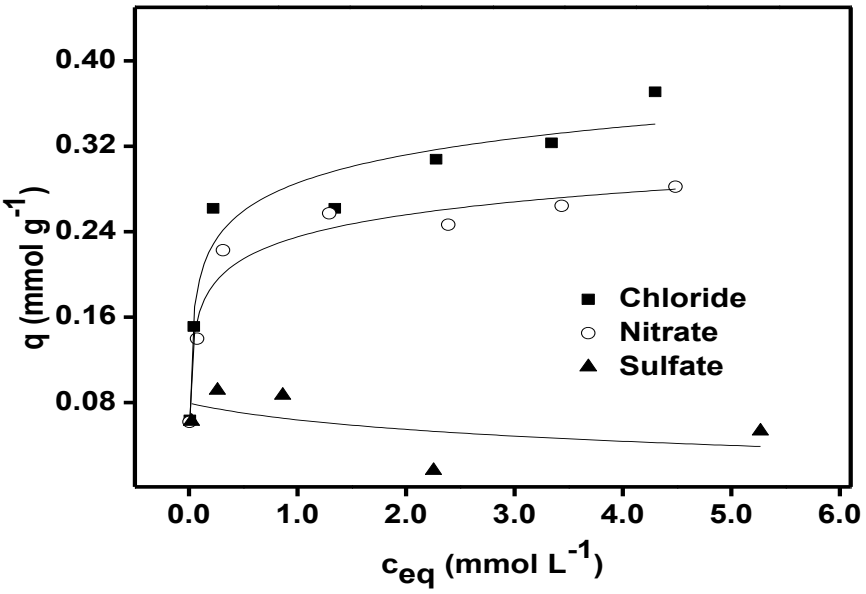

Figure 3.23. Sc(III) sorption from chloride, nitrate and sulfate media with the SILP Hbet-STFSI-PS-DVB. The initial Sc(III) concentration was varied between 0.2 and 5.6 mmol L^{-1}, pH_{ini} = 3.0, 90 min, 300 rpm, room temperature.

Table 3.5. Sorption isotherm data for Sc(III) sorption from chloride and nitrate media at room temperature.

Isotherm model	**Parameter**	**Chloride media**	**Nitrate media**
	q_m (mmol g^{-1})	0.36	0.29
Langmuir	K_L (L $mmol^{-1}$)	5.68	10.0
	R^2	0.98	0.99
	K_F ($mmol^{1-n}$ g^{-1} L^n)	0.11	0.10
Freundlich	n	4.18	4.62
	R^2	0.87	0.91

According to the Langmuir model, the total concentration of the sorbed compound increases when its concentration in the aqueous solution increases. This model suggests that sorption occurs on a homogenous monolayer surface where the number of sorption sites is finite and once a sorbate molecule occupies a site, no further sorption can take place at that site.[55,62]

3.3.4 Kinetic study

In order to examine the controlling step for sorption mechanism, the widely used pseudo-first-order and pseudo-second-order models were applied (*Eq. 1.8* and *Eq. 1.9*, Page 18, 1.3.1.1).[61,63,64,65]

The Sc(III) sorption kinetics data fitted well to the pseudo-second-order kinetics model (correlation coefficient of 0.99, from the plot of $t \cdot q_t^{-1}$ against t) at pH of 3, contrary to a low correlation coefficient when applying the pseudo-first-order kinetics model (0.53). This suggests that the reaction rate is controlled by a chemisorption process. It involves formation of chemical bonds through sharing or exchanging of electrons between sorbent and sorbate.[64] The SILP exhibited fast kinetics and within 15 min equilibrium was reached (Figure 3.24). This is a significant improvement in sorption kinetics in comparison with some conventional resins (6 to 48 h).[65,66]

The values of q_m and k_2 were equal to 0.30 mmol g^{-1} and 2.78 g $mmol^{-1}$ min^{-1}, respectively. In the batch sorption experiments, a wet SILP was used (average water content of 32 wt%) since drying can cause increase in the hydrophobicity and collapse of the structure rendering reactive sites inaccessible and thereby affecting sorption kinetics.[39,67,68] Moreover, when using sorbent in column chromatography, the sorbent is in general preconditioned before it is added to the column, and therefore the wet sorbent would even better reflect the behaviour of the SILP in column chromatography separations.[69]

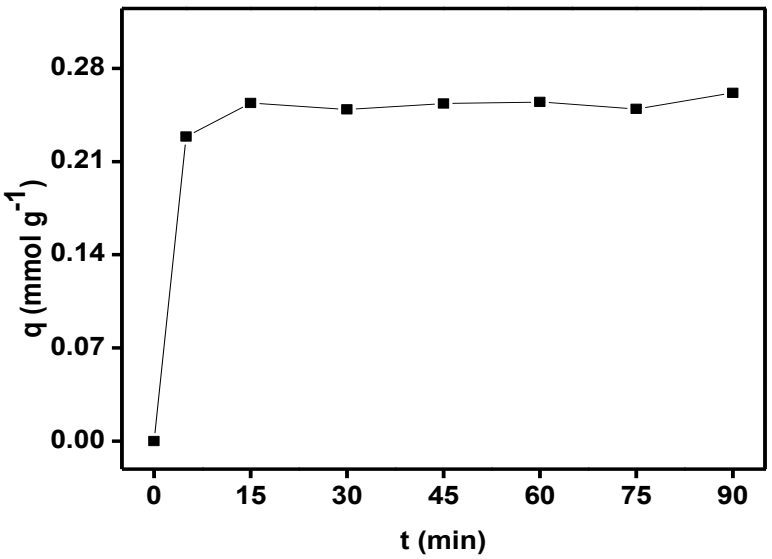

Figure 3.24. Kinetic study of Sc(III) sorption with SILP Hbet-STFSI-PS-DVB: aqueous phase = 10 mL, 0.05 g of SILP, Sc(III) concentration 1.1 mmol L^{-1}, pH_{ini} = 3.0, pH_{eq} = 2.5, 300 rpm, room temperature.

3.3.5 Effect of interfering ions

The sorption of Sc(III) in the presence of other associated major elements in secondary resources (e.g. bauxite residue) such as Fe(III), Al(III) and Ca(II) was investigated.[1] Multi-element, equimolar solutions were investigated in order to elucidate the sorption preference of the selected ions. The selectivity was tested under acidic conditions (pH from 0.5 to 1.8), to assure that no hydrolysis would occur, especially of Fe(III). The same trend of increase in sorption efficiency with the increase of pH was observed as with single element solutions. Moreover Sc(III) was preferentially sorbed over the other tested elements (Figure 3.25). Two main factors could have contributed to the selectivity of the SILP: the electrostatic interactions and the hydration energy. A general rule is that ion-exchangers sorb ions following the order starting from the higher valence, because the electrostatic attraction is directly proportional to the ionic charge and inversely proportional to the ionic radius.[70] Therefore Ca(II) ions were least sorbed by the SILP. Another factor is hydration energy. According to Eisenman's model for selectivity of sorbents the less hydrated ions are easier to dehydrate and, therefore, these are more likely to be selectively sorbed by the sorbent. Among the tested trivalent ions Sc(III) hydration enthalpy

is the lowest, which is in an agreement with the selectivity of the SILP.[71,72] In conclusion, valence and hydration energy could explain the preferential uptake of ions by the SILP. Since Sc(III) and Fe(III) have similar chemical behaviour and the expected concentration of Fe(III) in leach solutions is significantly higher than that of Sc(III), the selectivity of the SILP was further tested from a binary solutions of Sc(III) and Fe(III) at pH ≈ 1.0 (Figure 3.26). From the binary equimolar solution Sc(III) was preferentially sorbed. It must be noted that the amount of Sc(III) and Fe(III) sorbed by the SILP from the binary solution was higher than that from the multielement solution (Figure 3.25) at the same pH of approximately 1.0. This can be most likely attributed to the varation in sorption capacity between different batches of the SILP. With the increase of Fe(III) concentration, the amount of sorbed Sc(III) decreased (Figure 3.26). When the initial concentration of Fe(III) was five times higher than that of Sc(III), the amount of sorbed Sc(III) decreased up to 47% of the amount sorbed from the equimolar solution.

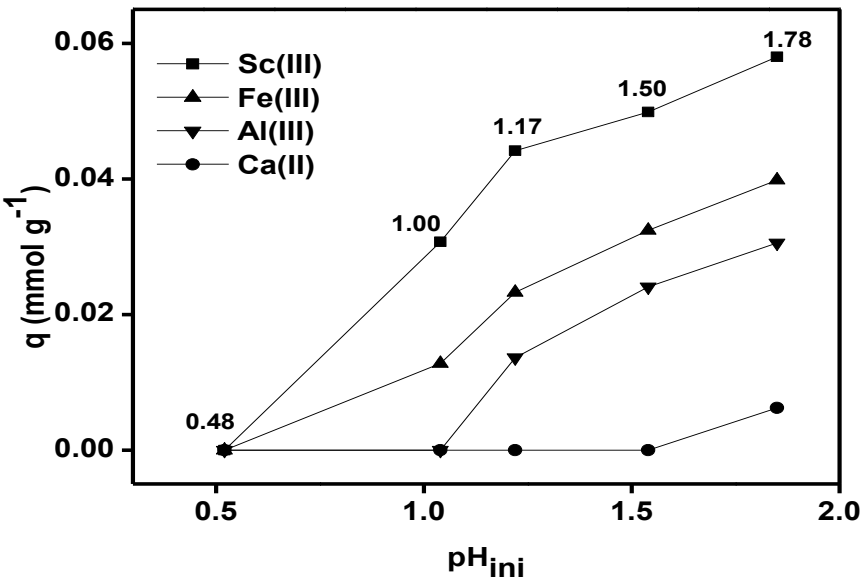

Figure 3.25. Influence of initial (pH_{ini}) and equilibrium pH (pH_{eq} values are labeled in the graph) on the sorption of major elements and Sc(III) with the SILP [Hbet-STFSI-PS-DVB]: aqueous phase = 10 mL, 0.05 g of SILP, multi-element equimolar solution with total concentration of elements 1.1 mmol L^{-1}, 90 min, 300 rpm, room temperature.

These results suggest that Fe(III) should be removed as much as possible (for instance by smelting reduction)[73] prior to the preconcentration of Sc(III) with the SILP. Previously reported sorbents comprising carboxylic groups were found to be suitable for selective Sc(III) sorption over major elements [chitosan-silica sorbent functionalised with ethyleneglycol tetraacetic acid (EGTA), resin with glycol amic acid group].[10,13,57] In terms of selectivity over major elements compared with reported sorbents, the SILP showed lower performance in batch sorption experiments. However, accounting for other important parameters like kinetics, sorption capacity under acidic conditions, preferential uptake of Sc(III) over major elements from equimolar solutions and the relatively simple synthesis procedure, would justify the preferred use of the SILP for further optimisation for Sc(III) recovery.

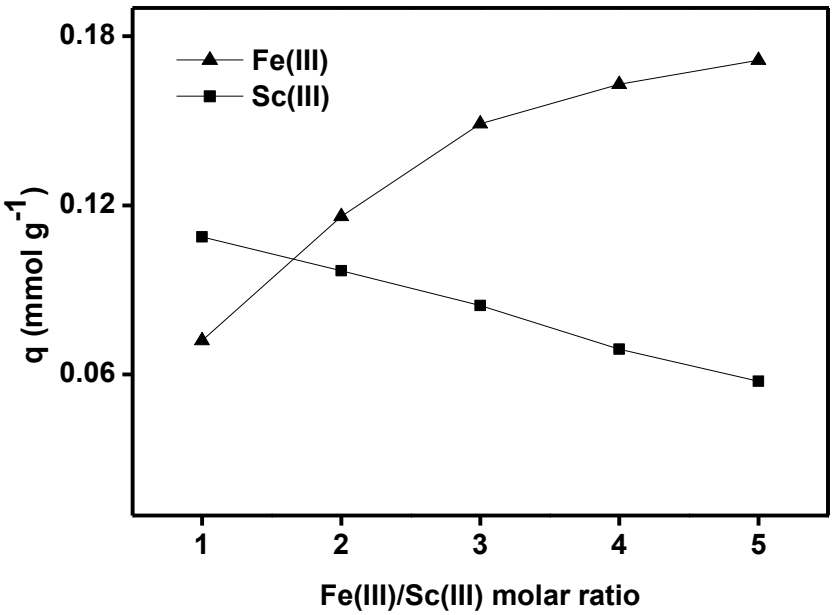

Figure 3.26. Fe(III) and Sc(III) selectivity for the SILP [Hbet-STFSI-PS-DVB]: aqueous phase = 10 mL, 0.05 g of SILP, c_{ini}[Sc(III)] = 1.1 mmol L^{-1}, c_{ini}[Fe(III)] from 1.1 mmol L^{-1} to 5.5 mmol L^{-1}, $pH_{ini} \approx pH_{eq} \approx 1.0$, 90 min, 300 rpm, room temperature.

Moreover, the SILP was tested for the sorption of Sc(III) in the presence of other REEs that can be found in bauxite residue [Y(III), Nd(III) Dy(III)].[1] Over the investigated pH range (from 0.5

to 3.0) all REEs were sorbed from multielement solutions by the SILP (Figure 3.27). Selectivity of the SILP for Sc(III) over other REEs was therefore not superior to previously reported metal phosphate ion-exchangers applied for Sc(III) recovery from bauxite residue.[74,75] However, results imply that the SILP could be used for sorption of REEs from acidic media and then Sc(III) could be further separated from other elements in a chromatography column (after optimising chromatographic conditions such as proper eluent, flow rate *etc.*).

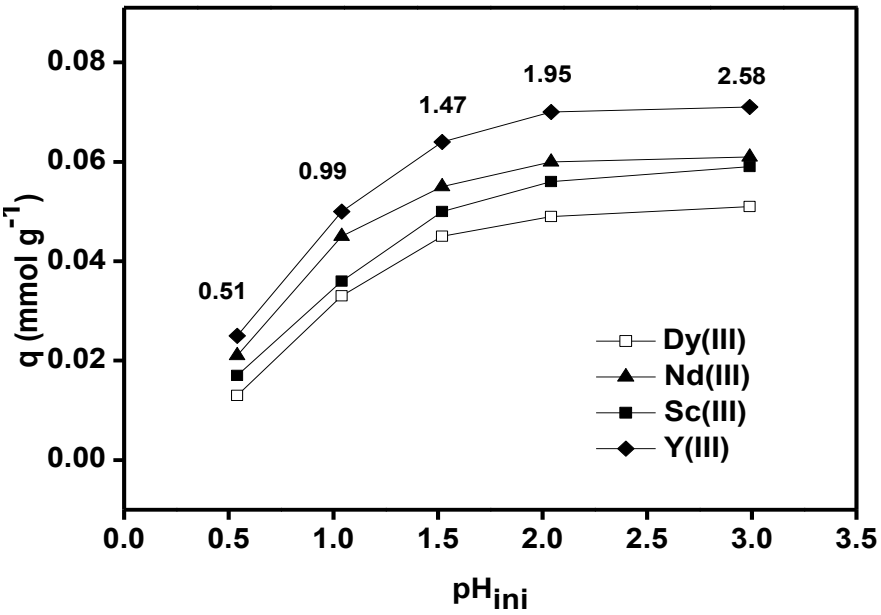

Figure 3.27. Influence of initial (pH_{ini}) and equilibrium pH (pH_{eq} values are labeled in the graph) on the sorption of REEs with the SILP [Hbet-STFSI-PS-DVB]: aqueous phase = 10 mL, 0.05 g of SILP, multi-element equimolar solution with total concentration of elements 1.1 mmol L^{-1}, 90 min, 300 rpm, room temperature.

3.3.6 Desorption and reusability of the SILP [Hbet-STFSI-PS-DVB]

In order to recover Sc(III) from the SILP the desorption efficiency of HCl, HNO_3 and H_2SO_4 was investigated. The desorption efficiency increased with an increase in acid concentration (Figure 3.28). Quantitative desorption of Sc(III) was possible even with 1 mol L^{-1} H_2SO_4. By desorption with 2 mL of H_2SO_4, Sc(III) was four times concentrated compared to its initial concentration.

This indicates that the covalent SILP Hbet-STFSI-PS-DVB could be used for preconcentration of Sc(III) from diluted solutions using chromatography, provided that the concentration of major interfering ions is minimised, especially of Fe(III). The fact that the highest desorption efficiency corresponds to H_2SO_4 could be attributed to scandium sulfate complex formation, as previously discussed.

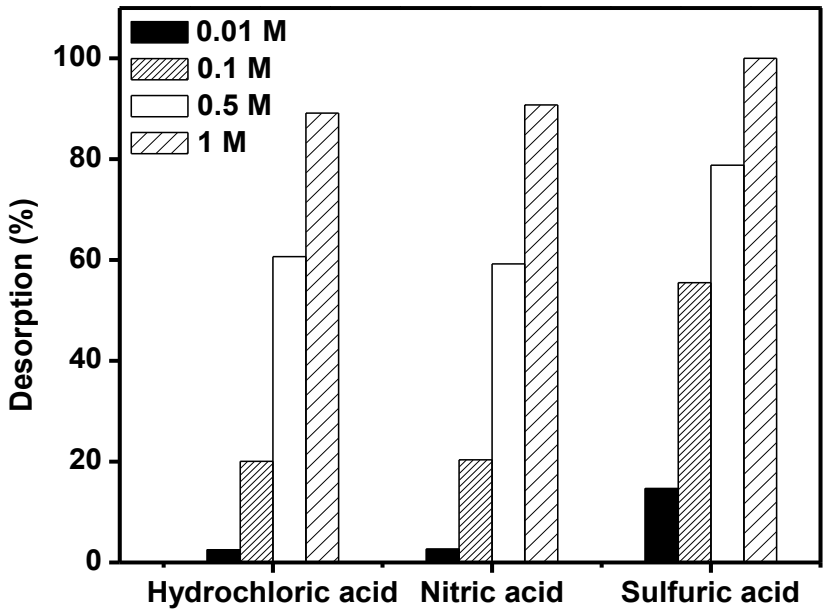

Figure 3.28. Desorption (%) of Sc(III) with different concentration of acids (2 mL of HCl, HNO_3, H_2SO_4) from 0.05 g of SILP [Hbet-STFSI-PS-DVB] previously loaded with ≈ 0.2 mmol g^{-1} of Sc(III). Desorption conditions: 30 min, 300 rpm, room temperature.

To apply the synthesised [Hbet-STFSI-PS-DVB] for the recovery of Sc(III) in a scaled-up process, the SILP has to be reusable. Thus, the SILP was tested in a seven consecutive sorption/desorption cycles, in duplicate. The complete desorption of the previously sorbed Sc(III) was performed with 1 mol L^{-1} H_2SO_4 (Figure 3.29). From one cycle to the next one, there were random differences in the sorption of Sc(III). These variations are more likely attributable to the experimental errors of the batch tests. The sorbed amount of Sc(III) in the first cycle was comparable to the amount sorbed in the last two cycles. The difference between the *q* value of

each cycle and the mean *q* value was additionally confirmed by Wilcoxon's statistical test.[76] The statistical tests suggested that the sorption efficiency of the SILP did not significantly change with 95% confidence level. In batch sorption reusability studies, the source of random errors arises from the potential losses of sorbent during handling or dilution of the fresh feed by residual amounts of ultrapure water used for pretreatment between cycles.

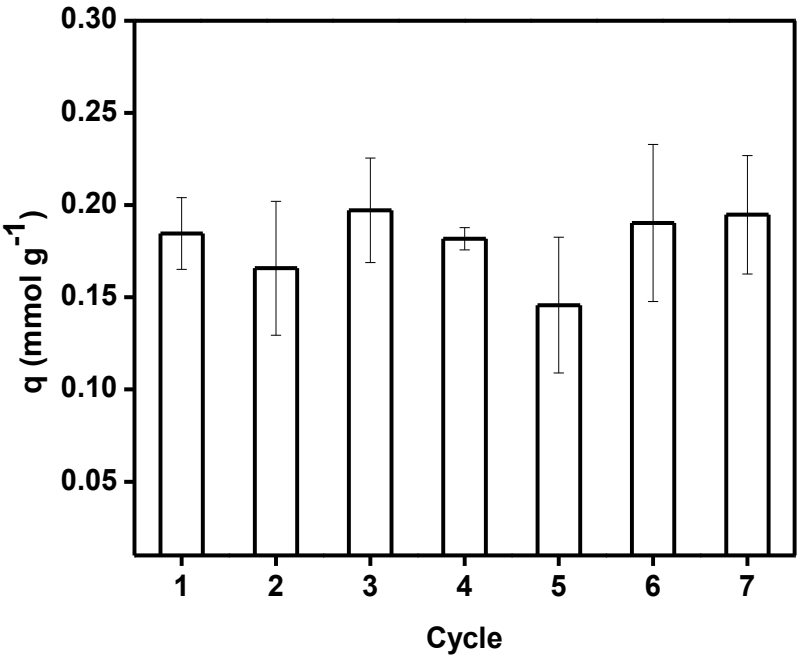

Figure 3.29. Reusability of SILP [Hbet-STFSI-PS-DVB] by desorption with 2 mL of 1 mol L^{-1} H_2SO_4, previously loaded with ≈ 0.2 mmol g^{-1} of Sc(III). Sorption/desorption time 30 min, 300 rpm, room temperature.

The reproducibility of the results was achieved probably due to the covalent bonding of the IL onto the support. This additionally confirmed the success in the preparation of a sustainable sorbent material for Sc(III) recovery from acidic aqueous solutions.

3.4 CONCLUSIONS

SILP-based sorbent [Hbet-STFSI-PS-DVB], which was synthesised by covalent linking of the ion pairs, showed good sorption properties for Sc(III) from acidic aqueous solutions. The formation of Sc(III) sulfate complexes resulted in a low sorption efficiency, but high desorption efficiencies. From chloride and nitrate media the sorption was effective and followed a Langmuir sorption isotherm. The pseudo-second-order kinetic model best describes the kinetic sorption processes of Sc(III) by the SILP. In addition, when using the SILP a short contact time was sufficient (15 min) due to the fast sorption kinetics. In the presence of other common impurities such as Fe(III), Al(III) and Ca(II), the highest sorption efficiency of the SILP was found for Sc(III) when equimolar solutions were used. However, in the presence of substantially higher concentrations of Fe(III), the Sc(III) sorption decreased. In batch experiments, the quantitative desorption for the recovery of the Sc(III) sorbed on the SILP with H_2SO_4 was shown and reusability of the SILP without affecting its efficiency after repeating the process seven times. Moreover, the loss of IL to the aqueous phase was prevented. Thus, SILPs can be designed as sorbents for the recovery and separation of targeted elements. The complete separation of Sc(III) from other accompanying elements can be optimised, for instance, in chromatography columns, which is the subject of the next chapter.

3.5 REFERENCES

1 C. R. Borra, Y. Pontikes, K. Binnemans, T. Van Gerven, *Miner. Eng.*, 2015, **76**, 20–27.
2 S. A. Cotton, *Polyhedron*, 1999, **18**, 1691–1715.
3 W. Wang, Y. Pranolo and C. Y. Cheng, *Hydrometallurgy*, 2011, **108**, 100–108.
4 EMC Metals Corporation, http://www.scandiummining.com/i/pdf/Scandium-White-PaperEMC-Website-June-2014-.pdf. Accessed on 01.02.2017.
5 K. Binnemans, P. T. Jones, B. Blanpain, T. Van Gerven, Y. Pontikes, *J. Clean. Prod.*, 2015, **99**, 17-38.
6 Y. Liu, R. Naidu, *Waste management (N.Y.)*, 2014, **34**, 2662-2673.
7 B. Onghena, K. Binnemans, *Ind. Eng. Chem. Res.*, 2015, **54**, 1887-1898.
8 M. T. Ochsenkühn-Petropoulou, K. S. Hatzilyberis, L. N. Mendrinos, C. E. Salmas, *Ind. Eng. Chem. Res.*, **2002**, 41, 5794-5801.
9 W. Wang, C. Y. Cheng, *J. Chem. Technol. Biotechnol.*, 2011, **86**, 1237-1246.

10 N. Van Nguyen, A. Iizuka, E. Shibata, T. Nakamura, *In: Proceedings of the World Congress on Mechanical, Chemical, and Material Engineering*, 20-21 July 2015, Barceloona, Spain, 338-1 - 338-4.
11 J. P. Faris, J. W. Warton, *Anal. Chem.*, 1962, **34**, 1077-1080.
12 V. Korovin, Y. Shestak, *Hydrometallurgy*, 2009, **95**, 346-349.
13 Z. Zhao, Y. Baba, W. Yoshida, F. Kubota, M. Goto, *J. Chem. Technol. Biotechnol.*, 2016, 2779–2784.
14 J. Jerez, A. C. Isaguirre, C. Bazan, L. D. Martinez, S. Cerutti, *Talanta*, 2014, **124**, 89-94.
15 H. Zhou, D. Li, Y. Tian, Y. Chen, *Rare Met.*, 2008, **27**, 223-227.
16 J. Ma, Z. Wang, Y. Shi, Q. Li, *RSC Adv*., 2014, **4**, 41597-41604.
17 A. N. Turanov, V. K. Karandashev, N. S. Sukhinina, V. M. Masalov, G. A. Emelchenko, *J. Environ. Chem. Eng.*, 2016, **4**, 3788-3796.
18 K. K. Yadav, D. K. Singh, M. Anitha, L. Varshney, H. Singh, *Sep. Purif. Technol.*, 2013, **118**, 350-358.
19 A. N. Turanov, V. K. Karandashev, A. N. Yarkevich, Z. V. Safronova, Russ. *J. Inorg. Chem.*, 2010, **55**, 1305-1311.
20 S. Shahida, A. Ali, M. H. Khan, *J. Iran. Chem. Soc.*, 2013, **10**, 461-470.
21 L. Zhu, Y. Liu, J. Chen, W. Liu, *J. Appl. Polym. Sci.*, 2011, **120**, 3284-3290.
22 S. Riaño, K. Binnemans, *Green Chem.*, 2015, **17**, 2931-2942.
23 T. Vander Hoogerstraete, S. Wellens, K. Verachtert, K. Binnemans, *Green Chem*., 2013, **15**, 919-927.
24 S. Wellens, B. Thijs, K. Binnemans, *Green Chem.*, 2012, **14**, 1657-1665.
25 P. Davris, E. Balomenos, D. Panias, I. Paspaliaris, *Hydrometallurgy*, 2016, **164**, 125-135.
26 D. Dupont, K. Binnemans, *Green Chem*., 2015, **17**, 856-868.
27 R.-S. Juang, *Proc. Natl. Sci. Counc. ROC(A)*, 1999, **23**, 353-364.
28 L. Zhu, L. Guo, Z.J. Zhang, J. Chen, S.M. Zhang, *Sci. China Chem*., 2012, **55**, 14791487.
29 C. P. Mehnert, R. A. Cook, N. C. Dispenziere, M. Afeworki, *J. Am. Chem. Soc.*, 2002, **124**, 12932-12933.
30 A. Riisager, *J. Catal*., 2003, **219**, 452-455.
31 J.-Q. Wang, X.-D. Yue, F. Cai, L.-N. He, *Catal. Comm.*, 2007, **8**, 167-172.
32 C. Van Doorslaer, J. Wahlen, P. Mertens, K. Binnemans, D. De Vos, *Dalton Trans*., 2010, **39**, 8377-8390.
33 E. Guibal, A. F. Piñol, M. Ruiz, T. Vincent, C. Jouannin, A. M. Sastre, *Sep. Sci. Technol.*, 2010, **45**, 1935-1949.
34 I. L. Odinets, E. V. Sharova, O. I. Artyshin, K. A. Lyssenko, Y. V. Nelyubina, G. V. Myasoedova, N. P. Molochnikova, E. A. Zakharchenro, *Dalton Trans.*, 2010, **39**, 4170-4178.
35 X. Sun, B. Peng, Y. Ji, J. Chen, D. Li, *Sep. Purif. Technol.*, 2008, **63**, 61-68.
36 F. Giacalone, M. Gruttadauria, *ChemCatChem*, 2016, **8**, 664-684.
37 N. Kabay, J. L. Cortina, A. Trochimczuk, M. Streat, *React. Funct. Polym.*, 2010, **70**, 484-496.
38 M. Cox, *Chem. Eng. J*., 2001, **84**, 107-113.
39 T. Vincent, A. Parodi, E. Guibal, S*ep. Purif. Technol.*, 2008, **62**, 470-479.
40 A. Ahmad, J. A. Siddique, M. A. Laskar, R. Kumar, S. H. Mohd-Setapar, A. Khatoon, R. A. Shiekh, *J. Environ. Sci. China*, 2015, **31**, 104-123.

41 H. Matsunaga, A. A. Ismail, Y. Wakui, T. Yokoyama, *React. Funct. Polym*., 2001, **49**, 189-195.
42 Q. Cai, W.-Y. Lin, F.-S. Xiao, W.-Q. Pang, X.-H. Chen, B.-S. Zou, *Microp. Mesop. Mat.*, 1999, **32**, 1-15.
43 P. Nockemann, B. Thijs, K. van Hecke, L. Van Meervelt, K. Binnemans, *Cryst. Growth Des.*, 2008, **8**, 1353-1363.
44 J. Goworek, A. Kierys, W. Gac, A. Borówka, R. Kusak, *J. Therm. Anal. Calorim.*, 2009, **96**, 375–382.
45 S. Liang, J. Xu, J. Chen, *J. Therm. Sci.*, 2004, **13**, 187–192.
46 D. Depuydt, W. Dehaen, K. Binnemans, *Ind. Eng. Chem. Res.*, 2015, **54**, 8988–8996.
47 J. S. Preston, *Hydrometallurgy*, 1985, **14**, 171–188.
48 T. Vander Hoogerstraete, B. Onghena, K. Binnemans, *Int. J. Mol. Sci.*, 2013, **14**, 21353–21377.
49 A. El Kadib, P. Hesemann, K. Molvinger, J. Brandner, C. Biolley, P. Gaveau, J. J. E. Moreau, D. Brunel, *J. Am. Chem. Soc.*, 2009, **131**, 2882–2892.
50 P. R. Haddad, P. E. Jackson, *Ion Chromatography. Principles and applications*, Elsevier, Amsterdam, 1st edn., 1990.
51 P. Nockemann, B. Thijs, S. Pittois, J. Thoen, C. Glorieux, K. Van Hecke, L. Van Meervelt, B. Kirchner, K. Binnemans, *J. Phy. Chem. B*, 2006, **110**, 20978–20992.
52 G. W. Bodammer, R. Kunin, *Industr. Eng. Chem.*, 1953, **45**, 2577–2580.
53 R. Bogoczek, E. Kociolek Bagawejlek, *React. Polym.*, 1987, 57–62.
54 L. J. Bellamy, *The Infra-red Spectra of Complex Molecules*, Chapman and Hall Ltd., London, 1975.
55 R. Hema Krishna, A.V.V.S Swamy, *Int. J. Eng. R&D*, 2012, **4**, 29–38.
56. N. Takeno, http://www.eosremediation.com/download/Chemistry/Chemical%20Properties/Eh_pH_Diagrams.pdf. Accessed on 01.02.2017.
57 J. Roosen, S. Van Roosendael, C. R. Borra, T. Van Gerven, S. Mullens, K. Binnemans, *Green Chem.*, 2016, **18**, 2005–2013.
58 J. Liu, X. Yang, X. Cheng, Y Peng, H Chen, *Anal. Methods*, 2013, **5**, 1811–1817.
59 J. Zhang, B. Zhao, B. Schreiner, *Separation and hydrometallurgy of rare earth elements*, Springer, Cham, Switzerland, 2016.
60 S. Schrodle, W. Wachter, R. Buchner, G. Hefter, *Inorg. Chem.*, 2008, **47**, 8619–8628.
61 B. N. Kumar, S. Radhika, M. L. Kantam, B. R. Reddy, *J. Chem. Technol. Biotechnol.*, 2011, **86**, 562–569.
62 G. Alberti, V. Amendola, M. Pesavento, R. Biesuz, *Coord. Chem. Rev.*, 2012, **256**, 28–45.
63 Sidney W. Benson, *The Foundations of Chemical Kinetics*, McGRAW - Hill Book Company, INC, New York, USA, 1960.
64 Y.S. Ho, G. McKay, *Proc. Biochem.*, 1999, **34**, 451–465.
65 N. Van Nguyen, A. Iizuka, E. Shibata, T. Nakamura, *Hydrometallurgy*, 2016, **165**, 51–56.
66 D.I. Srnirnov, T.V. Molchanova, *Hydrometallurgy*, 1997, **45**, 249–259.
67 R. Navarro, I. Saucedo, C. Gonzalez, E. Guibal, *Chem. Eng. J.*, 2012, **185-186**, 226–235.
68 A. R. Vaino, K. D. Janda, *J. Comb. Chem.*, 2000, **2**, 579–596.
69 X.Y. Yang,.P. Zhang, L. Guo, H. Zhao, Y. Zhang, J. Chen, *Transac. Nonferr. Met. Soc. China*, 2012, **22**, 3126–3130.
70 J. K. R.M Barrer, *J. Chem. Soc., Faraday Trans., 1*, **0**, 2080–2091.

71 D.W. Smith, *J. Chem. Educ.*, 1977, **54**, 540–542.
72 B. J. Teppen, D.M. Miller, *Soil Sci. Soc. Am. J.*, 2006, **70**, 31–40.
73 C. R. Borra, B. Blanpain, Y. Pontikes, K. Binnemans, T. Van Gerven, *J. Sustain. Metall.*, 2016, **2**, 28–37.
74 W. Zhang, R. Koivula, E. Wiikinkoski, J. Xu, S. Hietala, J. Lehto, R. Harjula, http://conference2015.redmud.org/wp-content/uploads/2015/10/PS7_Preliminary-investigation-of-rare-earth-separation-by-titanium-phosphate-materials.pdf. Accessed on 02.03.2017.
75 W. Zhang, R. Koivula, E. Wiikinkoski, J. Xu, S. Hietala, J. Lehto, R. Harjula, *Sustainable Chem. Eng.*, 2017, **5**, 3103–3114.
76 P. Coletti, Advanced statistics, http://www.paolocoletti.it/books/AdvancedStatistics.pdf. Accessed on 10.03.2017.

Chapter 4

Efficient separation of rare earths recovered by a supported ionic liquid from bauxite residue leachate

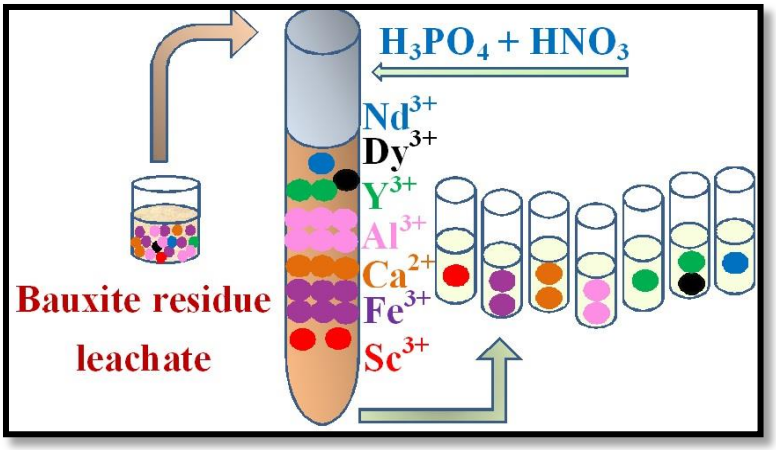

Rare earths are separated from base metals in bauxite residue leachate by a supported ionic liquid phase.

This chapter is based on the published paper:

Avdibegović D., Regadío M., Binnemans K. (2017). Efficient separation of rare earths recovered by a supported ionic liquid from bauxite residue leachate, *RSC Advances*, **8**, 11886–11893.

The text may contain slight adjustments compared to the original publication.

Author contributions:

K.B., M.R. and D.A. conceived the research. D.A. conducted all experiments and wrote the manuscript. All the authors commented on the manuscript.

ABSTRACT

Bauxite residue (BR) contains substantial concentrations of rare-earth elements (REEs), but their recovery is a challenge. Acidic BR leachates typically comprise much higher concentrations of base elements (g L^{-1}) than those of the REEs (mg L^{-1}). Thus, sorbents that are highly selective for the REEs over the base elements are required for the separation. The novel supported ionic liquid phase (SILP) betainium sulfonyl(trifluoromethanesulfonylimide) poly(styrene-*co*-divinylbenzene) [Hbet-STFSI-PS-DVB] was evaluated for the uptake of REEs (Sc, Y, Nd, Dy) in the presence of base elements (Ca, Al, Fe) from BR leachates. Breakthrough curves from acidic nitrate and sulfate media were investigated, as both HNO_3 and H_2SO_4 are commonly used for leaching of BR. The SILP exhibited a superior affinity for REEs in both media, except in the case of Sc(III) from the sulfate feed. The recovery rates of the trace amounts of REEs from the real nitrate feed were remarkably high (72–100%) *via* a simple chromatography separation, without requiring complexing agents or a pretreatment for the removal of interfering elements. The REEs were purified from the base elements and separated into three sub-groups (scandium, light REEs and heavy REEs) by an optimized elution profile with H_3PO_4 and HNO_3 in a single chromatographic separation step.

4.1 INTRODUCTION

The rare-earth elements (REEs) are nowadays considered as strategic elements because of their importance for modern technology and clean-tech applications.[1,2] REEs deposits in China and the United States constitute the largest percentage of REE economic resources worldwide.[1] In fact, China is the major supplier of REEs to the European Union.[3] European Union complete dependency on the REEs import classifies REEs as critical materials and enforces the search for innovative recycling schemes.

Bauxite residue (BR) or red mud is a by-product generated after alkali leaching of bauxite for alumina production in the Bayer process.[4–8] The variation in BR composition is extremely wide but generally BR is rich in Fe_2O_3 (5 - 60 wt%), Al_2O_3 (5 - 30 wt%), TiO_2 (0.3 – 15 wt%), CaO (2 – 14 wt%), SiO_2 (3 – 50 wt%) and Na_2O (1 – 10 wt%).[9,10] Apart from the base elements, BR comprises trace amounts of REEs. In the Bayer process REEs pass almost entirely from bauxite into the BR.[11] For instance, Sc and Y concentrations in a typical BR are 121 g tonne^{-1} and 75.7 g tonne^{-1}, respectively.[12] These values exceed the reported concentrations of Sc (48.9 g tonne^{-1}) and Y (18.8 g tonne^{-1}) in the ion-sorption REE ore from the Yunnan Province of China.[13] Considering its high annual production (140 million tonnes), BR represents an interesting and valuable by-product for REEs recovery. Leaching of BR with mineral acids is a frequent process prior to REEs recovery by solvent extraction or ion exchange.[12,14–20] The leaching process depends on the type of BR since its mineralogical composition is complex and comprises some minerals which are present in the bauxite and others that are produced during the Bayer process.[9,18,21] The leachates typically have high concentrations of base elements that are normally present in the BR and significantly lower concentrations of REEs.[10,12,18,22] This diversity of compounds and concentration range of the REEs in the BR leachates makes the REE recovery and separation a challenging task.

Previously the synthesis of the novel supported ionic liquid phase (SILP) betainium sulfonyl(trifluoromethanesulfonylimide) poly(styrene-co-divinylbenzene) [Hbet-STFSI-PS-DVB] by covalent bonding of ion pairs onto the PS-DVB matrix was described (Figure 4.30).[23] The SILP was specially designed for the efficient Sc(III) uptake from acidic solutions. The SILP

stands out for its fast sorption kinetics and higher Sc(III) uptake in the presence of equimolar concentrations of Ca(II), Al(III) and Fe(III). In the present paper, the possibility of REEs recovery and separation from BR leachates by the SILP and column chromatography operation was further explored.

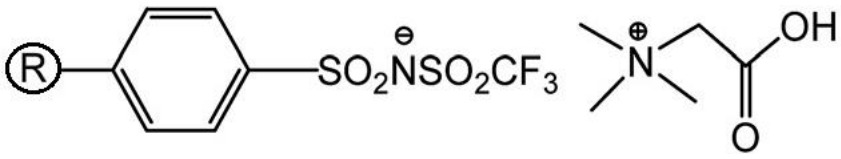

Figure 4.30. Structure of the SILP betainium sulfonyl(trifluoromethanesulfonylimide) poly(styrene-*co*-divinylbenzene) [Hbet-STFSI-PS-DVB].

4.2 EXPERIMENTAL

4.2.1 Chemicals

Nitric acid (65%), $Al_2(SO_4)_3 \cdot 18H_2O$ (100-110%), standard solutions of scandium, yttrium, neodymium, dysprosium, lanthanum, gallium, aluminum, iron, titanium, silicium and calcium (1000 ± 10 µg mL^{-1}) were purchased from Chem-Lab NV (Zedelgem, Belgium). $Sc(NO_3)_3 \cdot 5H_2O$ (99.9%), $Nd(NO_3) \cdot 6H_2O$ (99.9%), $Dy(NO_3) \cdot 6H_2O$ (99.9%) and $YCl_3 \cdot 6H_2O$ (99.9%) were purchased from Strem Chemicals (Newburyport, USA). $CaSO_4 \cdot 2H_2O$, $FeNO_3 \cdot 9H_2O$ (>99%), $Fe_2(SO_4)_3 \cdot xH_2O$ (p.a.) were purchased from Vel (Leuven. Belgium). $Nd_2(SO_4)_3 \cdot xH_2O$ (99.9%) and $CaCO_3$ (99.999%) were purchased from Alfa Aesar (Karlsruhe, Germany). $DyCl_3 \cdot 6H_2O$ (99.9%) was purchased from abcr (Karlsruhe, Germany). $Al(NO_3)_3 \cdot 9H_2O$ (>98.5%) was purchased from Sigma-Aldrich (Steinheim, Germany). Phosphoric acid (85%) was purchased from Ashland Chemicals (Columbus, USA). Betaine hydrochloride (99 %), triethylamine (99%), and sulfuric acid (96%) were purchased from Acros Organics (Geel, Belgium). Sodium hydroxide (97%) was purchased from VWR (Leuven, Belgium). Polystyrene-divinylbenzene

(PS-DVB) sulfonyl chloride resin (0.91 mmol g^{-1}, 200-400 mesh) was purchased from RappPolymere (Tübingen, Germany). Trifluoromethanesulfonamide (98%) was purchased from J&K Scientific GmbH (Pforzheim, Germany). Dichloromethane (DCM) (*p.a.*) and acetone (*p.a.*) were purchased from Fisher Chemical (Loughborough, UK). Sc_2O_3 (99.99%) was kindly provided by Solvay (La Rochelle, France). Hydrated $Sc_2(SO_4)_3$ was prepared from Sc_2O_3 as previously described in the literature.[24] Hydrated $Y_2(SO_4)_3$ and $Dy_2(SO_4)_3$ were prepared in the same manner from YCl_3 and $DyCl_3$, respectively. $Ca(NO_3)_2$ was prepared from $CaCO_3$ by dissolution in HNO_3. The concentrations of the stock solutions were measured by TXRF or ICP-OES (see next section).

4.2.2 Equipment

Batch sorption experiments were performed using a VWR International water bath shaker (Type 462-0355). A fraction collector CF-2 (Spectrum Laboratories, Inc.) equipped with drop sensor and IPC 8-channel peristaltic pump (ISMATEC) was used for sampling during the chromatography studies. An inductively coupled plasma - optical emission spectrometer (ICP-OES) (Perkin Elmer OPTIMA 8300) was used to measure concentrations of elements in the solutions. The calibration solutions and all samples were prepared by dilution with 2 wt% HNO_3. Lanthanum (5 ppm) was used as an internal standard. The following spectral lines were used for quantification (wavelengths in nm): Ca 317.933, Fe 238.204, Sc 361.383, Y 371.029, Al 308.215, Nd 401.225, Dy 394.468, Si 251.611, Ti 334.940, La 408.672.

4.2.3 Batch sorption tests

Typically, 0.050 g of the SILP (32 wt% of moisture) was placed in a 20 mL glass vial and 10 mL of synthetic equimolar feed solution of Sc(III), Y(III), Nd(III) and Dy(III) with total concentration of 1.2 mmol L^{-1} and with previously adjusted pH was added. The samples were shaken for 90 minutes at room temperature and 300 rpm. Further, the samples were filtered through a syringe filter with 0.20 μm pore size. The filtrate was then diluted to an appropriate

concentration for ICP-OES analysis, typically 10 times, with 2 wt% HNO_3 prior to the measurement. The amount of metal ions sorbed onto the SILP was calculated from *Eq. 1.1* (1.3.1.1) and the separation factors from the *Eq. 1.4* and *Eq. 1.5* (Page 17, 1.3.1.1).

4.2.4 Column chromatography tests

A gravity flow glass column (BIO-RAD) of 30 cm length and 0.7 cm diameter was used in chromatography separation experiments. The column was packed with the SILP (1.36 g of the SILP, dry mass) by a wet method to a bed volume (*BV*) of approximately 10.8 mL. Unless otherwise stated, the SILP was preconditioned with HNO_3 or H_2SO_4 solution (pH = 1.5) prior to each experiment. For breakthrough curve experiments, a 1.1 mmol L^{-1} equimolar solution of Sc, Y, Nd, Dy, Fe, Al, Ca in nitrate or sulfate media (initial pH, pH_{ini} = 1.5) was pumped through the column until complete saturation of the SILP was reached. For optimisation of the separation process, 10.0 mL of an equimolar solution was loaded onto the SILP. The pH_{ini} was set to 1.5 to mimic the sorption from acidic BR leachates. To remove possible impurities in the sample tubes, HNO_3 or H_2SO_4 was loaded prior to the eluting agent for the subsequent separation process. Typically, 5 mL of the corresponding acid with pH equal to the pH_{ini} of the sample was used. Prior to and after loading of the real BR leachate, 15.0 mL of HNO_3 (pH = 1.2) was used for the preconditioning and washing step. For each experiment, 5.0 mL fractions were collected and analysed by ICP-OES. The recovery of metal ions (%) was calculated from the equation *Eq. 1.11* (Page 19, 1.3.1.2). All column chromatography experiments were conducted at room temperature. Unless otherwise stated, the flow rate was set at 0.5 mL min^{-1}. This value corresponds to a space velocity (*SV*) of 2.7 h^{-1} [ratio of the volumetric flow rate (mL h^{-1}) to the *BV* (mL)].[25]

4.2.5 Leaching of bauxite residue

A sample of BR was kindly provided by Aluminium of Greece (Agios Nikolaos, Greece).[12] The characterisation of Greek BR has been previously reported in several studies.[12,15,26] The leaching

of BR was performed as described in previous studies.[12] About 4 g of BR was air-dried for 20 hours at 105 °C. An amount of 20.0 mL of 0.7 mol L^{-1} HNO_3 was added to 2.00 g of BR. The mixture was shaken for 6 hours on a Thermo Fisher shaker at 250 rpm at room temperature. The samples were filtered through a 0.20 μm pore size syringe filter and 2.0 mL of the freshly prepared leachate was used for a chromatography separation experiment.

4.3 RESULTS AND DISCUSSION

The effect of the solution pH on the REEs sorption was studied in batch sorption tests with the SILP from nitrate and sulfate synthetic solution, as the pH is one of the predominant parameters that can affect the sorption by the SILP. Moreover, for the study of REEs purification from the base elements, sorption and elution tests of the SILP in a column setup were performed with synthetic nitrate and sulfate multi-element equimolar solutions. Finally, the performance of the SILP for REEs separation and purification was studied and verified with the real HNO_3 BR leachate.

4.3.1 Sorption of REEs by the SILP in batch experiments

HNO_3 and H_2SO_4 are commonly used for BR leaching.[12,16,22] In different media, different REEs complexes form, which might affect the REEs uptake and selectivity. Therefore, the sorption experiments were initially conducted batchwise from both nitrate and sulfate media.[27] It was confirmed that the SILP can sorb the REEs under acidic conditions from both media (Figure 4.31). With the increase in the equilibrium pH value (pH_{eq} from 0.5 to 2.5), the amount of the REEs sorbed by the SILP increased. The uptake of Sc(III) was less pronounced than that of other REEs at $pH_{eq} < 2.5$. The small ionic radius of Sc(III) and therefore high charge density and hydration enthalpy might partially explain the lower uptake of Sc(III).[27–29]

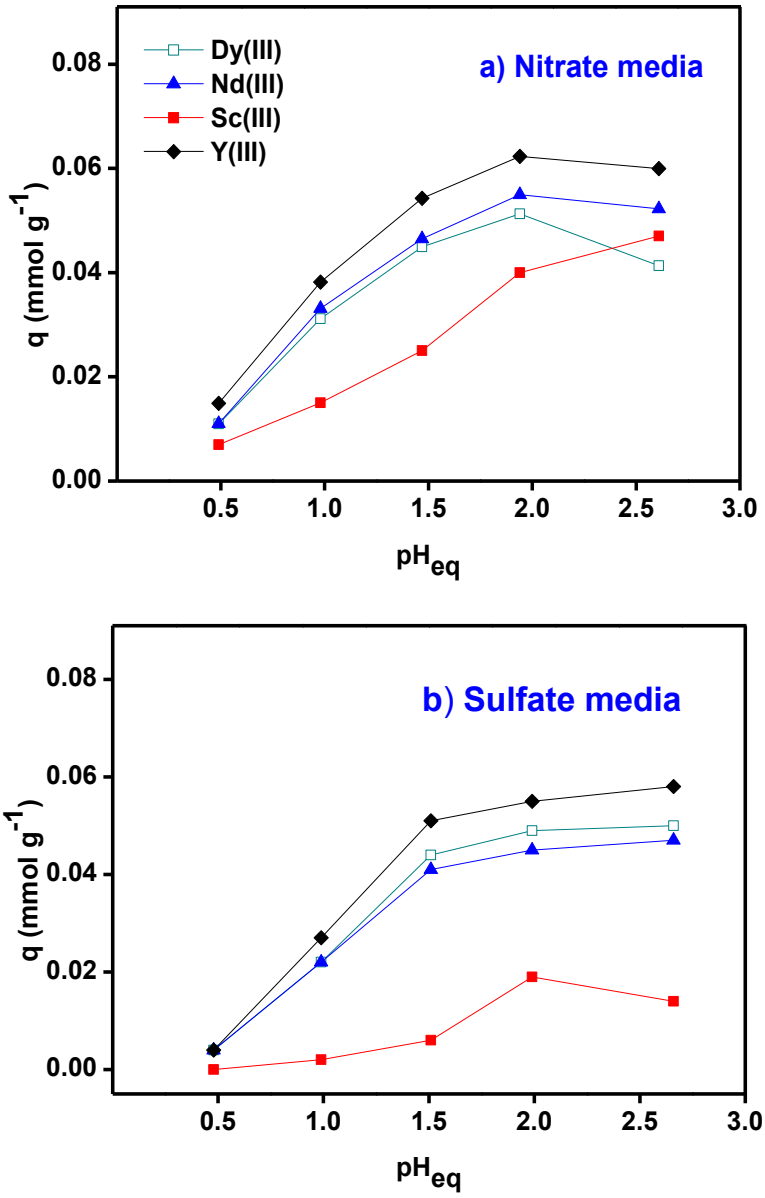

Figure 4.31. Sorption of REEs by the SILP from multi-element equimolar solution (total $c \approx 1.2$ mmol L^{-1}) as a function of the equilibrium pH from (a) nitrate and (b) sulfate media. The relative standard deviation (RSD) of triplicate measurement by ICP-OES was lower than 3%.

In the presence of sulfate anions Sc(III) can form negatively charged sulfato complexes which cannot undergo cation exchange with the proton of the SILP.[22,30] Therefore, in the sulfate media the resulting q was < 0.02 mmol g^{-1}. As a result, the calculated separation factors (*Eq. 1.4* and

Eq. 1.5, Page 17, 1.3.1.1) between Sc(III) and other REEs were up to 4.2. The other three investigated REEs, Dy(III), Nd(III) and Y(III), were sorbed to a similar extent resulting in low separation factors (from 1.1 to 1.5). Thus, to improve the separation of the REEs by the SILP, column chromatography needed to be considered (*vide infra*).

4.3.2 Breakthrough curves by the SILP in a fixed bed column

The preferential uptake and dynamic loading capacity of the SILP were estimated based on breakthrough curves with the assumption of a Langmuir isotherm (Figure 4.32). The breakthrough point was set at c/c_0 = 0.05 and the exhaustive point at c/c_0 = 1. Generally, a high preferential uptake of REEs by the SILP was evident from the high values of bed volume (*BV*) at the breakthrough and exhaustive points (Table 4.6). In the case of the sulfate feed, the uptake affinity order at a space velocity *SV* = 2.7 h^{-1} was: Sc(III) < Fe(III) < Ca(II) < Dy(III) < Al(III) < Y(III) < Nd(III). As elucidated from the batch sorption experiments (Figure 4.31), the SILP exhibited low affinity for Sc(III) from the sulfate media and high affinity for the other REEs. The uptake affinity order from the nitrate feed at *SV* = 2.7 h^{-1} was favorable for all REEs compared to the base metals: Ca(II) < Al(III) ≈ Fe(III) < Sc(III) < Y(III) ≈ Dy(III) < Nd(III). The SILP was then tested at *SV* = 10.8 h^{-1} (flow rate of 2.0 mL min^{-1}) to simulate a *SV* value within the typical range used for commercial sorbents applied in metal recovery (between 5 and 40 h^{-1}).[25] The breakthrough points (*BV* = 6.04) were equal for Fe(III), Sc(III), Y(III) and Dy(III). The *BVs* at the exhaustive points followed a similar order as at *SV* = 2.7 h^{-1}: Ca(II) < Al(III) < Sc(III) < Fe(III) < Y(III) < Dy(III) < Nd(III). A higher *BV* at the exhaustive point for Fe(III) compared to the *BV* for Sc(III) at *SV* = 10.8 h^{-1} indicates that the kinetics of the Fe(III) sorption are faster.

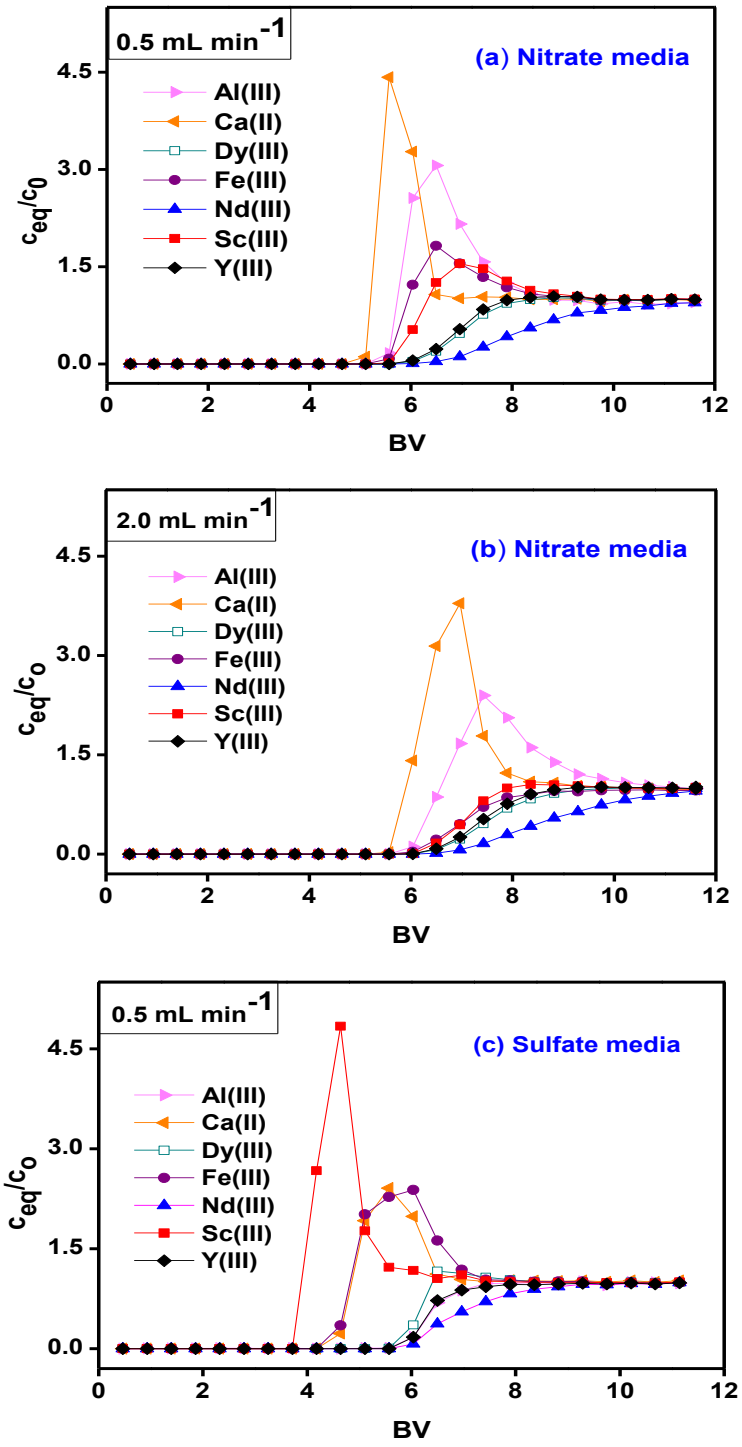

Figure 4.32. Breakthrough curves as a function of bed volume (*BV*) from (a) nitrate media at 0.5 mL min^{-1}, (b) nitrate media at 2.0 mL min^{-1} and (c) sulfate media at 0.5 mL min^{-1}. Feed 1.1 mmol L^{-1} multi-element equimolar solution. pH_{ini} = 1.5. pH_{eq} ranges from 1.2 to 1.5.

Sorption capacities at the breakthrough ($q_{0.05}$) and exhaustive point (q) were investigated under acidic conditions (pH = 1.5). The average $q_{0.05}$ value of 0.345 mmol g^{-1} calculated from the three breakthrough curves (Table 4.6) (RSD = 10.4%), and the average q value of 0.409 mmol g^{-1} (RSD = 15.8%) are comparable with sorption capacities of cation-exchange resins and sorbents used for REEs recovery.[16,31] The sorption capacity at $SV = 10.8\ h^{-1}$ did not significantly differ from the sorption capacity at $SV = 2.7\ h^{-1}$. The fast sorption kinetics indicated practical applicability of the SILP.

Table 4.6. Summary of bed volumes (BV) and sorption capacities $q_{0.05}$ and q at breakthrough and exhaustive point, respectively: (a) nitrate feed at 0.5 mL min^{-1} ($SV = 2.7\ h^{-1}$), (b) nitrate feed at 2.0 mL min^{-1} ($SV = 10.8\ h^{-1}$) and (c) sulfate feed at 0.5 mL min^{-1} ($SV = 2.7\ h^{-1}$).

	BV (mL) at $c/c_0 = 0.05$			BV (mL) at $c/c_0 = 1$			$q_{0.05}$ (mmol g^{-1})			q (mmol g^{-1})			$q_{0.05}/q$		
	a	b	c	a	b	c	a	b	c	a	b	c	a	b	c
Ca(III)	4.64	5.57	4.64	5.57	6.04	5.11	0.047	0.057	0.042	0.051	0.062	0.045	0.918	0.919	0.921
Al(III)	5.11	5.57	5.57	6.04	6.96	7.43	0.035	0.046	0.042	0.038	0.050	0.050	0.929	0.923	0.841
Fe(III)	5.11	6.04	4.18	6.04	8.82	5.11	0.050	0.057	0.045	0.054	0.073	0.048	0.928	0.776	0.933
Sc(III)	5.57	6.04	3.71	6.50	8.36	4.18	0.045	0.052	0.029	0.050	0.064	0.029	0.892	0.821	1.000
Y(III)	6.04	6.04	5.57	8.36	9.29	11.1	0.059	0.066	0.057	0.070	0.084	0.065	0.846	0.779	0.888
Dy(III)	6.04	6.04	5.57	8.82	10.2	6.50	0.051	0.046	0.050	0.058	0.060	0.057	0.887	0.766	0.880
Nd(III)	6.50	6.50	5.57	11.6	12.1	11.1	0.058	0.058	0.044	0.081	0.085	0.054	0.711	0.686	0.811

The vast majority of sorbents reported in the literature show higher affinity towards heavy REEs.[6,31–33] With the SILP, Nd(III) sorption resulted in the highest BV at breakthrough and exhaustive point and the lowest $q_{0.05}/q$ ratio under all investigated conditions (Table 4.6) revealing the applicability of the SILP for the recovery and separation of light REEs. It may be assumed that the high preferential uptake of Nd(III) was enabled by high electrostatic interactions between the Nd(III) ion and the carboxylic group on the SILP (compared to the

interactions with Ca(II)). Additionally, the uptake might be enhanced by the lower hydration enthalpy of Nd(III) compared to those of other tested trivalent ions.[29] In the present work the use of complexing agents or volatile solvents was not required for the uptake and selectivity of REEs sorption, contrary to the previously reported processes.[34,35] Therefore, the SILP gives the opportunity to efficiently recover all REEs from acidic nitrate BR leachates in the presence of Ca(II), Al(III) and Fe(III).

4.3.3 Elution curves by the SILP in a fixed bed column

Higher binding constants for REEs than that for base elements in nitrate media were evident from the breakthrough curves (Figure 4.32, Table 4.6). However, in order to obtain purified fractions of REEs by a column chromatography, optimisation of a selective elution had to be considered. Several attempts were made to separate the REEs from the base elements by the SILP. First, the separation was tested with a pH gradient elution with H_3PO_4 (Figure 4.33). The resulting elution sequence was: Sc(III) > Fe(III) > Al(III) > Ca(II) ≈ Dy(III) ≈ Y(III) > Nd(III). Despite their similar properties and challenging separation, Sc(III) was well separated from Fe(III) and moreover completely separated from Al(III), Ca(II) and other REEs. Nearly complete separation of Fe(III) and Al(III) from the other REEs was possible by a pH gradient elution. However, Ca(II) was eluted together with the remaining REEs when applying only H_3PO_4 for elution.

A second elution was then performed with H_3PO_4 and HNO_3 (Figure 4.34). The elution sequence was very similar to the previous one: Sc(III) > Fe(III) > Ca(II) > Al(III) ≈ Dy(III) ≈ Y(III) ≈ Nd(III). Sc(III) and Fe(III) were separated by H_3PO_4. Ca(II) was well separated from the other tested elements by HNO_3 (pH = 0.5). However, with HNO_3 (pH ≤ 0.0), Al(III) was co-eluted with the remaining REEs.

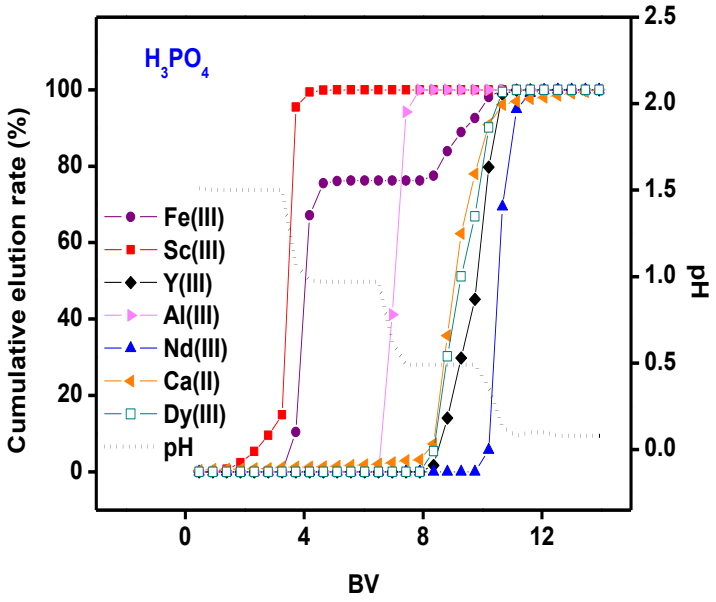

Figure 4.33. pH gradient elution with H_3PO_4 as a function of the bed volume (*BV*). Feed 10.0 mL 1.1 mmol L^{-1} multi-element equimolar solution in nitrate media. Flow rate 0.5 mL min^{1}.

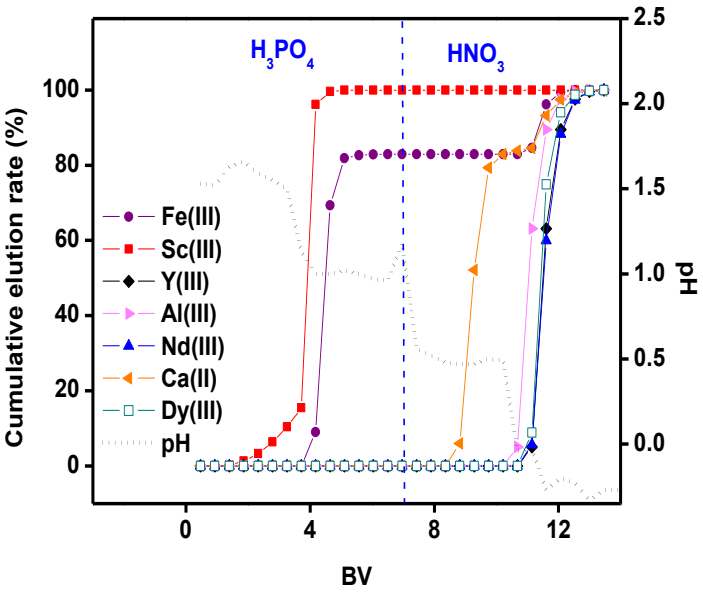

Figure 4.34. pH gradient elution with H_3PO_4 and HNO_3 as a function of the bed volume (*BV*). Feed 10.0 mL of 1.1 mmol L^{-1} multi-element equimolar solution in nitrate media. Flow rate 0.5 mL min^{-1}.

Therefore a third three-step elution profile comprising H_3PO_4 and HNO_3 was applied (Figure 4.35a). First, Sc(III) and Fe(III) were eluted with H_3PO_4 (pH between 1.5 and 1.0). Then Ca(II) was eluted with HNO_3 (pH = 0.5). Lastly, Al(III) was removed by further decreasing pH gradient with H_3PO_4 (pH from 0.5 to 0.1) resulting in a good separation from Dy(III), Y(III) and Nd(III). Moreover, when the REEs were eluted with H_3PO_4, Nd(III)/Dy(III) and Nd(III)/Y(III) molar ratios were much higher than when eluting with HNO_3 (Table 4.7), indicating their better separation with H_3PO_4. Using the same optimal elution profile, but a higher flow rate (2.0 mL min^{-1}) (Figure 4.35b), the molar ratios and therefore the separation between light and heavy REEs decreased (Table 4.7).

Moreover, with the higher elution flow rate Sc(III)/Fe(III) molar ratio and their separation also decreased (Figure 4.35 and Figure 4.36). The contact time between eluent and the sorbent was not sufficient for the effective elution and separation of ions with similar physico-chemical properties.

Optimal elution with H_3PO_4 and HNO_3 was tested as well with the sulfate media (Figure 4.37). The elution trend remained the same as with the nitrate media: Sc(III) > Fe(III) > Ca(II) > Al(III) > Dy(III) ≈ Y(III) > Nd(III). With the sulfate media, Sc(III)/Fe(III) and Nd(III)/REEs molar ratios exceeded the values found when using the nitrate media (Figure 4.36, Table 4.7). The total amount of all elements (n ≈ 0.0077 mmol) in the sulfate feed was much lower than the *q* of the SILP (0.409 mmol g^{-1}). Therefore, the Sc(III) uptake rate was not diminished by the presence of other elements. The lower Sc(III) binding constant from equimolar sulfate feed and consequently lower retention time on the column, improved the Sc(III)/Fe(III) separation. In a similar manner, Y(III) and Dy(III) migrated through the SILP faster than Nd(III) due to stronger electrostatic interactions of the smaller ions of Y(III) and Dy(III) with the sulfate ligand.

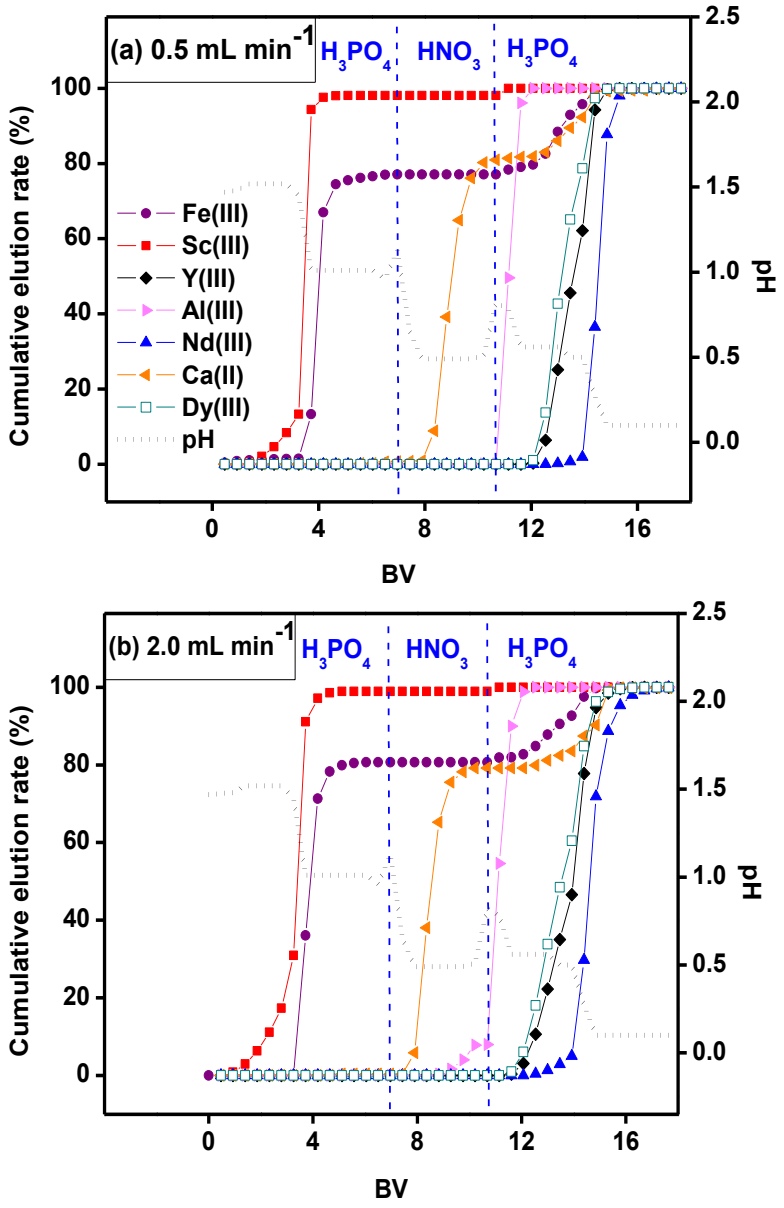

Figure 4.35. Optimised pH gradient elution with H_3PO_4 and HNO_3 as a function of the bed volume (*BV*). Feed 10.0 mL of 1.1 mmol L^{-1} multi-element equimolar nitrate solution. Flow rate (a) 0.5 mL min^{-1} and (b) 2.0 mL min^{-1}.

Table 4.7. Comparison of Nd(III)/Dy(III) and Nd(III)/Y(III) molar ratios in fractions after elution with H_3PO_4 and HNO_3. Feed 10.0 mL of 1.1 mmol L^{-1} multi-element equimolar solutions. pH_{ini} = 1.5.

Eluent	HNO_3	H_3PO_4	H_3PO_4	H_3PO_4
Media	Nitrate	Sulfate	Nitrate	Nitrate
Flow rate, mL min^{-1}	0.5	0.5	0.5	2.0
BV	11.6-12.5	14.9-17.2	14.9	14.9
Nr. of fractions	3	6	1	1
Nd/Dy	0.96	26.8	18.2	3.80
Nd/Y	0.76	13.9	7.85	2.06

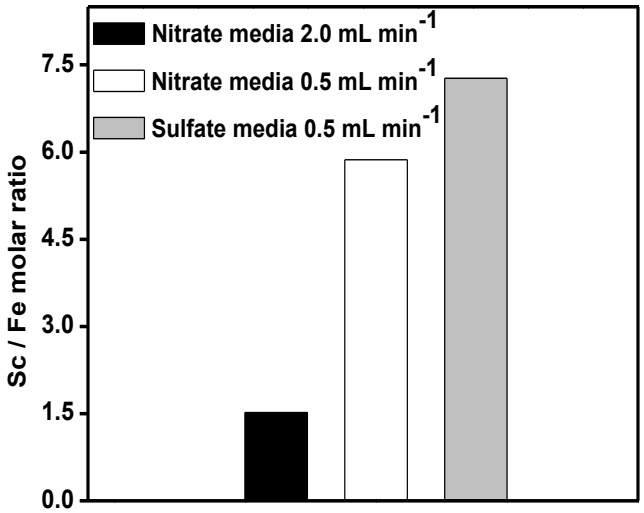

Figure 4.36. Comparison of Sc(III)/Fe(III) molar ratios after chromatography separation from 10.0 mL of 1.1 mmol L^{-1} multi-element equimolar solutions. Eluent 0.12 mol L^{-1} H_3PO_4 (pH = 1.5). *BV* = 3.7 mL, single fraction of 5.0 mL. pH_{ini} = 1.5.

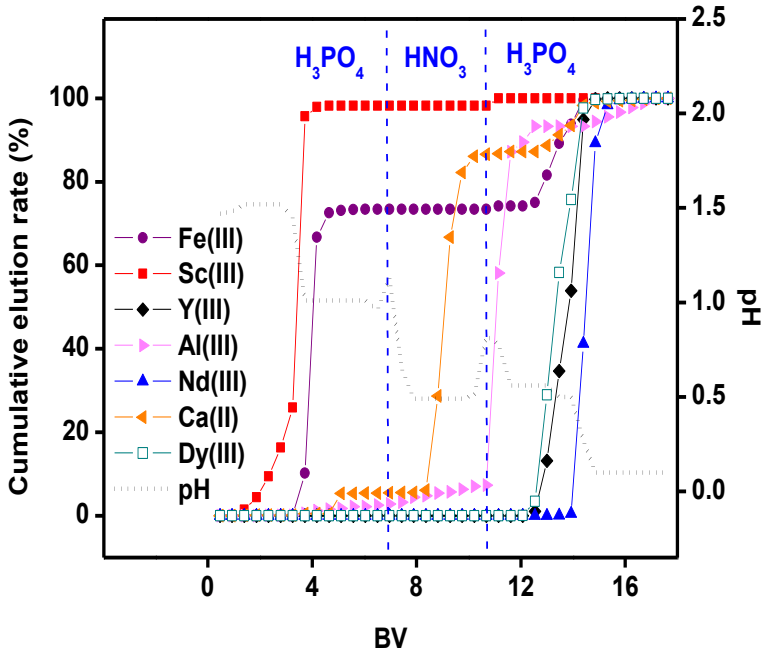

Figure 4.37. Optimized pH gradient elution with H_3PO_4 and HNO_3 as a function of the bed volume (*BV*). Feed 10.0 mL of 1.1 mmol L^{-1} multi-element equimolar solution in sulfate media. Flow rate 0.5 mL min^{-1}.

A promising separation between the REEs and base elements from the synthetic feeds was accomplished by an optimised elution with H_3PO_4 and HNO_3. However, in real BR leachates, the concentrations of the accompanying elements are much higher than those of the REEs. Therefore, a real nitrate leachate was tested (Figure 4.38) and its initial composition and the recovery of elements (*Eq. 1.11*, Page 19, 1.3.1.2) are summarised in the Table 4.8. Trace amounts of Sc(III) and Y(III) (up to 3.7 mg L^{-1}) were effectively recovered by the SILP even in the presence of accompanying elements in concentrations up to 4.9 g L^{-1}. Despite the high affinity of the SILP towards Nd(III), about 29% of Nd(III) was lost during the washing step between the sample and the eluting agent. The extremely complex matrix of the leachate gave rise to diminished Nd(III) uptake. Besides a wide range of base and minor elements, BR comprises a variety of organic compounds derived from bauxite and/or the Bayer process, which can be also present in the leachate.[10] Although Dy(III) could not be detected in the initial feed

composition due to the matrix effects, it was collected in the fractions which were purified from the majority of the compounds initially present.

Table 4.8. Composition of BR leachate and recovery (%) of elements by the SILP.

	Al	Ca	Si	Ti	Fe	Nd	Sc	Y	Dy
Initial concentration (mg L^{-1})	2454	4929	2031	822	611	7.1	3.7	3.2	*
Recovery (%)	97.9	70.9	4.7	18.3	99.1	71.8	100	100	*

*The Dy concentration in the leachate was too low to detect it by ICP-OES in the presence of very high concentrations of other elements, which is natural, since the Dy content in BR is generally low.[12] However, Dy could be quantified in the fractions purified from the major elements.

Most of Si(IV) and Ti(IV) were already removed from the column in the washing step, resulting in a recovery by the SILP of 4.7% and 18.3%, respectively. Probably, the remaining amounts could have been removed by a prolonged washing step between the sample loading and elution. The elution sequence with the real BR leachate was in agreement with the optimised elution sequence tested with the synthetic feed: Si(IV) ≈ Sc(III) > Fe(III) ≈ Ti(IV) > Ca(II) > Al(III) > Dy(III) ≈ Y(III) > Nd(III). Highly concentrated Ca(II) and Al(III) ions migrated faster through the column. Elution of Ca(II) and Al(III) started at eluent pH of 1.5 and 1.0, respectively. Ca(II) elution was enhanced with HNO_3 (pH = 0.5). Compared to the feed, the REEs in the resulting fractions were significantly purified from the major elements in BR (Figure 4.39) and the recovered amounts of REEs from the BR leachate and wt% of impurities in REEs fractions are summarised in the Table 4.9. Equilibrium versus initial molar ratio of Nd(III) towards Ca(II), Fe(III), Al(III) reached values up to 37, 300 and 660, respectively.

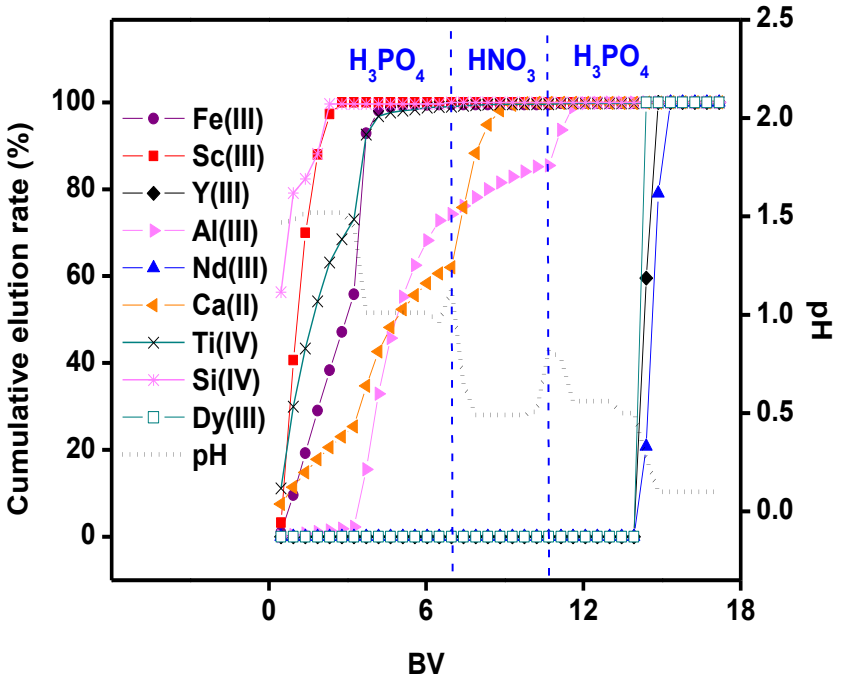

Figure 4.38. pH gradient elution with H_3PO_4 and HNO_3 as a function of the bed volume (*BV*). Feed 2.0 mL of BR leachate with 0.7 N HNO_3. pH_{ini} = 1.2, flow rate of 0.5 mL min^{-1}.

Table 4.9. Summary of REEs quantity and purity in fractions collected after purification by the SILP from 2.0 mL of real BR leachate.

REEs	*m* (mg)	Impurities (wt%)									*V* (mL) H_3PO_4	Ordinal Nr. of fraction	*BV*
		Al	Ca	Dy	Fe	Nd	Sc	Si	Ti	Y			
Sc	0.007	4.25	63.8	0.00	24.0	0.00	0.27	1.18	6.48	0.00	30.0	1–6	0.46–2.79
Y Dy	0.005 0.001	13.9	29.4	2.06	5.33	16.6	0.00	0.24	1.12	12.9	22.5	29–33	13.5–15.3
Nd	0.010	23.6	36.9	1.66	6.90	19.7	0.00	0.20	0.90	10.2	22.5	31–35	14.4–16.2

In a previous study of Sc(III) recovery from the BR, Na_2SO_3 was used for on-column Fe(III) (100 mg L^{-1}) reduction to Fe(II).[36] Moreover, Sc(III) recovery was achieved only after a number

of collected fractions (*e.g.* up to 115 *BV*).[16,36] In those studies other REEs were not considered for recovery and purification. Furthermore, when a commercial cation-exchange resin was used for the recovery of REEs from BR, 4–24% of Y(III) was co-eluted with Sc(III).[37] In the present study with the SILP, Sc(III) was effectively recovered and especially separated from other REEs in only several initial fractions (up to 11 fractions, 5.1 *BV*). Sc(III)/Fe(III) separation can be further enhanced by depleting Fe(III) concentration (611 mg L^{-1}) in the leachate.[14] A good separation of Nd(III), Y(III) and Dy(III) from other elements was achieved (Figure 4.37, Figure 4.38, Table 4.7). The SILP was reused in all conducted experiments (at least 9 times), confirming its high reusability.

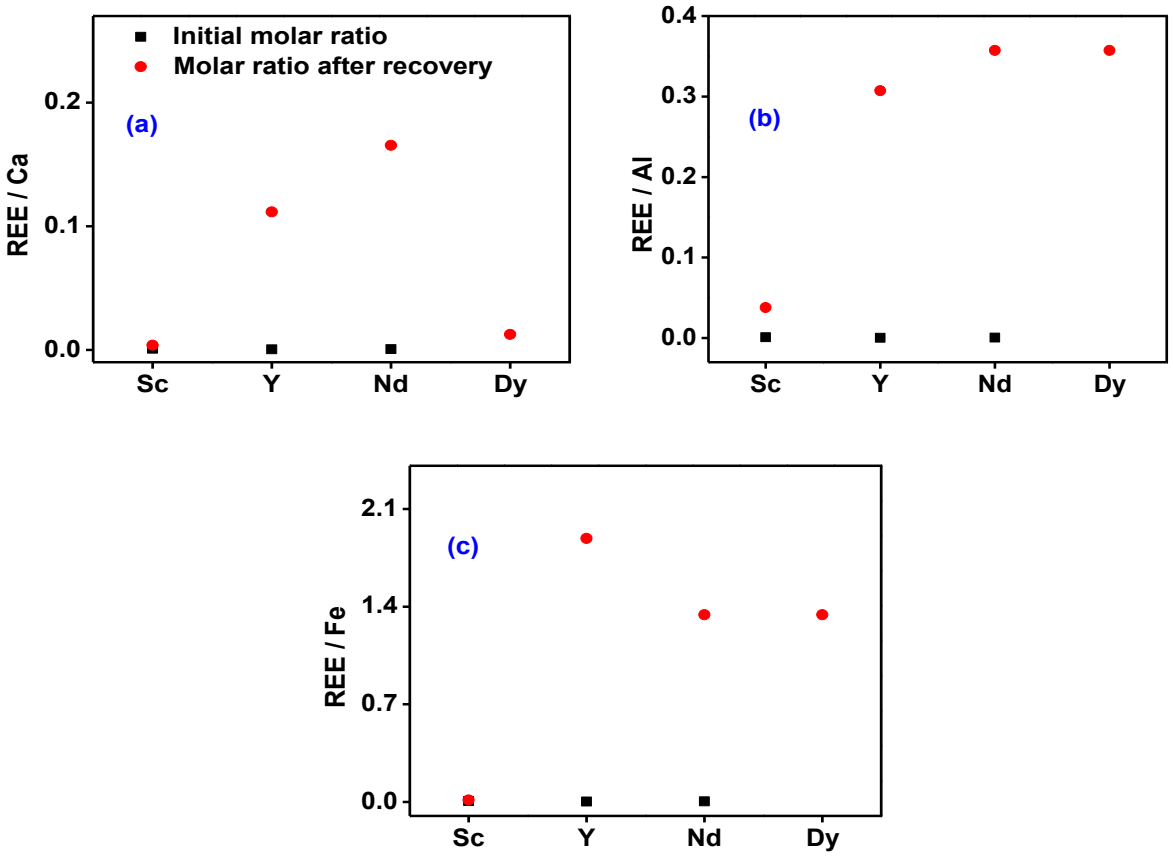

Figure 4.39. Molar ratios between REEs and a) Ca, b) Al, and c) Fe, in the real BR leachate before the recovery by the SILP (■) and in the fractions collected after optimized elution with H_3PO_4 and HNO_3 (●).

The high separation and recovery of elements opens the way to the BR valorization. Note that better results can probably be achieved taking into account that the tested BR leachate was obtained after a non-optimized leaching process. In the present study, the possibility for REEs recovery and separation by the novel SILP from a secondary resource such as BR was explored on a laboratory scale. The results with the leachate were used for a proof–of-concept. The chromatography process with the SILP can be further designed to exploit its maximum performance in terms of REEs separation and purification.[38] The developed separation procedure could be utilised in diverse applications, *e.g.* the recovery of Nd from spent NdFeB magnets or the separation of light from the rest of REE (with higher risk of under-supply), the latter being a key pre-processing step in the production of REEs.

4.4 CONCLUSIONS

The SILP [Hbet-STFSI-PS-DVB] was evaluated for the REEs uptake from acidic nitrate and sulfate media. Breakthrough curve experiments revealed generally preferential uptake of REEs (Sc, Y, Nd, Dy) over the base elements (Ca, Al, Fe) in BR, except in the case of Sc(III) from sulfate media due to its interactions with the sulfate ligands. Fast sorption kinetics indicated a potential applicability of the SILP for a large-scale process. The separation of REEs into three groups (Sc, light REEs and heavy REEs) was achieved by an optimised 3-step pH gradient elution with H_3PO_4 and HNO_3. The elution followed the sequence: Sc(III) > Fe(III) > Ca(II) > Al(III) > Dy(III) ≈ Y(III) > Nd(III). The REEs were enriched and purified from the base elements from the real BR leachate. The recovery and purification results are even more valuable when considering the fact that there was no optimization of the leaching process, neither pretreatments to remove interfering major elements, nor chelating agents to sorb only the elements of interest. Furthermore, the SILP showed high reusability and stability without decreasing the recovery efficiencies. In conclusion, this novel chromatographic method is promising for efficient separation and purification of REEs.

4.5 REFERENCES

1 V. Fernandez, *Resour. Policy*, 2017, **53**, 26-45.
2 K. Binnemans, P.T. Jones, B. Blanpain, T. Van Gerven, Y. Pontikes, *J. Clean. Prod.*, 2015, **99**, 17-38.
3 European Commission, *Report on the critical raw materials for the EU*, 2017, 1-8.
4 Z. Liu, Y. Zong, H. Li, D. Jia, Z. Zhao, *J. Rare Earths*, 2017, **35**, 896-905.
5 P. Smith, *Hydrometallurgy*, 2009, ***98***, 162-176.
6 Z.H. Wang, G.X. Ma, J. Lu, W.P. Liao, D.Q. Li, *Hydrometallurgy*, 2002, **66**, 95-99.
7 S. Liu, X. Guan, S. Zhang, C. Xu, H. Li, J. Zhang, *Mater. Lett.*, 2017, **191**, 222-224.
8 S. Rai, D.H. Lataye, M. J. Chaddha, R.S. Mishra, P. Mahendiran, J. Mukhopadhyay, C.K. Yoo, K.L. Wasewar, *Adv. Mater. Sci. Eng.***,2013**, 2013, 1-7.
9 K. Evans, *J. Sustain. Metall.*, 2016, **2**, 316-331.
10 K. Evans, In: *Y. Pontikes (ed) Proc. Bauxite Residue Valoris. Best Pract. Conf.*, 5–7 October 2015, Leuven (Belgium), 113-127.
11 S. P. Yatsenko, I. N. Pyagai, *Theor. Found. Chem. Eng.*, 2010, **44**, 563-568.
12 C. R. Borra, Y. Pontikes, K. Binnemans, T. Van Gerven, *Miner. Eng.*, 2015, **76**, 20-27.
13 Y. C. Y. Gao, *J. Rare Earths*, 2010, **28**, 622-626.
14 M. Ochsenkuhn-Petropulu, Th. Lyberopulu, T. Ochsenkuhn, G. Parissakis, *Anal. Chim. Acta* 1996, **319**, 249-254.
15 M. Th. Ochsenkühn-Petropoulou, K.S. Hatzilyberis, L.N. Mendrinos, C. E. Salmas, *Ind. Eng. Chem. Res.*, 2002, **41**, 5794-5801.
16 C. R. Borra, B. Blanpain, Y. Pontikes, K. Binnemans, T. Van Gerven, *J. Sustain. Metall.*, 2017, **3**, 393-404.
17 R. M. Rivera, G. Ounoughene, C. R. Borra, K. Binnemans, T. Van Gerven, *Miner. Eng.* 2017, ***112***, 92-102.
18 J. Roosen, S. Van Roosendael, C. R. Borra, T. Van Gerven, S. Mullens, K. Binnemans, *Green Chem.*, 2016, **18**, 2005-2013.
19 A. Akcil, N. Akhmadiyeva, R. Abdulvaliyev, Rinat, P. M. Abhilash, *Miner. Process. Extr. Metall. Rev.*, 2017, **4**, 1-7.
20 S. Reid, J. Tam, M. Yang, G. Azimi, *Sci. Rep.*, 2017, **7**, 15252.
21 P.E. Tsakiridis, S. Agatzini-Leonardou, P. Oustadakis, *J. Hazard. Mater.*, 2004, **116**, 103-110.
22 B. Onghena, C. R. Borra, T. Van Gerven, K. Binnemans, *Sep. Purif. Technol.*, 2017, **176**, 208-219.
23 D. Avdibegović, M. Regadío, K. Binnemans, *RSC Adv.*, 2017, **7**, 49664-49674.
24 J.-G. Li, T. Ikegami, T. Mori, *J. Mater. Res.*, 2003, **18**, 1816-1822.
25 T. Ogata, H. Narita, M. Tanaka, *Hydrometallurgy*, 2015, **155**, 105-109.
26 P. Davris, E. Balomenos, D. Panias, I. Paspaliaris, *Hydrometallurgy*, 2016, **164**, 125-135.
27 J. Zhang, B. Zhao, B. Schreiner, *Separation Hydrometallurgy of Rare Earth Elements*, Springer, Cham, Switzerland, 2016.
28 S. Cotton, *Lanthanide and Actinide Chemistry*, Wiley, Chichester, United Kingdom, 2006.
29 D.W. Smith, *J. Chem. Educ.*, 1977, **9**, 540-542.

30 S. Schrödle, W. Wachter, R. Buchner, G. Hefter, *Inorg. Chem.*, 2008, **47**, 8619-8628.
31 Y. Takahashi, K. Kondo, A. Miyaji, Y. Watanabe, Q. Fan, T. Honma, K. Tanaka, *PLoS One*, 2014, **9**, e114858 (1-15).
32 T. Ogata, H. Narita, M. Tanaka, M. Hoshino, Y. Kon, Y. Watanabe, *Sep. Purif. Technol.*, 2016, **159**, 157-160.
33 B. Nagaphani Kumar, S. Radhika, B. Ramachandra Reddy, *Chem. Eng. J.*, 2010, **160**, 138-144.
34 H. Hubicka, D. Kołodyńska, *Hydrometallurgy*, 2004, **71**, 343-350.
35 J. P. Faris, J. W. Warton, *Anal. Chem.*, 1962, **34**, 1077-1080.
36 W. Zhang, R. Koivula, E. Wiikinkoski, J. Xu, Junhua, S. Hietala, J. Lehto, R. Harjula, Risto, *Sustainable Chem. Eng.*, 2017, **5**, 3103-3114.
37 L.-A. Tsakanika, M. Ochsenkuehn-Petropoulou, In: *Y. Pontikes (ed) Proc. Bauxite Residue Valoris. Best Pract. Conf.*, 5–7 October 2015, Leuven (Belgium), 309-315.
38 T. S. J. Siitonen, *Chem. Eng. Sci.*, 2015, **122**, 436-451.

Chapter 5

Rare earths separation from leach liquor of bauxite residue slag

This chapter is based on the published paper:

Avdibegović D., Regadío M., Rivera R.M., Ounoughene G., Van Gerven T., Binnemans K.

Purification of low concentrations of rare earths from high concentration impurities in leach liquor of bauxite residue slag by a supported ionic liquid phase. In: *Y. Pontikes (ed) Proceedings of the 2nd International Bauxite Residue Valorisation and Best Practices Conference*, 7-10 May 2018, Athens, Greece, 381-386.

The text may contain slight adjustments compared to the original publication.

Author contributions:

K.B., M.R., G.O., T.V.G., R.M.R. and D.A. conceived the research. R.M.R conducted leaching experiments and D.A. conducted column chromatography experiments. D.A. drafted the manuscript. All the authors commented on the manuscript.

ABSTRACT

Liquid-solid extraction is often required in hydrometallurgy for the recovery of trace amounts of valuable metals from leaching solutions. Supported ionic liquid phases (SILPs) are a new class of sorbents which involve covalently attached ionic liquid fragments on the surface of a solid material. In this work, we examined the recovery and separation of rare-earth elements (REEs) from leachate of high-pressure HCl leaching of bauxite residue (BR) slag in a column setup by a specially designed SILP with high affinity for REEs. The SILP showed higher sorption affinity for the selected REEs (Sc(III), Y(III), Nd(III), Dy(III)] than for the base elements [Ca(II), Al(III), Fe(III), Si(IV), Ti(IV)] of BR. Purification of the REEs from the co-sorbed base elements was achieved by a three-step elution with dilute H_3PO_4 and HNO_3. Moreover, Sc(III) was completely separated from Y(III) and other REEs. Nd(III) was enriched over Dy(III) in the collected fractions. This indicates good separations between Sc(III), light REEs, heavy REEs and base metals.

5.1 INTRODUCTION

The rare-earth elements (REEs) seldomly occur in concentrated deposits and no primary production of REEs exists in the European Union (EU). The REEs are one of the most critical raw materials for the EU, due to the EU reliance on Chinese production and its quotas/export taxes.[1] Over 95% of the trace metal value in bauxite residue (BR) is attributed to the presence of REEs and to scandium in particular.[2] For instance, Greek BR contains up to 121 g tonnne^{-1} of scandium.[2] With its high worldwide production rate (140 million tonnes year^{-1}), BR is a potential source of REEs, although the concentration of REEs in BR depends on the type of bauxite deposit.[3]

Compounds consisting entirely of ions, better known as ionic liquids (ILs) are enjoying a strong research interest due to their unique properties.[4] ILs are considered as green, non-volatile, non-flammable compounds with broad electrochemical windows and low melting points. The affinity of metal complexes towards ILs can easily be tuned by careful selection of the cation or anion of the IL. Thus, ILs are increasingly being considered as good candidates for organic solvents in liquid-liquid extraction. The main problem encountered there is that ILs often exhibit a high viscosity, especially after metal loading. This issue can be solved by immobilising ILs on the surface of a solid support, forming supported ionic liquid phases (SILPs) which can be used for liquid-solid extraction.[5] Due to a diversity of available ILs that can be adhered to a variety of solid supports, SILPs can be well-designed for the recovery of targeted species.

We have previously reported the synthesis of the SILP betainium sulfonyl(trifluoromethanesulfonylimide) poly(styrene-*co*-divinylbenzene) [Hbet-STFSI-PS-DVB], which was specially designed for the uptake of the REEs and of scandium in particular.[6,7] The aim of the present work was to validate the performance of this SILP for the recovery and separation of REEs [Sc(III), Y(III), Nd(III), Dy(III)] from a real HCl leachate, obtained after high-pressure acid leaching (HPAL) of a slag generated during smelt reduction of the BR.

5.2 EXPERIMENTAL

A BR sample, kindly provided by Aluminium of Greece (AoG, Agios Nikolaos, Greece), was smelted in an electric arc furnace and in a graphite crucible by adding 10 wt% of graphite powder (99.5% purity), 8 wt% of CaO and 10 wt% of SiO_2 at a temperature of 1500 °C. A slag obtained after the reduction process was then subjected to the HPAL with 1 mol L^{-1} HCl acid in a 10:1 liquid-to-solid ratio at 180 °C for 1 h. The resulting mixture was then filtered for phase separation. The leachate was further used in the subsequent chromatography experiments, after pH adjustment to 1.5 with dilute HCl.

The chromatography experiments were performed in a 30 cm long and 0.7 cm wide column. Approximately 10.8 mL (1.36 g, dry mass) of bed volume (BV) of the SILP was packed in the chromatography column, by a wet method. A sample of 2.0 mL of the BR slag leachate (pH = 1.5) was used as feed in the chromatography separation experiments. For each experiment, 5.0 mL fractions were collected and analyzed by Inductively Coupled Plasma - Optical Emission Spectrometer (ICP-OES, Perkin Elmer OPTIMA 8300). All column chromatography tests were conducted at room temperature and with a flow rate of 0.5 mL min^{-1}.

5.3 RESULTS AND DISCUSSION

Among other compounds, BR is generally rich in Fe_2O_3, although the variation in its concentration is very wide (5 – 60 wt%).[3] Smelting of BR is a well-researched method for iron separation.[7,8] The smelting process of BR for iron separation applied in this work yields a slag phase enriched in oxides of the other elements found in BR, and in particular of REEs.[7,8] Subsequently, HPAL with HCl of the BR slag was applied mainly to inhibit silica-gel formation and to reduce the dissolution of major metals (*e.g.*, Al, Ti, Fe) in the slag leachate.[8,9] Decreasing silica-gel formation in the leachate is beneficial for the downstream processing to selectively recover REEs by solvent extraction or ion-exchange. Therefore, the leachate formed by HPAL of

the BR slag resulted in enhanced physico-chemical properties which were desirable for a straightforward chromatography process.

Since the sorption of metal ions is taking place *via* the carboxyl functional group of the SILP, a high pH dependency upon metal ion sorption was presumed. It is well known from our previous studies that the SILP is able to sorb the REEs from acidic media.[7] Therefore, the leachate with the adjusted pH at 1.5 was used for chromatography studies. At this value, the sorption capacity of the SILP was high enough for the REEs sorption whereas, at the same time, the hydrolysis of base metal ions and the REEs co-precipitation was circumvented.

Despite the benefits of the smelting process and HPAL in the resulting leachate the concentrations of the base metals were very high and those of the REEs were very low (Table 5.10). However, less iron is dissolved from the BR slag by HPAL compared to direct acid leaching of BR.[8] Regardless of the high concentrations of the base metals, the SILP showed a high affinity towards the REEs, with remarkably high sorption efficiencies (97.7−100%) of the REEs (Table 5.10).

Table 5.10. Composition of the BR slag leachate (feed) and sorption efficiencies (%) by the SILP.

	Ca	Al	Fe	Si	Ti	Nd	Y	Sc	Dy
Concentration in the leachate (mg L^{-1})	4209	1972	518	48.9	3.31	7.70	7.50	1.04	0.90
Sorption efficiency (%)	49.8	71.7	34.3	0.0	100	100	97.7	100	100

However, significant amounts of the base metals were sorbed together with the REEs during the loading of the SILP, due to their much higher concentrations in the feed (Table 5.10). The combination of H_3PO_4 and HNO_3 acids, within a three-step pH gradient elution from 1.5 to approximately 0.0, was tested for the selective elution (Figure 5.40). This resulted in a good separation of the REEs from the base elements, according to the following elution sequence: Sc(III) > Ti(IV) > Fe(III) > Ca(II) > Al(III) > Y(III) ≈ Dy(III) > Nd(III). Equilibrium REEs and

base metals molar ratios increased after the chromatography separation compared to their molar ratios in the leachate (Table 5.11). With an enrichment of the REEs over the base metals ranging from 3 to 3200 in the collected fractions, the combination of the H_3PO_4 and HNO_3 acids proved to be efficient for separating the REEs from the base metals.

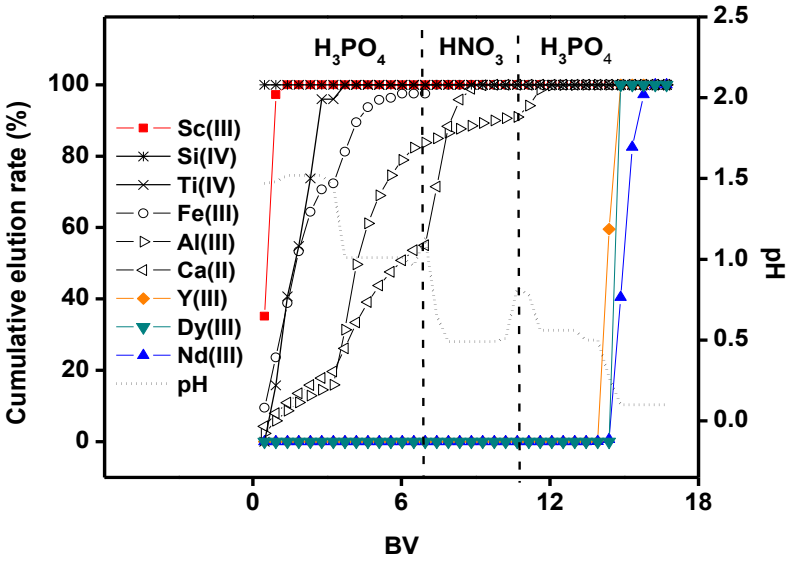

Figure 5.40. pH gradient elution with H_3PO_4 and HNO_3 as a function of the bed volume (*BV*). Feed = 2.0 mL of BR slag leachate with HCl. pH_{ini} = 1.5, flow rate of 0.5 mL min^{-1}.

Table 5.11. Equilibrium versus initial molar ratio of REEs and base elements after chromatography separation.

	Al(III)	Ca(II)	Fe(III)
Sc(III)	11	6	3
Y(III)	16	374	2835
Nd(III)	2293	698	2563
Dy(III)	1491	1327	3232

[a]Si and Ti were omitted due to their low concentration and sorption by the SILP.

In addition to the selective separation of the REE from the base elements, the applied elution profile enabled mutual separation between the REEs into sub-groups (Figure 5.40). In only several initial fractions, Sc(III) was completely separated from Y(III) and other REEs, as well as

from the majority of the base elements. The remaining REEs [Y(III), Nd(III), Dy(III)] were well separated from all other elements. Besides, the Nd/Dy initial molar ratio of 9.7 increased to an equilibrium ratio of 18.8. The results reveal a possibility for separating light and heavy REEs; the two sub-categories in which the REEs are split based on their chemical and physical properties.[2]

5.4 CONCLUSIONS

The performance of the SILP [Hbet-STFSI-PS-DVB] for the REEs recovery was tested with HCl leachate of a BR slag in a chromatography column. The SILP showed high affinity towards trace amounts (up to 7.7 mg L^{-1}) of the REEs in the presence of high concentrations (up to 4 g L^{-1}) of base metals. The sorption efficiencies of REEs were higher than those of base metals, but still large absolute quantities of the base metals were sorbed by the SILP due to the high concentrations of the base metals in the leachate. The different compounds were separated effectively in a three-step elution process with H_3PO_4 and HNO_3 as eluents.

5.5 REFERENCES

1 C. R. Borra, Y. Pontikes, K. Binnemans, T. Van Gerven, *Miner. Eng.*, 2015, **76**, 20–27.
2 European Commission, "Report on the Critical Raw Materials for the EU", 4–7 (2017).
3 K. Evans, *J. Sustain. Metall.*, 2016, **2** (4), 316-331.
4 N. V. Plechkova, K. R. Seddon, *Chem. Soc. Rev.*, 2008, **37**, 123–150.
5 F. Giacalone, M. Gruttadauria, *ChemCatChem*, 2016, **8**, 664–684.
6 D. Avdibegović, M. Regadío, K. Binnemans, *RSC Adv.*, 2017, **7**, 49664–49674.
7 D. Avdibegović, M. Regadío, K. Binnemans, *RSC Adv.*, 2018, **8**, 11886–11893.
8 G. Alkan, B. Xakalashe, B. Yagmurlu, F. Kaussen, B. Friedrich, *World of Metallurgy – ERZMETALL*, 2017, **70** (2), 5–12.
9 C. R. Borra, B. Blanpain, Y. Pontikes, K. Binnemans, T. Van Gerven, *J. Sustain. Metall.*, 2016, **2**, 28–37.
10 R. M. Rivera, G. Ounoughene, C. R. Borra, K. Binnemans, T. Van Gerven, *Min. Eng.*, 2017, **112**, 92–102.

Chapter 6

Combined multi-step precipitation and supported ionic liquid phase chromatography

This chapter is based on the collaborative manuscript, submitted for publication.

Avdibegović D., Yagmurlu B., Dittrich C., Regadío M., Friedrich B., Binnemans K.

"Combined multi-step precipitation and supported ionic liquid phase chromatography for the separation of rare earths from the base elements in bauxite residue leachates"

Author contributions:

B.F., B.Y., C.D., K.B., M.R., and D.A. conceived the research. B.Y. performed precipitation experiments and D.A. conducted column chromatography experiments. D.A. drafted the manuscript. All authors commented on the manuscript.

ABSTRACT

The supported ionic liquid phase (SILP) betainium sulfonyl(trifluoromethanesulfonylimide) poly(styrene-*co*-divinylbenzene) [Hbet-STFSI-PS-DVB] exhibits the highest affinity towards the rare-earth elements (REEs) among other elements in acidic bauxite residue (BR) leachates. The SILP can be used for purification of REEs from HNO_3, HCl and H_2SO_4 BR leachates. Leaching with H_2SO_4 is much cheaper than leaching with other mineral acids. However, uptake of Sc(III) from H_2SO_4 leachates is difficult due to strong electrostatic interactions between small Sc(III) ions and sulfate anions. Moreover, H_2SO_4 leachates generally contain high concentrations of base metals like iron and this reduces the efficiency of [Hbet-STFSI-PS-DVB] for uptake of REEs. Therefore, a precipitation step with an aqueous NH_3 solution was introduced to remove Fe(III), as a pretreatment step of a simulated H_2SO_4 BR leachate, prior to the REEs recovery by the [Hbet-STFSI-PS-DVB] column. Precipitation of Fe(III) from H_2SO_4 BR leachate increased the efficiency of column chromatography purification. In addition, $ScPO_4$ precipitation was alternatively performed after Fe(III) removal in order to compare and assess the optimum route for Sc(III) purification. After $ScPO_4$ precipitation, the recovery and purification of the remaining REEs on the [Hbet-STFSI-PS-DVB] column were also examined and shown to result in a higher purity of these REEs.

6.1 INTRODUCTION

The rare-earth elements (REEs) greatly contribute to modern technology, but there are only few mineable REE deposits.[1–3] Their most important applications are in permanent magnets for wind turbines, electric vehicles, computer hard-disk drives and mobile phones, alloys for rechargeable batteries, high-performance aluminium and magnesium alloys, as well as lamp phosphors.[2–5] The high economic importance of the REEs is reflected by their leading position in the list of the critical raw materials (CRMs) of the European Commission.[2,6] Since 2014 the REEs are no longer considered as one group in the list of CRMs, but are split into light and heavy REEs, whereas scandium was assessed separately from other REEs. In the 2017 update of the CRMs list, the light REEs were assessed as the CRMs with the highest supply risk. Moreover, the steadily growing demand for scandium (Sc), especially in high-strength aluminium alloys, necessarily increased its criticality and intensified the need for its production.[2,6,7] Although scandium resources have been identified across the globe, its concentration in the ores is generally low, so scandium is mainly produced as a by-product during processing of various ores or recovered from previously processed tailings or residues.[7–9]

The scarcity of naturally occurring REEs deposits, presents an opportunity for utilisation of secondary resources. In fact, in a quest for an alternative source of REEs, bauxite residue (BR), a waste material abundantly produced by the alumina industry, has recently drawn a lot of research attention. The REEs in BR are enriched by a factor of two compared to the bauxite ore.[10,11] It is well known that more than 90% of the trace metal value in BR can be attributed to the presence of Sc.[12–14] For instance, Greek BR is rich in Sc, with a concentration of around 120 g per tonne [12]. However, the base elements, namely iron (Fe), aluminum (Al), calcium (Ca), silica (Si), titanium (Ti) and sodium (Na), are much more abundant in BR (*e.g.* 5-60% of Fe_2O_3), which represents one of the major drawbacks for BR utilisation in REEs recovery.[15] Several flow-sheets are proposed for the selective recovery of REEs from the BR matrix, including alkali roasting–smelting for the separation of Al and Fe.[16] The residue can then be further treated by leaching with mineral acids.[9] These methods are either energy-intensive, consume large volumes of chemicals, and are thus not economically feasible.

Borra et al. (2015) reported that leaching of Greek BR gave similar results for HCl, HNO_3 and H_2SO_4, with a maximum scandium leaching efficiency of 80%.[12] However, from an economical point of view, H_2SO_4 is the preferred lixiviant.[16] In our previous studies, REEs were recovered from HCl, HNO_3 and H_2SO_4 media by the supported ionic liquid phase (SILP) betainium sulfonyl(trifluoromethanesulfonylimide) poly(styrene-*co*-divinylbenzene) [Hbet-STFSI-PS-DVB] (Figure 6.41).[17,18] In contrast to HCl and HNO_3 media, [Hbet-STFSI-PS-DVB] did not exhibit a very high tendency for Sc(III) uptake from H_2SO_4 media, especially in the presence of high concentrations of base elements. This issue sparked the idea of introducing a pretreatment step for H_2SO_4 BR leachates prior to the recovery of REEs, and Sc(III) in particular, by [Hbet-STFSI-PS-DVB]. Precipitation of highly concentrated and interfering ionic species from solutions is a commonly used treatment method in hydrometallurgy [8,19–24]. The focus of the present study was to purify the REEs from a simulated H_2SO_4 BR leachate by a tandem process involving a multi-step precipitation and [Hbet-STFSI-PS-DVB] column chromatography. The precipitation steps comprised Fe(III) removal by addition of an aqueous ammonia solution and selective $ScPO_4$ precipitation. The tested leachate consisted of substantial concentrations of REEs (Sc, Y, Nd, Dy) and base elements (Fe, Al, Ca) which are typically difficult to separate from the REEs and present in high concentrations. Still, real BR leachates contain a variety of elements not considered in the present study which might, to some extent, cause deviation of results compared to our study with a simulated leachate. Typical BR acidic leachates comprise only several mg L^{-1} of REEs and thousand times more concentrated base elements, so a significant loss of REEs due to co-precipitation with base elements can be anticipated.[12] Procedures for selective enrichment of REEs in the BR leachate have been developed.[25,26] Since it is elaborate to obtain a substantial amount of enriched BR leachates, a simplified study with the simulated leachate composed by realistic metal concentrations to a typical BR leachate was performed.[12,15,25,27] The main goal of this work is to give insight into the performance of the tandem process for the separation of REEs and base elements.

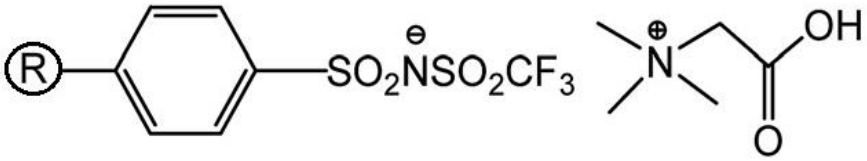

Figure 6.41. Structure of the SILP betainium sulfonyl(trifluoromethanesulfonylimide) poly(styrene-*co*-divinylbenzene) [Hbet-STFSI-PS-DVB] for REEs recovery and separation in column chromatography.

6.2 EXPERIMENTAL

6.2.1 Chemicals

HNO_3 (65%), $Al_2(SO_4)_3{\cdot}18H_2O$ (100-110%), standard solutions of scandium, yttrium, neodymium, dysprosium, lanthanum, aluminium, iron and calcium (1000 $\mu g\ mL^{-1}$) were purchased from Chem-Lab NV (Zedelgem, Belgium). $CaSO_4{\cdot}2H_2O$ was purchased from Vel (Leuven. Belgium). $Nd_2(SO_4)_3{\cdot}xH_2O$ (99.9%) was purchased from Alfa Aesar (Karlsruhe, Germany), $DyCl_3{\cdot}6H_2O$ (99.9%) from abcr (Karlsruhe, Germany) and $YCl_3{\cdot}6H_2O$ (99.9%) from Strem Chemicals (Newburyport, USA). H_3PO_4 (85%) was purchased from Ashland Chemicals (Columbus, USA). $(NH_4)_2HPO_4$ (98%) and NH_3 solution (25%) were purchased from Merck KGaA (Darmstadt, Germany). Betaine hydrochloride (99%), triethylamine (99%), and H_2SO_4 (96%) were purchased from Acros Organics (Geel, Belgium). Polystyrene-divinylbenzene (PS-DVB) sulfonyl chloride resin (0.91 $mmol\ g^{-1}$, 200-400 mesh) was purchased from RappPolymere (Tübingen, Germany). Trifluoromethanesulfonamide (98%) was purchased from J&K Scientific GmbH (Pforzheim, Germany). Dichloromethane (DCM) (p.a.) and acetone (p.a.) were purchased from Fisher Chemical (Loughborough, UK). Sc_2O_3 (99.99%) was kindly provided by Solvay (La Rochelle, France). Hydrated $Sc_2(SO_4)_3$ was prepared from Sc_2O_3 according to a literature procedure [28]. Hydrated $Y_2(SO_4)_3$ and $Dy_2(SO_4)_3$ were prepared in a similar manner from YCl_3 and $DyCl_3$, respectively.

6.2.2 Equipment

pH measurements were performed with WTW ProfiLine pH 197 series pH-meter with a Sentix 81 precision electrode. A fraction collector CF-2 (Spectrum Laboratories, Inc.) equipped with a drop sensor and an IPC 8-channel peristaltic pump (ISMATEC) was used for sampling during the chromatography studies. An inductively coupled plasma optical emission spectrometer (ICP-OES) (Perkin Elmer OPTIMA 8300) was used to measure the concentrations of the elements in solutions. The calibration solutions and all samples were prepared by dilution with 2 wt% HNO_3. Lanthanum (5 mg L^{-1}) was used as an internal standard. The following spectral lines (wavelengths in nm) in axial view were used for quantification: Fe 238.204, Al 308.215, Ca 317.933, Sc 361.383, Y 371.029, Dy 394.468, Nd 401.225, La 408.672.

6.2.3 Preparation of a simulated BR leachate and selective Fe and Sc precipitation

A simulated H_2SO_4 BR feed was prepared by dissolving the sulfate salts of the REEs and base elements in water, and the pH was adjusted to 1.50, typically with a 4 mol L^{-1} H_2SO_4 solution. The generated feed was used for column chromatography tests and for Fe(III) removal by a selective hydroxide precipitation with an ammonia solution.

Fe(III) was selectively removed by a dual-step precipitation procedure [29]. First, the largest part of Fe(III) was precipitated by addition of 10 wt% $NH_{3(aq)}$, until the pH of the solution reached the value of 3.3 and then the mixture was filtered. Secondly, a 10 wt% $NH_{3(aq)}$ was further added to the generated filtrate to remove the remaining Fe(III), until the pH of the solution reached the value of 3.7. The mixture was filtered and the solution pH was re-adjusted by dilute H_2SO_4 solution to 2.0 to aid the selectivity of the following $ScPO_4$ precipitation step. In this step, the remaining leachate after Fe(III) precipitation was further treated with 1 mol L^{-1} $(NH_4)_2HPO_4$ solution to selectively precipitate Sc(III) as a phosphate ($ScPO_4$), until the equilibrium pH reached the value of 2.7.

After Fe(III) and Sc(III) precipitations, aliquots of 10 mL of the leachates were taken for column chromatography separation studies. The total dilution factors after the Fe(III) and Sc(III) precipitation steps were 1.08 and 1.15, respectively, including the additional dilutions for pH adjustments prior to column chromatography tests. These dilution factors were taken into an account when calculating the precipitation percentage for each element.

The precipitation of metal ions was calculated from the *Eq. 6.12*.

$$Precipitation\ (\%) = \frac{c - c_1}{c} \cdot 100 \qquad (Eq.\ 6.12)$$

c and c_1 are the metal concentrations (mg L^{-1}) in the feed and in the solution after precipitation, respectively. c_1 is corrected by a dilution factor after the pH adjustments.

6.2.4 Test with the SILP in a column chromatography

The SILP [Hbet-STFSI-PS-DVB] used in chromatography studies was prepared following an earlier reported literature procedure.[17] A gravity flow glass column (BIO-RAD) of 30 cm length and 0.7 cm diameter was used in chromatography separation experiments. Approximately 10.8 mL bed volume (the total volume of the SILP in the column including the void volume, *BV*) of [Hbet-STFSI-PS-DVB] was packed in a column by a wet method (1.36 g of [Hbet-STFSI-PS-DVB], dry mass). [Hbet-STFSI-PS-DVB] was preconditioned with H_2SO_4 solution (pH = 1.5) prior to each experiment. For every chromatography separation, the column was loaded with 2 mL of synthetic BR leachate, of which the pH was adjusted to 1.5. An aliquot of 5 mL of H_2SO_4 (pH = 1.5) was added to remove remaining impurities in the column, prior to flowing the eluting solution through the column for the separation process. H_3PO_4 and HNO_3 were used as eluting agents, according to the previously optimized column chromatography process for the separation of REEs and base elements in BR.[18] During each experiment, 5 mL fractions were collected and analyzed by ICP-OES. All column chromatography experiments were conducted at room temperature with a set flow rate of 0.5 mL min^{-1}. The recovery of metal ions by [HBET-STFSI-PS-DVB] was calculated from *Eq. 1.11* (Page 19, 1.3.1.2).

6.3 RESULTS AND DISCUSSION

Dual-step Fe(III) precipitation as a pretreatment of BR leachate prior to recovery and purification of REEs by the [HBET-STFSI-PS-DVB] column chromatography was examined. Three simulated BR leachates were studied: 1) H_2SO_4 leachate with very high concentrations of base elements and lower concentrations of REEs, 2) H_2SO_4 leachate after Fe(III) removal with ammonia, and 3) H_2SO_4 leachate after Sc(III) precipitation with dibasic phosphate solution from the Fe(III) depleted leachate.

6.3.1 Selective precipitation

Selective removal of Fe(III) was attempted in order to increase the efficiency of the SILP column chromatography operation for REEs (and especially Sc) purification from H_2SO_4 medium. An ammonia solution was used as an efficient and selective precipitating agent for the two-stage removal of Fe(III) from the solution.[29] Then, Sc(III) was precipitated from the Fe(III) depleted solution with di-ammonium phosphate to produce a Sc concentrate.

The precipitation tests were conducted on a H_2SO_4 solution, with a composition similar to real BR leachate with enriched REEs concentrations (Table 6.12).[12,25,29] Sc(III), Y(III), Nd(III) and Dy(III) were studied taking into consideration their concentration in BR, high supply risk and economic importance [6,12]. Nd(III) was studied as a representative element of the light REEs and Dy(III) of the heavy REEs. In highly concentrated Fe(III) solutions, such as the simulated H_2SO_4 BR leachate, an increase in pH favors dimerisation, which proceeds according to *Eq. 6.13*.[30]

$$2Fe^{3+} + 2OH^- \rightarrow [Fe_2(OH)_2]^{4+} \qquad (Eq.\ 6.13)$$

The product $[Fe_2(OH)_2]^{4+}$ undergoes polymerization and larger iron(III)-hydroxo compounds are most likely being formed by the displacement and ionization of adjacent water molecules with other iron(III)-containing monomers and oligomers. The resulting species are the precursors to self-nucleated Fe(III) oxide/Fe(III) hydroxide precipitates.

Table 6.12. Metal concentrations in the simulated H_2SO_4 BR leachates: (1) initial H_2SO_4 BR leachate, (2) after dual-step Fe(III) removal, and (3) after $ScPO_4$ precipitation. For comparison, the concentrations are corrected by dilution factors after pH adjustments.

Elements	H_2SO_4 BR leachates		
	(1)	(2)	(3)
	Concentration (mg L^{-1})		
Al	3145	2991	2261
Fe	2942	23	7
Ca	390	390	367
Dy	31	12	9
Nd	25	22	11
Sc	16	14	5
Y	10	10	9

A decrease in Fe(III) concentration from approximately 2900 mg L^{-1} to 20 mg L^{-1} (99% removal) confirmed the efficiency of the dual-step precipitation (Table 6.12, Figure 6.42). Upon Fe(III) precipitation, 2 mg L^{-1} of Sc(III) and 19 mg L^{-1} of Dy(III) were co-precipitated (Table 6.12, Figure 6.42). The total removal of other elements in the feed was even lower than that of Sc(III) (Figure 6.42). It appears that Fe(III) precipitation step is more beneficial for the later Sc(III), Y(III) and light REEs recovery by [HBET-STFSI-PS-DVB], due to their low co-precipitation, than for the heavy REEs. This is even more important considering that the concentration of light REEs in the BR is generally higher than that of the heavy REEs [8,12,31]. The highest of co-precipitation occurs during the second Fe(III) removal step, where minor amount of Fe(III) is being precipitated.[29] The co-precipitated REEs can still be recovered by re-dissolving the precipitate and further processing of the solution by a column chromatography.

Selective precipitation of Sc(III) from the Fe(III) depleted BR leachate was studied by addition of $(NH_4)_2HPO_4$. After this step, 56% of Sc(III) initially present in the Fe(III) depleted BR leachate was precipitated as $ScPO_4$ (Figure 6.42). However, during Sc(III) precipitation, the co-precipitation of other REEs increased compared to their co-precipitation rate during Fe(III) removal with ammonia. In particular, the Nd(III) co-precipitation rate increased from 9%, during

Fe(III) removal, to 55% during Sc(III) precipitation. The co-precipitated REEs could eventually be recovered by re-dissolving $ScPO_4$ and performing [Hbet-STFSI-PS-DVB] column chromatography. The solution that can be generated in this way would have low concentrations of the base elements, due to their limited co-precipitation with Sc(III) (Figure 6.42). Hence this feed composition is a convenient source for downstream processes to easily obtain high-purity fractions of REEs by [Hbet-STFSI-PS-DVB] column chromatography.

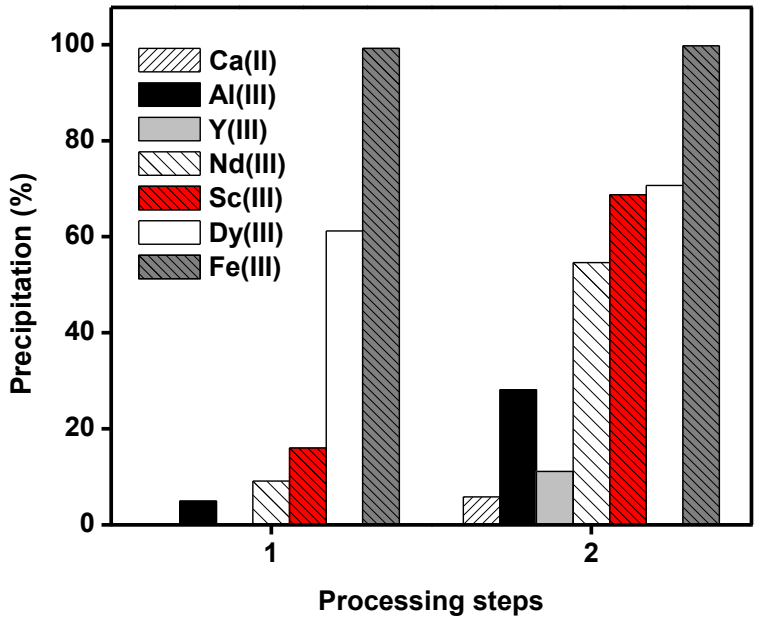

Figure 6.42. Precipitation (%) of elements in: (1) Fe(III) dual-step removal with ammonia, and (2) $ScPO_4$ precipitation step with di-ammonium phosphate.

6.3.2 Purification of REEs by the SILP in a fixed bed column

The recovery of REEs by the SILP in column chromatography was studied by making use of the [Hbet-STFSI-PS-DVB] SILP as the solid support, since this material has a proven ability to recover REEs from acidic media.[3,3,17] The possibility to obtain high-purity REEs fractions by column chromatography with [Hbet-STFSI-PS-DVB] was examined for the three simulated H_2SO_4 BR leachates (Table 6.12).

Firstly, the simulated H_2SO_4 BR leachate was tested prior to any precipitation treatment. As expected, Sc(III) sorption from this leachate was much lower compared to that of all other elements (Figure 6.43). The low affinity of [Hbet-STFSI-PS-DVB] towards Sc(III) in H_2SO_4 solution was previously explained by the high electrostatic interactions between the small Sc(III) cations and sulfate anions, which tightly retain Sc(III) in the solution.

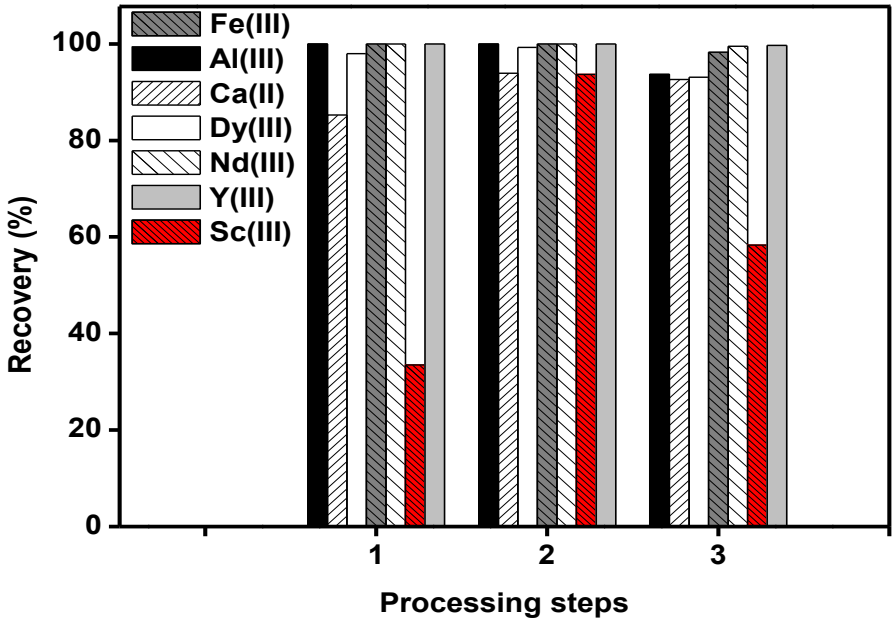

Figure 6.43. Recovery (%) of elements by [Hbet-STFSI-PS-DVB] after loading of: (1) simulated H_2SO_4 BR leachate, (2) leachate after dual-step Fe(III) removal by addition of ammonia, and (3) leachate after $ScPO_4$ precipitation.

[17,32] In addition, Sc(III) uptake was hindered by the high concentration of base elements, especially of Fe(III) which exhibits very similar physico-chemical behavior to Sc(III). Recovery rate of the base elements from the sulfate feed was nearly complete (Figure 6.43). The electrostatic interactions between sulfate anions and metal ions were less pronounced for other REEs (Y(III), Nd(III), Dy(III)) than for Sc(III), resulting in their quantitative recovery.

Since the base elements were recovered by [Hbet-STFSI-PS-DVB] to a great extent, separation from the REEs was performed by applying a pH gradient elution with H_3PO_4 (from pH 1.5 to approximately 0.0). HNO_3 (pH = 0.5) was used to specifically enhance Ca(II) elution (Figure 6.44). With the applied elution profile, Sc(III) and other REEs were separated from the other elements of the simulated H_2SO_4 BR leachate in the following sequence: Sc(III) > Fe(III) > Ca(II) > Al(III) > Dy(III) ≈ Y(III) > Nd(III).

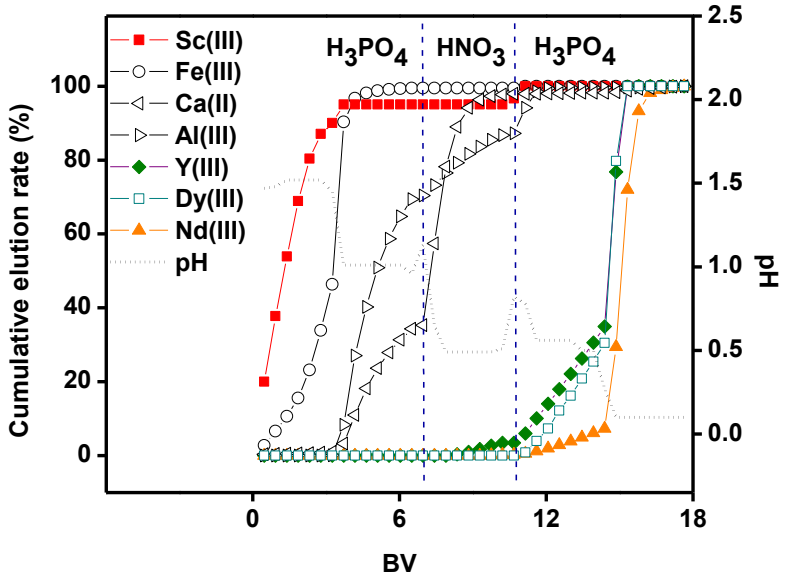

Figure 6.44. pH gradient elution with H_3PO_4 and HNO_3. Feed: 2 mL of simulated H_2SO_4 BR leachate (pH = 1.5). Flow rate 0.5 mL min^{-1}.

The second test was performed with the leachate obtained after precipitating Fe(III) with ammonia. Here, the Sc(III) recovery by [Hbet-STFSI-PS-DVB] increased dramatically from 33% to 94% (Figure 6.43). The interaction between the carboxyl group of [Hbet-STFSI-PS-DVB] and Sc(III) ions was facilitated, since the binding sites on [Hbet-STFSI-PS-DVB] are no longer occupied by Fe(III) ions. Therefore, Fe(III) removal by precipitation as $Fe(OH)_3$ had a positive impact on the Sc(III) recovery from the H_2SO_4 leachate by [Hbet-STFSI-PS-DVB]. The recovery of other REEs and base elements still remained nearly quantitative (Figure 6.43).

The elution sequence of the REEs recovered by [Hbet-STFSI-PS-DVB] from the feed after Fe(III) removal, followed the same trend as with the BR H_2SO_4 leachate without Fe(III) precipitation (Figure 6.45). Sc(III) was eluted within the first three fractions. The remaining REEs started to partially elute already with HNO_3, although with original leachate, the REEs were only eluted with H_3PO_4 at a pH below 0.5 (Figure 6.44, Figure 6.45). These results indicate that ammonium ions in the feed, not consumed during the Fe(III) removal step, may have partially occupied the available ion-exchange sites of [Hbet-STFSI-PS-DVB]. As a consequence of increased competition, the REEs migrated further through the column during the loading of the feed, and eventually started eluting earlier, already during the HNO_3 elution step.

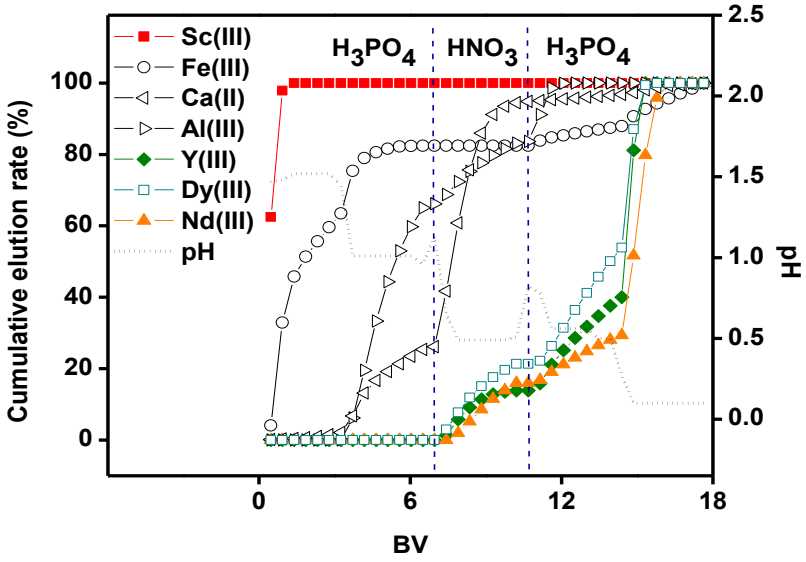

Figure 6.45. pH gradient elution with H_3PO_4 and HNO_3. Feed: 2 mL of simulated H_2SO_4 BR leachate after Fe(III) precipitation (pH = 1.5). Flow rate 0.5 mL min^{-1}.

The last tests were performed with the simulated H_2SO_4 BR leachates after two consecutive precipitation steps, where Fe(III) and Sc(III) had been extensively removed by precipitation with NH_3 and $(NH_4)_2HPO_4$ solutions, respectively. [Hbet-STFSI-PS-DVB] exhibited a maximum recovery of 58% of trace amount of Sc(III) that could not be sorbed and persisted in the solution (Figure 6.43). Although the Fe(III) concentration in the tested feed was negligible (Table 6.12),

presumably the presence of phosphate anions that remained after Sc(III) precipitation inhibited trace Sc(III) recovery by [Hbet-STFSI-PS-DVB]. Nevertheless, the recovery of other REEs remained remarkably high (> 98%). It must be noted that the REEs concentrations in the feed after Sc(III) precipitation were lower than in the initial H_2SO_4 leachate and after Fe(III) removal, due to their co-precipitation (Table 6.12).

The elution sequence in the column chromatography for the separation of REEs and base elements from the leachate after Sc(III) precipitation was in agreement with the previous ones (without precipitation and after Fe(III) removal) (Figure 6.46). The trace amount of Sc(III) recovered by [Hbet-STFSI-PS-DVB] was eluted with H_3PO_4 in only two fractions and the remaining REEs were eluted with H_3PO_4. The REEs did not migrate faster through the column than in the case with the leachate after Fe(III) removal by ammonia. The influence of ammonium ions was less pronounced in the presence of phosphate counter-ions that were primary added for Sc(III) precipitation.

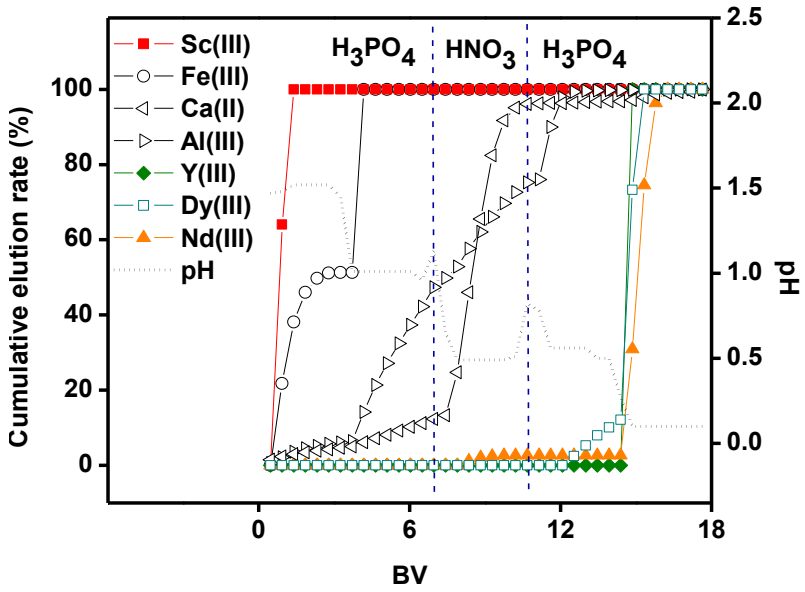

Figure 6.46. pH gradient elution with H_3PO_4 and HNO_3. Feed: 2 mL of simulated BR H_2SO_4 leachate after $ScPO_4$ precipitation (pH = 1.5). Flow rate 0.5 mL min^{-1}.

6.3.3 Assessment of the different combinations: precipitation – SILP chromatography

In all three tested cases, the REEs collected in the fractions after [Hbet-STFSI-PS-DVB] column chromatography were largely purified from the base elements (Figure 6.47). The most efficient Sc(III) recovery and purification route was found to be by [Hbet-STFSI-PS-DVB] column chromatography after Fe(III) removal (Figure 6.43). The purity of Sc(III) in the fractions obtained when performing only Fe(III) removal prior to the chromatography separation, was superior to the purity of Sc(III) concentrate obtained by the phosphate precipitation (Figure 6.48). However, by $ScPO_4$ precipitation generally higher feed volumes can be treated per purification step in comparison with [Hbet-STFSI-PS-DVB] column chromatography, making the former process more suitable for large-scale scandium production. The amount of the feed solution treated with [Hbet-STFSI-PS-DVB] column chromatography is limited by the presence of large concentrations of base elements. Sc(III) precipitation resulted in feed with lower concentrations of interfering elements, which was beneficial for the subsequent column chromatography separation of other REEs. As a result, the purity of the REEs fractions was better compared to the purity obtained after separation from the simulated H_2SO_4 BR leachate, before and after Fe(III) precipitation (Figure 6.47, Figure 6.48). Hence, the precipitation and column chromatography tandem process enables recovery and purification of scandium and other REEs *via* two routes, which are split based on the resulting purity degree of REEs (Figure 6.49). The proposed routes aim for simultaneous utilization of BR as a secondary source of several critical REEs, outreaching previously reported processes which are mainly focused on the recovery of a single REE, mainly scandium.[26,33,34]

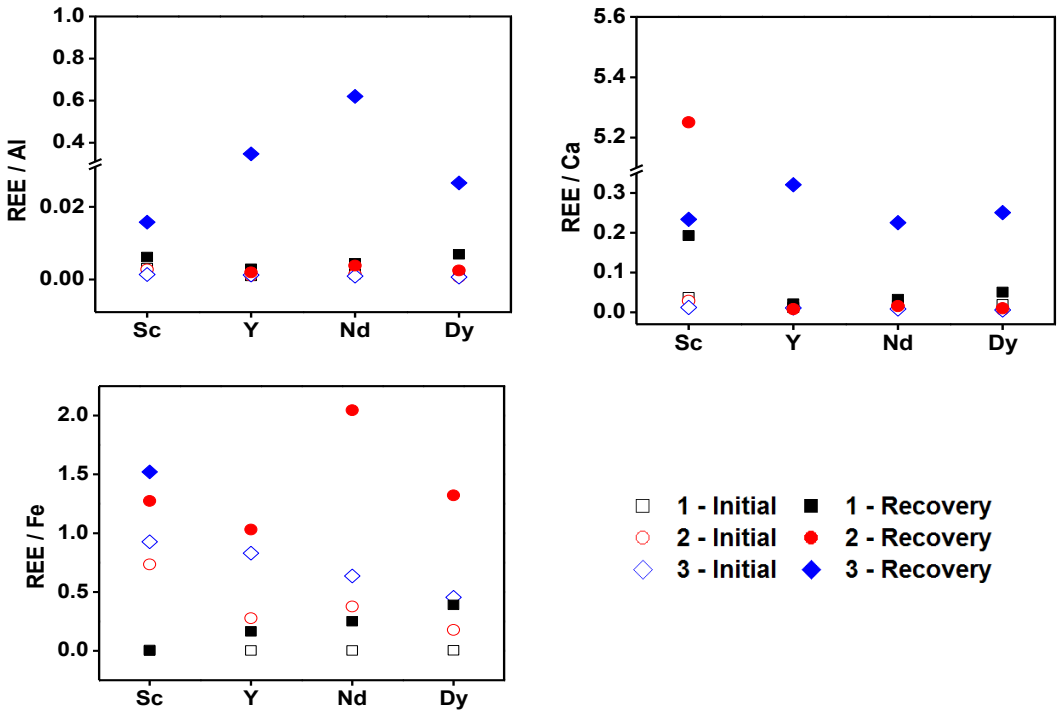

Figure 6.47. Molar ratios of REEs and base elements in the feed solutions (open symbols) and after recovery and elution in the [Hbet-STFSI-PS-DVB] column (filled symbols) with: (1) H_2SO_4 BR leachate, (2) leachate after Fe(III) removal, and (3) leachate after $ScPO_4$ precipitation.

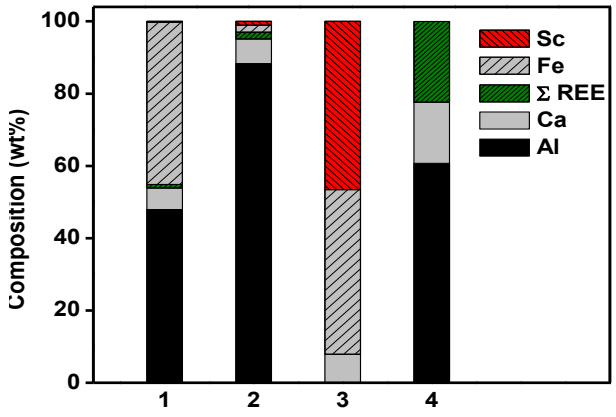

Figure 6.48. Summary of the compositions (wt%) of: (1) simulated H_2SO_4 BR leachate, (2) $ScPO_4$ precipitate, (3) Sc(III) chromatography fractions after Fe(III) removal, and (4) REEs chromatography fractions after $ScPO_4$ precipitation.

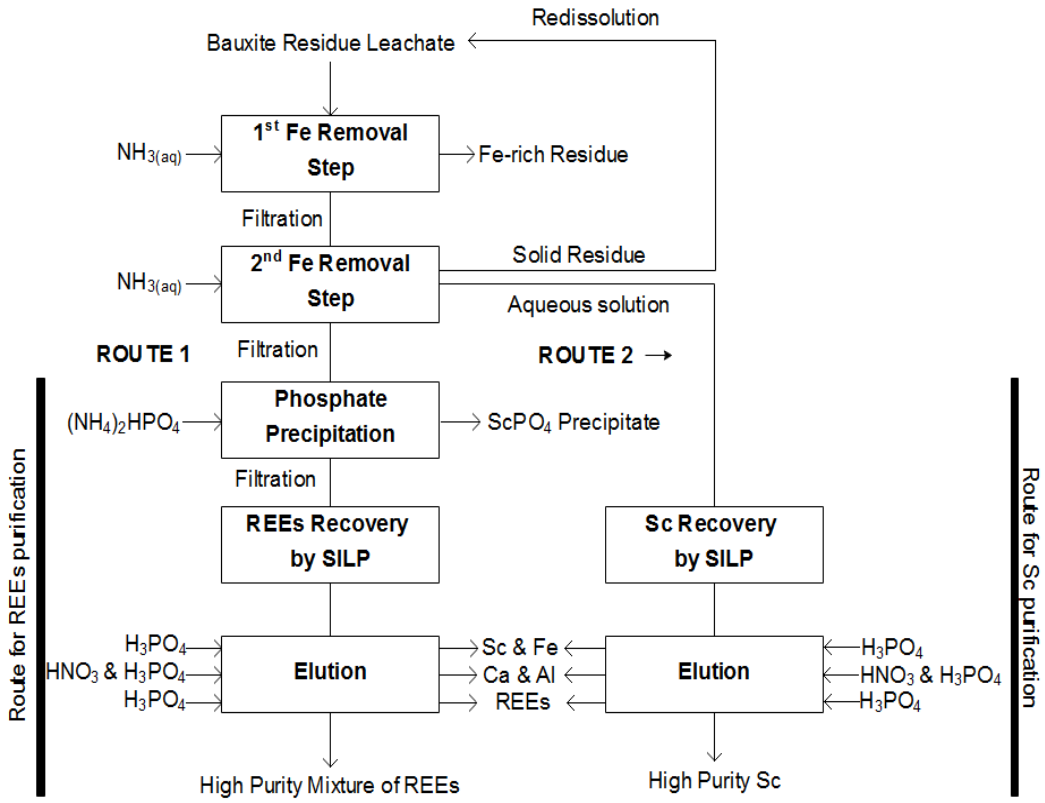

Figure 6.49. Flow-sheet for REEs purification (route 1), including scandium (route 2), by a precipitation and [Hbet-STFSI-PS-DVB] column chromatography tandem processes.

6.4 CONCLUSIONS

The REEs Y(III), Nd(III) and Dy(III) were efficiently (≈100%) recovered by [Hbet-STFSI-PS-DVB] from three simulated BR leachates: 1) H_2SO_4 leachate with very high concentrations of base elements and lower concentrations of REEs, 2) the same leachate after Fe(III) removal with ammonia, and 3) the latter leachate after additional precipitation of Sc(III) with a dibasic phosphate solution. Sc(III) recovery from the H_2SO_4 leachate by [Hbet-STFSI-PS-DVB] was only efficient after Fe(III) precipitation. A subsequent column chromatography separation step resulted in Sc(III) fractions of purity superior to $ScPO_4$ precipitate. Therefore, the precipitation of Fe(III) prior to Sc(III) recovery by [Hbet-STFSI-PS-DVB] appeared to be the most promising

route to separate Sc(III) from the base elements in H_2SO_4 leachates of BR. The obtained Sc(III) purity (47%) may be further improved by an additional column chromatography cycle. The highest REEs purity (23% for the group of REEs) was achieved for the feed solution after Sc(III) precipitation. In other words, precipitation of interfering elements as a pretreatment of BR H_2SO_4 leachates boosted the efficiency of the [Hbet-STFSI-PS-DVB] column chromatography towards obtaining purified fractions of Sc(III) and other REEs.

6.5 REFERENCES

1 V. Fernandez, *Resour. Policy*, 2017, **53**, 26–45.
2 K. Binnemans, P.T. Jones, T. Müller, L. Yurramendi, *J. Sustain. Metall.*, 2018, **53**, 1–21.
3 J. Zhang, B. Zhao, B. Schreiner, *Separation Hydrometallurgy of Rare Earth Elements*, Springer, Cham, Switzerland, 2016.
4 M. V. Riesgo García, A. Krzemień, M. A. Manzanedo Del Campo, M. Menéndez Álvarez, M.R. Gent, *Resour. Policy*, 2017, **53**, 66–76.
5 K. Binnemans, P.T. Jones, B. Blanpain, T. Van Gerven, Y. Pontikes, *J. Clean. Prod.*, 2015, **99**, 17–38.
6 European Commission, Directorate-General for Internal Market, Industry, Entrepreneurship and SMEs, *Study on the review of the list of Critical Raw Materials: executive summary*, 2017.
7 K. Pyrzyńska, K. Kilian, M. Pęgier, *Sep. & Purif. Rev.*, 2018, **9**, 1–13.
8 R. P. Narayanan, N. K. Kazantzis, M.H. Emmert, *ACS Sustainable Chem. Eng.*, 2017, **6**, 1478–1488.
9 M. T. Ochsenkühn-Petropoulou, K. S. Hatzilyberis, L.N. Mendrinos, C.E. Salmas, *Ind. Eng. Chem. Res.*, 2002, **41**, 5794–5801.
10 M. T. Ochsenkühn-Petropulu, T. Lyberopulu, K. Ochsenkühn, G. Parissakis, *Anal. Chim. Acta*, 1996, **319**, 249–259.
11 É. Deady, E. Mouchos, K. Goodenough, B. Williamson, F. Wall, *in: Proceedings ERES2014 1st European Rare Earth Resources Conference*, 4-7 September, Milos, Greece.
12 C. R. Borra, Y. Pontikes, K. Binnemans, T. Van Gerven, *Min. Eng.*, 2015, **76**, 20–27.
13 Y. Liu, R. Naidu, Ravi, *Waste manag.*, 2014, **34**, 2662–2673.
14 H. L. Z. Liu, *Hydrometallurgy*, 2015, **155**, 29–43.
15 K. Evans, *J. Sustain. Metall.*, 2016, **2**, 316–331.
16 C. R. Borra, B. Blanpain, Y. Pontikes, K. Binnemans, T. Van Gerven, *J. Sustain. Metall.*, 2016, **2**, 365–386.
17 D. Avdibegović, M. Regadío, K. Binnemans, *RSC Adv*, 2017, **7**, 49664–49674.
18 D. Avdibegović, M. Regadío, K. Binnemans, *RSC Adv*, 2018, **8**, 11886–11893.

19 H. Han, W. Sun, Y. Hu, X. Cao, H. Tang, R. Liu, T. Yue, Tong, *Hydrometallurgy*, 2016, **165**, 318–322.
20 G. J.P. Deblonde, A. Chagnes, V. Weigel, G. Cote, *Hydrometallurgy*, 2016, **165**, 345–350.
21 D.K. Singh, K.N. Hareendran, T. Sreenivas, V. Kain, G.K. Dey, *Hydrometallurgy*, 2017, **171**, 228–235.
22 A. S. E. Güler, *Hydrometallurgy*, 2016, **164**, 118–124.
23 K. Mazurek, *Hydrometallurgy*, 2013, **134-135**, 26–31.
24 X. Wang, C. Xiao, M. Wang, W. Xiao, Weiliu, *Hydrometallurgy*, 2011, **107**, 133–136.
25 R. M. Rivera, B. Ulenaers, G. Ounoughene, K. Binnemans, T. Van Gerven, *Miner. Eng.*, 2018, **119**, 82–92.
26 B. Onghena, C. Borra, T. Van Gerven, K. Binnemans, *Sep. Purif. Technol.*, 2017, **176**, 208–219.
27 G. Alkan, B. Xakalashe, B. Yagmurlu, F. Kaussen, B. Friedrich, *World of Metallurgy–ERZMETALL*, 2017, **70**, 5–12.
28 J.G. Li, T. Ikegami, T. Mori, *J. Mater. Res.*, 2003, **18**, 1816–1822.
29 B. Yagmurlu, C. Dittrich, B. Friedrich, *J. Sustain. Metall.*, 2017, **3**, 90–98.
30 R. Coetzee, C. Dorfling and S. M. Bradshaw, *Hydrometallurgy*, 2018, **175**, 79–92.
31 É. Ujaczki, Y.S. Zimmermann, C. A. Gasser, M. Molnár, V. Feigl, M. Lenz, *J. Chem. Technol. Biotechnol.*, 2017, **92**, 2835–2844.
32 S. Cotton, *Lanthanide and Actinide Chemistry*, Wiley, Chichester, United Kingdom, 2006.
33 W. Zhang, R. Koivula, E. Wiikinkoski, J. Xu, S. Hietala, J. Lehto, R. Harjula, *ACS Sustain. Chem. Eng.*, 2017, **5**, 3103–3114.
34 J. Roosen, S. Van Roosendael, C. Borra, T. Van Gerven, S. Mullens, K. Binnemans, *Green Chem.*, 2016, **18**, 2005–2013.

Chapter 7

Selective ion-exchange separation of Sc(III) over Fe(III) by crystalline α-zirconium phosphate platelets from bauxite residue leachates

This chapter is written based on a collaborative manuscript, intended for publication.

Dženita Avdibegović, Wenzhong Zhang, Junhua Xu, Mercedes Regadío, Risto Koivula, and Koen Binnemans

"Selective ion-exchange separation of Sc(III) over Fe(III) by crystalline α-zirconium phosphate platelets from bauxite residue leachates"

Author contributions:

K.B., M.R., R.K., W.Z. and D.A. conceived the research. D.A., W.Z. and J.X. performed all experiments. D.A. and W.Z. analysed the data and D.A. drafted the manuscript. All authors commented on the manuscript.

Authors wish to thank Tobias Hertel (KU Leuven) for XRD measurements and Sami Hietala (University of Helsinki) for NMR measurements.

ABSTRACT

A continuous worldwide increase in scandium (Sc) criticality leads to a quest for secondary scandium resources. Among them, bauxite residue (BR) – a waste product from alumina refinery – often contains substantial amounts of scandium. However, the complexity in BR composition drives the need for developing a selective, efficient and cost-effective process to achieve separation and purification of scandium. Insoluble salts of tetravalent metallo-acids are inorganic acid-resistant ion-exchangers with well-established preparation procedures, but their potential use in rare-earth recovery and purification has not been extensively explored yet. Zirconium and titanium phosphates, both in amorphous and α-layered crystalline forms, were screened for Sc(III)/Fe(III) separation, as Fe(III) is one of the base elements in BR that is hard to separate from Sc(III). The studied α-zirconium phosphate (α-ZrP, $Zr(HPO_4)_2 \cdot H_2O$) exhibited the highest Sc(III)/Fe(III) separation factors (up to approximately 23) from HCl acidic solutions. Therefore, crucial parameters for Sc(III) ion-exchange by α-ZrP were investigated: influence of the pH, sorption isotherms, ion-exchange kinetics, and reusability. The metal selectivity of α-ZrP was considered to be affected by the solution pH, and the size and hydration enthalpy of the metal cations. Breakthrough curves for a binary Sc(III)/Fe(III) solution, composed by realistic metal concentrations to a typical BR leachate, revealed the selectivity of α-ZrP for Sc(III) under column operating conditions. Furthermore, chromatographic separation of Sc(III) from a real hydrochloric acid leachate of BR was successfully achieved on an α-ZrP column. Sc(III) fractions without measurable Fe(III), Al(III) or other rare-earth impurities were obtained after a simple two-step elution with HCl. Overall, this study highlights possibility for direct ion-exchange separation of Sc(III) from a much higher concentration of Fe(III), without the need of using reducing agents, the later resulting in higher process costs.

7.1 INTRODUCTION

Scandium (Sc) belongs to a group of rare-earth elements (REEs) which has long been recognised as a valuable commodity for various advanced applications. Currently, the primary use of scandium is in solid oxide fuel cells (SOFC).[1] Scandia-zirconia solid electrolytes can be used at lower temperatures than yttria-stabilised zirconia, because the former has a high ionic conductivity, resulting in increased operational stability of SOFC.[2] Scandium in its metallic form has found application in aluminium–scandium alloys that are used in aerospace, sports, transportation, and process industry.[3,4] These alloys are much stronger and lighter than other high-strength alloys, exhibit significant grain refinement, strengthen welds and are resistant to corrosion. Besides the bulk applications, addition of scandium compounds to high- pressure lamps renders a light spectrum which is extremely similar to the natural sunlight and increases the light output efficiency.[5] Moreover, scandium finds application as host matrix for lasers applied in dentistry.[6]

However, exploitable scandium-rich minerals and ores are rare.[7,8] Therefore, scandium is usually produced as a by-product from other metal extraction process. Already in 2014, the European Commission considered scandium as one of the critical raw materials for the European Union, whereas in 2017 the assessed criticality only increased.[9,10] The lack of primary production mines in Europe imposes a search for secondary resources of scandium and the technologies for extracting scandium from these resources.

Bauxites are the primary ores for alumina production through the well-established Bayer process. In Europe, karst bauxites are more often found than their lateritic counterparts, with the former relatively enriched in REEs.[11] The REEs from the bauxite are not extracted into the Bayer liquor and are concentrated consequently in the solid waste by a factor of two.[11] The generated solid waste, known as bauxite residue (BR) or red mud, typically contains 50 to 110 mg kg^{-1} of scandium.[11,12] The scandium content in BR depends on the source bauxite and precise processing route. For instance, Greek BR contains even around 120 mg kg^{-1} of scandium.[11,12] This concentration is much higher than the average abundance of scandium in the Earth's crust (22 mg kg^{-1}). Although BR can be considered as a potential scandium resource, other metals are concentrated in BR, especially iron, aluminum, calcium, sodium and titanium, which are energy

and process intensive to separate from scandium.[12–14] In principle, scandium can be recovered from a leachate produced by direct leaching of BR with mineral or organic acids, but in this way large amounts of undesired base elements are co-dissolved along with the scandium and other REEs.[12,15,16] Several hydro- and pyrometallurgical processes have been developed to recover the base elements from BR, i.e. magnetic separation for iron recovery, smelting of BR to produce pig iron, leaching of BR by organic or inorganic acids (H_2SO_4, HNO_3, HCl, CH_3SO_3H, citric acid, oxalic acid) or alkali roasting for alumina recovery.[17–21] The REEs can then be recovered in a subsequent step from the leachates, but the leachates generated in this way still cannot directly provide REEs compounds of high purity, thus further purification steps are required.[20] The commercial value of REEs depends on their purity, therefore it is important to separate them in a high purity from main base elements. Recovery and purification of scandium from BR leachates is generally performed using either solvent extraction, ion-exchange chromatography, precipitation, or by a combination of these techniques.[8,22–27] Ion-exchange chromatography possess the advantage of high preconcentration factors.[28,29] In BR leachates, the scandium concentration is in the order of several mg L^{-1}, whereas the inevitable impurities of base metals can reach the values of thousands of mg L^{-1}.[23] Iron is one of the base elements that is predominantly present in the BR leachates and it is often co-extracted along with scandium.[25,30] One way to tackle the issue with iron impurities is by reducing it from its trivalent to divalent state. Divalent iron has a much lower charge density than trivalent iron and is therefore easier to separate from trivalent scandium, for instance by solvent extraction with acidic extractants or by use of ion-exchangers.[26,31] However, this reduction step makes the process more costly. Ochsenkühn-Petropulu *et al.* purified scandium from the BR leachate in a Dowex 5OW-X8 column by eluting of base elements with 1.75 mol L^{-1} HCl.[25] Scandium and other REEs were subsequently eluted with 6 mol L^{-1} HCl. Nontheless, separation of scandium from other REEs involved an additional solvent extraction step with di(2-ethylhexyl)phosphoric acid (D2EHPA). It appears that finding a scandium-selective sorbent could address the issue of its recovery and purification from dilute, yet complex solutions like BR leachates.

Insoluble salts of multivalent metallo-acids have been extensively studied as ion-exchangers with high sorption capacities, acid, temperature and radiation resistance.[32] They can be prepared in crystalline layered forms, rendering them as excellent hosts for intercalation of a variety of guest molecules and for the synthesis of hybrid materials.[33–37] α-$Zr(HPO_4)_2 \cdot H_2O$ (α-ZrP, with

$P2_1/n$ space group) is an established inorganic ion-exchange material from the class of metal(IV) phosphates, and it has been used in the separation of metal ions, especially for radionuclide removal.[38,39] α-ZrP shows a high sorption capacity (*e.g.* 6.64 meq g^{-1} of exchanger).[40,41] The crystal structure of α-ZrP is layered and each layer consists of zirconium atoms lying in a plane and bridged by phosphate groups situated above and below the plane.[41] Although α-ZrP has been investigated to some extent for the separation of lanthanides, its interesting properties have not been completely explored for the uptake and separation of scandium.[42] As a need for new scandium sources exists, a simple and efficient procedure for the challenging Sc/Fe separation from sources such as BR is required. In the present work, Sc(III) and Fe(III) separation by α-ZrP was investigated in detail. In order to assess and compare the selectivity of the same class of ion-exchangers and to reveal the origin of difference in their selectivity, amorphous zirconium and titanium phosphate (am-ZrP, am-TiP) and crystalline titanium phosphate (α-$Ti(HPO_4)_2 \cdot H_2O$ or α-TiP) were screened as well.

7.2 EXPERIMENTAL

7.2.1 Chemicals

$ZrOCl_2 \cdot xH_2O$ (>99.9%, Alfa Aesar, Karlsruhe, Germany), $TiCl_4$ (>99.9%, Sigma-Aldrich, Helsinki, Finland) and H_3PO_4 (85%, Ashland Chemicals, Columbus, USA) were used for synthesis of sorbents. HNO_3 (65%) and standard solutions of scandium, yttrium, neodymium, dysprosium, lanthanum, aluminium, iron, titanium, silicium, cerium, zirconium and calcium (1000 μg mL^{-1}) from Chem-Lab NV (Zedelgem, Belgium), NaCl (>99.5%, Fisher Scientific, Loughborough, United Kingdom), HCl (37%, VWR, Leuven, Belgium), Sc_2O_3 (99.99%, kindly provided by Solvay, La Rochelle, France), hydrated $ScCl_3$ (prepared by dissolving Sc_2O_3 in concentrated HCl) and anhydrous $FeCl_3$ (98%) (Acros Organics, Geel, Belgium) were used for solution preparation. Greek BR was kindly provided by Aluminium of Greece (Agios Nikolaos, Greece)

7.2.2 Equipment

X-ray powder diffraction (XRD) patterns were collected from the 2θ angle of 5° to 35° in the Bragg-Brentano geometry on a Bruker D2 PHASER X-ray diffractometer equipped with a CuKα radiation operating at a voltage of 45 kV and a current of 30 mA. Solid-state ^{31}P magic angle spinning (MAS) nuclear magnetic resonance (NMR) spectra were recorded by a Bruker Avance III 500 MHz spectrometer equipped with a 4 mm H/X/Y MAS probe. The samples were packed in a 4-mm zirconia rotor and spun at a MAS rate of 12 kHz. The spectra were acquired with a 90° pulse (77 kHz RF), a 100 s recycle delay, and 64 scans. The ^{31}P chemical shifts were referred to external 85% H_3PO_4 (at 0 ppm). The morphology of the platelets was observed by a Hitachi S4800 field emission-scanning electron microscope (FE-SEM) after the sample was sputter-coated with a 3-nm layer of Au-Pd alloy. Batch sorption experiments were performed at room temperature on a VWR International water bath shaker (Type 462-0355). Eppendorf Centrifuge 5804 was used for phase disengagement. A fraction collector CF-2 (Spectrum Laboratories, Inc.) equipped with drop sensor and IPC 8-channel peristaltic pump (ISMATEC) was used for sampling during the chromatography studies. An inductively coupled plasma - optical emission spectrometer (ICP-OES) (Perkin Elmer OPTIMA 8300) was used to measure concentrations of elements in the solutions. The following spectral lines were used for quantification (wavelengths in nm): Al 308.215, Ca 317.933, Ce 413.762, Dy 394.468, Fe 238.204, La 408.672, Nd 401.225, Sc 361.383, Si 251.611, Ti 334.940, Y 371.029.

7.2.3 Synthesis of metal(IV) phosphate inorganic ion-exchangers

α-ZrP was prepared by the reflux method.[43] Briefly, 200 mL of 0.5 mol L^{-1} $ZrOCl_2$ was added dropwise to 200 mL of 6 mol L^{-1} H_3PO_4 and refluxed for 48 h at 94 °C. The product was rinsed with water, centrifuged and air-dried at 70 °C overnight.

A hydrothermal synthesis method was used to synthesize α-TiP.[26] An amount of 10 mL of $TiCl_4$ was added dropwise into 50 mL of water with strong magnetic stirring (300 rpm) until it became transparent, and 40 mL of concentrated H_3PO_4 was added. The mixture was heated at 180 °C in a

Teflon-lined stainless autoclave for 12 h. The product was filtered, washed with water until a pH of 3.5 was reached, and then air-dried at 70 °C overnight.

The precipitation method was used for the synthesis of am-ZrP and am-TiP.[26,44] Briefly, 30.7 g of $ZrCl_4$ or 25 g of $TiCl_4$ was added quickly to 430 mL of 2 mol L^{-1} HCl solution under strong magnetic stirring (300 rpm) until it gave a totally transparent solution. The prepared solution was added dropwise into 400 mL of 1.25 M H_3PO_4 solution with stirring at 150 rpm. The resulting white solid was let stand in the mother solution for 24 h before filtering out. am-ZrP was subsequently washed with 2 mol L^{-1} H_3PO_4, 1 mol L^{-1} HNO_3 and with water until a pH of 3.0 was reached. am-TiP was washed only with water until the pH of 3.5 was attained. The products were then air-dried at 70 °C overnight.

7.2.4 Batch sorption studies

Typically, 0.050±0.001 g of the ion-exchanger was placed in a 20 mL glass vial and 20 mL of synthetic feed solution of Sc(III) and/or Fe(III) with preadjusted pH was added. Unless otherwise specified, concentrations of Sc(III) and Fe(III) were 1.0 mmol L^{-1}, the shaking speed was 300 rpm and the equilibration time was 18 h. The experiments were carried out at room temperature in HCl media. The uptake of Sc(III) and Fe(III) from a 3 mol L^{-1} NaCl solution was investigated under the same experimental conditions. After equilibration, the samples were filtered through 0.20 μm PVDF syringe filters. The filtrate was then diluted to a concentration suitable for ICP-OES analysis. The reusability of α-ZrP for Sc(III) uptake was examined by repeating the sorption-desorption steps for three times. α-ZrP was equilibrated with 20 mL of Sc(III) solution (initial pH, pH_{ini} = 1.6), centrifuged for 15 min at 2880 *g* and the supernatant was taken by a pipette. Then, α-ZrP was washed two times with 10 mL of ultrapure water, centrifuged and air-dried for 2 h at 50 °C in a vacuum, before 20 mL of an equimolar 1.5 mol L^{-1} HNO_3 and H_3PO_4 mixture was introduced for Sc(III) desorption. Desorption experiments were conducted for 24 h at the same shaking conditions as for the uptake experiments.

The amount of the metal ions sorbed onto the ion-exchangers *q* was calculated from the *Eq. 1.1* (Page 16, 1.3.1.1), the distribution coefficient (K_d) was calculated following the *Eq. 1.4*. (Page 17, 1.3.1.1), and the separation factor ($SF_{A/B}$) following the *Eq. 1.5* (Page 17, 1.3.1.1).

7.2.5 Column chromatography sorption studies and bauxite residue leaching

A low-pressure vertical glass column (BIO-RAD) of 10 cm length with an inner diameter of 1 cm was used in chromatography separation experiments. A slurry with 1.0 g of α-ZrP and 10 mL of a 1 mol L^{-1} NaCl solution was prepared and the column was packed to a bed volume (*BV*) of approximately 2.0 mL (the total volume of the α-ZrP together with the void volume in the column). The remaining NaCl impurities were washed by pumping through 5 *BV* of 1.5 M HCl. α-ZrP was preconditioned with HCl solution of pH = 0.8 prior to breakthrough curve experiments and pH = 2.2 prior to elution studies with the HCl BR leachate. The breakthrough curves were constructed by pumping the binary solution of 0.04 mmol L^{-1} Sc(III) and 1.72 mmol L^{-1} Fe(III), with pH_{ini} of 0.8, through the α-ZrP column. All column chromatography experiments were conducted at room temperature and with the flow rate of 2 mL h^{-1}. The collected fractions after elution column chromatography were analysed by ICP-OES.

Leaching of Greek BR (Agios Nikolaos, Greece) was performed as described elsewhere.[12] Briefly, BR was air-dried for 20 h at 105 °C in an oven. An aliquot of 100.0 mL of 0.7 mol L^{-1} HCl was added to 10.0 g of BR. The mixture was shaken for 6 h on a rotary mixer at 60 rpm and at room temperature. The leachate was filtered through a 0.20 μm PVDF syringe filter and 5.0 mL of the freshly prepared leachate was used for a chromatographic separation experiment with pH_{ini} = 2.2, without any further treatments. The recovery of elements from the BR leachate by the α-ZrP column was calculated from the *Eq. 1.11* (1.3.1.2).

7.3 RESULTS AND DISCUSSION

7.3.1 Characterisation of α-ZrP

The synthesised α-ZrP platelets have been extensively studied and characterised in the literature.[45,46] As the focus of the present study falls on the metal separation behaviour, only typical characterisations to check the purity of the obtained α-ZrP platelets were run. The XRD patterns (Figure 7.50) showed typical peaks for the α-ZrP phase, with the peak at around 11.8° (2θ) being the most intensive one. This peak represents the diffraction from the (002) plane and hence indicates the interlayer distance of the α-ZrP at 7.6 Å.[42] According to the formula of α-ZrP ($Zr(HPO_4)_2 \cdot H_2O$), only one kind of phosphate group should be present, which can serve as an indicator for the material purity. The solid-state ^{31}P MAS NMR spectrum (Figure 7.51) of the α-ZrP platelets appears with only one dominant peak (-18.4 ppm) with two shoulders (-16.8 and -20.3 ppm) within the ^{31}P chemical shift region of $–HPO_4$ groups. It was reported that the dominating peak could be assigned to the $–HPO_4$ groups of the interlayer, while the shoulders could be assigned to the phosphate groups on the edges of the platelet (with possible partial hydrolysis and dehydration).[43,47] The absence of a resonance peak at 0 ppm indicated that no residual H_3PO_4 was left behind in the material. Morphologically speaking, the α-ZrP particles are highly ordered hexagonal platelets with a diameter of approximately 3 μm, as shown by the SEM images (Figure 7.52).

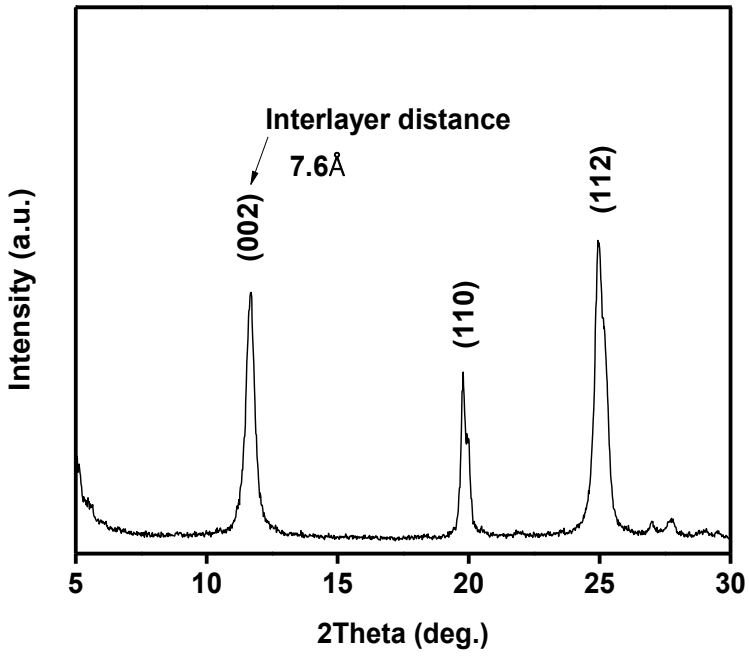

Figure 7.50. XRD patterns of the synthesised α-ZrP platelets.

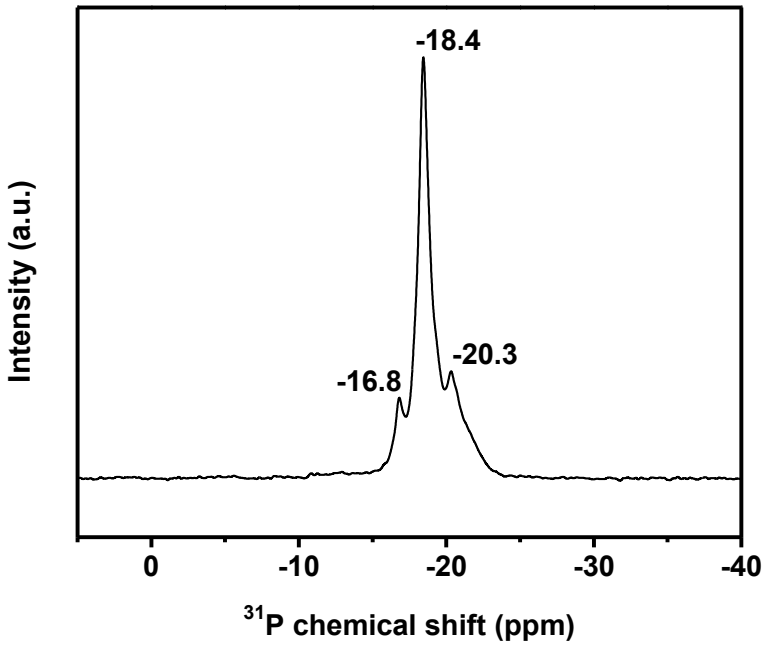

Figure 7.51. Solid-state ^{31}P MAS NMR spectrum of the synthesised α-ZrP platelets.

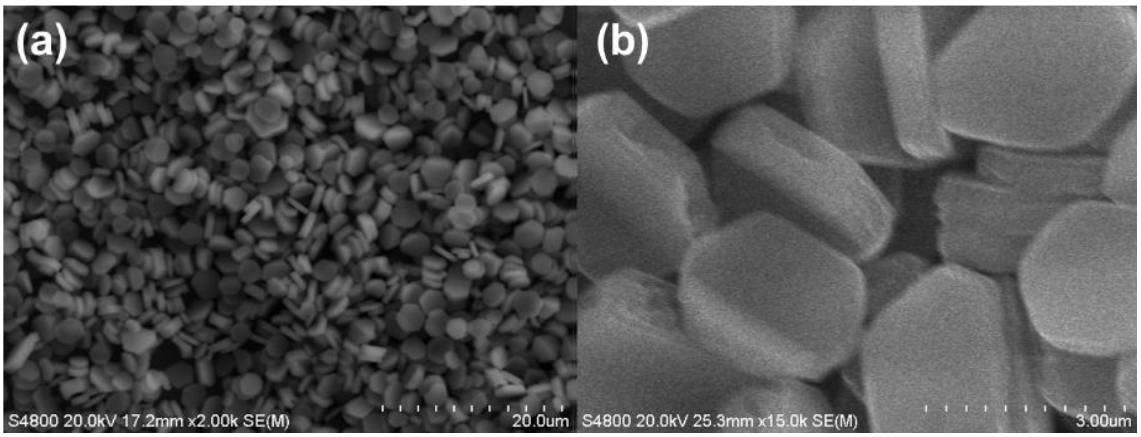

Figure 7.52. SEM micrographs of the synthesised α-ZrP platelets at different magnifications: (a) 2000 and (b) 15000.

7.3.2 Selectivity of metal(IV) phosphate inorganic ion-exchangers

ZrP and TiP are widely investigated metal(IV) phosphates that can be obtained in the metal(IV)–H_3PO_4 system. In the present study, their amorphous and crystal forms (am-ZrP, am-TiP, α-ZrP and α-TiP) have been investigated for Sc(III)/Fe(III) separation from acidic media (Figure 7.53). Both amorphous and crystalline TiP and ZrP exhibited the preferential uptake of Sc(III) over Fe(III). This selectivity for Sc(III) might be explained by the lower hydration enthalpy of Sc(III) than that of Fe(III), as less energy is utilised for Sc(III) dehydration to occupy ion-exchange sites.[48,49] Although the amorphous forms of ion-exchangers exhibited higher uptake capacity for both Sc(III) and Fe(III) (especially am-ZrP), α-ZrP exhibited the highest Sc(III)/Fe(III) separation factors (Figure 7.55). Besides of the superior selectivity of α-ZrP over am-ZrP for Sc(III), for reproducible performance the crystalline form is highly preferred over the amorphous form of metal phosphates, and it is more stable over a wide pH range. With the increase of pH a general decrease in separation factors was observed, presumably as a consequence of the increase in the availability of ion-exchange sites, which resulted in an elevated Fe(III) uptake. Ion-exchange properties of metal(IV) phosphates depend on the central atom and their crystalline structure.[50] Based on the lattice radius of 6-coordinate Ti(IV) (0.74 Å) and of Zr(IV) (0.86 Å) and high polarising power of Ti(IV), it might be assumed that the acidity

of the phosphate group in α-TiP is higher than in α-ZrP.[49] Still, α-ZrP possesses higher free area around the phosphate group (24.0 $Å^2$) than α-TiP (21.6 $Å^2$), indicating that there is more available cavity around the exchange sites for guest species.[50,51] The phosphate groups in ZrPs are believed to have a greater mobility compared to those in TiPs, because the lesser covalent nature of the Zr–O bonds with regards to the Ti–O bonds. Higher free area and greater phosphate mobility are both convenient for accommodating larger species, and as the ionic radius of Sc(III) is larger than that of Fe(III), the uptake of Sc(III) was facilitated. The prominent selectivity of α-ZrP is an overall result of different effects: hydration enthalpy, the pH of solution, and accessibility of phosphate groups. As a consequence, only α-ZrP was selected for further detailed study.

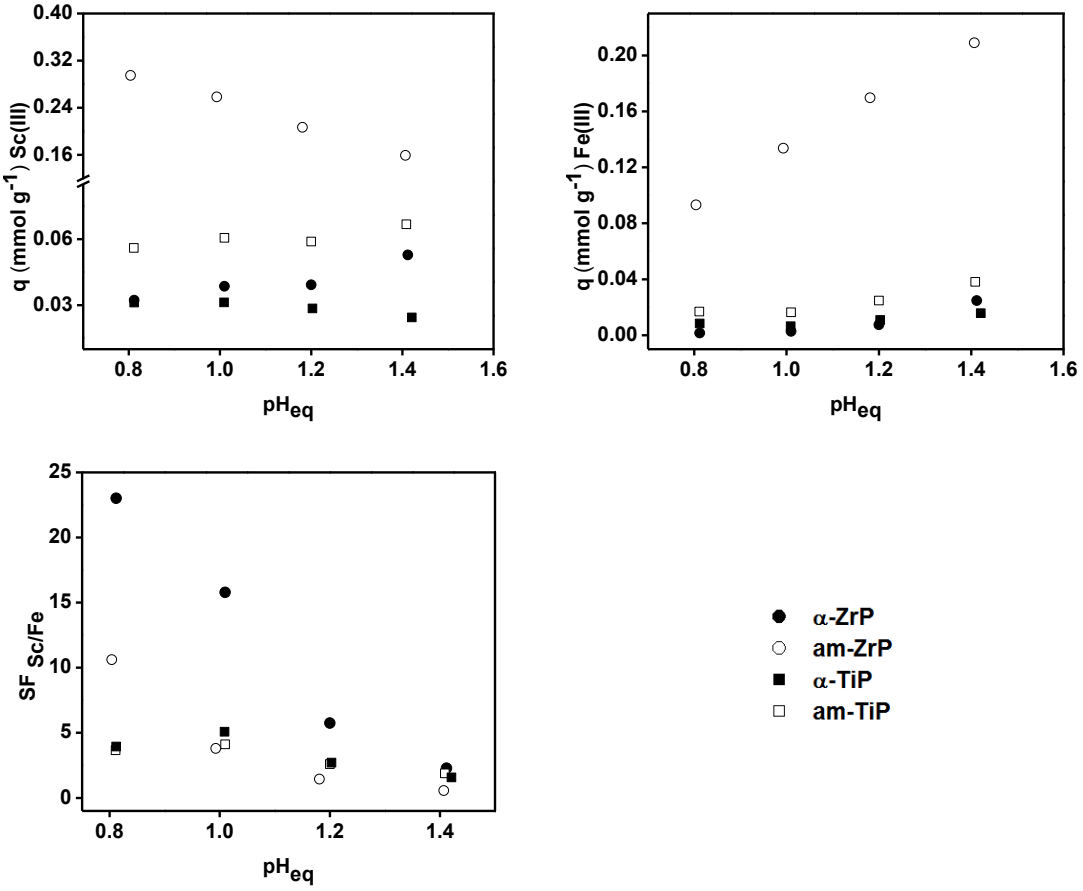

Figure 7.53. Sc(III) and Fe(III) uptake (*q*) and separation factors (*SF*) as a function of pH_{eq} with different inorganic ion-exchangers. Feed: binary equimolar solutions c_{ini} = 0.9 mmol L^{-1}, *V* = 20 mL. *m* = 0.05 g, 300 rpm, room temperature.

7.3.3 pH dependence

The solution pH is one of the crucial parameters that can affect the uptake of metal ions and the selectivity of an ion-exchanger. The ion-exchange uptake of metal ions (M^{n+}) on α-ZrP can be expressed using *Eq. 7.14* (crystalline water is omitted for clarity): [37]

$$Zr(HPO_4)_2 + 1/n\ M^{n+} \leftrightarrow Zr(M_{1/2n}PO_4)_2 + 2H^+ \qquad (Eq.\ 7.14)$$

Obviously, lowering solution pH would drive the equilibrium towards the left-hand side, resulting in lower metal uptake. The influence of the pH was further investigated from single-element solution and Sc(III)/Fe(III) binary HCl solutions. As expected, an increase in metal ions uptake was observed as the pH_{eq} increased, both from single and binary solutions (Figure 7.54). The uptake of Sc(III) was generally more favorable than the uptake of Fe(III). However, the uptake of Sc(III) from acidic media (0.42 mmol g^{-1} from single Sc(III) solution at pH 1.6) was well below the total sorption capacity of α-ZrP reported in the literature (6.64 meq g^{-1} or 2.21 mmol g^{-1} of Sc(III)).[41] α-ZrP exhibits a diprotic character, with pKa_1 = 3.3 and pKa_2 = 6.3.[42] Since the present sorption systems are operating at pH values far lower than the first acid dissociation constant, the obtained uptake values are expected.

The influence of pH on Sc(III) and Fe(III) uptake by α-ZrP was additionally investigated from the 3 mol L^{-1} NaCl solutions. Na(I) ions can act as ion-exchange reaction synergists, by entering the layers of α-ZrP and possibly by expanding the interlayer distance.[32] Na(I) ions can subsequently be exchanged by highly charged ions like Sc(III) and Fe(III), due to their stronger electrostatic interaction with α-ZrP. Moreover, Fe(III) and Sc(III) can form chloro complexes in the presence of an excess of chloride anions, which affect the charge of metal ions and may alter the selectivity of α-ZrP.[38,39] The total uptake of metal ions was higher from solutions with NaCl than without its addition, which confirmed Na(I) synergistic effect in the ion-exchange reaction (Figure 7.54, Figure 7.55). However, the increase in the interlayer space of α-ZrP after Na(I) and Sc(III) exchange was not observable in the XRD spectra (Figure 7.56). At such low pH, a low amount of lattice water molecules was displaced by metal ions, and therefore the change in the distance between the adjacent α-ZrP layers was not possible to detect by powder XRD.[45]

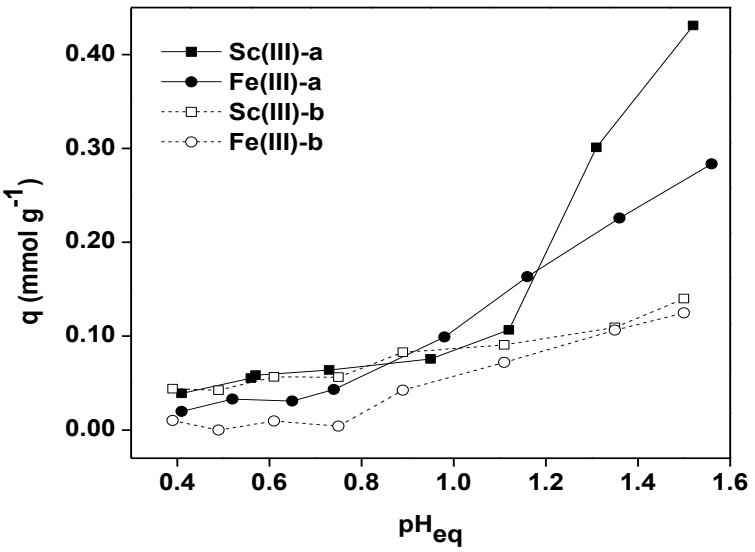

Figure 7.54. Uptake of Sc(III) and Fe(III) by α-ZrP from HCl solutions of: (a) single-element solutions, and (b) equimolar binary mixture of Sc(III) and Fe(III). Feed: c_{ini} = 1.1 mmol L^{-1}, V = 20 mL. m = 0.05 g. 300 rpm, room temperature.

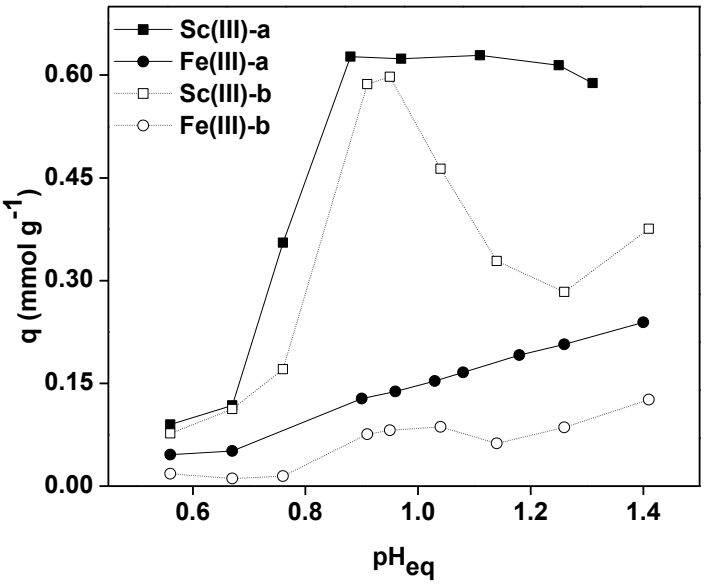

Figure 7.55. Uptake of Sc(III) and Fe(III) by α-ZrP from HCl solutions with 3 mol L^{-1} NaCl of: (a) single element solutions, and (b) binary solutions. Feed: $c_{ini} \approx$ 1.1 mmol L^{-1}, V = 20 mL. m = 0.05 g. 300 rpm, room temperature.

Furthermore, in the pH_{eq} region between 1.0 and 1.3, the uptake of Sc(III) from binary solutions started to decrease, followed by an increase in the uptake of Fe(III) (Figure 7.55). Na(I) and Fe(III) ion exchange was facilitated by an increase in pH, which presumably hindered Sc(III) exchange. Still, as the pH further increased ($pH_{eq} \approx 1.4$) the uptake of both Sc(III) and Fe(III) from a binary solution increased, as there are generally less H^+ ions competing in the ion-exchange reaction with metal ions. High Sc(III)/Fe(III) separation factors from NaCl solution can therefore only be attributed to the Na(I) synergistic effect.

The formation of Fe(III) chloro complexes did not diminish the uptake of Fe(III) by the α-ZrP, as its uptake was even higher from NaCl solutions due to the Na(I) synergistic effect (Figure 7.55, Figure 7.57). Only in a narrow pH_{eq} region, the calculated Sc(III)/Fe(III) separation factors from NaCl solutions significantly surpassed the separation factors obtained by the α-ZrP without NaCl addition (Figure 7.57). Therefore, the incremental selectivity enhancement of α-ZrP for Sc(III) with the addition of NaCl was not further explored. The salt addition would result in a more complex downstream process in practice. Note that the activity coefficient of H^+ in this solution is close to one, therefore the pH measurement was still reliable in the presence of 3 mol L^{-1} NaCl.[52]

To further elucidate the uptake mechanism of Sc(III) and Fe(III) from HCl solutions with and without NaCl, additional studies on α-ZrP with Raman spectroscopy, extended X-ray absorption fine structure (EXAFS) and ^{31}P MAS NMR were attempted. Unfortunately, due to a very low uptake of Sc(III) and Fe(III) from acidic solutions and small changes in the structure of α-ZrP, the spectra obtained by these techniques were inconclusive and therefore omitted here.

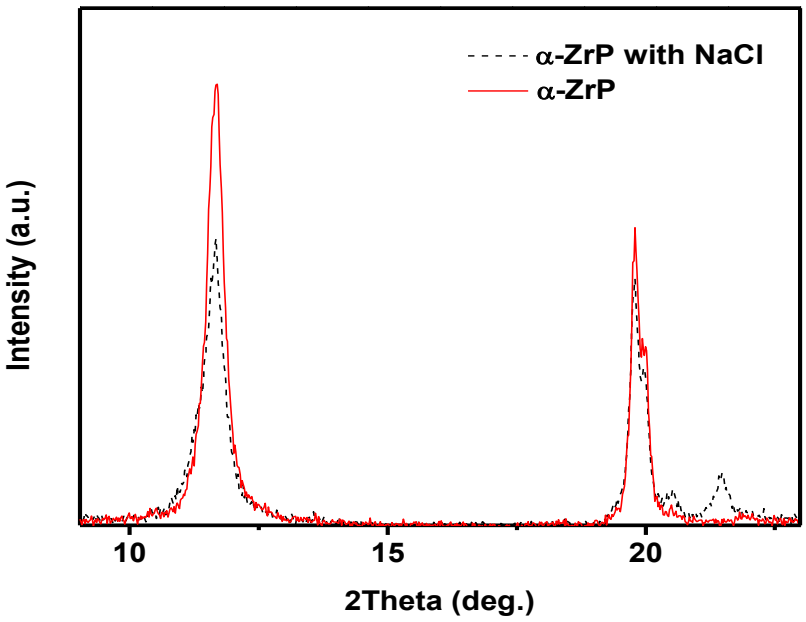

Figure 7.56. XRD patterns of α-ZrP platelets prior to and after Sc(III) uptake from 3 mol L^{-1} NaCl solution at pH_{eq} = 1.4.

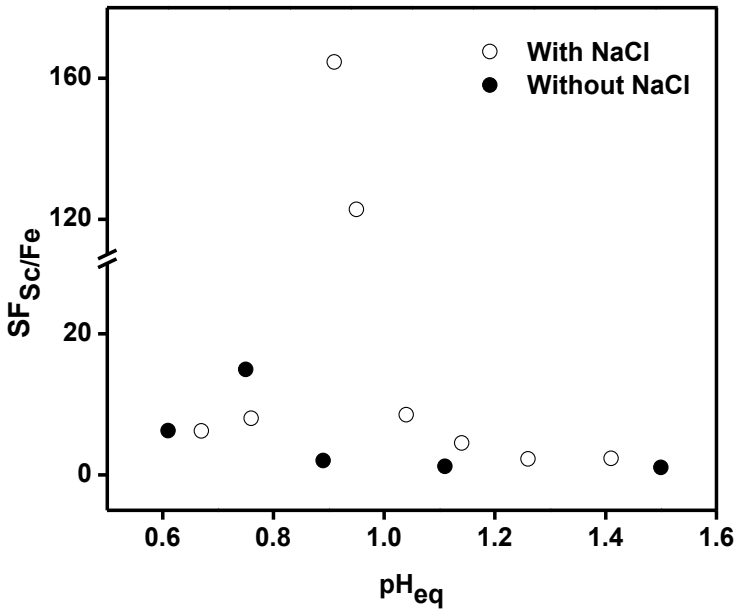

Figure 7.57. Sc(III)/Fe(III) separation factors with increasing pH_{eq} of Sc(III)/Fe(III) binary solutions with and without 3 mol L^{-1} NaCl. Feed: $c_{ini} \approx 1.1$ mmol L^{-1}, $V = 20$ mL. $m = 0.05$ g. 300 rpm, room temperature.

7.3.4 Sorption isotherms

The most common and the simplest models to describe the sorption of metal ions are the empirical Langmuir and Freundlich models. Therefore, the ion-exchange of Sc(III) and Fe(III) was investigated from HCl solutions at $pH_{eq} \approx 1.5$ by varying their concentration (Figure 7.58, Table 7.13), and the equilibrium data were fitted to linearised Langmuir (*Eq. 1.6*, Page 17, 1.3.1.1) and Frenudlich equations (*Eq. 1.7*, Page 18, 1.3.1.1). The Langmuir isotherm model much better described sorption of Sc(III) (regression coefficient, $R^2 = 0.999$) than the Freundlich model ($R^2 = 0.107$) (Table 7.13). The high uptake at low Sc(III) concentration indicates a very strong interaction between Sc(III) and α-ZrP. In addition, when the Sc(III) concentration increased, the saturation constant value was approached. Sorption of Fe(III) fitted both Langmuir and Freundlich isotherm models (R^2 of 0.982 and 0.942, respectively). The results suggest that monolayers of Sc(III) and Fe(III) were sorbed on the α-ZrP surface, but the sorption capacity of α-ZrP was higher for Sc(III) than that for Fe(III) (Table 7.13). The *n* value for Fe(III) indicates a high sorption intensity.

Table 7.13. Langmuir and Freundlich sorption isotherm parameters for Sc(III) and Fe(III).

Isotherm model	Langmuir		Freundlich	
	Sc	Fe	Sc	Fe
Correlation coefficient (R^2)	0.999	0.982	0.107	0.942
Intercept	0.003	0.272	-0.074	-0.402
Slope	1.199	2.347	0.132	0.404
Calculated q_m (mmol g^{-1})	0.83	0.43		
K_L (L $mmol^{-1}$)	468	9		
K_F ($mmol^{1-n}$ g^{-1} L^n)				0.4
n				2.5

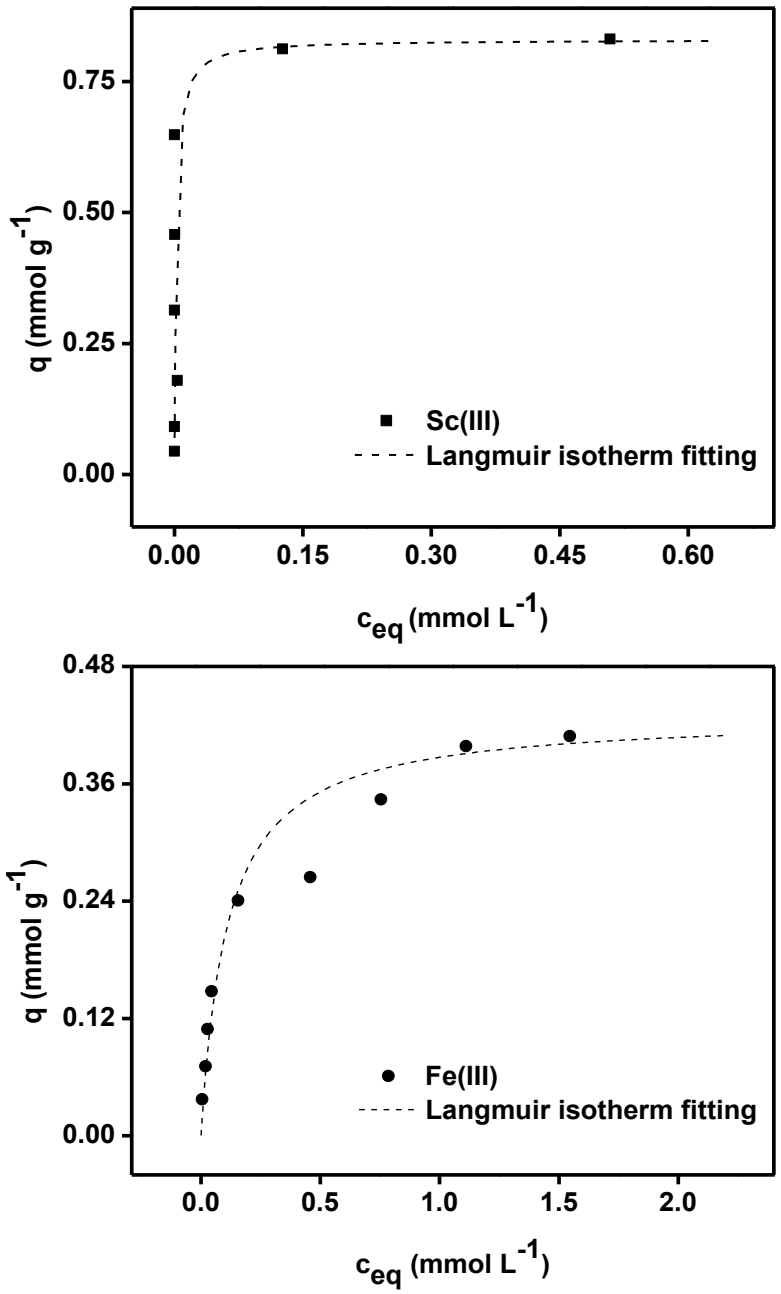

Figure 7.58. Sorption isotherms for Sc(III) and Fe(III) with α-ZrP. Initial concentration range from 0.1 to 2.6 mmol L^{-1}, and of Fe(III) $pH_{eq} \approx 1.5$, $m = 0.05$ g, $V = 20$ mL, 300 rpm, room temperature.

Sorption capacities of several sorbents for Sc(III) are given in the Table 7.14. Although the sorption capacities were determined under different pH, it is evident that even at low pH of 1.5

α-ZrP exhibits a remarkable sorption capacity for Sc(III), superior to other silica- or resin-based sorbents.

Table 7.14. Sorption capacities (q_m) of several sorbents for Sc(III).

Sorbent	pH	q_m (mmol g^{-1})	Reference
Aminocarbonylmethylglycine-immobilised resin (PA-AG)	3	0.28	[53]
Betainium sulfonyl(trifluoromethanesulfonylimide) poly(styrene-co-divinylbenzene) [Hbet-STFSI-PS-DVB]	3	0.36	[54]
Resin with glycol amic acid group	–	0.363	[55]
Amorphous titanium phosphate (am-TiP)	2	0.54	[26]
Saponified product of orange juice residue	4	0.60	[56]
Lysine modified SBA-15 silica	5	0.785	[57]
α-zirconium phosphate (α-ZrP)	1.5	0.83	Present work

7.3.5 Kinetic study

The reaction kinetics primarily defines the efficiency of an ion exchanger. In order to examine the controlling step for ion exchange, the widely used pseudo-first-order, pseudo-second-order and intra-particle diffusion kinetic models were applied (*Eq. 1.8*, *Eq. 1.9* and *Eq. 1.10*, respectively, Page 18, 1.3.1.1). The kinetics of Sc(III) ion exchange by α-ZrP fitted better the pseudo-second-order kinetics model ($R^2 = 0.999$) (Figure 7.59, Table 7.15) than the pseudo-first-order kinetics model ($R^2 = 0.473$) or the intra-particle diffusion model ($R^2 = 0.809$). The results suggest that the chemical reaction at the surface of α-ZrP is the rate-limiting step, rather than diffusion-related phenomena. Sc(III) uptake from HCl media with α-ZrP was remarkably fast and 95% of Sc(III) was exchanged within 15 minutes (Figure 7.59). The fast kinetics of Sc(III) ion-exchange significantly outstand the previously reported equilibration time of 72 hours for the REEs (neodymium and dysprosium) uptake by the α-ZrP.[42] This indicates the practicability of ion-exchanger for large-scale applications, *e.g.* column chromatography separations. Still, when an ion-exchanger is packed in a column, additional practical factors that affect the exchange of

metal ions have to be considered, like the flow rate of feed solution through the column, selectivity coefficient, particle size and operation temperature.

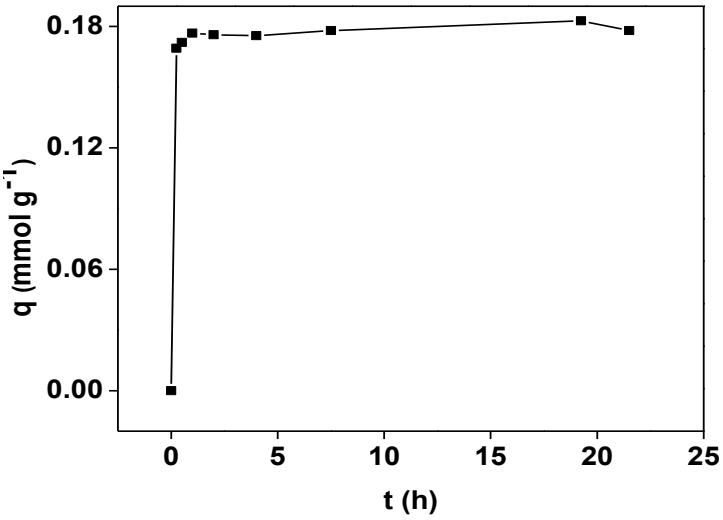

Figure 7.59. Kinetics of Sc(III) sorption by α-ZrP. Feed: c_{ini} = 0.5 mmol L^{-1}, pH_{eq} = 1.5, m = 0.05 g, V = 20 mL. 300 rpm, room temperature.

Table 7.15. Parameters calculated from the linear-fit of kinetic model equations

	Pseudo-second-order
Regression coefficient	0.999
Intercept	6.70
Slope	5.62
Calculated q_m (mmol g^{-1})	0.15
k_2 (gmmol min^{-1})	7.99

7.3.6 Reusability of α-ZrP

Prior to its application in a column chromatography for metal ions separation, the reusability of ion-exchanger must be examined. A mixture of HNO_3 and H_3PO_4 was used for desorption of

Sc(III), since this acid mixture has already been successfully applied for Sc(III) recovery from am-TiP (Figure 7.60).[26]

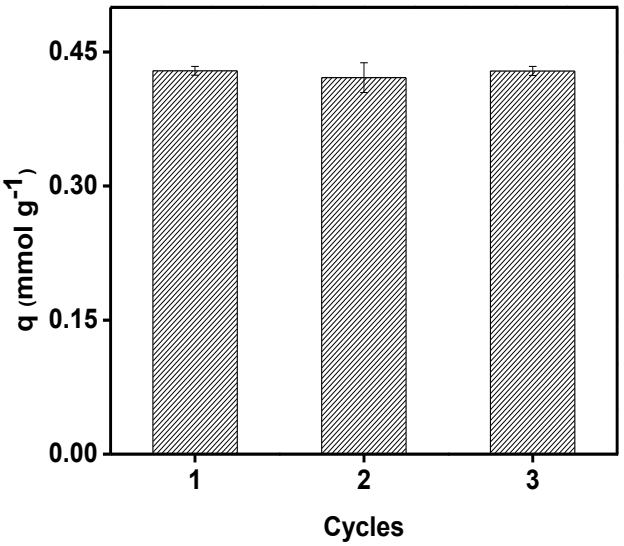

Figure 7.60. Reusability of α-ZrP (triplicate measurements). Sorption conditions: m = 0.05 g, 20 mL of 1.0 mmol L^{-1} Sc(III), pH_{ini} = 1.6, pH_{eq} = 1.5, 18 hours. Desorption conditions: 20 mL of 1.5 mol L^{-1} equimolar mixture of HNO_3 and H_3PO_4, 24 hours.

Accordingly, Sc(III) was quantitatively desorbed (100%) from α-ZrP with the acid mixture, and moreover α-ZrP was reused for three times, without any significant decrease in Sc(III) uptake.

7.3.7 Column chromatography studies

Since the vital parameters for Sc(III) recovery by α-ZrP from acidic solutions showed promising results (selectivity, sorption capacity, kinetics, reusability), α-ZrP was packed in a column and at first breakthrough curve with Sc(III)/Fe(III) binary solution was constructed. The synthetic solution was prepared by mimicking the Sc//Fe concentration ratio of a typical BR acidic leachate (Figure 7.61).

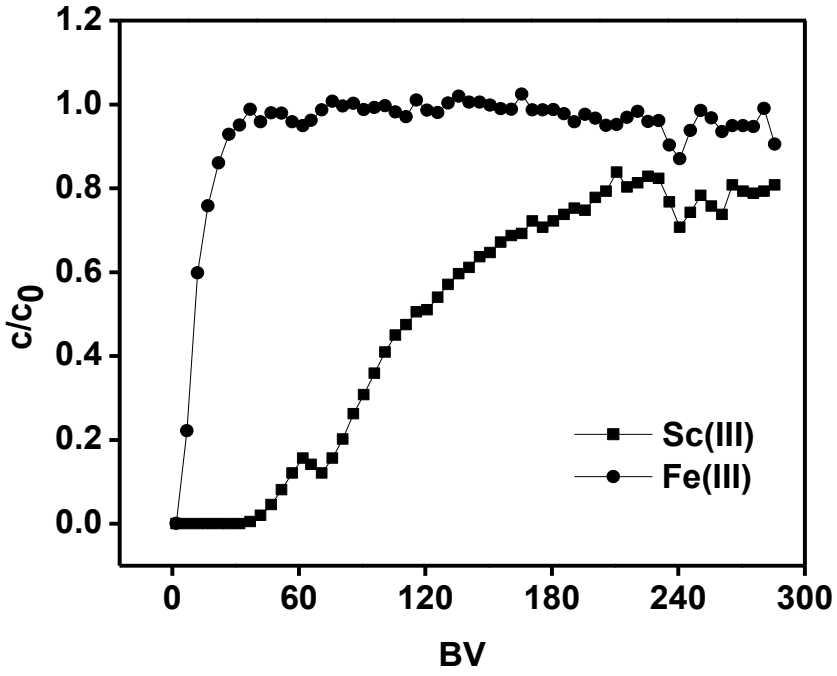

Figure 7.61. Breakthrough curve of Sc(III) and Fe(III) from binary HCl solution (pH_{ini} = 0.8). Feed: 0.04 mmol L^{-1} of Sc(III), Fe/Sc molar ratio = 43. Flow rate 2 BV h^{-1}.

Under acidic conditions, Fe(III) started to break through at 1 *BV*, while Sc(III) break through at 32 *BV*, confirming the remarkable selectivity of α-ZrP for Sc(III). The sorption performance of Sc(III) through the column could be analysed by established mathematical models: Thomas, Yoon-Nelson or Adams-Bohart model.[58] Since it has been confirmed batchwise that Sc(III) uptake by the α-ZrP follows Langmuir isotherm model and the pseudo-second-order reaction, it might seem reasonable to attempt fitting the data to the Thomas model. However, our dual metal loading process did not fit well with the Thomas model since the Sc(III) and Fe(III) are essentially competing with each other during the loading. Nevertheless, the breakthrough study revealed the potential applicability of α-ZrP for Sc(III) recovery and purification from BR leachates.

As a demonstration, a freshly prepared HCl BR leachate, without any further pH adjustments, was loaded onto the α-ZrP column. Although the Sc(III) concentration in the leachate was low

(2 mg L^{-1}), it was completely recovered by α-ZrP, even in the presence of highly concentrated base elements (Table 7.16).

Table 7.16. Composition of the HCl BR leachate and recovery of elements by the α-ZrP.

Elements	Concentration in the leachate (mg L^{-1})	Recovery (%) by the α-ZrP
Ca	5108	6.2
Al	2653	3.9
Si	1202	35.2
Fe	358	54.1
Ti	227	43.3
Ce	9.9	21.7
La	9.3	15.6
Nd	3.7	38.6
Sc	1.9	>99.9
Y	1.7	29.2
Dy	0.6	8.9

However, certain amounts of base elements, and especially of Fe(III) was recovered by α-ZrP along with Sc(III). In order to separate Sc(III) and other co-loaded elements, a simple concentration gradient elution with HCl was performed (Figure 7.62). The majority of elements recovered by the α-ZrP from the BR leachate break through at the first *BV* and were nearly completely eluted with 1 mol L^{-1} HCl at 31 *BV*. However, only 40% of Sc(III) was eluted at 31 *BV*. Therefore, Sc(III) elution was enhanced by 2 mol L^{-1} HCl and it was completely eluted at 48 *BV*, resulting in a remarkable separation from other elements of the remaining 60% of Sc(III). In the last 17 *BV*, where the majority of Sc(III) was eluted, no Fe(III), Al(III), Ca(II) or other REEs impurities were detected. The performed procedure outstands the previous studies on Sc(III) recovery form BR leachates by its simplicity, effectiveness and scandium purity.[26,59] When considering the fact that the BR leachate was obtained under non-optimised conditions and was tested without any further treatment, the results indicate that α-ZrP may offer a unique

possibility for obtaining high purity scandium from BR leachates. With the performed elution chromatography, a proof-of-principle for Sc(III) recovery and purification from the real BR leachate by α-ZrP was confirmed.

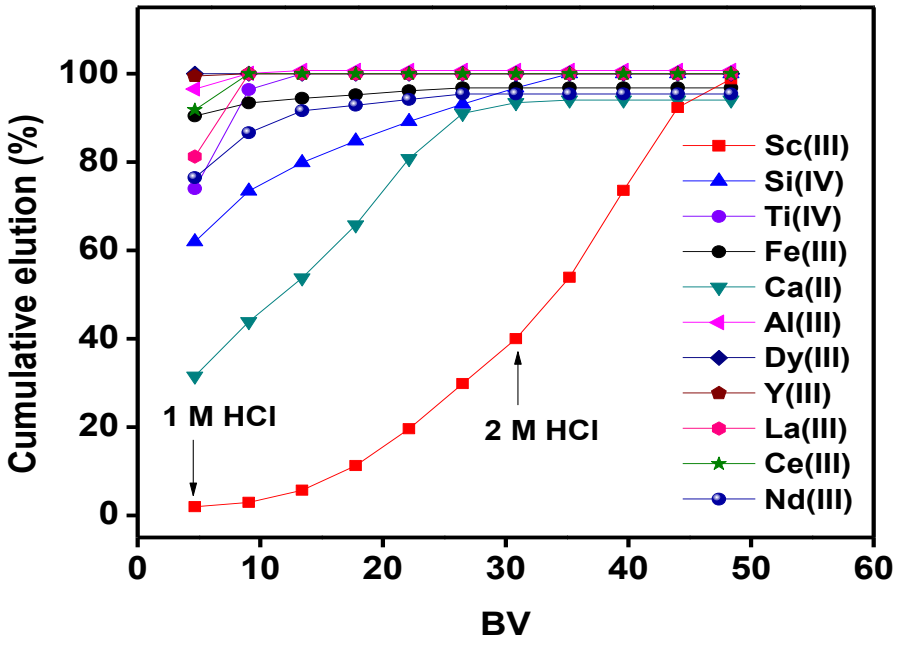

Figure 7.62. Cumulative elution of elements recovered by α-ZrP from BR HCl leachate. Eluent: 1-2 mol L^{-1} HCl. Feed: pH_{ini} = 2.2, V = 5 mL, flow rate 2 BV h^{-1}.

7.4 CONCLUSIONS

ZrP and TiP materials possess excellent selectivity towards Sc(III) in the presence of high concentrations of Fe(III). This interesting feature indicates a potential for applying these materials in Sc(III)/Fe(III) separation from BR leachates, as they are the two elements that exhibit similar properties and thus their separation is generally difficult. Among the tested materials (α-ZrP, am-ZrP, α-TiP, am-TiP), α-ZrP exhibited the highest Sc(III)/Fe(III) separation factors. Hydration enthalpy of Sc(III), ionic radii, crystallinity of the material and the pH of the solution were found to be the dominant factors that have an influence on the α-ZrP selectivity for

Sc(III). α-ZrP exhibited very fast kinetics for Sc(III) uptake, which indicated a practical applicability of the ion exchanger for column chromatography process. Furthermore, the applicability of α-ZrP was verified in a column chromatography by loading BR leachate with HCl, without any pretreatment. Most elements were not recovered by α-ZrP, whereas the recovery of Sc(III) was complete (>99.99%). Moreover, by elution with 2 mol L^{-1} HCl 60% of the recovered Sc(III) was well separated from the base elements in BR and other REEs. High-purity Sc(III) fractions were obtained after a single chromatography separation. α-ZrP presents a solution for purification of Sc(III) from very complex matrices, such as BR leachate.

7.5 REFERENCES

1 K. Binnemans, P. T. Jones, T. Müller, L. Yurramendi, *J. Sustain. Metall.*, 2018, **4**, 126–146.
2 S. Badwal, *Solid State Ionics*, 2000, **136-137**, 91–99.
3 J. Zhang, B. Zhao, B. Schreiner, *Separation Hydrometallurgy of Rare Earth Elements*, Springer, Cham, Switzerland, 2016.
4 Z. Ahmad, *JOM*, 2003, **55**, 35–39.
5 A. Bauer, 1963, US Patent US3351798A.
6 C.M. David, P. Gupta, *Int. J. of Adv. Health Sci.*, 2015, **2**, 7–13.
7 J. Röyset, *Metallurgical Science and Technology*, **25**, 2013.
8 W. Wang, Y. Pranolo, C.Y. Cheng, *Hydrometallurgy*, 2011, **108**, 100–108
9 European Commission, Directorate-General for Enterprise and Industry, 2014, Critical raw materials for the EU, Report of the Ad hoc Working Group on defining critical raw materials. Brussels.
10 European Commission, Directorate-General for Internal Market, Industry, Entrepreneurship and SMEs, 2017, Study on the review of the list of Critical Raw Materials: executive summary.
11 J J. Vind, A. Malfliet, B. Blanpain, P. Tsakiridis, A. Tkaczyk, V. Vassiliadou, D. Panias, *Minerals*, 2018, **8**, 77.
12 C. R. Borra, Y. Pontikes, K. Binnemans, T. Van Gerven, *Min. Eng.*, 2015, **76**, 20–27.
13 R. P. Narayanan, N. K. Kazantzis, M. H. Emmert, *ACS Sustain. Chem. Eng.*, 2017, **6**, 1478–1488.
14 R. P. Narayanan, L.-C. Ma, N. K. Kazantzis, M. H. Emmert, *ACS Sustain. Chem. Eng.*, 2018, **6**, 5333–5341.

15 R. M. Rivera, B. Ulenaers, G. Ounoughene, K. Binnemans, T. van Gerven, *Min. Eng.*, 2018, **119**, 82.
16 R. M. Rivera, G. Ounoughene, C. R. Borra, K. Binnemans, T. Van Gerven, *Min. Eng.*, 2017, **112**, 92–102.
17 L. Piga, F. Pochetti, L. J. Stoppa, *JOM*, 1993, 54–59
18 K. Hammond, B. Mishra, D. Apelian, B. Blanpain, *JOM*, 2013, **65**, 340–341.
19 C. R. Borra, B. Blanpain, Y. Pontikes, K. Binnemans, T. Van Gerven, *J. Sustain. Metall.*, 2016, **2**, 28–37.
20 C. R. Borra, B. Blanpain, Y. Pontikes, K. Binnemans, T. Van Gerven, *J. Sustain. Metall.*, 2017, **3**, 393–404.
21 C. R. Borra, B. Blanpain, Y. Pontikes, K. Binnemans, T. Van Gerven, *J. Sustain. Metall.*, 2016, **2**, 365–386.
22 W. Wang, Y. Pranolo,C.Y. Cheng, *Separation and Purification Technology* **2013**, *108*, 96.
23 B. Onghena, C.R. Borra, T. Van Gerven, K. Binnemans, *Sep. Purif. Technol.*, 2017, **176**, 208–219.
24 J. Roosen, S. Van Roosendael, C.B. Borra, T. Van Gerven, S. Mullens, K. Binnemans, *Green Chem.*, 2016, **18**, 2005–2013.
25 M. Ochsenkühn-Petropulu, Th. Lyberopulu, G. Parissakis, *Anal. Chim. Acta*, 1995, **315**, 231–237.
26 W. Zhang, R. Koivula, E. Wiikinkoski, J. Xu, S. Hietala, J. Lehto, R. Harjula, *ACS Sustain. Chem. Eng.*, 2017, **5**, 3103–3114.
27 D. Depuydt, W. Dehaen, K. Binnemans, *Ind. Eng. Chem. Res.*, 2015, **54**, 8988–8996.
28 L. Schmidt, J. S. Fritz, *J. Chromatogr. A*, 1993, **640**, 145–149.
29 Inamuddin, M. Luqman, *Ion exchange technology*, Springer, Dordrecht, The Nederlands, 2012.
30 B. Onghena, K. Binnemans, *Ind. Eng. Chem. Res.*, 2015, **54**, 1887–1898.
31 B. Onghena, C. R. Borra, T. Van Gerven, K. Binnemans, *Sep. Purif. Technol.*, 2017, **176**, 208–219.
32 G. Alberti, *Acc. Chem. Res.*, 1978, **11**, 163-170.
33 B. F. Alfonso, C. Trobajo, M. A. Salvadó, P. Pertierra, S. García-Granda, J. Rodríguez-Fernández, J. A. Blanco, J. R. García, *Z. Anorg. Allg. Chem.*, 2005, **631**, 2174–2180.
34 H. Xiao, W. Dai, Y. Kan, A. Clearfield, H. Liang, *Appl. Surf. Sci.*, 2015, **329**, 384–389.
35 A. Díaz, V. Saxena, J. González, A. David, B. Casañas, C. Carpenter, J. D. Batteas, J. L. Colón, A. Clearfield, M. D. Hussain, *ChemComm.*, 2012, **48**, 1754–1756.
36 C. Bisio, M. Nocchetti, F. Leroux, *Dalton trans.*, 2018, **47**, 2838–2840.
37 A. Clearfield, *Inorganic ion exchange materials*, CRC Press, Boca Raton, Florida, 1982.
38 Wolfram W. Rudolph, C. C. Pye, *J. Solution Chem.*, 2000, **29**, 955-986.
39 A. Stefánssona, K. H. Lemkeb, T. M. Sewardc, In: Proc. 15th International Conference on the Properties of Water and Steam, 8-11 September, 2008, Berlin, Germany.
40 B. Pan, Q. Zhang, W. Du, W. Zhang, B. Pan, Q. Zhang, Z. Xu, Q. Zhang, *Water res.*, 2007, **41**, 3103–3111.

41 A. Clearfield, W. L. Duax, A. S. Medina, G, D. Smith, J. R. Thomas, *J. Phys. Chem.*, 1969, **73**, 3424–3430.
42 J. Xu, E. Wiikinkoski, R. Koivula, W. Zhang, B. Ebin, R. Harjula, *J. Sustain. Metall.*, 2017, **3**, 646–658.
43 B. M. Mosby, A. Díaz, V. Bakhmutov, A. Clearfield, *ACS Appl. Mater. Interfaces*, 2014, **6**, 585–592.
44 J. Xu, R. Koivula, W. Zhang, E. Wiikinkoski, S. Hietala, R. Harjula, *Hydrometallurgy*, 2018, **175**, 170-178.
45 A A. Clearfield, J. Stynes, *J. Inorg. Nucl. Chem.*, 1964, **26**, 117–129.
46 L. Sun, W. J. Boo, H.-J. Sue, A. Clearfield, *New J. Chem.*, 2007, **31**, 39–43.
47 B. M. Mosby, M. Goloby, A. Díaz, V. Bakhmutov, A. Clearfield, *Langmuir*, 2014, **30**, 2513–2521.
48 D. W. Smith, *J. Chem. Educ*., 1977, **54**, 540–542.
49 R. Thakkar, U. Chudasama, *J. Hazard. Mater.*, 2009, **172**, 129–137.
50 G. Alberti, E. Torracca, A. Conte, *J. Inorg. Nucl. Chem.*, 1966, **28**, 607–613.
51 R. D. Shannon, *Acta Cryst. A*, 1976, **32**, 751–767.
52 W. Song, M. A. Larson, *AIChE J*., 1990, **36**, 1896-1900.
53 Z. Zhao, Y. Baba, W. Yoshida, F. Kubota, M. Goto, *J. Chem. Technol. Biotechnol.*, 2016, **91**, 2779- 2784.
54 D. Avdibegović, M. Regadío, K. Binnemans, *RSC Adv.*, 2017, **7**, 49664- 49674.
55 N. Van Nguyen, A. Iizuka, E. Shibata, T. Nakamura, *Hydrometallurgy*, 2016, **165**, 51-56.
56 H. Paudyal, B. Pangeni, K. Nath Ghimire, K. Inoue, K. Ohto, H. Kawakita, S. Alam, *Chem. Eng. J.*, 2012, **195-196**, 289-296.
57 J. Ma, Z. Wang, Y. Shi, Q. Li, *RSC Adv.*, 2014, **4**, 41597.
58 Z. Z. Chowdhury, S. M. Zain, A. K. Rashid, R. F. Rafique, K. Khalid, *J. Chem.*, 2013, 1-8.
59 D. Avdibegović, M. Regadío, K. Binnemans, *RSC Adv.* 2018, **8**, 11886- 11893.

Chapter 8

Titanium alkylphosphate functionalised mesoporous silica for enhanced uptake of rare earths

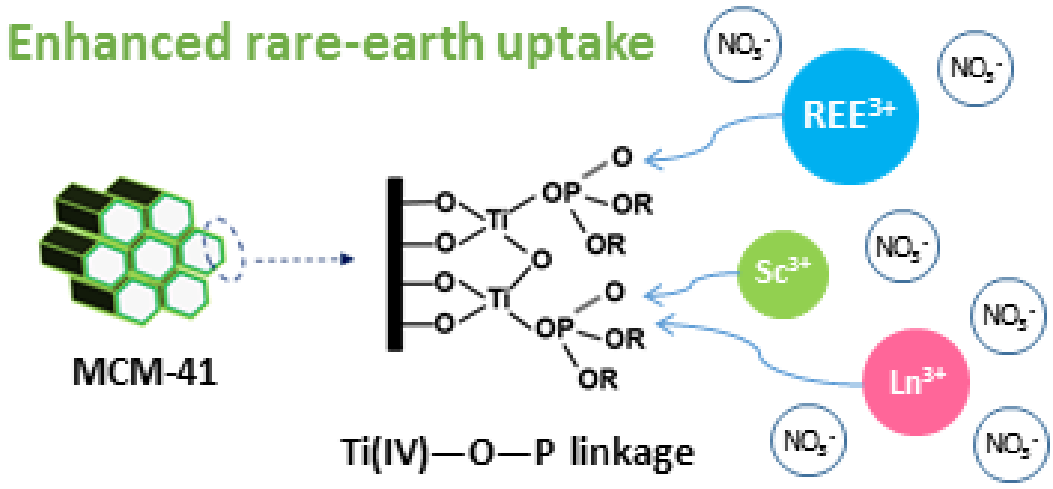

Sorbents for rare-earth ions are prepared by covalently binding organophosphate ligands on mesoporous silica *via* a versatile metal(IV)−O−P linkage.

This chapter is based on the published paper:

Zhang W., Avdibegović, D., Koivula R., Hatanpaa T., Hietala S., Regadío M., Binnemans K., Harjula R. (2017). Titanium alkylphosphate functionalised mesoporous silica for enhanced uptake of rare-earth ions, *Journal of Materials Chemistry A*, **5** (45), 23805-23814.

The text may contain slight adjustments compared to the original publication.

Author contributions:

W.Z., D.A., K.B and R.K. conceived the research. W.Z. and D.A. perfomed all experiments, except that T.H. conducted thermogravimetry analysis. S.H. discussed NMR data analysis. W.Z. and D.A. analysed the data and W.Z. drafted the manuscript. All authors commented on the manuscript.

Authors wish to thank Dr Sambhu Radhakrishnan and Dr Eric Breynaert (KU Leuven) for performing the solid-state ^{13}C and ^{31}P NMR measurements. Bart Van Huffel, Dirk Henot (KU Leuven) and Pasi Heikkilä (University of Helsinki) are acknowledged for BET, CHN and XRD analysis, respectively.

ABSTRACT

The separation of rare-earth elements (REEs) is usually carried out by a multi-stage solvent extraction process utilising organophosphorus extractants. Inspired by the structure of the solvating extractant tri-*n*-butyl phosphate (TBP), new sorbents were designed by covalently attaching short *n*-alkyl chains (ethyl, *n*-propyl and *n*-butyl) to titanium(IV) phosphate functionalised mesoporous MCM-41 silica by a layer-by-layer grafting route. Mesoporous MCM-41 silica served as a versatile porous support and the grafted titanium(IV) derivatives provided enhanced acid stability and solvating extraction capability. Various characterisation methods including solid-state ^{13}C, ^{29}Si and ^{31}P magic-angle spinning (MAS) nuclear magnetic resonance (NMR) and simultaneous thermogravimetry and differential scanning calorimetry–mass spectroscopy (TG/DSC-MS) were used to confirm the ligand attachment. The hybrid materials showed a better uptake of rare-earth ions from nitrate feed solution than the unmodified inorganic material. The optimal separation factor (*SF*) obtained for scandium-lanthanum separation is in excess of 100,000 at pH 2.1. The *SFs* calculated for dysprosium-neodymium are approximately 3, which is comparable to that of TBP in a typical solvent extraction setup. This study provides a new strategy to design inorganic–organic hybrid sorbents based on the structure of organophosphorus extractants *via* metal(IV)–O–P bonds.

8.1 INTRODUCTION

Rare-earth elements (REEs) nowadays play an increasing role as critical raw materials for the transition to cleaner energy and the production of high-tech devices.[1] They are used in wind turbines (Nd, Dy, Sm, Pr), hybrid and electric cars (Nd, Dy, La) and lamp phosphors (Eu, Gd, Tb, Yb, La).[2] For these applications, pure REEs are required. Liquid-liquid extraction and ion-exchange are the most important REE separation techniques. However, the separation of complex mixtures of REEs remains challenging owing to the similarity of their chemical properties.[3,4] The liquid-liquid extraction process involves the use of organic extractants which transfer the REE ions from the aqueous to the organic phase.[5] Usually, the organic phase consists of a diluent (kerosene) to dissolve the extractant, reduce the viscosity of the loaded organic phase and facilitate the hydrodynamics of the extracted species. Tri-*n*-butyl phosphate (TBP) is a classic solvating extractant used in the separation of REE.[6,7] The neutral REE-nitrate complexes are coordinated by the phosphoryl group in TBP, yielding an extractable complex (*Eq. 8.15*):[3,8,9]

$$REE^{3+}{}_{(aq.)} + 3NO_3^-{}_{(aq.)} + 3TBP_{(org.)} \leftrightarrows [REE(NO_3)_3TBP_3]_{(org.)} \qquad (Eq.\ 8.15)$$

The extraction of REEs must be carried out at high nitrate salt concentrations (often > 6 mol L^{-1}) to shift the equilibrium in *Eq. 8.15* to the right. The separation is based on the slightly different complex stability constants for different lanthanides.[9]

Liquid-solid extraction is regarded as an alternative for liquid-liquid extraction.[10-12] Recently, organic-inorganic hybrid materials, including metal phosphonates (metal-organic framework)[13,14] and ligand-functionalised silica (phosphine oxide,[15] phosphonates[16-18] and diglycolamide-derivatives[19-22]) have been developed as sorbents for REE separation. The major advantage of liquid-solid extraction over liquid-liquid extraction is the elimination of one of the liquid phases.[2]

Selective ion-exchange materials, which are used in liquid-solid extraction, take advantage of the differences in the acidity and ionic radii of REEs. Solid metal(IV) phosphates are a class of inorganic ion-exchange materials with a good stability against strong acids and a good thermal stability.[23] Recently it has been shown that titanium phosphates are useful for scandium recovery

from acidic media due to metal affinity towards the phosphate ligands and size selection.[24] However, one major drawback of these metal phosphates is the high framework density due to their densely packed layered structure, which leads to a relatively low surface area and slow kinetics. Decorating a porous support with metal phosphate could mitigate this issue. Silica materials are especially suitable to this end since they offer tuneable framework structures with high surface area. The mesoporous MCM-41 (M41) silica[25] consists of an ordered hexagonal pore array built up by unidimensional and hexagonal pores.[26] Many silanol groups are available on the surface of the pores, permitting post-synthetic functionalisation of the heteroatoms. M41 is generally extensively investigated because the other members in this family are either thermally unstable or difficult to obtain.

A solution-based layer-by-layer deposition has been developed to graft amorphous titanium phosphate onto silica.[27-29] The resulted grafted material showed enhanced metal uptake compared to that of pure silica support or to that of metal phosphate. The introduction of titanium also improves the acid stability of the phosphate group since direct Si–O–P linkages are prone to hydrolysis.[30]

Herein, we present the conceptual design and synthesis of a hybrid liquid-solid extraction material composed of M41 silica as a support and titanium(IV) alkylphosphate covalent grafts as the functional groups. The basicity of P=O groups is expected to be influenced by titanium(IV) and the organic *n*-alkyl chain lengths can impose steric effects[10] to facilitate molecular recognition events.[31] The surface alkylphosphate groups mimicking the TBP structure showed good performance for uptake of rare-earth nitrate complexes in acidic solutions using ammonium nitrate as the source of nitrate ions.

8.2 EXPERIMENTAL

8.2.1 Chemicals

Titanium(IV) isopropoxide ($Ti(OPr^i)_4$, >97%), tetraethyl orthosilicate (TEOS, >98%), hexadecyltrimethylammonium bromide (CTAB, >99%), neodymium(III) nitrate hexahydrate

(>99.9%), dysprosium(III) nitrate hydrate (>99.9%) and ammonia solution (25 wt.%) were purchased from Sigma-Aldrich (Helsinki, Finland). Pyridine (>99%), ethanol (>99.5%), *n*-propanol (>99.0%) and *n*-butanol (>99.4%) were purchased from Fisher Chemical (Helsinki, Finland). Scandium(III) oxide (>99.99%) were acquired from Alfa Aesar (Helsinki, Finland). Phosphorus oxychloride (>99%) was obtained from ACROS Organics (Helsinki, Finland). Ammonium nitrate was obtained from Riedel-de Haen GmbH (Seelze, Germany). All elemental (P, Dy, La, Nd, Sc, and Ti) single standard solutions (1000 mg L^{-1}, PrimAg-plus cert. ref. material) and nitric acid (SpA super purity, 67-69%) were purchased from Romil (Cambridge, UK). Milli-Q water (Millipore) with a resistivity of 18.2 MΩ cm was used throughout the experiments.

8.2.2 Synthesis of silica support

MCM-41 silica was synthesised according to a literature procedure.[32] At first, 2.0 g of CTAB was dissolved in a diluted ammonia solution (205 mL of 25 wt.% ammonia solution mixed with 270 mL of H_2O). Subsequently, 10 mL of TEOS was added drop-wise to the solution, giving rise to a white slurry. The slurry was then aged for 2 h before harvested by filtration and washing. To remove the template, the final product was calcined in air at 550 °C. The molar composition of the precursor was 525 H_2O: 69 NH_4OH: 0.125 CTAB: 1 TEOS.

8.2.3 Grafting of titanium(IV) alkylphosphate

The synthesis was carried out under argon atmosphere. In a typical experiment, 1 g of M41 was mixed with 20 mL of dry toluene in a two-neck flask sealed with a rubber septum, to which 3.4 mmol of $Ti(OPr^i)_4$ was added through a syringe at room temperature. The slurry was stirred and refluxed at 80 °C for 2 h. The obtained solid was washed three times with toluene to remove unreacted $Ti(OPr^i)_4$ precursor, washed again three times with water to hydrolyse the alkoxy groups and then dried in air at 80 °C. The modification of the phosphate groups was achieved by repeating the same procedure using 10.2 mmol of $POCl_3$ (except for the washing step). The obtained solid was then washed three times with 20 mL of toluene. The alkyl chains were

attached to the material through esterification reactions by corresponding alcohols. To a sealed two-neck flask, 20 mL of toluene was added together with the toluene-washed slurry. The mixture was stirred and the flask was cooled in an ice-water bath before slowly adding 30 mmol of pyridine and, afterwards, 60 mmol of alcohol (ethanol, n-propanol or n-butanol). After the addition was completed, the reaction mixture was heated slowly to 80 °C and held there for 2 h. The products were washed three times with 20 mL of acetone and three times with 20 mL of water before drying in vacuum at 50 °C. The final products are denoted as M41-TiEtP, M41-TiPrP and M41-TiBuP corresponding to ethyl-, *n*-propyl- and *n*-butyl- grafted materials, respectively. For comparative reasons, the inorganic titanium(IV) phosphate grafted M41 (denoted as M41-TiP) was also synthesised by direct hydrolysing the product with water after the reaction with $POCl_3$.

8.2.4 Characterisation

The surface morphology was examined using a Hitachi S-4800 FE-SEM (field-emission scanning electron microscopy) after coating with 3 nm of Pd-Au by sputtering. Powder X-ray diffraction (XRD) patterns were collected using a PANalytical X'Pert PW3710 MPD diffractometer coupled with a PW3020 vertical goniometer in Bragg-Brentano geometry. X-ray radiation was sourced from monochromatic CuKα line (λ=1.54056 Å) at 40 kV and 40 mA. All solid-state magic angle spinning (MAS) nuclear magnetic resonance (NMR) spectra were acquired on a Bruker Avance III 500 MHz spectrometer equipped with 4mm H/X/Y MAS probe. The samples were filled in a 4 mm ZrO_2 rotor and measured under MAS at 12 (for ^{29}Si) and 15 kHz (for ^{1}H, ^{13}C and ^{31}P). The ^{1}H spectra were acquired with a 90° pulse (83 kHz RF pulse), 5s recycle delay and 64 scans. All the ^{1}H spectra were referenced to the secondary ^{1}H reference adamantane (^{1}H peak at 1.773 ppm), which was referenced to the primary reference tetramethylsilane (TMS) at 0 ppm. ^{13}C spectra were recorded with ^{1}H-^{13}C cross-polarisation pulse sequence, 2048 scans, recycle delay of 5 s, spinal-64 ^{1}H decoupling and a contact time 0.5 ms. Line broadening of 50 Hz was applied for spectral processing. The spectra were referenced to the ^{13}C adamantane peak at 38.5 ppm, which was primarily referenced to the TMS peak at 0 ppm. ^{29}Si spectra were obtained with a 4.18 μs pulse, 200 s recycle delay and

256 scans. The spectra were externally referenced also to TMS. ^{31}P spectra were acquired with a 90° pulse (77 kHz RF), 100s recycle delay and 64 scans. ^{31}P NMR spectra were referenced to the ammonium dihydrogen phosphate peak at 0.8 ppm, which was further referenced to the primary reference 85% H_3PO_4 peak at 0 ppm. Infrared spectra (700–4000 cm^{-1}) were recorded on a Bruker Vertex 70 spectrometer (Bruker Optics) with a platinum ATR single reflection diamond attenuated total reflection (ATR) accessory. The CHN (carbon, hydrogen, nitrogen) elemental contents were analysed by a Thermo Scientific Interscience Flash 2000 Elemental analyser. The textural properties of the materials were determined by N_2 adsorption at 77 K, using a Quanta Chrome NOVA 2200e surface area and pore size analyser. Samples were degassed at 160 °C (M41 and M41-TiP) or at 80 °C (other samples) for 23 h prior to analysis. The BET surface area was calculated by the Brunauer, Emmett, and Teller (BET) method using the adsorption isotherms. Pore-size distributions were calculated using nonlocal density functional theory (NLDFT) with cylindrical silica pores. Simultaneous thermogravimetry and differential scanning calorimetry–mass spectroscopy (TG/DSC–MS) analysis was performed using a simultaneous TG/DSC apparatus (STA 449F3 Jupiter, Netzsch) connected to JAS-Agilent GCMS (7890GC/MSD5977A). In the dynamic TG measurements, the samples were heated from 30 °C to 800 °C. The heating rate was 20 °C min^{-1}, with a helium flow of 40 mL min^{-1}. A sample of 5 to 10 mg was placed in an open 90 μL alumina crucible. Part of the evolving gas mixture (50%) was led with aid of diaphragm pump through a heated transfer line with silico-steel capillary tubing to a heated gas sampling system (JAS valve), both maintained at 250 °C. From the sampling system on the top of an Agilent GC-MS (7890B GC/MSD5977A), part of the evolved gas mixture was continuously sampled into the GC-MS system. In the GC furnace held at 250 °C there was a 60 cm long GC capillary which acted as a pressure restrictor in front of the MS detector. Data collection was carried out with Agilent MassHunter software.

8.2.5 Batch sorption and desorption experiments

Typically, 0.050 g of material was placed in a polyethylene vial with 20 mL of test solution. Samples were equilibrated overnight on a constant rotary mixer (50 rpm). The solid/liquid separation was then achieved by centrifugation (15 min at 3000 ***g***), and an adequate amount of

the supernatant was filtered through a 0.45 μm PVDF syringe filter for concentration determination. Equilibrium pH was measured from the remaining solution. Two systems were evaluated: in the first system, a 1 mmol L^{-1} equimolar mixture of Sc and La (with and without 5 mol $L^{-1}NH_4NO_3$) were studied as a function of pH in the range of 1 to 4. The second system comprised a 1 mmol L^{-1} equimolar mixture of Nd and Dy (with 5 mol L^{-1} NH_4NO_3), sorption was studied as a function of the pH in the range of 1 to 5. The pH was adjusted with 1 mol L^{-1} HNO_3. Desorption experiments were conducted by first loading the materials with metals at appropriate equilibrium pH. After loading equilibrium was reached, the supernatant was decanted. The remaining material was quickly washed three times with 20 mL of acetone using centrifugation and re-dispersion, and the supernatants were all discarded. Note that ammonium nitrate is soluble in acetone. The acquired slurry was dried in an oven at 50 °C. After that, 20 mL of acid solution was introduced into the tube and samples were again equilibrated. Finally, after centrifugation, the supernatant was taken for metal analysis. The desorption solution used here were water, 0.01 mol L^{-1} HNO_3 and 0.1 mmol L^{-1} HNO_3. Cyclic sorption-desorption was performed for five cycles. Acid stability was measured by batch experiments using 0.01 mol L^{-1} and 0.1 mol L^{-1} HNO_3 with an equilibration time of 6 h.

Determination of metal concentrations was performed on a Perkin Elmer Optima 8300 inductively coupled plasma optical emission spectrometer (ICP-OES) in dual view, with a GemTip CrossFlow II nebuliser, a Scott Spray Chamber Assembly, a sapphire injector and a HybridXLT ceramic torch. Atomic emission lines were prioritised and possible spectrum interferences were minimised. Lanthanum or praseodymium were used as internal standard. The distribution coefficient (K_d) and separation factors (SF) were calculated based on the *Eq. 1.4* and *Eq. 1.5*, respectively (Page 17, 1.3.1.1).

8.3 RESULTS AND DISCUSSION

8.3.1 Synthesis and characterisation

The synthesis approach is shown in the Figure 8.63: the M41 silica was grafted with titanium(IV) phosphate *via* 'acid-base pair' precursors utilising $Ti(OPr^i)_4$ and $POCl_3$.[29] The reactivity of the P–Cl bonds was later harnessed for grafting alkoxy groups through reaction with the corresponding alcohol (ethanol, *n*-propanol and *n*-butanol). The reaction was carefully controlled (by drop-wise addition of the alcohol) to avoid the E2 elimination of the alcohol to an alkene. Additionally, HCl generated in the reaction was removed by a base (pyridine).

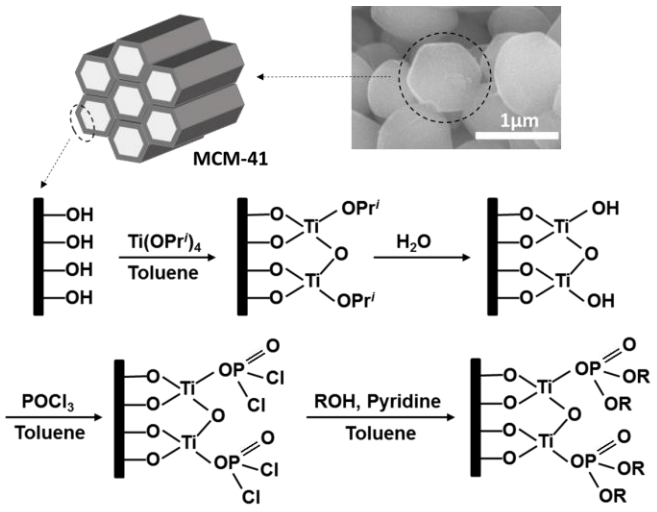

Figure 8.63. Layer-by-layer synthesis route of M41 silica functionalised titanium(IV) *n*-alkylphosphate materials (R = H, Et, *n*-Pr and *n*-Bu).

The FE-SEM images of those hexagonal-shape materials are available in Figure 8.64. All functionalised materials contained approximately 8 wt% of Ti and 4 wt% of P (Table 8.17). The small-angle XRD patterns of grafted hybrid materials showed well-resolved peaks at 2θ = 3-4° (Figure 8.65), confirming the preservation of the ordered hexagonal mesoporous structure. The

slight shift of the [100] diffraction peak to higher diffraction angles represents the decrease of the interplanar spacing (d).

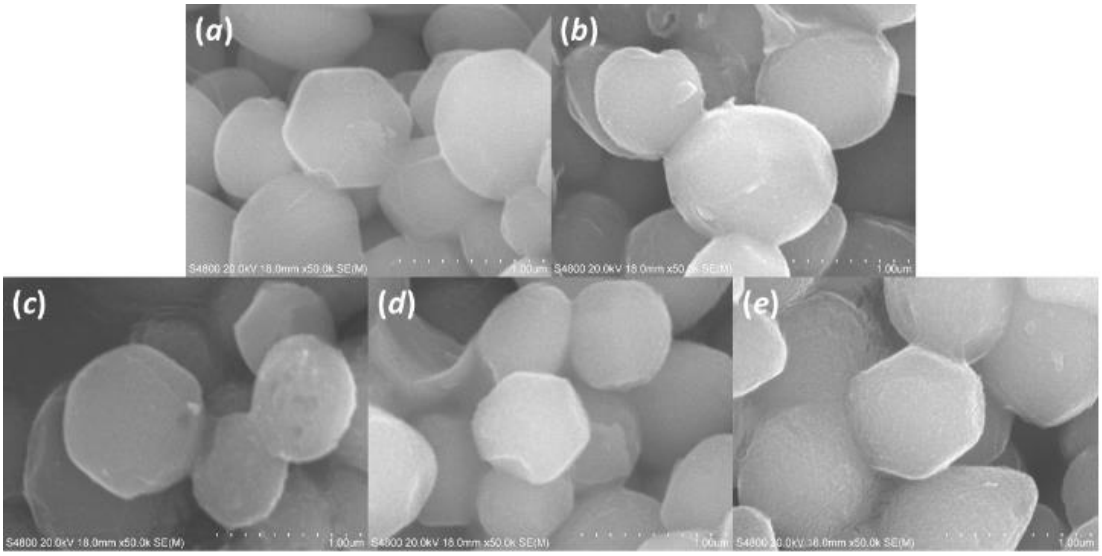

Figure 8.64. FE-SEM images of the (a) M41, (b) M41-TiP, (c) M41-TiEtP, (d) M41-TiPrP and (e) M41-TiBuP.

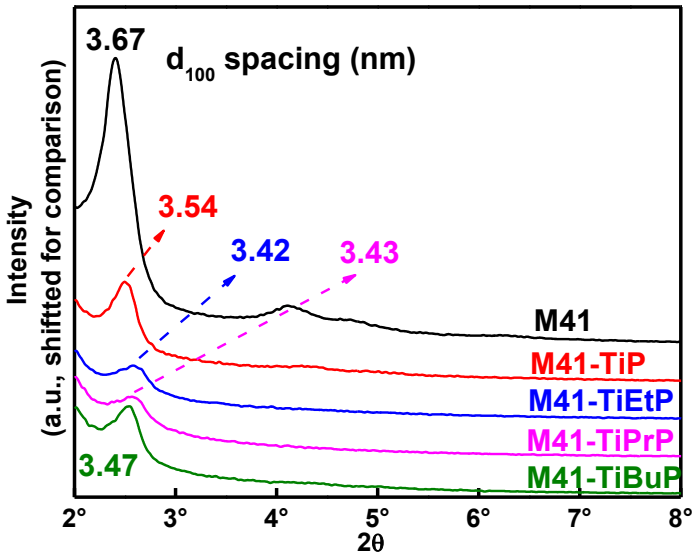

Figure 8.65. XRD patterns (2θ = 2–8°) of the synthesised materials.

The grafted alkyl chains occupy pore spaces and therefore lead to smaller *d* values (Table 8.17). However, due to the differences in reactivity and bulkiness of the different alcohols, the reaction yields varied (Table 8.17). More ethyl and *n*-propyl groups could be grafted compared to *n*-butyl groups. A similar trend was evident from the N_2 porosimetry results. The nitrogen adsorption-desorption isotherms and pore-size distributions are shown in Figure 8.66.

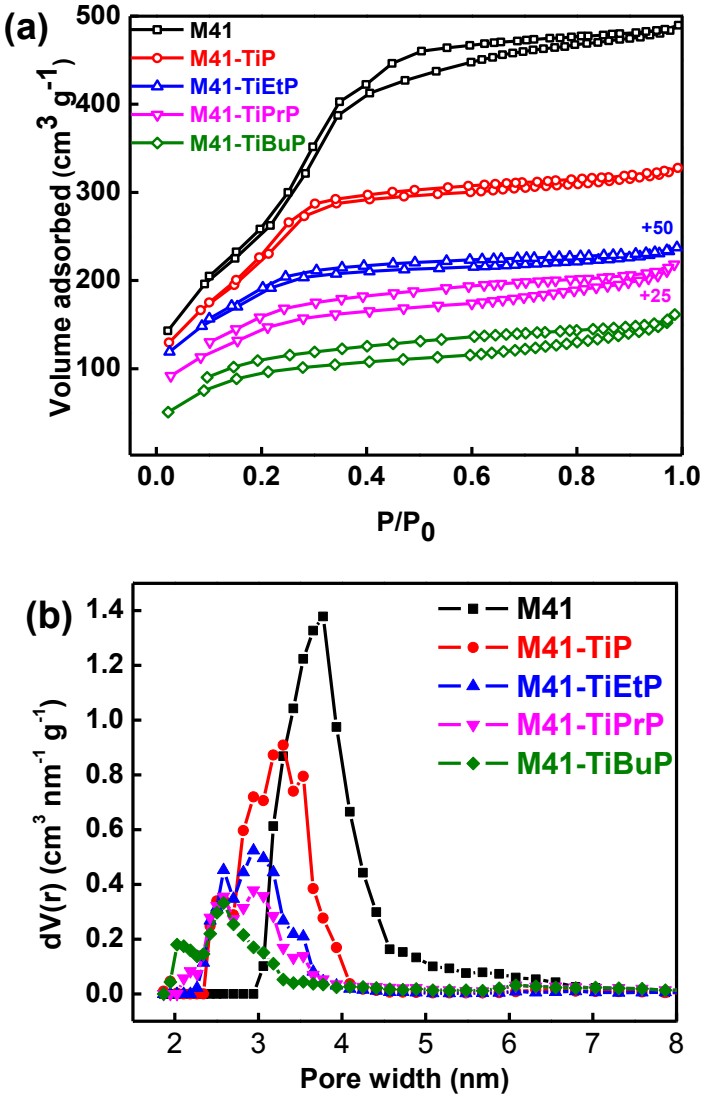

Figure 8.66. Nitrogen adsorption-desorption isotherms (a) and respective NLDFT pore-size distribution curves (b) of the synthesised materials.

All the materials exhibited type-IV isotherms and very narrow H1 type hysteresis loop, indicating the narrow channels of the M41 silica. The pore-size distribution results were in line with the calculated d_{100} spacing from XRD. The BET surface area decreased from M41 support (1022 m^2 g^{-1}) to M41-TiP (879 m^2 g^{-1}) and then to even lower values when alkyl chains were grafted (Figure 8.63).The Fourier transform infrared (FTIR) spectra of the synthesised materials are shown in Figure 8.67.

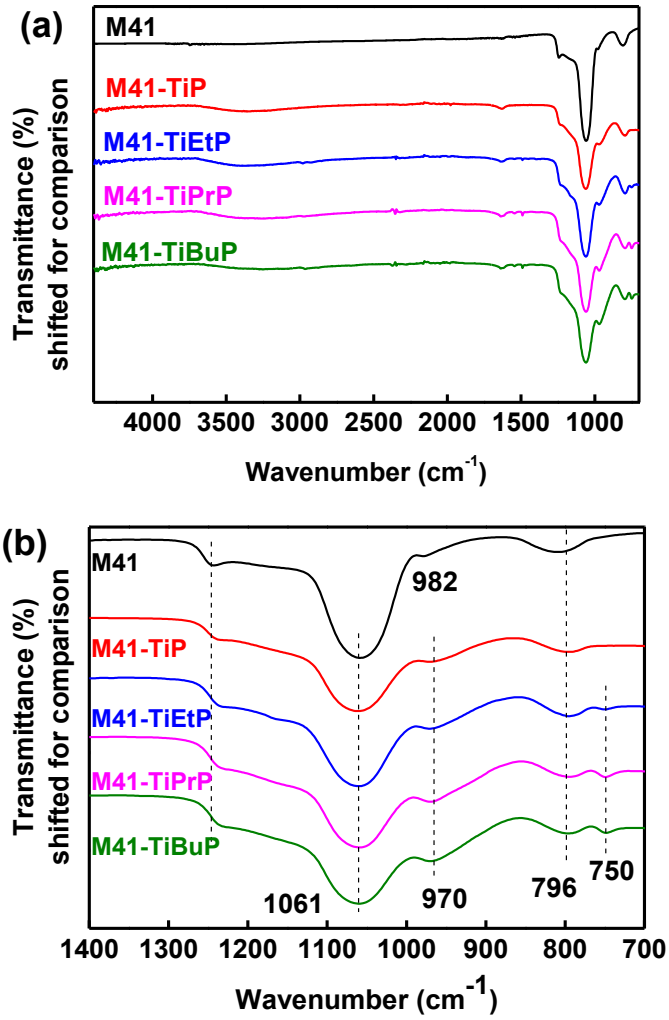

Figure 8.67. ATR-FTIR spectra of the synthesised materials (a) with an enlarged view on the wavenumber region from 700 to 1400 cm^{-1} (b).

Two bands centred at 1250 and 1060 cm^{-1} correspond to longitudinal and transversal optic of the asymmetric stretching vibrations of the siloxane groups. The peak at about 800 cm^{-1} can be assigned to the symmetric stretching vibration of the same group. The shoulder peak at 970–980 cm^{-1} is attributed to the Si–O^- stretching vibration of the silanol group.[33] The peaks centred at 750 cm^{-1} are only visible from the alkyl-grafted materials. It is due to the asymmetric P–O–C stretching vibration,[34] confirming the successful grafting process.

The deconvoluted ^{29}Si magic-angle spinning nuclear magnetic resonance (MAS NMR) spectra of these materials (Figure 8.68) show in general three peaks at -92, -101 and -110 ppm corresponding to geminal silanol ($(SiO)_2$*$Si(OH)_2$, Q^2 site), isolated silanol ($(SiO)_3$*SiOH, Q^3 site) and framework silicon sites ($(SiO)_4$*Si, Q^4 site).[35] Ti is considered isomorphic with Si and therefore the substitution of Si by Ti does not result in distinguishable changes in ^{29}Si resonance. Approximately 40% of the silicon are in surface silanol groups (Q^2 + Q^3). A general trend of the decrease in Q^2 and Q^3 resonances as well as the increase in Q^4 resonance is shown in Table 8.17. This intensity redistribution is a strong indication for surface modification of the silanol groups by titanium derivatives.

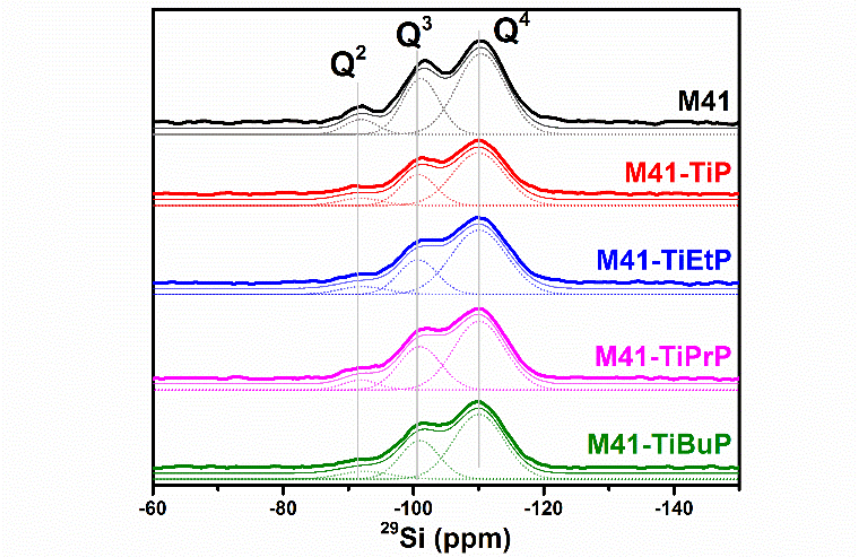

Figure 8.68. Solid-state ^{29}Si MAS NMR spectra of the synthesised materials with peak deconvolution.

Table 8.17. Physicochemical properties of the pristine and the grafted M41 materials.

Sample[a]	S_{BET}[b] ($m^2 g^{-1}$)	d_{100}[c] (nm)	V_{total}[d] ($cm^3 g^{-1}$)	Content[e]				Si sites[f]		
				wt%		mmol g^{-1}		Q^2 sites (%)	Q^3 sites (%)	Q^4 sites (%)
				Ti	P	Ti	P	$(SiO)_2$* $Si(OH)_2$	$(SiO)_3$* SiOH	$(SiO)_4$ *Si
M41	1022	3.67	0.76	-	-	-	-	7.4	31.5	61.1
M41-TiP	879	3.54	0.51	8.38	4.04	1.75	1.30	7.3	26.8	65.8
M41-TiEtP	514	3.42	0.29	7.45	3.65	1.56	1.18	7.1	25.3	67.7
M41-TiPrP	443	3.43	0.30	8.09	3.86	1.69	1.24	6.1	32.0	61.8
M41-TiBuP	350	3.47	0.25	7.89	3.65	1.65	1.18	7.4	29.3	63.3

[a] Samples denotation: MCM-41 silica (M41), titanium(IV) phosphate functionalised MCM-41 silica (M41-TiP) and *n*-alkyl chains (Et, Pr, Bu) grafted titanium(IV) phosphate functionalised MCM-41 silica (M41-TiEtP, M41-TiPrP and M41-TiBuP). [b] S_{BET}: BET specific surface area. [c] d_{100}: interplanar distance calculated by diffraction of [100] plane. [d] V_{total}: total pore volume estimated at a relative pressure of 0.99, assuming full surface saturation. [e] Chemical content determined by total digestion. [f] Relative peak areas calculated from the deconvoluted ^{29}Si MAS NMR spectra.

The ^{31}P MAS NMR spectra of the synthesised materials are shown in the Figure 8.69. The spectra were assigned based on literature data[36] and the relative content of different P species are listed in Table 8.18. The phosphate groups were linked not only to surface titanol but to silanol groups as well. Approximately 40% of the P species were surface titanium(IV) (alkyl)phosphates (**3, 4, 6**) and 30-49% were surface silicon (alkyl)phosphates (**1, 2, 5**). The titanium(IV) hydrogenphosphate (**7**) and pyrophosphate (**8**), representing the remaining 20% P species, most probably existed in quasi-amorphous state rather than being covalently linked to the surface.[36] The results indicated that the phosphate grafting rate was higher for titanium(IV) than for silicon, since the overall surface silanol groups were more abundant than titanol groups according to the elemental analysis and ^{29}Si NMR spectra. Therefore, the titanium(IV) layer enhanced the degree of functionalisation of the material.

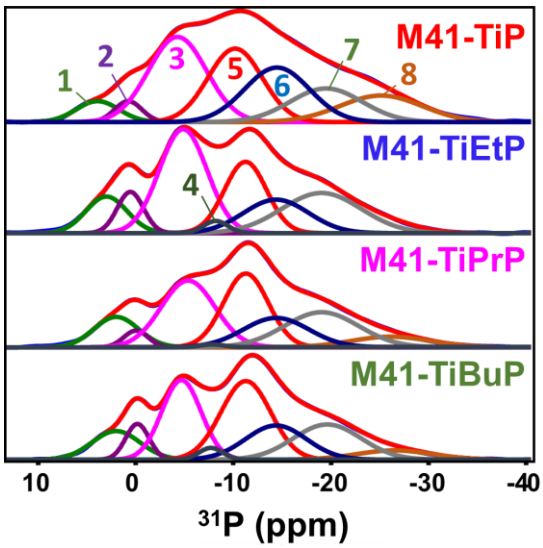

Figure 8.69. ^{31}P MAS NMR spectra with peak deconvolutions (numbers representing peak assignments are listed in Table 8.18).

Table 8.18. Assignments and relative quantification of P species from ^{31}P MAS NMR spectra (R = H, Et, *n*-Pr or *n*-Bu).

Position *ca.* (ppm)	**Species (Peak number in Figure 8.69)**	**Relative quantification (%)**			
		M41-TiP	M41-TiEtP	M41-TiPrP	M41-TiBuP
0 and 2	≡SiO-**P**O(OR)$_2$ **(1,2)**	8	16	13	15
-5 and -7.5	≡TiO-**P**O(OR)$_2$ **(3,4)**	27	31	26	23
-11	(≡SiO)$_2$-**P**O-(OR) **(5)**	21	18	23	27
-14.5	(≡TiO)$_2$-**P**O-(OR) **(6)**	19	13	14	14
-19	Ti(H**P**O$_4$)$_2$ **(7)**	13	19	18	16
-26	Ti**P**$_2$O$_7$ **(8)**	12	3	6	5

The grafting of organic moieties was investigated by two other methods. Solid-state ^{1}H-^{13}C cross polarisation (CP)/MAS NMR spectra in Figure 8.70 show peaks corresponding to grafted alkyl chains. For instance, in the M41-TiPrP sample, the peak at 60-70 ppm represents the first carbon atom (a) of the *n*-propyl group, while the peak at 25 and 10 ppm indicate the middle (b) and terminal (c) carbon atoms, respectively. The overlapping peaks are caused by the fact that some alkylphosphate groups are attached to Ti atoms and some to Si atoms.

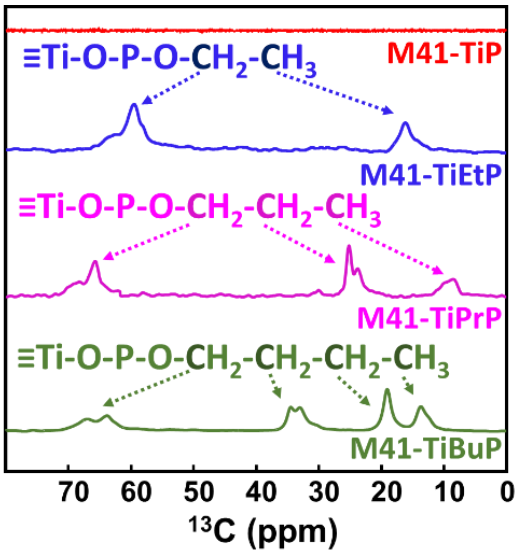

Figure 8.70. Solid-state ^{1}H–^{13}C CP/MAS NMR spectra of the synthesised materials.

Thereafter, simultaneous thermogravimetry and differential scanning calorimetry–mass spectroscopy (TG/DSC–MS) was utilised to study the thermal decomposition behaviour of the grafted materials. Figure 8.71 illustrates the ion intensity profile of selected *m/z* values representing ethylene, propene, butene and CO_2 with increasing temperature. The grafted *n*-alkyl chains started to decompose at approximately 200 °C *via* cis-elimination to produce acids and alkenes.[37] The reaction mechanism in producing butene is demonstrated in Figure 8.72. The produced alkene subsequently reduced phosphate and silica, thereby CO_2 was emitted in all the samples at temperature more than 400 °C.

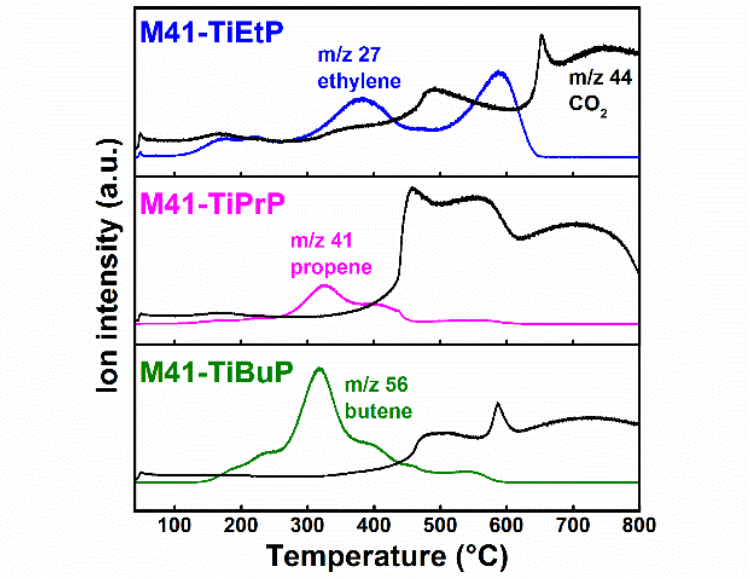

Figure 8.71. TG/DSC-MS profiles showing ion intensities corresponding to the evolved ethylene, propene, butene and CO_2.

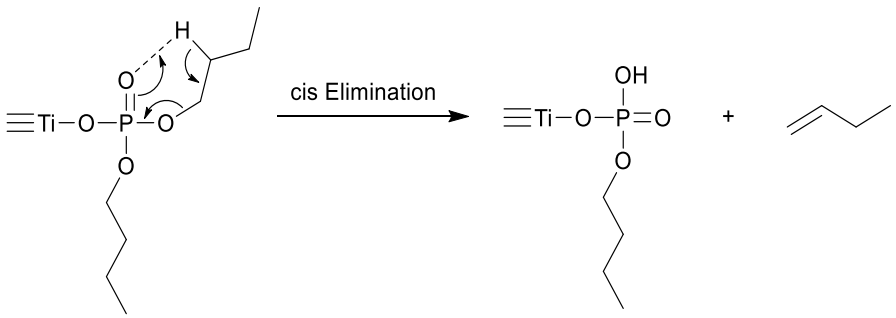

Figure 8.72. Thermal decomposition of surface titanium n-butyl phosphate *via* a cis elimination mechanism.

The overall characterisation suggested that the short *n*-alkyl chains were successfully grafted onto the M41-TiP material. However, it was not possible to fully functionalise all the surface silanol groups with Ti. Due to the differences in reaction activity and diffusion resistance of the alcohols, the degree of organic grafting differed and was not easily quantifiable. The mesoporous nature of the M41 silica support also resulted in residual acetone and pyridine left inside the final

products. Even after treatment in a vacuum oven at 50 °C for 2 days, it was not possible to remove them until below the detection limit.

8.3.2 Batch sorption experiments of lanthanum and scandium

Batch sorption studies were conducted to evaluate the uptake behaviour of different rare-earth ions on the synthesised hybrid materials. Among all the REEs, scandium is the lightest element and is almost always found in minerals together with yttrium and lanthanides. The uptake of scandium and lanthanides in their mixture could indicate the potential of separating them. To simplify the situation, lanthanum is used as a representative lanthanide here. Due to the solvating extraction nature of the prepared sorbents, batch uptake experiments were conducted in aqueous solutions with and without 5 mol L^{-1} NH_4NO_3 as the nitrate ion supply.

The values for distribution coefficients (K_d) of scandium and lanthanum along with their calculated separation factors are plotted in Figure 8.73. In our adopted system, a K_d value of 400 would mean 50% uptake and a K_d value of 3600 indicated 90% uptake. In, the Figure 8.73, K_d values for Sc increased with elevated pH throughout the investigated pH range (1.5 to 4) for the pristine M41 and M41-TiP. These materials also exhibited lower scandium uptake when 5 mol L^{-1} NH_4NO_3 was present in the solution. Presumably, only ion-exchange and physisorption sites were accounted for the uptake and the addition of competing cations resulted in lower uptake. For the hybrid materials, the situation was reversed. Higher scandium uptake was obtained under the presence of additional nitrate ions. Note that nearly all the scandium in the solution was taken up by M41-TiEtP and M41-TiPrP in the pH range of 2 to 4, translating into K_d values more than 10^6 mL g^{-1}. The lanthanum uptake was suppressed in this system, resulting in lesser K_d values ranging from 1 to 100 mL g^{-1} (Figure 8.73b).

In view of the separation factors for scandium and lanthanum ($SF_{Sc/La}$, in Figure 8.73c), scandium was clearly favoured by all the materials and the separation factors in the magnitudes of 10 to 100 were achieved using inorganic M41 and M41-TiP. Notably, separation factors over 100,000 were obtained for M41-TiEtP and M41-TiPrP under 5 mol L^{-1} NH_4NO_3 condition. This

demonstrates the excellent potential of the hybrid materials in the separation of scandium and lanthanides.

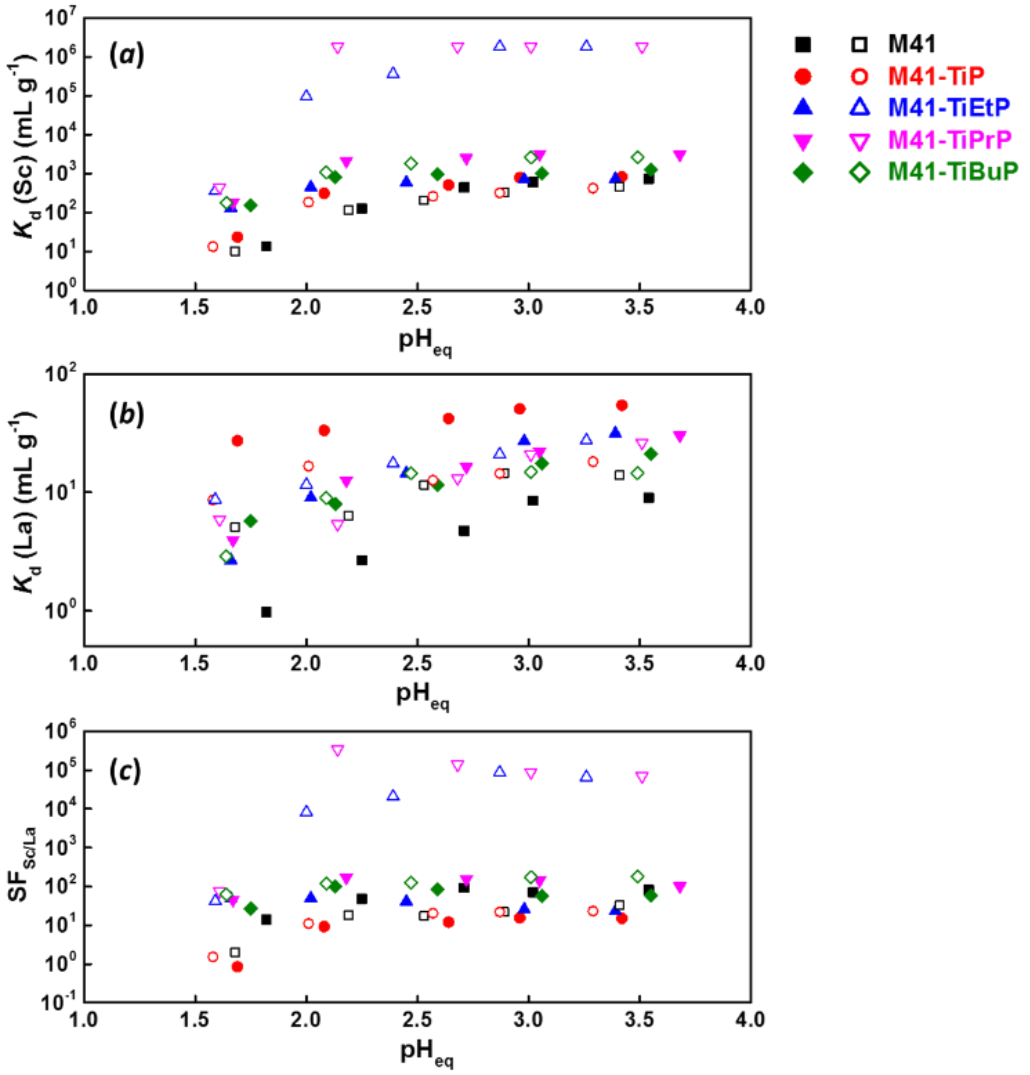

Figure 8.73. K_d values for Sc(III) (a) and La(III) (b) and the corresponding $SF_{Sc/La}$ values (c) as a function of equilibrium pH for sorption systems with 5 mol L^{-1} NH_4NO_3 (open symbols) and without NH_4NO_3 (closed symbols). Initial solution composition: 1 mmol L^{-1} of Sc and La, sorption solid-to-liquid ratio: 50 mg/20 mL.

In liquid-liquid operations, triethyl phosphate and tri-*n*-propyl phosphate are in general not used due to their higher solubility in the aqueous phase. However, their solvating behaviour towards REE nitrate complexes are similar compared to that of TBP. When the alkyl chains are

immobilised on a solid surface, their solubility in water is no longer an issue. The reason why M41-TiEtP and M41-TiPrP outperformed M41-TiBuP is very likely due to the higher organic loading in the two former materials.

8.3.3 Batch sorption experiments of lanthanides

The liquid-solid extraction capabilities of the synthesised grafted materials towards lanthanides were evaluated by batch sorption experiments using a binary 1 mmol L^{-1} equimolar neodymium and dysprosium mixture with 5 mol L^{-1} NH_4NO_3. Here, neodymium represented the light REEs and dysprosium represented the heavy REEs. This lanthanide pair was selected also due to its industrial relevance (recycling of NdFeB magnets). High concentrations of nitrate ions were used because of the solvating extractant nature of TBP. As demonstrated earlier, a very small amount of lanthanum was sorbed on M41 and M41-TiP. Similarly, the results in Figure 8.74a indicate that the M41 silica support and M41-TiP exhibited negligible total neodymium and dysprosium uptake, while the M41-TiEtP, M41-TiPrP and M41-TiBuP showed a significant uptake (0.12, 0.34 and 0.25 mmol g^{-1}, respectively) at an equilibrium pH of approximately 2. Comparable behaviour has been observed in uranyl sorption by phosphoryl and phosphoryl-ether-functionalised metal-organic framework, where the uptake was much higher in the ethoxy-protected materials rather than the phosphoric acid analogues.[38] In our cases, the differences in uptake among the hybrid materials originated from the variations in the degree of surface functionalisation by alkyl groups and from the differences in the stability of the ternary lanthanide-nitrate-alkylphosphate complexes.[9]

The K_d for neodymium and dysprosium were calculated at different equilibrium pH conditions in M41-TiPrP sample and shown in Figure 8.74c. The separation factors for dysprosium/neodymium ($SF_{Dy/Nd}$) were approximately 3 in all tested pH conditions. This is comparable with a solvent extraction system using TBP in benzene with 5 mol L^{-1} NH_4NO_3, where the distribution ratio obtained for neodymium is 0.029 and for dysprosium is 0.081,[39] thus resulting in a $SF_{Dy/Nd}$ of 2.8. The K_d and $SF_{Dy/Nd}$ values of M41-TiEtP and M41-TiBuP are given in Figure 8.74b and Figure 8.74d.

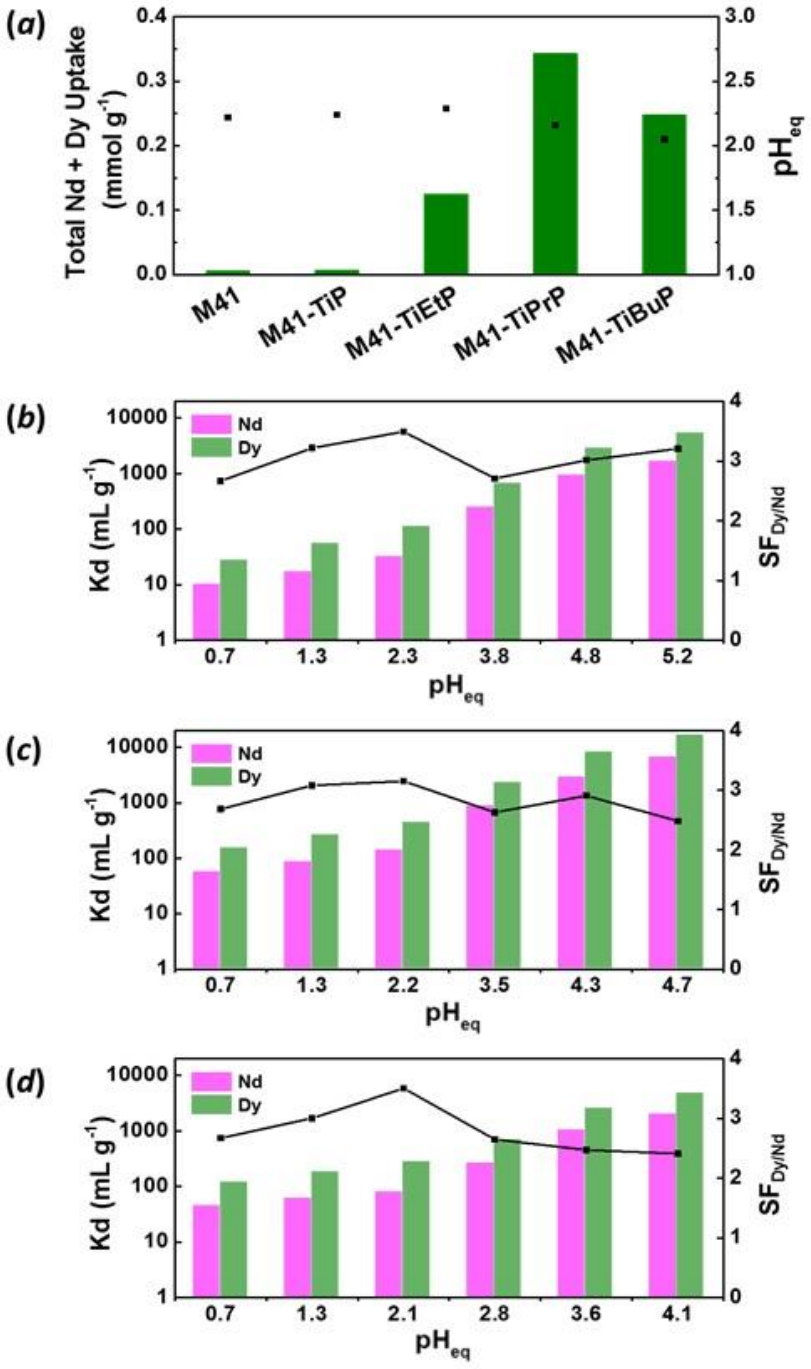

Figure 8.74. (a) Total Nd and Dy uptake (bars) of five synthesised materials and their corresponding equilibrium pH values (squares), K_d values (bars) and $SF_{Dy/Nd}$ (squares) as a function of equilibrium pH for (b) M41-TiEtP, (c) M41-TiPrP and (d) M41-TiBuP material. Initial solution composition: 1 mmol L^{-1} Nd, and Dy and 5 mol L^{-1} NH_4NO_3, sorption solid-to-liquid ratio: 50 mg/20 mL.

The increase in equilibrium pH increased both K_d values and had only a limited impact on the $SF_{Dy/Nd}$. The decrease in lanthanide uptake with increasing acidity is likely due to the competitive co-extraction of HNO_3.[40]

The desorption process was almost quantitative when using a 0.1 mol L^{-1} HNO_3 solution (Figure 8.75), in which H^+ inhibited the residual ion exchange sites (silanol and titanol) and low nitrate concentration favoured the breakdown of lanthanide nitrate complexes. Cyclic sorption-desorption tests (Figure 8.76) confirmed the reusability of our prepared hybrid sorbents. The $SF_{Dy/Nd}$ values remained stable throughout the five sorption cycles. Further column tests are needed to investigate the extraction and stripping behaviour (including kinetics) under extraction conditions.

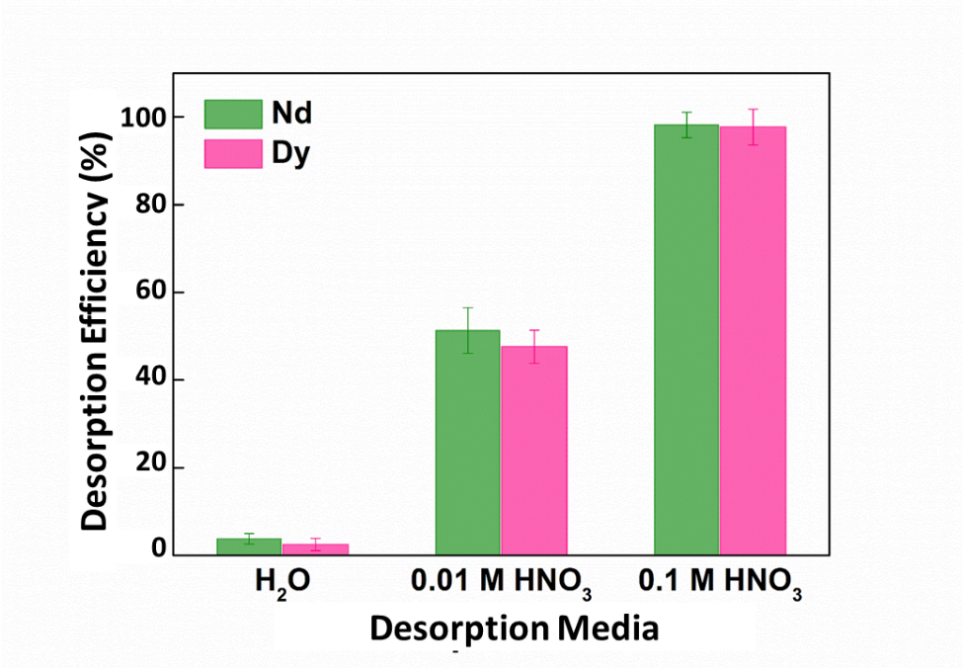

Figure 8.75. Desorption efficiencies using water, 0.01 mol L^{-1} and 0.1 mol L^{-1} nitric acid on M41-TiPrP material. Initial sorption solution composition: 1 mmol L^{-1} Nd and Dy and 5 mol L^{-1} NH_4NO_3, sorption solid-to-liquid ratio: 50 mg/20 mL and equilibrium pH ≈ 2. Desorption solid-to-liquid ratio: 50 mg/20 mL.

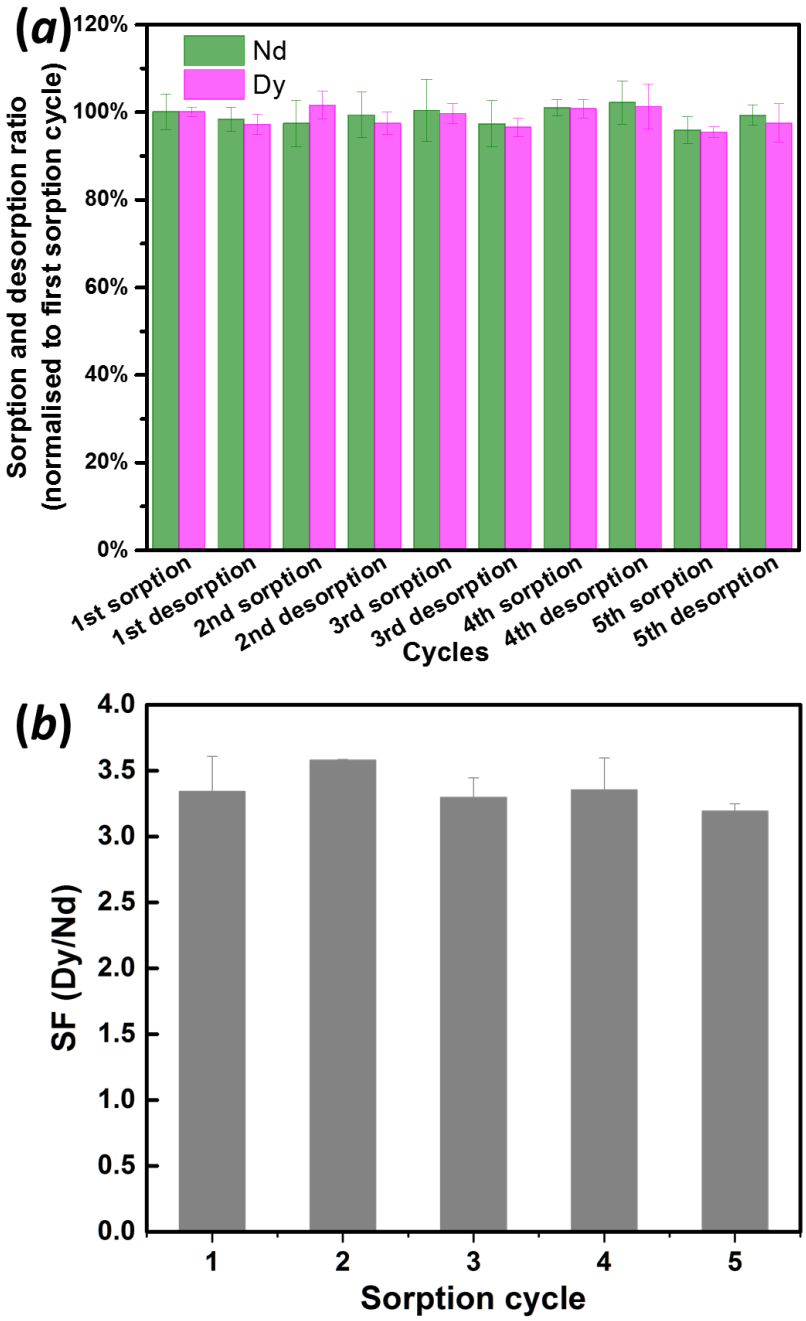

Figure 8.76. Cyclic sorption-desorption tests on M41-TiPrP material: (a) sorption and desorption ratios of Nd and Dy normalised to the first sorption cycle uptake, and (b) $SF_{Dy/Nd}$ values for each sorption cycle. Initial sorption solution composition: 1 mmol L^{-1} Nd and Dy and 5 mol L^{-1} NH_4NO_3, sorption solid-to-liquid ratio: 50 mg/20 mL and equilibrium pH ≈ 2. Desorption solution: 0.1 mol L^{-1} HNO_3 and desorption solid-to-liquid ratio: 50 mg/ 20 mL.

8.3.4 Stability towards strong acids

One major drawback of siliceous materials is their poor stability in strongly acidic solutions.[20] This hinders their application in hydrometallurgical conditions. It is known that titanium(IV) oxides and phosphates are less soluble in acidic media and therefore functionalisation of silica with titanium(IV) derivatives should lead to enhanced acid stability.[41] The reason that mesoporous titanium materials are not directly utilised for synthesis is because of comparatively difficult and unreproducible control over the synthesis. Table 8.19 summarises the amount and relative percentage of dissolved silicon and titanium in nitric acid solutions. More than 5% of the silica in M41 silica was dissolved in our batch system under 0.1 mol L^{-1} HNO_3 solution. Functionalisation with titanium phosphate led to apparent improvement in acid stability, with less than 0.6% of the silica from M41-TiP dissolved under the same condition. Notably, alkyl grafting further enhanced the acid stability of the materials most likely due to increased hydrophobicity.

Table 8.19. Acid stability of the pristine and the grafted M41 materials.[a]

Materials	0.1 mol L^{-1} HNO_3 (pH 1)				0.01 mol L^{-1} HNO_3 (pH 2)			
	Dissolved [b] Si		Dissolved Ti		Dissolved Si		Dissolved Ti	
	mg L^{-1}	%	mg L^{-1}	%[c]	mg L^{-1}	%	mg L^{-1}	%
M41	62.31	5.34%	-	-	21.9	1.88%	-	-
M41-TiP	6.15	0.53%	0.16	0.08%	3.71	0.32%	N.D.[d]	N.D.
M41-TiEtP	4.27	0.37%	0.08	0.04%	3.91	0.34%	N.D.	N.D.
M41-TiPrP	5.18	0.44%	0.12	0.06%	3.52	0.30%	N.D.	N.D.
M41-TiBuP	3.19	0.27%	0.09	0.05%	2.66	0.23%	N.D.	N.D.

[a] Batch solid-to-liquid ratio: 50 mg/20 mL acid, contact time: 6 h. [b] Passed through 0.45 mm syringe filter. [c] Percentage calculated based on elemental analysis results. [d] Not detected (<0.01 ppm).

8.3.5 Mechanistic consideration of uptake and selectivity

The prepared hybrid sorbents (M41-TiEtP, M41-TiPrP and M41-TiBuP) have different sorption sites for the uptake of rare-earth ions. First of all, the remaining silanol (−SiOH), titanol (−TiOH) and hydrogen phosphate groups (−HPO_4) have hydroxyl groups serving as cation-exchange sites. Secondly, the mesostructured materials have large surface areas, which accounts for the

physisorption. Finally and most importantly, the grafted alkylphosphate groups act as solvating extractants that are capable of immobilising the neutral rare-earth nitrate complexes by donating electrons. Ion exchange and physisorption are inhibited by the addition of ammonium nitrate (ammonium ions to compete with cation exchange sites). On the other hand, the solvating extraction behaviour is enhanced through the formation of rare-earth nitrate complexes.

Scandium and lanthanides are hard Lewis acids and phosphates are hard Lewis bases. The affinity of hard acids to hard bases are mostly ionic in nature. The ionic radius of scandium (74.5 pm, 6-coordinated) is smaller than that of the lanthanides (103.2 to 121.6 pm, 9-coordinated from the series La(III) to Lu(III)),[42] therefore scandium is a stronger Lewis acid and forms more stable coordination bond with phosphate (containing hard-atom O).

For the hybrid sorbents, based on the electronic effect, titanium atoms and the alkyl chains both donate electrons to the attached phosphoryl group (P=O), thereby increasing the electron density on the oxygen atom. The resulting titanium(IV) alkylphosphates are even stronger Lewis bases than TBP and inorganic phosphate, respectively. Therefore, a stronger Lewis acid with a small ionic radius is favoured and thus resulting in the enhanced uptake and the selectivity of Sc(III) over La(III). Due to lanthanide contraction, the ionic radius of Dy(III) is smaller than that of Nd(III) and subsequently Dy(III) is better retained by the hybrid materials. By selecting the metal which links the silica and the organophosphate group and by using different types of organophosphorus moieties, it is possible to further fine-tune the basicity of the phosphoryl ligands.

The length of the alkyl chains should affect the molecular recognition events (size-exclusion preferences) and the attachment of the alkyl chains to the solid matrix surface potentially adds to the overall rigidity of the complex. However, this behaviour cannot be fully elucidated in the current situation since the amounts of grafted alkyl chains vary for the different alkyl chains.

8.4 CONCLUSIONS

The feasibility of designing a hybrid composite material mimicking the structure of organophosphate solvent extractants was demonstrated. Mesoporous silica offers a high surface

area for heteroatom functionalisation and improved contact efficiency with aqueous solutions. A metal(IV) phosphate acts as a versatile acid-resistant platform for grafting of organic chains via a Ti(IV)−O−P bond. Our approach is different from the conventional organic grafting routes where silylation reagents containing the extractant structure are employed. The synthesised M41 silica grafted titanium(IV) alkylphosphate hybrid materials mimicking the TBP structure showed excellent scandium and lanthanum separation potential from nitrate feed solution. These materials also presented intra-lanthanide separation capabilities comparable to that of TBP in liquid-liquid extraction systems. Our proposed idea can be utilised for obtaining task-specific materials, e.g. covalently anchoring of longer organic chains (mimicking the D2EPHA, bis(2-ethylhexyl) phosphate, structure), which are more selective for intra-lanthanide separations. Alternatively, phosphonates and phosphinates can be synthetically introduced as metal(IV) derivatives, allowing precisely tuned selectivity. The knowledge gained from liquid-liquid extraction systems is transferable, to a certain extent, to guide the future design of hybrid materials for rare-earth separations by the liquid-solid exctraction mechanism.

8.5 REFERENCES

1 K. Binnemans, P. T. Jones, B. Blanpain, T. Van Gerven, Y. Yang, A. Walton, M. Buchert, J. *Clean. Prod.*, 2013, **51**, 1-22.
2 J. Florek, D. Larivière and F. Kleitz, *in Nanotechnology: Delivering on the Promise Volume 2, American Chemical Society*, 2016, **1224** (6), 107-117.
3 F. Xie, T. A. Zhang, D. Dreisinger, F. Doyle, *Miner. Eng*., 2014, **56**, 10-28.
4 B. Kronholm, C. G. Anderson, P. R. Taylor, JOM, 2013, **65**, 1321-1326.
5 T. Vander Hoogerstraete, S. Wellens, K. Verachtert, K. Binnemans, *Green Chem*., 2013, **15**, 919-927.
6 G. Baldwin, N. J. Bridges, J. C. Braley, *Ind. Eng. Chem. Res*., 2016, **55**, 13114-13119.
7 S. Mishra, J. Dwivedi, A. Kumar, N. Sankararamakrishnan, *New J. Chem*., 2016, **40**, 1213-1221.
8 E. Hesford, E. Jackson, H. McKay, *J. Inorg. Nucl. Chem*., 1959, **9**, 279-289.
9 Kalaya, C. Deacha, *J. Rare Earth*., 2011, **29**, 896-901.
10 Siva Kesava Raju, M. S. Subramanian, *J. Hazard. Mater*., 2007, **145**, 315-322.
11 V. Luca, J. J. Tejada, D. Vega, G. Arrachart, C. Rey, *Inorg. Chem*., 2016, **55**, 7928-7943.
12 J. Florek, S. Giret, E. Juere, D. Lariviere, F. Kleitz, *Dalton Trans*., 2016, **45**, 14832-14854.
13 J. Veliscek-Carolan, T. L. Hanley, V. Luca, *Sep. Purif. Technol*., 2014, **129**, 150-158.
14 R. Silbernagel, C. H. Martin, A. Clearfield, *Inorg. Chem*., 2016, **55**, 1651-1656.

15 W. Zhang, G. Ye, J. Chen, *J. Mater. Chem. A*, 2013, **1**, 12706-12709.
16 P. J. Lebed, K. De Souza, F. Bilodeau, D. Lariviere, F. Kleitz, *Chem. Comm*., 2011, **47**, 11525-11527.
17 T. Ogata, H. Narita, M. Tanaka, *Hydrometallurgy*, 2015, **155**, 105-109.
18 P. J. Lebed, J.-D. Savoie, J. Florek, F. Bilodeau, D. Larivière, F. Kleitz, *Chem. Mater*., 2012, **24**, 4166-4176.
19 J. A. Shusterman, H. E. Mason, J. Bowers, A. Bruchet, E. C. Uribe, A. B. Kersting, H. Nitsche, *ACS Appl. Mater. Interfaces*, 2015, **7**, 20591-20599.
20 J. Shusterman, H. Mason, A. Bruchet, M. Zavarin, A. B. Kersting, H. Nitsche, *Dalton Trans*., 2014, **43**, 16649-16658.
21 J. Florek, F. Chalifour, F. Bilodeau, D. Larivière, F. Kleitz, *Adv. Funct. Mater*., 2014, **24**, 2668-2676.
22 D. Juere, J. Florek, D. Lariviere, K. Kim, F. Kleitz, *New J. Chem*., 2016, **40**, 4325-4334.
23 Bortun, L. N. Bortun, A. Clearfield, S. A. Khainakov, V. V. Strelko, V. N. Khryashevskii, A. P. Kvashenko, I. I. Voitko, *Solvent. Extr. Ion. Exc*., 1997, **15**, 515-532.
24 W. Zhang, R. Koivula, E. Wiikinkoski, J. Xu, S. Hietala, J. Lehto, R. Harjula, *ACS Sustain. Chem. Eng.*, 2017, **5**, 3103-3114.
25 G. E. Fryxell, H. Xu, Y. Lin, W. J. Shaw, J. C. Birnbaum, J. C. Linehan, Z. Nie, K. Kemner, S. Kelly, *J. Mater. Chem*., 2004, **14**, 3356-3363.
26 M. Grün, K. K. Unger, A. Matsumoto, K. Tsutsumi, *Micropor. Mesopor. Mater*., 1999, **27**, 207-216.
27 J. Zhang, Z. Ma, J. Jiao, H. Yin, W. Yan, E. W. Hagaman, J. Yu, S. Dai, *Micropor. Mesopor. Mater*., 2010, **129**, 200-209.
28 Hoffmann, M. Cornelius, J. Morell, M. Fröba, *Angew. Chem. Int. Ed*., 2006, **45**, 3216-3251.
29 J. Zhang, Z. Ma, J. Jiao, H. Yin, W. Yan, E. W. Hagaman, J. Yu, S. Dai, *Langmuir*, 2009, **25**, 12541-12549.
30 Styskalik, D. Skoda, Z. Moravec, J. G. Abbott, C. E. Barnes, J. Pinkas, *Micropor. Mesopor. Mater*., 2014, **197**, 204-212.
31 Cao, H. G. Hong, T. E. Mallouk, *Acc. Chem. Res*., 1992, **25**, 420-427.
32 Q. Cai, W.-Y. Lin, F.-S. Xiao, W.-Q. Pang, X.-H. Chen, B.-S. Zou, *Micropor. Mesopor. Mater*., 1999, **32**, 1-15.
33 L. Liu, D. K. Wang, D. L. Martens, S. Smart, E. Strounina, J. C. D. Da Costa, *RSC Adv*., 2014, **4**, 18862-18870.
34 Socrates, Infrared and Raman characteristic group frequencies: tables and charts, Wiley, New York, USA, 2004.
35 X. Zhao, G. Lu, A. Whittaker, G. Millar, H. Zhu, *J. Phys. Chem. B*, 1997, **101**, 6525-6531.
36 T. Kovalchuk, H. Sfihi, A. Korchev, A. Kovalenko, V. Il'in, V. Zaitsev, J. Fraissard, *J. Phys. Chem. B*, 2005, **109**, 13948-13956.
37 S. Gaan, G. Sun, K. Hutches, M. H. Engelhard, *Polym. Degrad. Stab*., 2008, **93**, 99-108.
38 M. Carboni, C. W. Abney, S. Liu, W. Lin, *Chem. Sci*., 2013, **4**, 2396-2402.
39 M. Majdan, *Hydrometallurgy*, 1994, **35**, 179-185.
40 T. Vander Hoogerstraete, K. Binnemans, *Green Chem*., 2014, **16**, 1594-1606.
41 M. Shahadat, T. T. Teng, M. Rafatullah, M. Arshad, *Colloids Surf. B*., 2015, **126**, 121-137.
42 R. Shannon, *Acta Cryst. A*, 1976, **32**, 751−767.

Chapter 9

Conclusions and outlook

One of the main goals of this PhD thesis was to develop new sorbents for the recovery of REEs from acidic leachates of bauxite residue (BR). The leachates can be generated by direct acid leaching of BR or after a number of processing steps for the removal of major components such as iron, aluminium or titanium. In these leachates, the concentrations of REEs are low (typically < 50 mg L^{-1}) and base metal impurities are inevitable (even up to several g L^{-1}). Liquid-solid extractions are generally suitable for metal recovery from dilute solutions due to a high sample throughput. If a sorbent selective for REEs is used in these processes, they can be concentrated from dilute solutions. The resulting concentrated solution of REEs can already be purified from the majority of other elements present in BR. The concentrate can also be further treated by well-established liquid-liquid extraction systems or sorbents selective for specific REE to obtain high-purity of individual REEs.

The existing knowledge in liquid-liquid extractions of REEs gained over the last years can be a starting point for choosing the functional groups that need to be incorporated into the novel sorbents. The IL [Hbet][Tf_2N] has been used in solvent extraction of Sc(III). The extraction properties of [Hbet][Tf_2N] can be ascribed to the carboxylic functional group. Therefore, a SILP [Hbet-STFSI-PS-DVB] with similar structure as [Hbet][Tf_2N] was synthesised. [Hbet-STFSI-PS-DVB] was characterised by a range of analytical techniques. Then the SILP was investigated batchwise for Sc(III) sorption from acidic media. Fast sorption kinetics (15 minutes), moderate sorption capacity (0.36 mmol g^{-1}) and good reusability (7 cycles) of the [Hbet-STFSI-PS-DVB] appeared to be promising results for Sc(III) recovery. The batch sorption study was extended to other REEs (Y, Nd, Dy) and the ability of [Hbet-STFSI-PS-DVB] to recover also these REEs from acidic solutions was confirmed. The [Hbet-STFSI-PS-DVB] was packed in a column and was investigated for the uptake of REEs in the presence of base metals in BR from HNO_3 and H_2SO_4 solutions. The breakthrough curves revealed the higher affinity of the [Hbet-STFSI-PS-DVB] towards the REEs. The uptake affinity order from HNO_3 solutions followed the trend: Ca(II) < Al(III) ≈ Fe(III) < Sc(III) < Y(III) ≈ Dy(III) < Nd(III). The results suggested that the REEs could be recovered by the [Hbet-STFSI-PS-DVB] even in the presence of high concentrations of base elements. Despite the higher affinitiy of the [Hbet-STFSI-PS-DVB] for the REEs, base metal ions impurities were still recovered along with the REEs, and an elution column chromatography was necessary to separate the REEs. By an optimised pH gradient

elution with H_3PO_4 and HNO_3 the REEs and the base metal ions were well separated and followed the trend: Sc(III) > Fe(III) > Al(III) > Ca(II) ≈ Dy(III) ≈ Y(III) > Nd(III). The SILP was then tested for the uptake of REEs from a BR leachate. The leachate was obtained by direct leaching of BR with HNO_3. The REEs were recovered (71.7–100%) and separated from the base elements by the optimised elution chromatography. The elution sequence with the real BR leachate followed the trend as anticipated from the elution studies. The breakthrough curve study with H_2SO_4 solutions revealed different uptake affinity order: Sc(III) < Fe(III) < Ca(II) < Dy(III) < Al(III) < Y(III) < Nd(III). In this case, the lowest affinity of [Hbet-STFSI-PS-DVB] towards Sc(III) indicated that H_2SO_4 BR leachates require a pretreatment step prior to the [Hbet-STFSI-PS-DVB] column chromatography. In a study with a simulated H_2SO_4 BR leachate Fe(III) selective precipitation with ammonia strongly increased the subsequent recovery of Sc(III) by [Hbet-STFSI-PS-DVB]. The REEs, including Sc(III), were then purified by the optimised elution chromatography. Besides, another way to recover scandium by precipitating as $ScPO_4$ from the Fe(III) depleted solution was also tested. The purity of scandium after column chromatography was found to be superior to the purity of the $ScPO_4$ precipitate. [Hbet-STFSI-PS-DVB] was additionally tested for the recovery of REEs from a leachate obtained by high-pressure HCl leaching of a slag obtained after smelting reduction of BR for iron recovery. Although the tested leachate was still composed of high amount of base metals, the recoveries of REEs by [Hbet-STFSI-PS-DVB] were high (97.7–100%), with a modest selectivity over base elements. The separation of REEs by elution chromatography was in accordance with the results obtained with the HNO_3 BR leachate and simulated H_2SO_4 BR leachate.

All studies with the real or simulated BR leachate confirmed a proof-of-principle for REEs recovery by [Hbet-STFSI-PS-DVB]. However, due to a lack in selectivity of [Hbet-STFSI-PS-DVB], concentrated REEs fractions could not be achieved. The base metals of BR were in each case recovered along with the REEs. This diminished the efficiency of [Hbet-STFSI-PS-DVB], and imposed the three-step elution for purification of REEs. Therefore, [Hbet-STFSI-PS-DVB] should be rather applied in an integrated process for BR valorisation, where the vast majority of base metals are recovered in advance. The performance of [Hbet-STFSI-PS-DVB] should be studied on a larger scale and with an optimised leachate. Although the SILP was tested exclusively for the separation of REEs and base metals in BR leachates, the elution study might

be implemented to other relevant processes (*e.g.* the recovery of Nd from spent NdFeB magnets). The chromatography separation can be tuned based on the feed composition and targeted elements.

In a quest for a sorbent selective for Sc(III), insoluble salts of multivalent metaloacids (α-ZrP, α-TiP, am-ZrP, and am-TiP) were investigated batchwise for the uptake of Sc(III) in the presence of Fe(III) from acidic solutions. α-ZrP exhibited the highest selectivity towards Sc(III). The selectivity of α-ZrP was an overall result of different effects: hydration enthalpy, the pH of solution and accessibility of phosphate groups. Besides of a good selectivity for Sc(III), fast sorption kinetics (15 minutes) and high sorption capacity (0.83 mmol g^{-1}) indicated that α-ZrP might give even more promising results in a column chromatography. α-ZrP was packed in a column and a breakthrough curve experiment with a binary solution of Sc(III) and Fe(III) confirmed the selectivity for Sc(III). The performance of α-ZrP was further evaluated with a real BR leachate obtained after direct leaching with HCl, without any further pH adjustments or pretreatments. Sc(III) was quantitatively (>99.9%) recovered by the α-ZrP from this complex leachate. Fe(III) recovery was around 54%, while all other elements including other REEs were recovered at even lower rate. The co-sorbed Fe(III) and other elements were eluted with 1 mol L^{-1} HCl, whereas around 40% of Sc(III) was eluted in this step. The remaining 60% of Sc(III) was eluted with 2 mol L^{-1} HCl, with no impurities of Fe(III), Al(III), Ca(II) or other REEs. The results appear to be very promising for Sc(III) recovery from BR leachates.

One way how to further increase the selectivity of α-ZrP column could be by adjusting the initial pH of the leachate. At low pH α-ZrP might still recover Sc(III), whereas the recovery of other elements is not anticipated, and then large sample volumes could be treated. This can be a way to concentrate Sc(III) in a column, and produce high purity Sc(III) fractions. The performance of α-ZrP should be further investigated with large volumes of BR leachate. A drawback of the method is that low flow rates must be maintained in the α-ZrP column, due to a difficult percolation of liquids through the fine particles of α-ZrP and further improvement in this aspect is required.

Additionally, new sorbents for effective mutual separation of REEs were synthesised by covalently attaching short *n*-alkyl chains (ethyl, *n*-propyl and *n*-butyl) to titanium(IV) phosphate functionalised mesoporous MCM-41 silica. The materials were characterised by various

analytical techniques. The performances of the modified materials for REEs recovery were compared with the unmodified materials. The hybrid materials showed a better uptake of REEs from nitrate feed solution than the MCM-41 silica. MCM-41 silica served as a versatile porous support and the grafted titanium(IV) derivatives provided solvating extraction capability. The modified materials showed excellent Sc(III) and La(III) separation potential from nitrate solution. These materials also presented intra-lanthanide separation capabilities. The separation factors of Dy(III)/Nd(III) are approximately 3, which are comparable to that of TBP in a typical solvent extraction setup.

The hybrid materials could be optimised for separation of REEs mixtures to individual elements or sub-groups. The study confirmed that the knowledge gained from liquid-liquid extraction systems is transferable, to a certain extent to liquid-solid extraction systems. In order to derive the appropriate conclusion about the influence of the alkyl chain length in selectivity for REEs, it is necessary to further optimise the synthesis procedure of these materials. The experimental conditions should be adjusted so that all materials are grafted to the same extent. Moreover, the degree of functionalisation should be increased, as the grafted groups have the essential role in extraction properties. The materials should also be investigated for separation of REEs in the presence of base metals of BR. Column chromatography separation of REEs can further be developed with these materials.

Generally, there is still plenty of room for improvement in liquid-solid extractions of REEs, either by tuning the characteristics of sorbents or by optimising the operating parameters. Firstly, deepening our understanding of the sorption processes of REEs with the existing sorbents would alow to predict and better control their performance under real operating conditions. Moreover, the gained knowledge could be used as a source of ideas for designing new sorbents with a desirable selectivity. Therefore, more detailed studies are necessary on the sorption mechanisms of REEs with all sorbents tested during this PhD. However, measuring low concentrations of REEs in sorbents is challenging with the vast majority of analytical techniques (EXAFS, XRD, Raman). One possibility to tackle the issue is to increase the number of functional groups on the sorbent which can then sorb substantial amounts of REEs. Besides, computer simulation techniques can be used for elucidating the sorption mechanisms. Moreover, a large amount of literature data related to the application of other sorbents for REEs can be elaborated to correlate

the structure of sorbents and sorption conditions with the selective uptake of REE. Diglycolamide (DGA) acid and phosphoric acid-based sorbents can be particularly interesting to work out, as the research on the recovery of REEs with these sorbents appears promising.

A key point of the optimisation of column chromatography process is the choice of a suitable sorbent. Apart from that, a number of column operating parameters (*e.g.* flow rate, pressure, temperature, column dimensions) can affect the separation and these should be optimised in such way to achieve a reduction of costs and an overall ease of operation. By optimising column operating parameters purified and/or preconcentrated fractions of REEs should be obtained in a short time, with a minimum consumption of reagents used for preconditioning of the sorbent and for the elution of metal ions. This also includes a minimum production of secondary waste. When this is not possible, the secondary waste should be considered for other applications or made non-hazardous for storage, and these options should be explored. One way how to tackle these issues is to recover metals other than REEs with the most efficient and near-zero waste process (*e.g.* Orbite) prior to column chromatography separation of REEs with the most effective sorbent (*e.g.* α-ZrP for Sc(III) recovery). Computer simulation techniques can also be used here to predict the performance of column operations and in a shorter time than when performing practical experiments. These techniques can be useful when extending the research on the column performance to various BR leachates (pre-treated leachates) or various operating conditions (*e.g.* further studies with SILP or α-ZrP in an integrated flowsheet). At last, operational lifetime of columns packed with the synthesised sorbents needs to be carefully investigated, especially after multiple column operation cycles for treatment of real BR leachates.

In conclusion, during this PhD several new sorbents were synthesised and investigated for REEs recovery. The conducted studies can be used as a starting point for further development of new sorbents or for the optimisation of large-scale processes for the recovery and purification of REEs.

List of publications

Avdibegović D., Regadío M., Binnemans K. (2018). Efficient separation of rare earths recovered by a supported ionic liquid from bauxite residue leachate, *RSC Advances*, **8**, 11886–11893.

Avdibegović D., Regadío M., Binnemans K. (2017). Recovery of scandium(III) from diluted aqueous solutions by a supported ionic liquid phase (SILP). *RSC Advances*, **7**, 49664-49674.

Zhang W., Avdibegović, D., Koivula R., Hatanpaa T., Hietala S., Regadío M., Binnemans K., Harjula R. (2017). Titanium alkylphosphate functionalised mesoporous silica for enhanced uptake of rare-earth ions. *Journal of Materials Chemistry A*, **5** (45), 23805-23814. *Joint first author with Wenzhong Zhang.*

Avdibegović, D., Yagmurlu, B., Dittrich, C., Regadío, M., Friedrich, B., Binnemans, B., Combined multi-step precipitation and supported ionic liquid phase chromatography for the separation of rare earths from the base elements in bauxite residue leachates. *Manuscript under revision. Joint first author with Bengi Yagmurlu.*

Avdibegović, D., Zhang, W., Xu, J., Regadío, M., Koivula, R., Binnemans, K. Selective ion-exchange separation of Sc(III) over Fe(III) by crystalline α-zirconium phosphate platelets from bauxite residue leachates. *Manuscript under preparation. Joint first author with Wenzhong Zhang.*

Attended conferences and trainings

Conferences

Avdibegović D., Regadío M., Rivera R.M., Onoughene G., Van Gerven T., Binnemans K., Purification of low concentration of rare earths from high concentration impurities in leach liquor of bauxite residue slag by a supported ionic liquid phase. Oral presentation and a conference paper in: *Y. Pontikes (ed) Proceedings of the 2nd International Bauxite Residue Valorisation and Best Practices Conference*. 7-10 May 2018, Athens, Greece, 381-386.

Avdibegovic D., Regadío M., Binnemans K. (2018). The importance of the preparation method of supported ionic liquid phases for their reuse in metal recovery and separation processes. *ChemCYS Chemistry Conference for Young Scientists*. 21-23 February 2018, Blankenberge (Belgium). Poster presentation

Avdibegovic D., Regadío M., Binnemans K. (2016). Preconcentration of scandium from bauxite residue leachates by a supported ionic liquid phase. *4th International Conference on Methods and Materials, "Separation Science – Theory and Practice" (SCTP2016).* 4-8 September 2016 Brunów (Poland). Poster presentation

Secondments

University of Helsinki, Helsinki, Finland

15th September – 13th November 2016. Experimental work in synthesis of hybrid MCM-41 silica materials.

MEAB, Aachen, Germany

20th March – 20th April 2017. Experience with solvent extraction and mixer-settlers.

Safety aspects

The experimental work performed during this PhD thesis was executed in compliance with the guidelines of the Good Laboratory Practice of the Department of Chemistry.

Before handling a chemical compound the KU Leuven Hazardous Substances Database in KU Loket was consulted for safety measures. Safety goggles, lab coat and gloves were worn while performing the experiments.

Risk assessments were approved before each experiment and are available at:

- https://www.groupware.kuleuven.be/sites/depchemrisico/Risk%20Assessments/Forms/Per%20division.aspx

For unsupervised experiments, additional risk assessments were prepared and approved, according to the procedure:

- https://admin.kuleuven.be/sab/vgm/kuleuven/EN/riskactivities/ue/continuous-activities

Particular care was taken when working with compounds classified as E4+, such as phosphoryl trichloride (highly toxic and causes severe burns), acetone or toluene (highly flammable) which were used during the synthesis of sorbents.

The following safety trainings were attended:

- Introductory safety course (March 2015)
- Industrial and lab safety (May, 2015)
- Radiation protection (November 2016)